博士論文

論文題目　Organic aerosol production in reducing atmospheres and its influence on the radiation fields on Titan and early Earth
（還元的大気における有機物エアロゾルの生成とタイタンおよび原始地球における放射伝達過程への影響）

氏　名　洪　鵬

Doctoral Dissertation

Organic aerosol production in reducing atmospheres and its influence on the radiation fields on Titan and early Earth.

Department of Complexity Science and Engineering,

Graduate School of Frontier Science,

University of Tokyo

Peng Hong

Wed, Dec 11, 2013

Abstract

Organic aerosols are considered to be produced in CH_4-containing, reducing atmospheres, such as Titan, early Earth, and exoplanets. Physical processes (radiative transfer and microphysical processes of the organic aerosols) and chemical processes (photochemical and ion reactions to form organic aerosols) in these atmospheres are mutually dependent on each other. Thus, self-consistent coupling of the physical and chemical processes is essential to understand atmospheric and environmental evolution of these planets and satellites. Many of the previous studies, however, discuss the physical and chemical processes independently, and there are only a few studies that couple these two processes.

One of the largest obstacles that prevent the coupling between the physical and chemical processes is uncertainty of production mechanism of organic aerosols in reducing planetary atmospheres. In order to filling the gap between the chemical and physical processes, we conduct laboratory experiments of formation of organic aerosol analogues, called tholin, using a hydrogen/helium lamp and gas analysis of intermediate molecules formed by photochemical reactions. We also perform photochemical calculations that simulate reactions in the laboratory experiments to identify the parent molecules and corresponding reactions that control the tholin production in the experiments. We measure the dependences of tholin production rate on both actinic UV flux and CH_4/CO_2 ratio. Our experimental results show that the tholin production rate is a linear function of UV flux, which suggests that the aerosol production is limited by polymerization reactions between intermediate products, i.e., parent molecules, produced from the photochemistry of CH_4. We also found that the aerosol production rate remains almost constant for a wide range of CH_4/CO_2 ratio when the CH_4/CO_2 ratio is in excess of unity. On the other hand, the tholin production rate decreases dramatically with a decline in CH_4/CO_2 ratio when the CH_4/CO_2 ratio becomes less than unity. Our photochemical calculations show that this behavior of tholin production rate is in a good agreement with polymerization reaction rates involving aromatic hydrocarbons, benzene. These results suggest that benzene is the parent molecule that controls the tholin production. On the other hand, polymerization reactions involving polyynes do not explain the measured tholin production rate as a function of CH_4/CO_2 ratio. Our results are considered to be applicable to estimate the production of monomers in a CH_4-contaitning reducing atmosphere using a one-dimensional photochemical model, which is necessary to couple the chemical processes with the physical processes in the atmospheres.

Based on our experimental results, we calculate the atmospheric composition, organic aerosol production, and its optical depth for variable planetary

atmospheres, using a coupled photochemical-microphysical-radiative transfer models. In Titan's atmosphere, the primary energy source for organic aerosol formation has been unclear. Our results show that polymerization reactions of benzene induced by solar far UV light cannot explain the proposed aerosol production rates in Titan's atmosphere. In contrast, our results suggest that the organic aerosols in Titan's atmosphere are largely produced by nitrile polymerization, which is initialized by irradiations of high-energy particles. These results suggest that the irradiation of high-energy particles is the primary energy source for the formation of thick aerosol layers in Titan's atmosphere. These conclusions further imply that Titan's climate and surface environments would have been very sensitive to variations in the magnetic field of Saturn and solar wind flux.

In early Earth's atmosphere, organic aerosols formed from atmospheric CH_4 are suggested to play key roles in determining the surface temperature. If their UV optical depth were thick, the organic aerosols would have possessed indirect greenhouse effect, which shields strong greenhouse gas such as NH_3 from UV light. On the other hand, if their optical depth in visible wavelength were thick, they in turn would have had anti-greenhouse effect, which cools the surface. Whether the organic aerosols work as indirect greenhouse or anti-greenhouse critically depends on their production rate in the atmosphere. Our results show that the organic aerosol layers produced by benzene polymerization induced by solar UV would have been optically thin, insufficient to have both indirect greenhouse and anti-greenhouse effects. The absence of strong anti-greenhouse effect in turn suggests that the greenhouse effect of ethane would have worked efficiently to keep early Earth's surface above freezing point of H_2O, especially under CH_4-rich atmospheric conditions. The supply and loss of both CO_2 and CH_4 through biogeochemical processes vary with surface temperature. Given that ethane concentration also changes with CH_4/CO_2 ratio of the atmosphere, there would have been a feedback relationship between surface temperature and ethane concentration. On the other hand, we found that thick aerosol layers would have been formed if aerosol production also proceeds through nitrile polymerization, induced by irradiation of high-energy particles. Such thick aerosol layers are optically thick sufficient for shielding NH_3 from UV light on early Earth. Further investigation of nitrile polymerization by laboratory experiments will be important in future studies to evaluate the role of organic aerosols in early Earth's atmosphere.

Acknowledgments

I would like to thank to my PhD advisors, Professor Seiji Sugita and Doctor Yasuhito Sekine, for supporting me during these past five years. I owe this dissertation to their constructive comments and encouragements. My two advisors, showing professionalism, enthusiasm and dedication to science, are the exemplary scientists I wish to become someday. I am also very grateful to the researchers in Boulder, Colorado, Professor Owen Toon of the University of Colorado at Boulder, Doctor Erika Barth and Doctor Timothy Michaels of the Southwest Research Institute. Without their instructive and technical help about microphysical and radiative transfer model, I surely could not have done this study. I also thank the member of my PhD committee, Professors Kiyoshi Kuramoto, Takehiko Sasaki and Takeshi Imamura for their contribution to improve this thesis. I would like to extend my gratitude to other researchers, who gave me various comments and suggestions, useful ideas, criticism and advice to my research, including Eiichi Tajika, Masahiro Ikoma, Yutaka Abe, Hiroko Nagahara, Hidenori Genda, Takanori Sasaki.

I thank the graduate students and alumni, as colleagues and as friends. Yuichiro Cho, Tiger Hamura, Yoshiyasu Watanabe, Natsuko Okamura: they are the same class with me in the graduate school and have worked hard together. I shared most of the time with them when I was in the lab. The alumni of the lab, Doctors Kousuke Kurosawa, Shunichi Kamata, Kazumi Ozaki are good seniors, providing guidance to me. The Master's thesis of Tsutoni Sasamori, a graduate of our lab, directs my PhD study. Hideharu Kuwahara, Mariko Harada, Shintaro Kadoya, Yui Joh, Eri Tatsumi, Toshiyuki Morimi, Shun Fukushima, Kouichi Hagura, Kenya Kodama, Junpei Kobayashi, Kana Oide, Megumi Mori, Sumire Koga: They are good friends and make my life easier Among them, I have to address my special gratitude to Hideharu Kuwahara, who conducted the measurement of fragmentation pattern for QMS gas analysis, described in the section 1.3.4., when I was in the US. It is needless to say that I could not have advanced without his data. I am also grateful to the members of Professor Toon's research group, including Erik Larson, Eric Wolf, Pengfei Yu. Especially to Erik: thank you so much for your tremendous help throughout my stay in Colorado. You were a good tutor, helping me to get used to American culture, feeding me lots of hot dogs and giving me several stitches. All of them are good memories now, and remember, it was your unexpected visit to Japan that led me to Colorado. I cannot thank you enough.

I am also endlessly grateful to the other PhD students who entered doctoral course at the same time with me: Hideyuki Hotta, Shin Toriumi, Risa Sakai, Akiko Takeo, Katsuaki Higashimori, Hiroki Terashima, Yasuhiko Igarashi, Hiroki Terashima, Yasuhiko Igarashi, Yosuke Otsubo, Hiroshi Saito. They are good friends as well as good rivalries. I wish we will keep inspiring each other. Many friends in Boulder made my

life pleasant, especially those who were living at Horizon International Student Center. Kim Burb, Khalid, Chandan, Raphael, Marx, Sheeraz, Shahid, Caleb, Ashley, Summer, Joe, Steve, Aimee, Lily, Mona, Javier, Taty, Rickey, Aki, Kevin, Nico, Todd, Edi, Ken, Cynthia: You are not only my friends, but my brothers and sisters, uncles and aunts in the US. I would have never imagined to have that awesome friends before came to Boulder. Only the beautiful memories with you kept me sane for the last few months. We will meet again someday.

Finally, I wish to express my best thanks to my family for all the love and spiritual and material support over the years. The Japan Society for the Promotion of Science has also provided me financial support.

To everyone else not named above, thank you, too.

Table of Contents

General Introduction

Understanding physical and chemical processes in planetary atmospheres is important to investigate the long term evolution of climate and surface environments. The physical processes involve the radiative transfer processes, which include scattering and absorption of both short- and long-wavelength light due to gas molecules and solid particles in the atmospheres, and the microphysical processes, which include the formation and growth of both cloud and aerosol particles. On the other hand, the chemical processes in the atmosphere involve photochemistry and ion chemistry driven by the irradiations of ultraviolet (UV) light and high-energy particles.

These physical and chemical processes have an interdependent relationship in planetary atmospheres. For instance, in methane-rich reducing atmospheres, such as the atmospheres of Titan and early Earth, organic aerosol layers are considered to be produced by the growth and coagulation of the precursors of aerosol particles called monomers (i.e., the microphysical processes) (e.g., Toon et al., 1992; Waite et al., 2007; Trainer et al., 2006) (Figure 1). In the atmospheres, the monomers are originally formed by complex photochemical and ion-chemical reactions (i.e., the chemical processes) (e.g., Yung et al., 1984; Pavlov et al., 2001). Because the organic aerosol layers significantly influence the radiative transfer processes in the atmosphere, the surface temperature and atmospheric structure are not determined only by the atmospheric compositions but also these microphysical and chemical processes. Meanwhile, the chemical processes also depend on the radiative transfer processes. For instance, solar UV light, energy source for photochemical reactions, is attenuated by absorption and scattering due to gas molecules and aerosol particles (e.g., McKay et al., 1989; Tomasko et al., 2008a). Chemical reactions also highly depend on the temperature profile determined by radiative transfer processes (Hebrard et al., 2006; 2007). Thus, to understand the evolution of planetary climate and surface environments, a theoretical model, which calculates both the physical and chemical processes consistently, is required. However, many of the previous studies discuss the physical or chemical processes independently (e.g., Yung et al., 1984; Toublanc et al., 1995; Lara et al., 1996; Wilson and Atreya, 2004; Krasnopolsky 2009; Toon et al., 1980; 1992; McKay et al., 1989; Pavlov et al., 2001; Haqq-Misra et al., 2008; Wolf and Toon, 2010), and there are a few studies that couple these two processes (Lavvas et al., 2008a, b).

One of the large obstacles, which prevent the coupling between the physical and chemical processes especially in reducing atmospheres, is the uncertainty of production mechanism of organic aerosols. Nevertheless, a general picture of the

formation of organic aerosols in Titan's atmosphere now can be drawn owing to the Cassini mission (e.g., Waite et al., 2007; Tomasko and West, 2009; Krasnopolsky, 2009). Organic aerosols in Titan's atmosphere are considered to be complex, high-molecular-weight hydrocarbons and nitriles with thousands atomic mass (Waite et al., 2007; Tomasko et al., 2008b), which are presumed to be formed from simple hydrocarbons, such as C_6H_6, C_4H_2, HCN, and C_2H_2 (Wilson and Atreya, 2003; 2004; Lavvas et al., 2008a, b; Krasnopolsky, 2009). Figure 1 is a schematic of photochemical and microphysical processes of the formation of organic aerosols in Titan's atmosphere, after Lavvas et al. (2011). Organic aerosol formation initiates with the photolysis of methane, subsequently producing various gaseous hydrocarbons, e.g., C_6H_6, C_4H_2 and C_2H_2 (Yung et al., 1984; Wilson and Atreya, 2004; Lavvas et al., 2008a, b; Krasnopolsky, 2009). The gas-phase reactions among those gas species are considered to result in the production of monomers (Wilson and Atreya, 2003; Trainer et al., 2006), which are the fundamental blocks to constitute large aerosol particles (McKay et al., 1989; Toon et al., 1992). The monomers would be coagulated each other through various microphysical processes in the atmosphere, like Brownian motion, gravitational settling, coagulation by Van der Waals and Coulomb forces (Seinfeld and Pandis, 2006; Pruppacher and Klett, 2010). In addition to coagulation, the reactions on the surface of monomers with highly-reactive gas species would result in the growth of the monomer size (Lavvas et al., 2011). The aggregate particles are considered to experience particle rounding due to the increased monomer size by the surface growth (Lavvas et al., 2011). Finally, large organic aerosol particles would be produced in Titan's atmosphere (McKay et al., 2001). Similar chemical and microphysical processes are considered to have been occurred in CH_4-containing, early Earth's atmosphere before the rise of O_2 (Sagan and Chyba, 1997; Pavlov et al., 2001; Trainer et al., 2006; Hasenkopf et al., 2010).

Since the rate coefficients of the reactions of high-molecular-weight hydrocarbons are largely unknown, all of the chemical reactions, which lead to the formation of monomers, cannot be included in photochemical models of planetary atmospheres. The previous photochemical models of Titan and early Earth assume that all high-molecular-weight hydrocarbons (e.g., $\geq$ C_4–C_6 hydrocarbons) become monomers (e.g., Pavlov et al., 2001, Lavvas et al., 2008a, Krasnopolsky 2009). Using the obtained vertical profile of presumed formation rate of monomers, the microphysical models obtained the vertical profile of organic aerosol layers by calculating the growth and coagulation of these monomers in the atmosphere (Toon et al., 1980; 1992; McKay et al., 1989). The chemical pathways for the formation of monomers from gaseous molecules, however, remain poorly understood. In especially, all of aliphatic and aromatic hydrocarbons higher than C_4–C_6 would not always become the monomers. Thus, although there are a few coupled atmospheric models (Lavvas et al., 2008a; 2008b), a large uncertainly still remains in the calculation of aerosol monomer

production rate. On the other hand, laboratory experiments have measured aerosol production rates for several experimental conditions simulating Titan's atmosphere (e.g., Trainer et al., 2006; Sciamma-O'Brien et al., 2010). Nevertheless, no experimental data have been obtained to constrain the chemical reactions that control the aerosol production. Dependence of aerosol production rate on UV fluxes and of atmospheric compositions is also largely unclear, which is essential to estimate the influence of organic aerosol layers on the radiative transfer processes in long term evolution.

Self-consistent coupling of the photochemistry and microphysics could provide significant implications to atmospheric chemistry and climatic evolution. In Titan's atmosphere, the organic aerosols would be produced by the solar UV and those by other energy sources, such as high-energy electrons from Saturn's magnetosphere (e.g., Krasnopolsky, 2009). However, the major energy source for generating organic aerosols remains unclear. The organic aerosols formed by different energy sources could have different chemical compositions and optical properties (Hasenkopf et al., 2010). For instance, because of the low energy of far UV (FUV: 120–200 nm) photons compared to the high-energy particles and extreme ultraviolet (EUV: <120 nm) photons, organic aerosol produced by FUV would not incorporate nitrogen atoms (Raulin et al., 1982; Trainer et al., 2012). On the other hand, high-energy particles are considered to efficiently dissociate both N_2 and CH_4 to form nitriles in Titan's atmosphere (e.g., Yung et al., 1984; Wilson and Atreya, 2004; Krasnopolsky, 2009). In fact, previous experiments showed that the optical property and chemical structure of organic aerosols formed by plasma irradiation are different from those formed by EUV irradiations (See a review by Cable et al., 2012). The fluxes of solar UV and high-energy particles are suggested to vary throughout Titan's history. Thus, changes in these energy fluxes could have affected the production rate and optical depth of organic aerosols and thus the radiative transfer processes in the atmosphere. This in turn would have remarkably affected the surface temperature and atmospheric structure. Determining the major energy source for organic aerosol formation in Titan's atmosphere is important to understand not only the chemical processes in the current atmosphere but also the stability of the atmosphere and climate in response to changes in energy fluxes. To draw a clearer view of the energy source for organic aerosol production and the climatic stability of Titan in response to a change in energy fluxes, a self-consistent, physical and chemical model of the atmosphere would be needed.

A self-consistent modeling would also provide another implication to understand the habitability on early Earth, especially regarding the faint young Sun paradox (Pollack, 1979; 1991; Crowley, 1983; Barron, 1984; Kasting and Grinspoon, 1991; Kasting 1993; Rampino and Caldeira, 1994; Nisbet and Sleep, 2001; Kasting and Catling, 2003; Zahnle et al., 2007; Güdel, 2007; Shaw, 2008; Nisbet and Fowler, 2011; Feulner, 2012). Based on solar evolution models, the bolometric luminosity of the young Sun at 4.5 Gyr ago is suggested to have been about 30% smaller than that of the

current Sun (e.g., Gough, 1981). Under the low luminosity of young sun, the surface temperature of early Earth at > 2 Gyrs ago could have been below H_2O's freezing temperature if the atmospheric compositions were same as that of today (Sagan and Mullen, 1972). There are, however, geologic evidences for the presence of liquid surface water during the Archean (> 2.5 Gyr ago) (Lowe, 1980; Walker, 1982; Walker et al., 1983; Fowler et al., 2002; Eriksson et al., 2004; Benn et al., 2006). Thus, in order to account for, so called, the early faint Sun paradox, an enhanced greenhouse effect would be needed in early Earth's atmosphere (e.g., Sagan and Mullen, 1972; Owen et al., 1979). A thick CO_2 atmosphere has been suggested to resolve the early faint sun paradox (e.g., Owen et al., 1979). Geochemical analyses of paleosols and banded iron formations, however, suggest that the CO_2 partial pressures at 2.8 Gyr ago would have been too low to solve the paradox (Rye et al., 1995; Sheldon, 2006; Driese et al., 2011). Ammonia has been suggested as another solution to the faint young Sun paradox (Sagan and Mullen, 1972), since ammonia is a strong greenhouse gas because of its strong and broad absorption feature around 10 μm (e.g., Wang et al., 1976). However, the photochemical models show that ammonia would have been destroyed by solar UV in less than a decade, which is significantly shorter than the outgassing time scale of NH_3 (e.g., Kuhn and Atreya, 1979). Sagan and Chyba (1997) proposed that optically thick organic aerosol layers would have been formed in a CH_4-rich atmosphere on Earth before the rise of O_2. They suggested that organic aerosols have yielded a strong indirect greenhouse effect on an early Earth, by protecting ammonia from UV photolysis. In contrast, the photochemical model considering Mie scattering of aerosol particles shows the organic aerosol layer could have possessed a strong anti-greenhouse effect due to its optical thickness at the visible wavelengths (Pavlov et al., 2001; Haqq-Misra et al., 2008). Whether the organic aerosol layers could have possessed indirect greenhouse or anti-greenhouse effect on early Earth depends critically on the aerosol production rate in the atmosphere (Trainer et al., 2006; Wolf and Toon, 2010). In particular, given an uncertainty in the atmospheric composition in early Earth's atmosphere (e.g., see Feulner, 2012), the experimental data on aerosol production for a wide range of CO_2/CH_4 ratio would be essential. Furthermore, a small change in the CO_2/CH_4 ratio in the atmosphere could have changed the aerosol production rate, which may have affected the atmospheric structure and surface temperature through the radiative transfer processes. This in turn could have resulted in a large change in the CO_2/CH_4 ratio in the atmosphere, through biogeochemical processes, such as silicate weathering (e.g., Walker et al., 1981; Berner et al., 1983). To discuss such feedback mechanism and climatic stability in an atmosphere with thick organic haze, self-consistent coupling of the physical and chemical processes is required.

In the Chapter 1 of this dissertation, we conducted laboratory experiments of organic aerosol formation using a FUV H_2/He lamp for various gas mixtures of CH_4 and CO_2. Then, the results of aerosol production rate and gas analyses were compared with

photochemical calculations to constrain the chemical reactions that control the organic aerosol production. In the Chapter 2, we coupled a one-dimensional photochemical model of planetary atmospheres to a microphysical and radiative transfer models. Using the photochemical models, we calculated the production rate of monomers in the atmosphere based on the experimental results of rate-limiting reactions of organic production. Using the results, microphysical model calculated the profile of organic aerosol layers, by which the atmospheric structure and radiative transfer processes are in turn calculated. We then investigate the influence of organic aerosols on the radiative transfer process in the atmospheres of Titan and early Earth using the coupled photochemical/microphysical/radiative transfer model. Finally we summarize the results and implications.

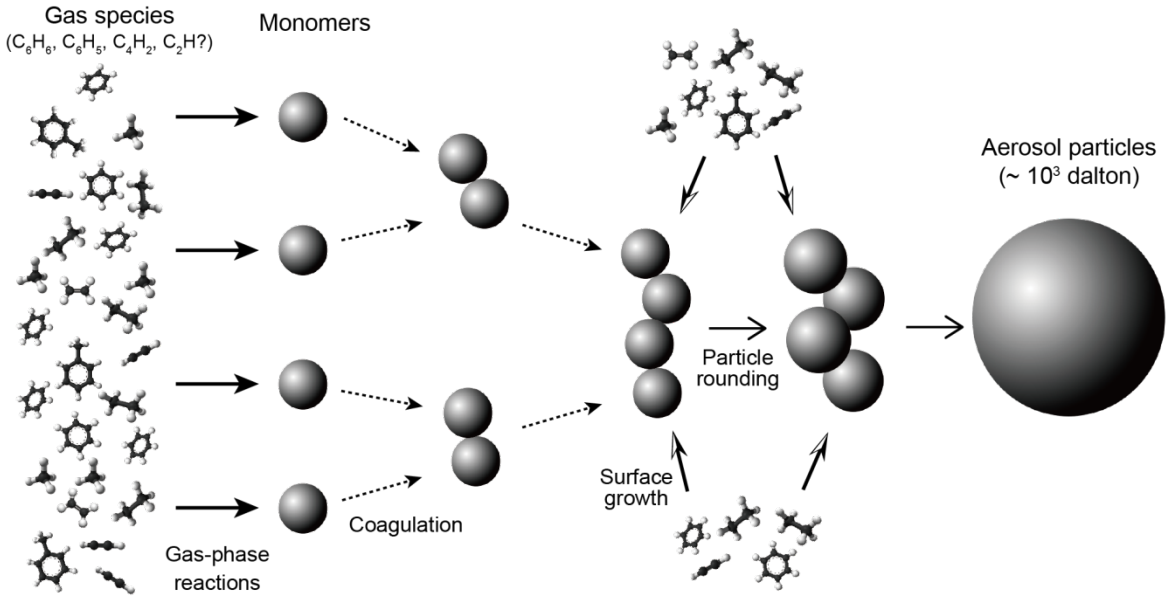

Figure 1. Photochemical and microphysical processes that lead simple gas species to large organic aerosol particles, after Lavvas et al. (2011). Hydrocarbon chemistry produces various gas species such as C_6H_6, C_4H_2 and C_2H_2 (e.g., Yung et al., 1984; Krasnopolsky, 2009). Gas-phase reactions among those gas species would further lead to the formation of monomers (e.g., Wilson and Atreya, 2004; Lavvas et al., 2008a, b; Krasnopolsky, 2009). The monomers are considered to be coagulated with microphysical processes in the atmosphere (Toon et al., 1980; 1992; McKay et al., 1989). The surface reactions on the monomers would also occur, resulting in the growth of the monomer size (Lavvas et al., 2011). The aggregate particles would experience particle rounding due to the increased monomer size by the surface growth (Lavvas et al., 2011).

Chapter 1. Organic aerosol production mechanism constrained by laboratory experiments and photochemical calculations

1.1 Introduction

In CH_4-rich reducing planetary atmospheres, Titan and early Earth, organic aerosol layers are considered to be produced through complex photochemical reactions (Yung et al., 1984; Wilson and Atreya, 2004; Waite et al., 2007; Lavvas et al., 2008a, b; Krasnopolsky, 2009; Tomasko and West, 2009). Organic aerosols in Titan's atmosphere would be solid particles of high-molecular-weight hydrocarbons with thousands atomic mass (Waite et al., 2007; Tomasko et al., 2008b), which are presumed to be formed via polymerization of simple hydrocarbons (e.g., Yung et al., 1984; Wilson and Atreya, 2004; Waite et al., 2007; Lavvas et al., 2008a, b; Krasnopolsky, 2009; Waite et al., 2007). The previous photochemical models assume that the polymerization reactions of all of C_4-C_6 hydrocarbon carbons produce precursors of organic aerosols, called monomers (Yung et al., 1984; Toublanc et al., 1995; Wilson and Atreya, 2004; Waite et al., 2007; Lavvas et al., 2008a, b; Krasnopolsky, 2009). Using the vertical profile of formation rate of monomers in the atmosphere, the growth and coagulation of monomers and atmospheric structure in Titan' atmosphere were discussed using the microphysical and radiative transfer models (Toon et al., 1980; 1992; McKay et al., 1989; Lavvas et al., 2008a, b). However, the chemical network and rate coefficients for formation of high-molecular-weight hydrocarbons are largely unknown due to a lack of laboratory data. Thus, it is highly uncertain whether polymerization of all of C_4–C_6 hydrocarbons would result in the formation of the monomers. In fact, the efficiency of polymerization would be different between aliphatic and aromatic hydrocarbons. Furthermore, the uncertainty in the formation mechanisms of monomers prevents to discuss the long term evolution of Titan's atmosphere and extrapolation of the organic aerosol production rate to early Earth and exoplanets, given a large uncertainty in a change in aerosol production rate in response to a change in the flux and spectra of UV light. As organic aerosol layers could play a key role in determining the atmospheric structure and surface temperatures of these planets and satellite, filling a gap between the reactions of C_4–C_6 hydrocarbons and the monomer production rate is essential to discuss the atmospheric chemistry and its long term evolution.

Laboratory experiments have been performed to produce laboratory analogues of organic aerosols, so called "tholin", by irradiating various energy sources (e.g., cold and hot plasma discharge, UV irradiation, Gamma rays, soft X-rays, Electron beam, and Proton beam) to CH_4-containing gas mixture (e.g., Khare et al., 1984a; 1987; Imanaka et al., 2004; Imanaka and Smith, 2007; 2010; Trainer et al., 2006; 2012; Sekine et al., 2008a; Hasenkopf et al., 2010). The optical constants, mainly complex refractive index, of the tholins produced by the cold plasma irradiation to gas mixtures of N_2 and CH_4 sufficiently reproduce Titan's planetary albedo retrieved by the spacecraft and

ground-based observations (e.g., McKay et al., 1989; Toon et al., 1992). These results indicate that the tholins produced in laboratories would be good analogue materials for the organic aerosols in Titan's atmosphere. Most of the previous experiments have investigated the reaction conditions (e.g., temperature, pressure, and composition of gas mixtures), under which the optical properties of the produced tholins can explain the planetary albedo of Titan (e.g., Khare et al., 1984a; 1987; Imanaka et al., 2004; Hasenkopf et al., 2010). Nevertheless, most of the previous studies have not focused on the rate and mechanism for the formation of tholins.

Recently, Trainer et al. (2006) measured the production rate of tholins as a function of CH_4 concentration for CH_4/N_2 gas mixture using a deuterium lamp as a simulated solar FUV source. They observed that the aerosol production initially increases with added CH_4 and then decreases with further increases in CH_4. Based on these results, they proposed two mechanisms for the aerosol production:

Mechanism I:

$$CH_4 + h\nu \rightarrow A \qquad (1.1)$$

$$A + h\nu \rightarrow \text{aerosol products} \qquad (1.2)$$

Mechanism II:

$$CH_4 + h\nu \rightarrow A \qquad (1.3)$$

$$A + A \rightarrow \text{aerosol products} \qquad (1.4)$$

$$A + CH_4 \rightarrow \text{nonaerosol products} \qquad (1.5)$$

where A is an intermediate product. In the mechanism I, increased CH_4 shields the production of intermediate A and therefore decreases the aerosol production rate at high CH_4 abundances. Meanwhile, the mechanism II assumes an aerosol production from the reaction of intermediate species; however, the intermediate can also react with CH_4, producing nonaerosol particles such as saturated hydrocarbons. In this case, very high levels of CH_4 suppress the aerosol production. An important difference between mechanisms I and II is the difference in aerosol production rate in response to a change in UV fluxes (Trainer et al., 2006). When the abundance of CH_4 limits the aerosol production, the aerosol production rate in the mechanism I would become a second-order function of actinic flux, because there are two photolysis reactions (see the reactions 1.1 and 1.2). On the other hand, the mechanism II results in an aerosol production rate as a first-order function of actinic flux, since there is only one photolysis

reaction (see the reactions 1.3, 1.4, and 1.5). Nevertheless, it has been unclear whether the tholin formation proceeds through the mechanism I or II.

Trainer et al. (2006) also measured tholin production rates as a function of initial CH_4/CO_2 gas ratio to simulate organic aerosol formation in early Earth's atmosphere. They show that, at the CH_4/CO_2 ratio of > 1, the tholin production rate becomes almost constant. Their experimental results, however, indicate that that dramatically decrease with an increase in CO_2 levels when the CH_4/CO_2 ratio of < 0.1. Although they did not provide detailed explanation for this behavior, they suggested oxygen species could participate in the aerosol production. To understand the behavior of the tholin formation rate and its mechanism, chemical analyses of intermediate gas species would be required. Nevertheless, they did not perform the gas analyses during the experiment. Furthermore, Trainer et al. (2006) used a deuterium lamp as an energy source of the reactions. As described below, a deuterium lamp would not be a good energy source to simulate solar UV light, in which the Lyman α line is predominant.

In this chapter, we measured the dependence of aerosol production rate on actinic flux, in order to distinguish which mechanisms (i.e., the mechanism I or II) is dominant. The dependence of aerosol production rate on actinic flux is also important when one estimates the organic aerosol production rates on an early Earth and exoplanet based on Titan's production rate:

$$F = \beta \cdot F_{\mathrm{Titan}} \cdot \left(\frac{I}{I_{\mathrm{Titan}}}\right)^{m} \cdot \left(\frac{\chi_{\mathrm{CH4}}}{\chi_{\mathrm{CH4,\ Titan}}}\right) \qquad (1.6)$$

where F_{Titan} and F are the aerosol fluxes on Titan and early Earth, respectively. I and I_{Titan} are the FUV flux on an early Earth and Titan. χ and χ_{Titan} are methane mixing ratios. β is an enhancement factor experimentally obtained. Due to the uncertainty of m, the reaction order of aerosol formation rate as a function of UV flux (i.e., m = 1 or 2), the previous estimates of aerosol production rates on early Earth contain a large uncertainty on the order of 10^3 (Trainer et al., 2006; Wolf and Toon, 2010). In addition to the dependence on UV flux, we measured the variation in tholin production rate as a function of initial CH_4/CO_2 gas ratio of the reactant gas. To understand the reaction mechanism and parent reactions/molecules to be converted in to the tholin, we performed gas analyses of the intermediate products. We compared the experimental results of intermediate gas products with those of photochemical calculations. If the parent molecules/reactions for the formation of tholin were identified, we will be able to incorporate the production rate of monomers in the microphysical models (see Chapter 2). Thus, the identification of the parent molecules/reactions are a key for constructing a self-consistent coupling model of photochemical, microphysical, and radiative transfer processes.

1.2 Experimental apparatus

Figure 1.1 shows a schematic diagram of the experimental apparatus for our tholin formation experiments. The system is an open-flow system, which consists mainly of two quartz glass tubes (Makuhari Rikagaku Glass Inc.) for a reaction cell and UV light source. The two parts are separated by a MgF_2 window with 1 mm thickness (IR SYSTEM Co., Ltd.) having UV cutoff at 110 nm (Duncanson and Stevenson, 1958). Thus, UV light at >110 nm from the light source can transmit into the reaction cell through the window, whereas the reactant gas and hydrogen/helium gas are not combined each other. The UV lamp has a cross sectional area of 3.8 cm^2. Reactant gases are introduced into the reaction cell constantly through mass flow controllers (KOFLOC, Model 3200 series) from gas cylinders and evacuated by a rotary pump with a liquid nitrogen cold trap in between. The cold trap prevents pump oil from diffusing back into the line. Likewise, the hydrogen/helium mixture gas is introduced to the chamber next to the reaction cell through the mass flow controller and evacuated by a rotary pump. When evacuated, the reaction cell and the chamber of light source have a background pressure of 10^{-3} torr, as measured by thermocouple gauges (Varian Inc., ConvecTorr P-Type). Since the thermocouple gauges are able to measure only relative pressure, they are calibrated with a capacitance manometer (MKS, 622B Baratron Absolute Capacitance Manometer) to derive absolute pressure. Figure 1.2 is the calibration result of the thermocouple gauge using the capacitance manometer, showing that the thermocouple gauge always underestimates the pressure about a factor of five. A part of the reactant and/or product gases are introduced to a quadruple mass spectrometer, or QMS (ULVAC, Qulee CGM) to perform mass spectrometry. An ultraviolet/visible spectrometer (Ocean Optics, USB 2000) was inserted at the opposite end of the reaction cell to the light source to measure the time evolution of attenuation of UV flux from the lamp. The UV/VIS spectrometer is also separated by a MgF_2 window from the reaction cell. Reactant gases are photolyzed and the radicals produced initiate complex photochemistry in the reaction cell, especially in the vicinity of UV lamp, eventually leading to formation of higher-molecular-weight hydrocarbons. The tholins produced deposit on the MgF_2 window, forming a thin organic film. We measured the thickness of the film with a spectroscopic ellipsometer (HORIBA Jobin Yvon, Auto SE Lambda 650).

The previous tholin experiments simulating hydrocarbon photochemistry driven by solar FEV irradiation have employed deuterium lamps as the solar UV flux (Adamkovics and Boering, 2003; Trainer et al., 2006; 2012; 2013; Hasenkopf et al., 2010). One of the spectra of the deuterium lamps (Hamamatsu Photonics Co., L1835) is shown in Figure 1.3. It has a distinctive strong emission line around 160 nm due to

hydrogen and deuterium molecular emissions, which is not significant in the actual solar UV flux. On the other hand, since the solar atmosphere contains a large number of hydrogen atoms, the Lyman α line at 121.6 nm dominates the actual solar ultraviolet radiation (Kuroiwa et al. (1992)). Because CH_4 and CO_2 have very different absorption cross sections around 160 nm (Figure 1.3), the use of a deuterium lamp as an UV source could cause significantly different photochemical reactions with those by actual solar ultraviolet flux. By adding noble gases to H_2 gas and exciting the gases with a power source, meta-stable noble gases with high energy can collide with hydrogen molecules and dissociate H_2 into atomic hydrogen, which suppresses molecular emission lines (Davis and Braun, 1968; Boduch et al., 1992). We used a premixed hydrogen/helium gas mixture with H_2:He = 1:9 (Purity 99.9999%, Japan Fine Products Co.) and introduced it with a pressure of ~1 torr. The hydrogen/helium gas mixture is excited by a high frequency (RF) power source (13.56 MHz, Nihon Koshuha Co., Ltd.,). Previous studies show that the use of helium results in a stronger Lyman α emission line compared with other noble gases due to the high energies of meta-stable He atoms (Kuroiwa et al., 1992; Rahman et al., 2004). Kuroiwa et al. (1992) measured the emission spectrum of H_2/He lamp with H_2:He = 1:20, shown in Figure 1.3, which has a strong Lyman α emission line similar to the actual solar UV flux. With the similar experimental settings with Kuroiwa et al. (1992), we expect that the Lyman α line would dominate the vacuum ultraviolet irradiated from our H_2/He lamp. Although the molecular emissions around 160 nm are sometime observed with these hydrogen/helium lamps (Fuchs et al., 1995; Cottin et al., 2003), we confirmed that the Lyman a line is the dominant emission from our H_2/He lamp by performing N_2O and CO_2 actinometry (see the next section below).

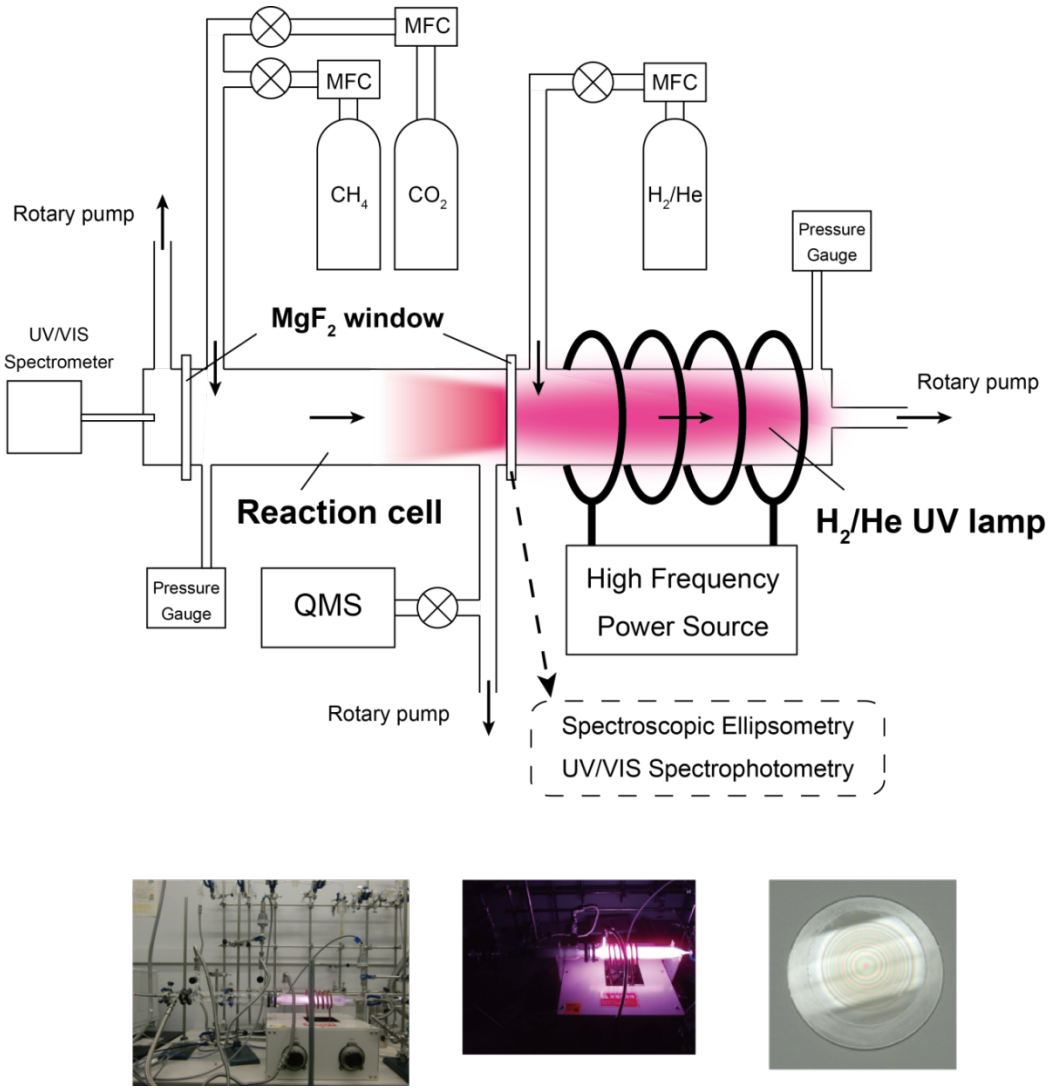

Figure 1.1. Experimental apparatus for organic aerosol experiments. QMS, MFC stand for quadruple mass spectrometer and mass flow controller, respectively. Solid black arrows represent the directions of gas flow. The pressure gauges used in the experiments are thermocouple gauges. The right bottom picture is an organic film produced on a MgF_2 window with 35 mm of diameter, showing Newton's rings. The left bottom picture shows the reaction cell, UV lamp and high frequency power source. The center bottom picture is a close-up of the UV lamp.

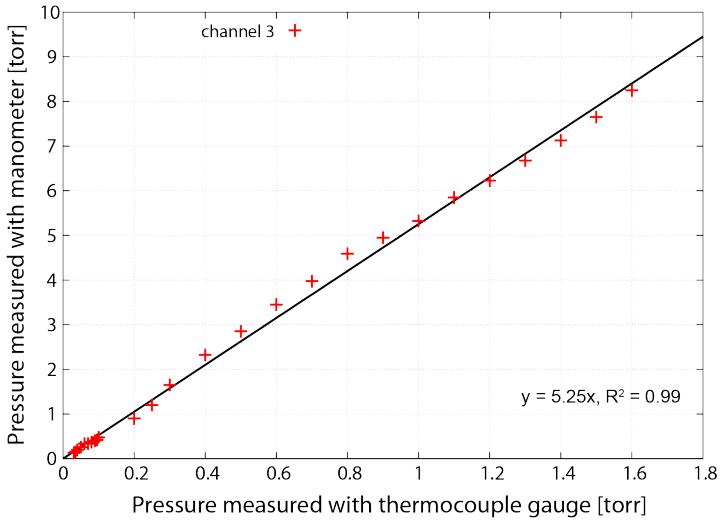

Figure 1.2. Calibration result of a thermocouple gauge using a capacitance manometer, showing the thermocouple gauge overestimates the pressure by a factor of 5.

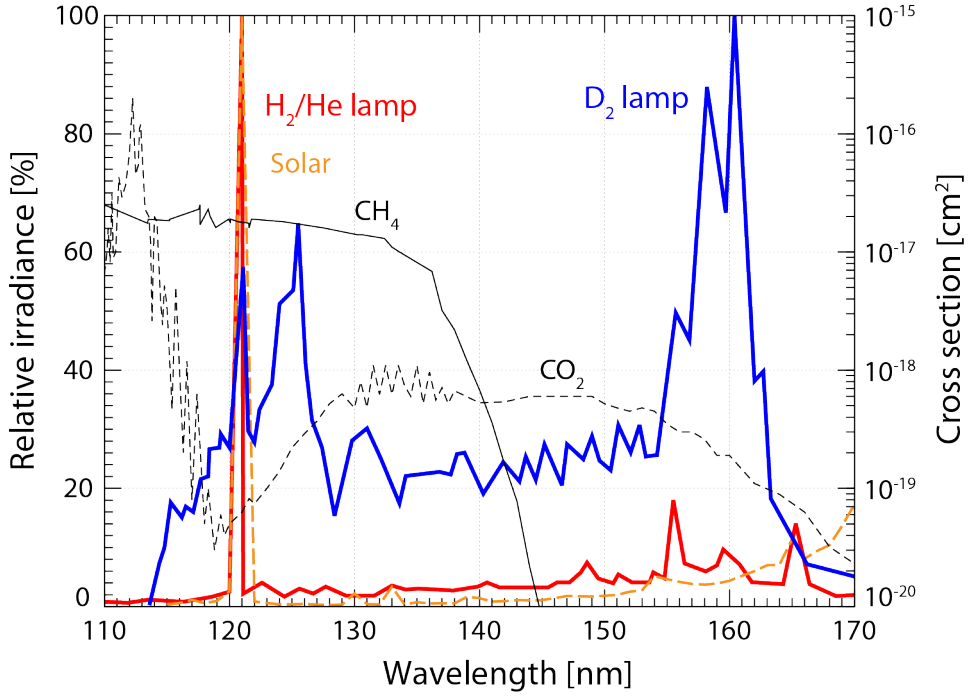

Figure 1.3. Vacuum ultraviolet spectra of hydrogen/helium lamp (solid red line) and deuterium lamp (solid blue line). The spectrum of H_2/He lamp was obtained by Kuroiwa et al. (1992), while that of D_2 lamp is obtained by Hamamatsu Photonics Co. (L1835). Also shown are solar ultraviolet flux (yellow dashed line) observed by Mount and Rottman (1983) and the absorption cross sections of CH_4 (solid black line) and CO_2 (dashed black line). The references of the cross sections are listed in Table 2.3.

1.3 Experimental results

1.3.1 Measurement of actinic flux of H_2/He lamp by N_2O/CO_2 actinometry

The measurement of the vacuum UV flux (wavelengths shorter than 200 nm) is of importance, since most of the gas species in planetary atmospheres significantly absorb vacuum ultraviolet (Young and DeMore, 1999). In order to measure the relationship between organic aerosol production rates and actinic flux, we first measured the actinic flux emitted from the hydrogen/helium lamp by performing N_2O and CO_2 actinometry (e.g., Rajappan et al., 2010).

We estimated the actinic flux from the lamp by the following procedure. We consider that, before the UV irradiation, the gas abundance in the reaction cell reaches steady state between the supply of gas mixtures from the mass flow controller and evacuation with the rotary pump,

$$\frac{dn_{\text{before}}}{dt} = f_{\text{in}} - v_{\text{out}} n_{\text{before}} = 0$$
$$n_{\text{before}} = \frac{f_{\text{in}}}{v_{\text{out}}} \qquad (1.7)$$

where n_{before} is the gas abundance (molecule) before the UV irradiation, f_{in} is the flux of inflow controlled with the mass flow controller (molecule s^{-1}), v_{out} is the pumping efficiency of the rotary pump (s^{-1}). In the above equation, we assumed that the pumping speed is a first order function of the gas abundance, i.e. $v_{\text{out}} \times n$ (molecule s^{-1}). Since the observable variable about the flux of inflow, $f_{\text{in,obs}}$, has a unit of (cm^3 s^{-1}), f_{in} is calculated with $f_{\text{in,obs}}$ and the ideal gas law,

$$f_{\text{in}} = f_{\text{in,obs}} \frac{n_{\text{before}}}{V_{\text{before}}} = f_{\text{in,obs}} \frac{p_{\text{before}}}{RT} \qquad (1.8)$$

where V_{before} is an effective volume (cm^3), p_{before} is the pressure of reactant gas (Pa), R is the gas constant (1.381×10^{-17} cm^3 Pa K^{-1} $molecule^{-1}$) and T is the temperature (K). After and during the UV irradiation, the gas abundance in the reaction cell reaches another steady state,

$$\frac{dn_{\text{after}}}{dt} = f_{\text{in}} - v_{\text{out}} n_{\text{after}} - q\sigma I n_{\text{after}} = 0$$
$$n_{\text{after}} = \frac{f_{\text{in}}}{v_{\text{out}} + q\sigma I} \qquad (1.9)$$

where n_{after} is the gas abundance (molecule) during the UV irradiation, q is the quantum yield (molecule photon^{-1}), σ is the absorption cross section of reactant gas (cm^2 molecule^{-1}) and I is the actinic flux to be estimated (photon cm^{-2} s^{-1}). By substituting (1.7) to (1.9), we can eliminate v_{out} from the equation and obtain the following equation about the actinic flux:

$$I = \frac{f_{\text{in}}}{q\sigma}\left(\frac{1}{n_{\text{after}}} - \frac{1}{n_{\text{before}}}\right) \qquad (1.10)$$

In the equations from (1.7) to (1.10), the gas abundances, n_{before} and n_{after}, do not mean the whole gas abundances in the reaction cell, because the equation (1.9) does not hold everywhere in the reaction cell. In the reaction cell, vigorous photochemical reactions occur in a region near the UV lamp. Thus the equation (1.9) holds only within the effective region. We consider that the effective region has a cross sectional area S (cm^2) and a length d (cm) measured from the end that connects to the hydrogen/helium lamp.

$$V_{\text{eff}} = d \times S \qquad (1.11)$$

where V_{eff} is the volume of the effective region where the above equations hold. Meanwhile, the optical depth τ in the reaction cell is calculated as follows,

$$\tau = \sigma \frac{n}{V_{\text{eff}}} d \qquad (1.12)$$

We assumed that the length of the effective region corresponds to one optical depth ($\tau = 1$). Thus, d can be calculated as follows,

$$d = \frac{V_{\text{eff}}}{\sigma n} = \frac{RT}{\sigma p_{\text{eff}}} \qquad (1.13)$$

where p_{eff} is the pressure in the effective region. For 1.0 torr of N_2O gas, d is about 2 cm at a wavelength at the Lyman-α line (The length of the reaction cell is 26 cm). By substituting (1.13) to (1.11), V_{eff} is calculated as follows,

$$V_{\text{eff}} = \frac{RTS}{\sigma p_{\text{eff}}} \qquad (1.14)$$

With the equation (1.14), the gas abundances in the effective region are calculated as follows,

$$\begin{aligned} n_{\text{before}} &= \frac{p_{\text{before}} V_{\text{eff}}}{RT} = \frac{p_{\text{before}} S}{\sigma p_{\text{eff}}} \\ n_{\text{after}} &= \frac{p_{\text{after}} V_{\text{eff}}}{RT} = \frac{p_{\text{after}} S}{\sigma p_{\text{eff}}} \end{aligned} \qquad (1.15)$$

where p_{before} and p_{after} are the partial pressures of the reactant gas before and during the UV irradiation, respectively. Those partial pressures are measured with the QMS in the downstream of the reaction cell (Figure 1.1). By substituting (1.8) and (1.15) into (1.10) and assuming p_{eff} is p_{before}, the actinic flux is calculated only with observable variables:

$$I = \frac{f_{\text{in,obs}} p_{\text{before}}^2}{qSRT} \left(\frac{1}{p_{\text{after}}} - \frac{1}{p_{\text{before}}} \right) \qquad (1.16)$$

It is noted here that the actinic flux calculated by (1.16) does not explicitly depend on the absorption cross sections of the reactant gases if the cross sections of the reactant gases have the same cut-off wavelength. This is because we assumed that the effective region has a length corresponding to one optical depth. The larger the absorption cross section of the reactant gas has, the shorter the optical depth becomes and vice versa. If the cross sections of the reactant gases have different cut-off wavelengths, the actinic flux calculated would change. For example, if a molecule A can absorb UV flux at a wider wavelength region than a different molecule B, the actinic flux calculated with the molecule A would be larger than that by molecule B.

The absorption cross sections of N_2O measured by the previous studies (Hitchcock et al. (1980), Chan et al. (1994), Selwyn et al. (1977), Hubrich and Stuhl (1980) and Nicolet and Peetermans (1972)) are shown in Figure 1.4. The N_2O molecule is sensitive for Lyman-α emission since the absorption cross section above 140 nm is negligible. The previous studies agree that the photochemistry of N_2O using Lyman-α radiation can be explained by the following reactions (Groth and Schierholz, 1959; Hampson and Okabe, 1970; Gilpin and Welge, 1971; McEwan et al., 1974; Okabe, 1967)

$$N_2O + h\nu \rightarrow N_2 + O$$

$$N_2O + h\nu \rightarrow NO + N$$

$$O + N_2O \rightarrow N_2 + O_2$$

$$O + N_2O \rightarrow 2NO$$

$$\text{(net) } 6N_2O + 4h\nu \rightarrow 3N_2 + 2N + O_2 + 4NO$$

which results in an overall quantum yield of 0.67 photons/N_2O (decomposed by both the photolysis and subsequent reactions).

Carbon dioxide is photolyzed by UV under 205 nm. The absorption cross section of CO_2 is shown in Figure 1.3.

$$CO_2 + h\nu \rightarrow CO + O$$

The O atom produced is in the ground state, $O(^3P)$, at wavelengths longer than 167 nm, but at wavelengths shorter than 167 nm, the atom could be excited state $O(^1D)$. The excited oxygen atom is, however, quickly quenched to the ground state by collisions with background gases. The reaction between CO and $O(^3P)$ is very slow, since it is spin-forbidden (Yung and DeMore, 1999).

$$CO + O(^3P) \rightarrow CO_2$$

The reaction between CO_2 and $O(^3P)$ is also extremely slow (reaction rate constant at room temperature is about 10^{-50} cm^3 $molecule^{-1}$ s^{-1} based on Tsang and Hampson, 1986).

$$CO_2 + O(^3P) \rightarrow CO + O_2$$

Thus, without any other radicals like OH and CH_2, CO_2 would be destroyed by only ultraviolet irradiation. Accordingly, we estimated the overall quantum yield of CO_2 photolysis to be 1 photons/CO_2.

The flux of the inflow is controlled with the mass flow controller. The flow flux depends on the size of molecule. We calibrated the mass flow controller using N_2O gas and a graduated cylinder. The result is shown in Figure 1.5. N_2O gas (purity 99.9%, Suzuki Shokan Co., Ltd.) or CO_2 gas (purity 99.999%, Taiyo Nippon Sanso

Corporation) were introduced into the reaction cell and irradiated by the hydrogen/helium UV lamp we used. Time evolutions of the QMS signal at m/z = 44 for N_2O or CO_2 gases were measured before and during the UV irradiations. Figure 1.7 shows a typical example of the time evolution of the QMS signal at m/z = 44 for a run using 0.59 torr of N_2O gas with 1.2 [mL min^{-1}] of influx. In this experiment, the hydrogen/helium UV lamp was discharged with a power of 90 W at 13.56 MHz for the RF generator. The background signal at m/z = 44 was 10^{-11} (a.u.). The actinic flux is calculated to be $1.77 \times 10^{14} \pm 6.2 \times 10^{11}$ [photon cm^{-2} s^{-1}]. We performed actinometry with power from 20 W to 120 W. The pressures of N_2O and CO_2 gases in the reaction cell range 1.0 – 6.5 torr. All of the experiments were performed at room temperature.

Figure 1.8 shows the results of actinometry using N_2O and CO_2 gases. At powers stronger than 60 W, the actinic fluxes are calculated to be 10^{14} [photon cm^{-2} s^{-1}], which is consistent with the results of a previous study (Westley et al., 1995). The actinic flux increases with an increase of the power discharged with the RF power source, however, the increase of actinic flux is not significant above 90 W. This may be due to the self-absorption effect of Lyman α (Holstein, 1947), because the Lyman α line is easily absorbed by the hydrogen atoms in the ground state and, with an increase of input power, more efficient dissociation of hydrogen molecules into hydrogen atoms is expected (Yamashita, 1975). Figure 1.8 also shows that there is no significant difference between the results by using N_2O and those by using CO_2 gas. This suggests that the UV spectra produced with our hydrogen/helium lamp is dominated by the Lyman α line, not by molecular emission lines around 160 nm. If a significant difference was observed, that would imply a significant amount of photons were originated from molecular emission lines around 160 nm, because CO_2 can absorb UV fluxes around 160 nm (Figure 1.3).

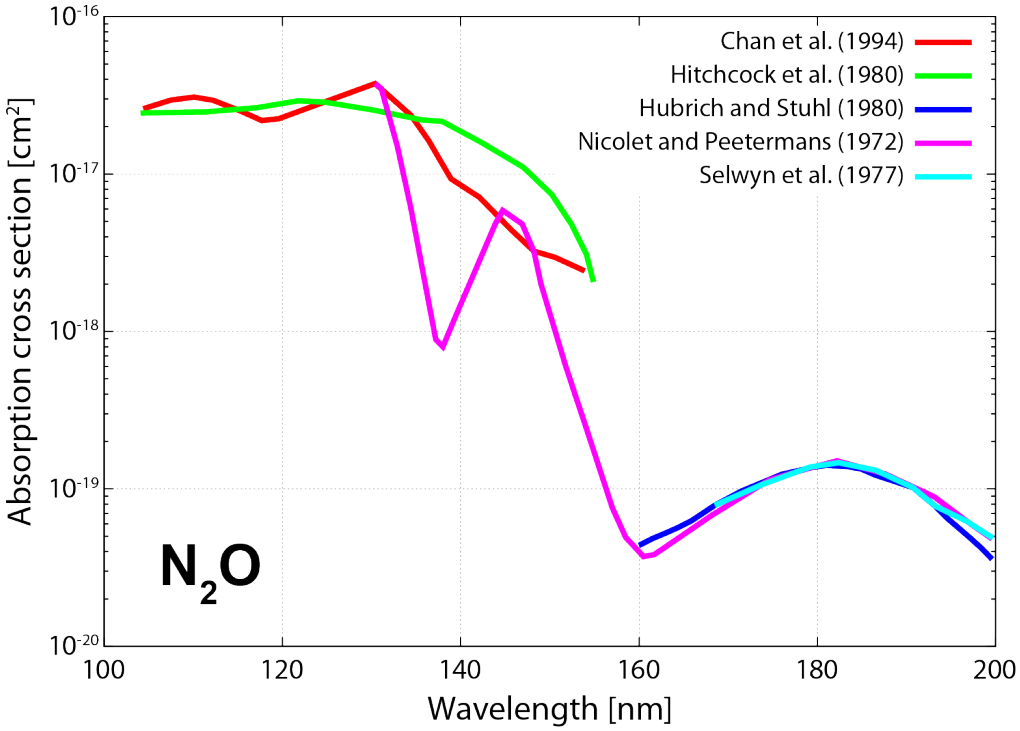

Figure 1.4. Absorption cross section of N_2O molecule after Rajappan et al. (2010). The data are from Hitchcock et al. (1980), Chan et al. (1994), Selwyn et al. (1977), Hubrich and Stuhl (1980) and Nicolet and Peetermans (1972).

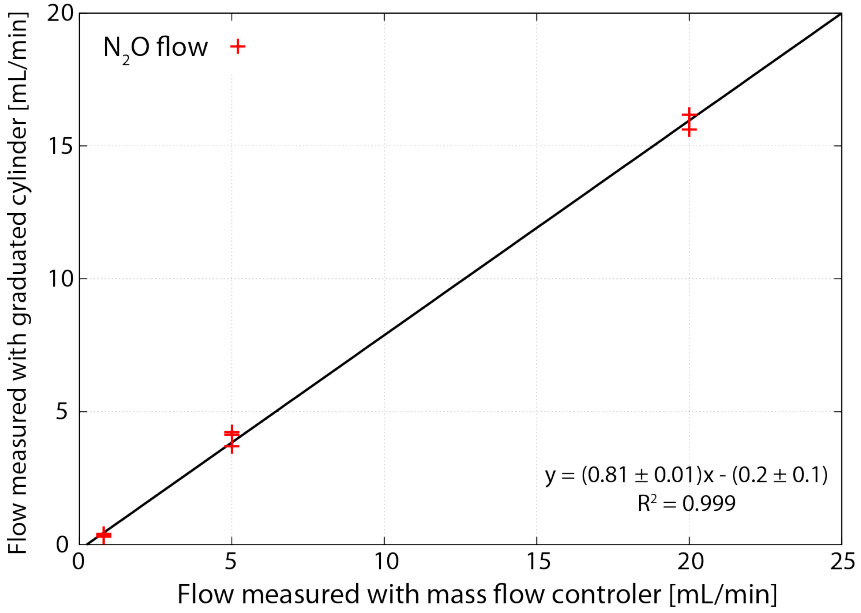

Figure 1.5. Calibration result of a mass flow controller using N_2O gas flow and a graduated cylinder.

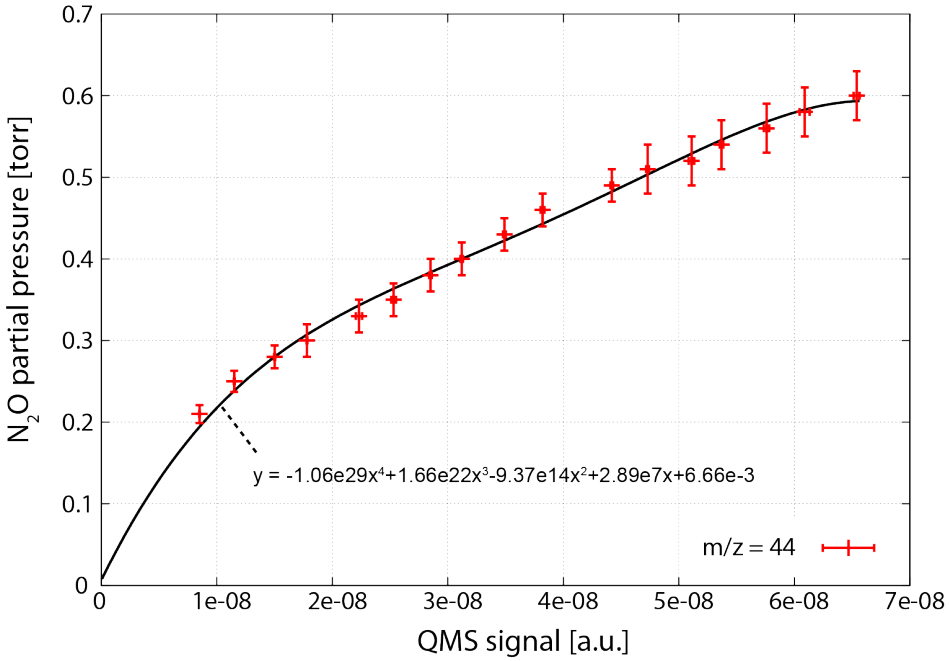

Figure 1.6. Calibration result of the QMS signal at m/z = 44 using N_2O gas. The background signal at m/z = 44 was 10^{-11} (a.u.). The N_2O partial pressure was measured with a thermocouple gauge and then calibrated using the calibration data shown in Figure 1.2 when the analysis.

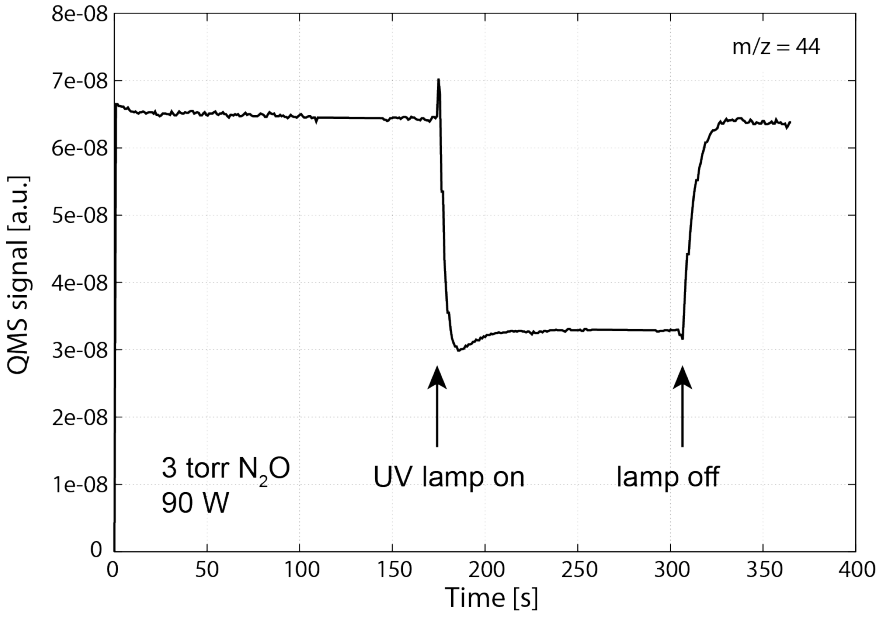

Figure 1.7. A typical example of the time evolution of QMS signal at m/z = 44 for 3 torr of N_2O gas. The H_2/He UV lamp was discharged with a power of 90 W at 13.56 MHz. The background signal at m/z = 44 was 10^{-11} (a.u.). This run yields $1.77 \times 10^{14} \pm 6.2 \times 10^{11}$ [photon cm^{-2} s^{-1}] of actinic flux.

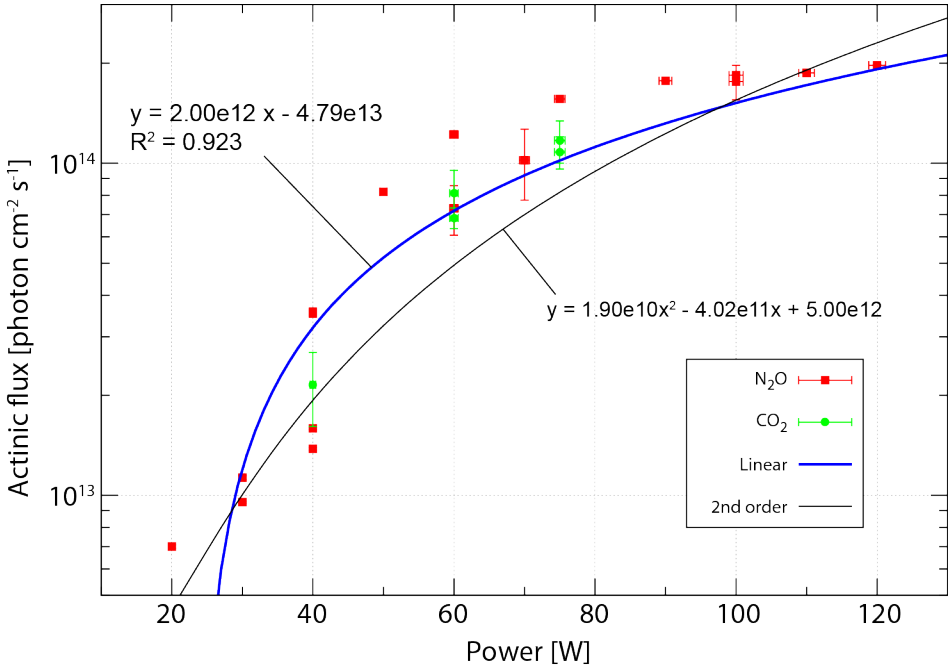

Figure 1.8. Results of the actinometry performed for the H_2/He UV lamp. The black and blue lines are the results of least squares fitting.

1.3.2 Organic aerosol production rates as a function of UV flux

With the relationship between the actinic flux and RF power obtained in Section 1.3.1, we measured the tholin production rates as a function of actinic UV fluxes. About 5 torr of CH_4 gas (purity 99.999%, Japan Fine Products Corporation) was introduced into the reaction cell through the mass flow controller with 1.5 [mL min^{-1}] of flow. Then we irradiated UV light with the hydrogen/helium lamp. After the irradiation of UV light, the MgF_2 window was removed from the quartz glass tube and analyzed with the spectroscopic ellipsometer. Because ellipsometry is nondestructive testing, the time evolution of thickness of tholin formed on the MgF_2 window can be measured as a function of reaction time. The tholin production rates were obtained from the slope of the time evolution of tholin thickness deposited on the MgF_2 window using spectroscopic ellipsometry (Azzam and Bashara, 1977).

Figure 1.12–Figure 1.16 show the typical results by ellipsometry and model results, while Figure 1.11 shows the measurement results for a MgF_2 window without organic film. The variables measured with the ellipsometer, *Is* and *Ic*, are described by the following equations:

$$Is = \sin(2\Psi)\sin(\Delta)$$

$$Ic = \sin(2\Psi)\cos(\Delta)$$

where Ψ is the amplitude ratio upon reflection between p and s components. These components are light polarized parallel and perpendicular to the plane of incidence, respectively (Azzam and Bashara, 1977). Δ is the phase difference upon reflection between p and s components. In the data analyses of ellipsometry, both thickness and optical property of each layer are free parameters and are varied in order to fit the observed *I*s and *I*c.

Figure 1.9 shows the physical parameter of the ellipsometer and a schematic diagram of the optical model for the data analysis. In the measurements, the incident angle of the beam is 66° ± 0.5°, wavelength of the beam varies from 425 nm to 1000 nm, and the diameter of the beam is 1 mm. We assumed a two-layer model for the data analysis of the results of ellipsometry (Figure 1.9), in which the produced tholin is composed of an upper thin, partially oxidized tholin layer and an lower un-oxidized tholin layer. This is because the surface of an organic thin film could be oxidized by oxygen when it is exposed to the air (Sciamman-O'Brien et al., 2010). However, since single-layer models without an upper oxidized layer show the thickness close to those obtained by the two-layer models, the influence of oxidation on the samples was small (within an uncertainty of 1%) for obtaining the formation rate of tholin. The complex refractive index of tholin used for the data analysis is shown in Figure 1.10. The complex refractive index of the oxidized layer is a mixture of that of amorphous carbon and air ($n = 1.000$, $k = 0$). The geometry of the organic film could be mountain-shaped rather than a layer with flat surface. Thus we measured the film thickness not only at the center of the MgF_2 window but also on several points 1 mm off from the center. Ellipsometry and the subsequent analysis showed, however, the geometry around the center of the window is almost flat, having only a few nanometers of roughness.

Figure 1.17 shows a typical result of the time evolutions of the tholin thickness as a function of irradiation time. The thickness increases linearly with the reaction time (e.g., see the results of RF power of 110 W, 90 W and 60 W). The results of 60 W of RF power show that once the tholin achieves a certain thickness, the growth would stop because the tholin blocks the UV right from the lamp, preventing further photochemical reactions in the reaction cell (Figure 1.17). As for the experiment with 75 W of RF power, we obtained only one datum of the tholin thickness. As the thicknesses at 90 W and 60 W of RF power show linear increases with the reaction time (Figure 1.17), we assumed that the time evolution of tholin thickness at 75 W would also be a linear function of time. As for the experiments with 40 W of power, the tholin

thicknesses in the reaction time of 20 and 25 minutes become similar. Thus, we consider that the tholin growth stopped between 10 and 20 minutes. We used only the data point at 10 minutes for the estimate of tholin production rate, assuming a linear growth with time.

Figure 1.18 shows the tholin production rate as a function of RF power. The tholin production rate shows a linear function of RF power. With the linear regression function obtained by actinometry (Figure 1.8), we are able to convert the RF power into actinic UV flux. Figure 1.19 shows that the tholin production rate is a linear function of UV flux. These results strongly suggest that the mechanism II is responsible for the tholin formation (see the reactions, 1.3, 1.4, and 1.5). In the mechanism II, reactions between intermediate gas species lead to tholin products. In the next section, we will further investigate the intermediate species (i.e., parent molecules) that limit the formation of tholin. Our results also shows that *m* in the equation (1.6) is 1, indicating a lower production rate when extrapolating Titan's aerosol production rate to another planet under high UV irradiation conditions, such as early Earth (Trainer et al., 2006; Wolf and Toon, 2010). Applying the aerosol production rate of Titan (Toon et al., 1992) using the experimental result ($\beta \approx 1.5$, Trainer et al., 2006) in equation (1.6), the aerosol production rate in early Earth's atmosphere become 4×10^{-13} g cm^{-2} s^{-1}, or 1×10^{13} g year^{-1} with 0.001 of CH_4 molar fraction in the atmosphere and with 1.4×10^{12} photon cm^{-2} s^{-1} of solar UV flux. As discussed in Trainer et al. (2006), this estimate of organic aerosol flux on an early Earth is comparable to the current carbon burial rate due to biological processes (i.e., 5×10^{13} g year^{-1}) (Lasaga et al., 1985).

In the experiments, we measured the growth of tholin deposited on the MgF_2 window, and then applied to early Earth's atmosphere. Thus, we implicitly assumed that the tholin growth rate on the MgF_2 window is proportional to organic aerosol production rate. Although the aerosol production rate in planetary atmospheres could not be proportional to the growth of aerosols, by an analogy with cloud production process on Earth's atmosphere, we believe this assumption could be valid. In the terrestrial atmosphere, it is well known that cloud condensation nuclei greatly accelerate the growth of cloud particles (e.g., Pruppacher and Klett, 2010). Without the help of such condensation nuclei, the cloud particles are not able to grow into larger particles, or not able to produce cloud droplets. Since the same microphysical process could apply to aerosol production (Seinfeld and Pandis, 2006; Pruppacher and Klett, 2010), it is likely that Titan's aerosol production is governed by the surface growth of monomers. Therefore, we believe that the observation of the growth rate of tholin could actually correspond to the limiting process of aerosol production in Titan's atmosphere. The y-intercept of the linear regression line in Figure 1.19 is not zero, probably due to the poor fitting in low-power region in actinometry and the negative y-intercept of the linear regression line (Figure 1.8). Or the non-zero y-intercept in Figure 1.19 could mean the film growth rate is nonlinear in a low actinic flux region where $I < 3 \times$

10^{13} photon cm^{-2} s^{-1}. Nevertheless, since a second-order or higher-order function cannot fit the experimental results, the film growth rate should be at least a first-order or lower-order function of actinic flux.

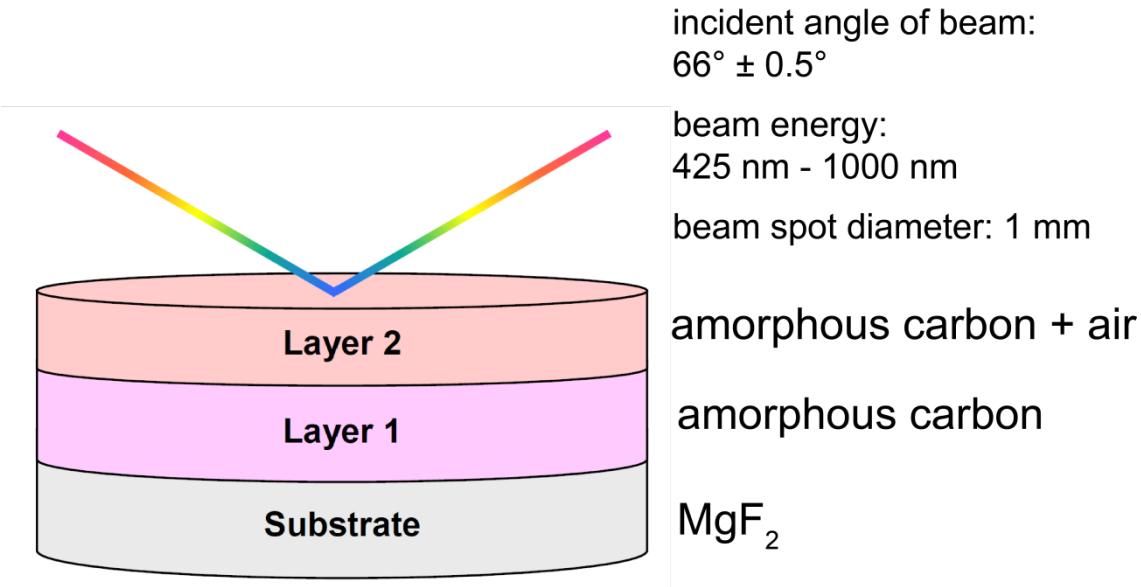

Figure 1.9. Physical parameters of the ellipsometer and a schematic diagram of two-layer model for the data analysis.

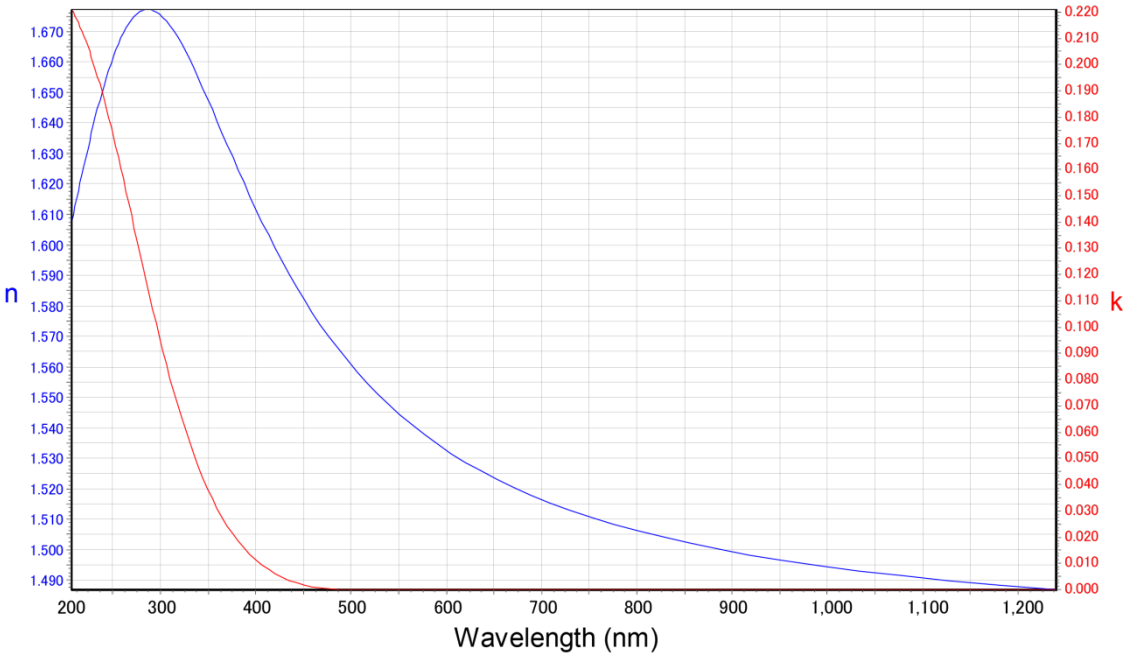

Figure 1.10. Complex refractive index of amorphous carbon used for the data analysis.

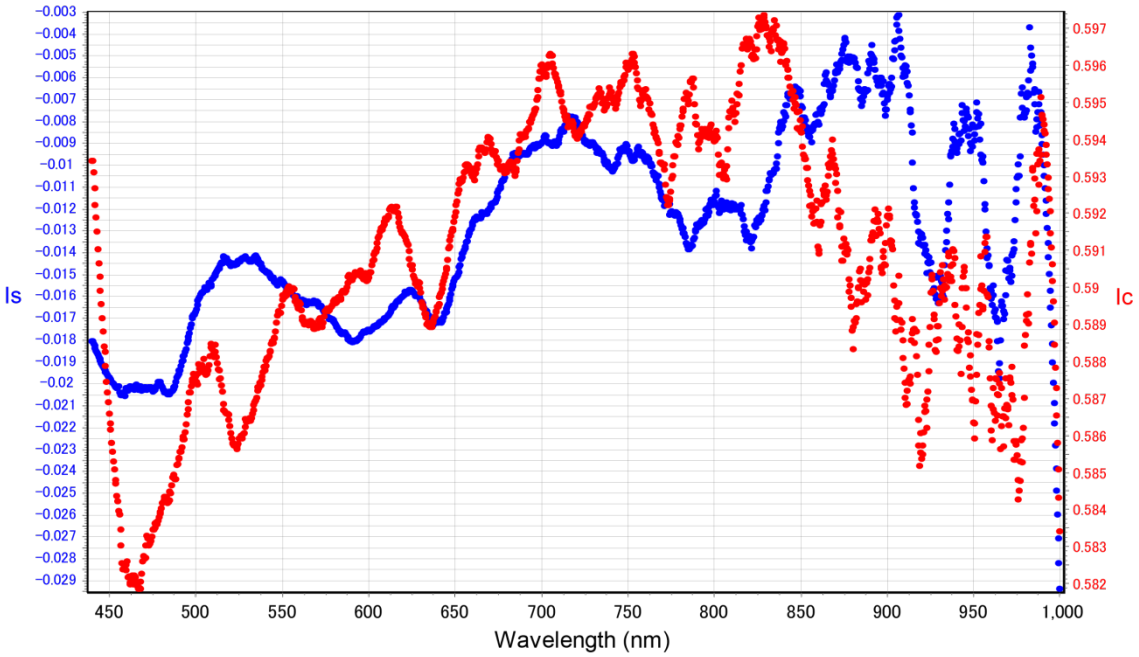

Figure 1.11. Measurement results of ellipsometry for a MgF_2 window with no organic film.

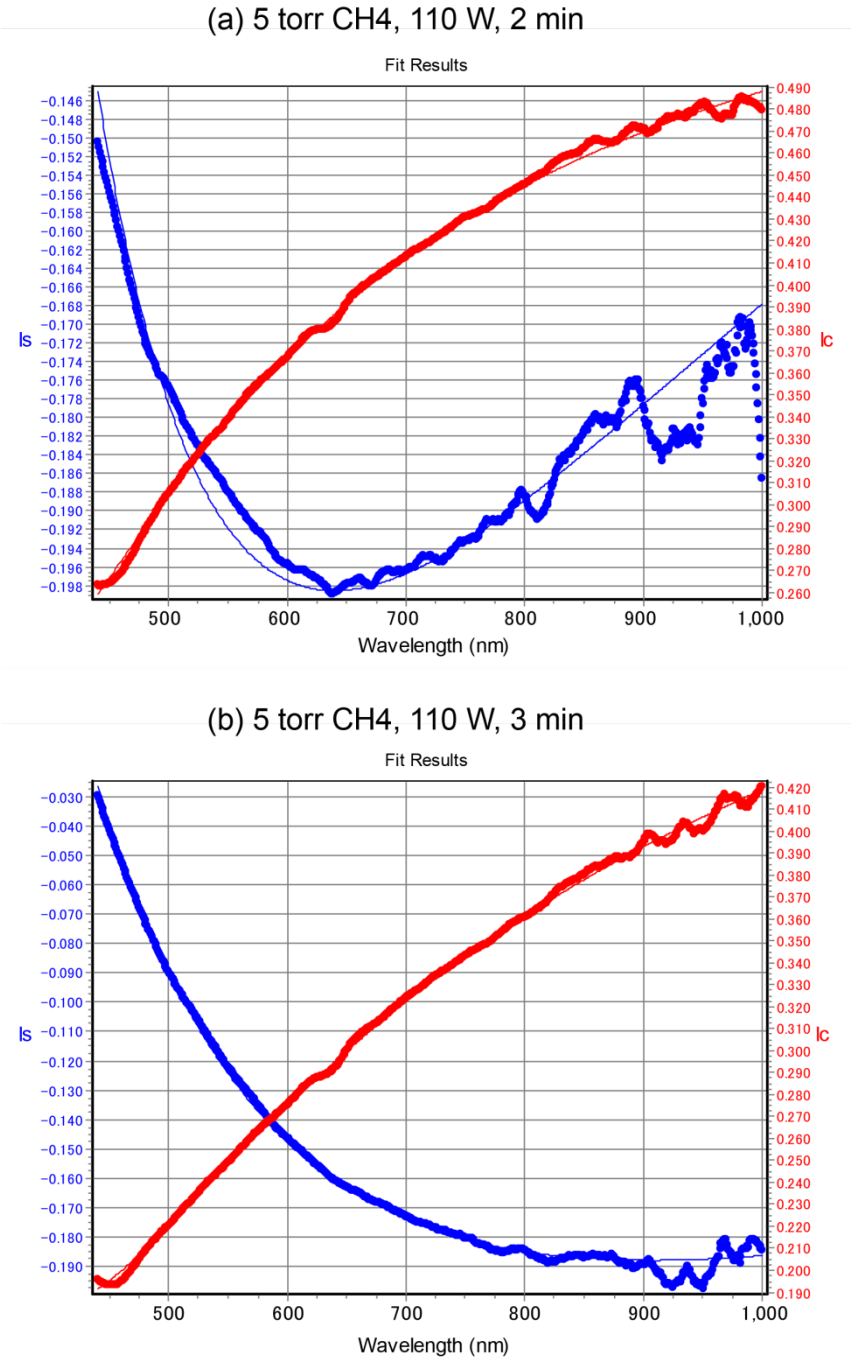

Figure 1.12. Measurement results of ellipsometry (thick lines) and model results (thin lines) of the sample produced in 5 torr of CH_4 and with a power of 110 W. (a) Results after 2 minutes of total irradiation time. Film thickness is 39.0 ± 0.3 nm and $\chi^2 = 0.057$. (b) Results after 3 minutes of total irradiation time. Film thickness is 64.1 ± 0.2 nm and $\chi^2 = 0.039$.

(a) 5 torr CH4, 90 W, 10 min

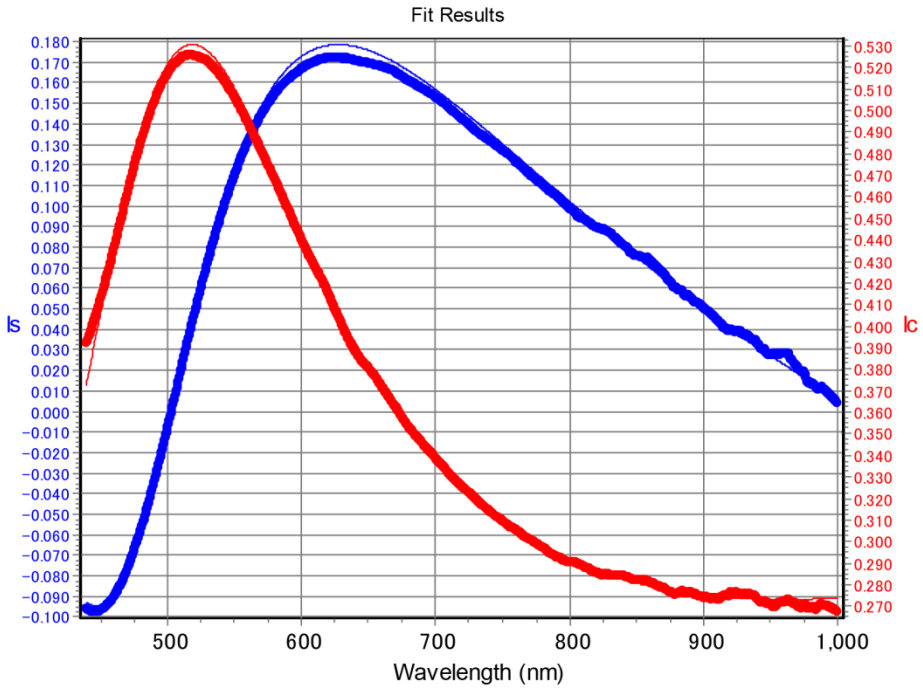

(b) 5 torr CH4, 90 W, 20 min

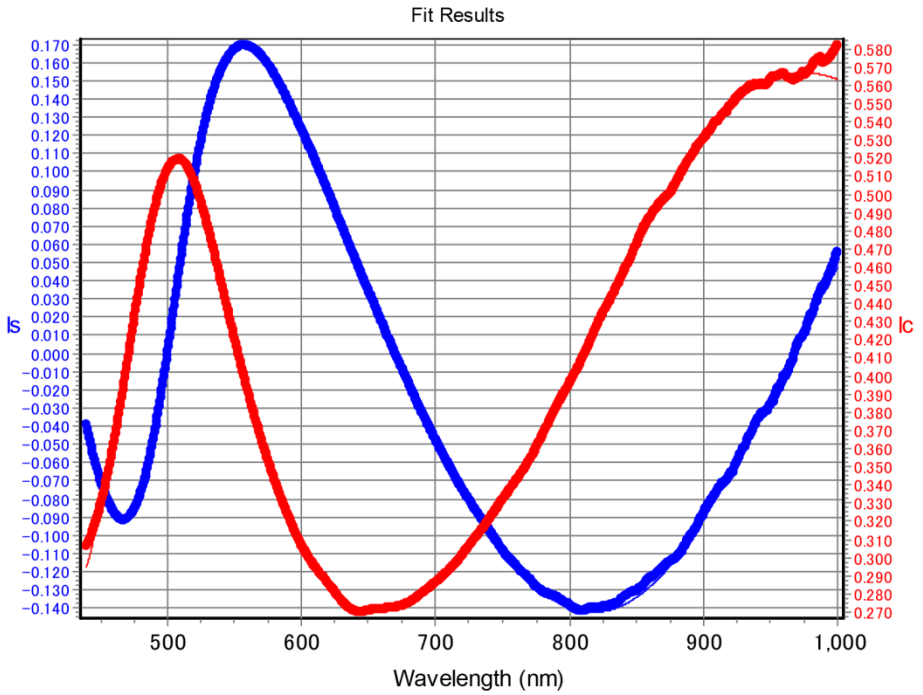

Figure 1.13. – *Continuted.*

(c) 5 torr CH4, 90 W, 30 min

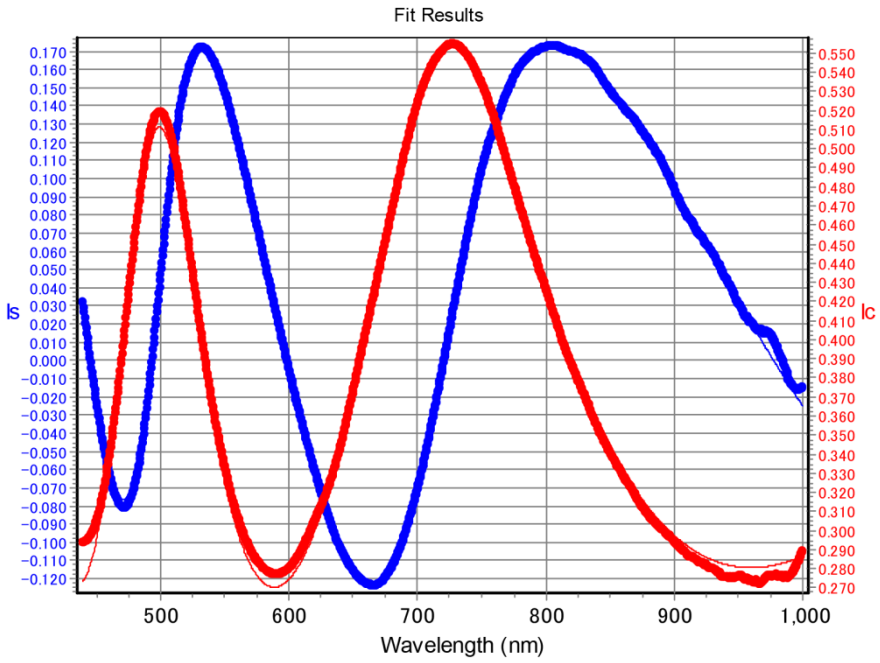

(d) 5 torr CH4, 90 W, 40 min

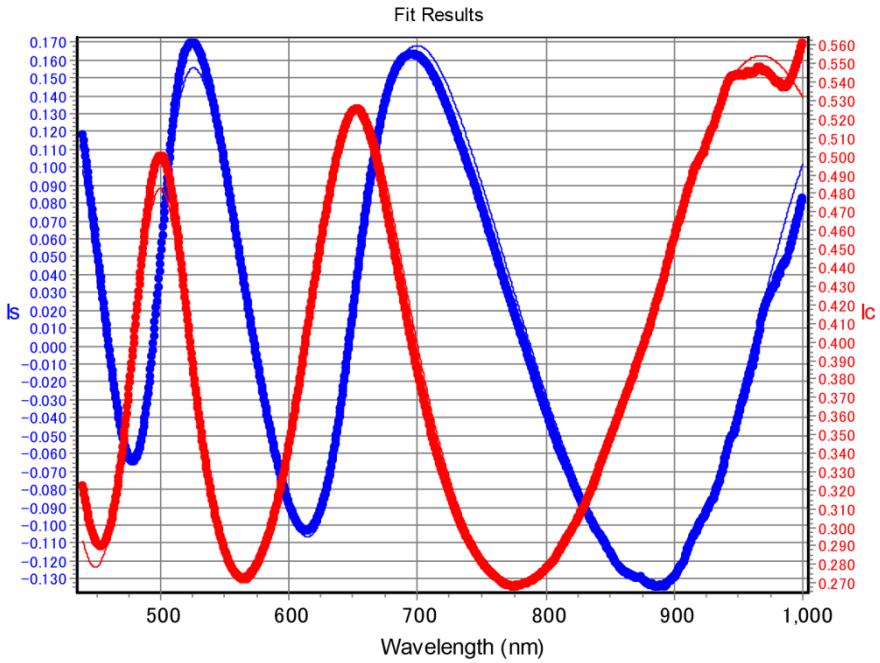

Figure 1.13. – *Continuted.*

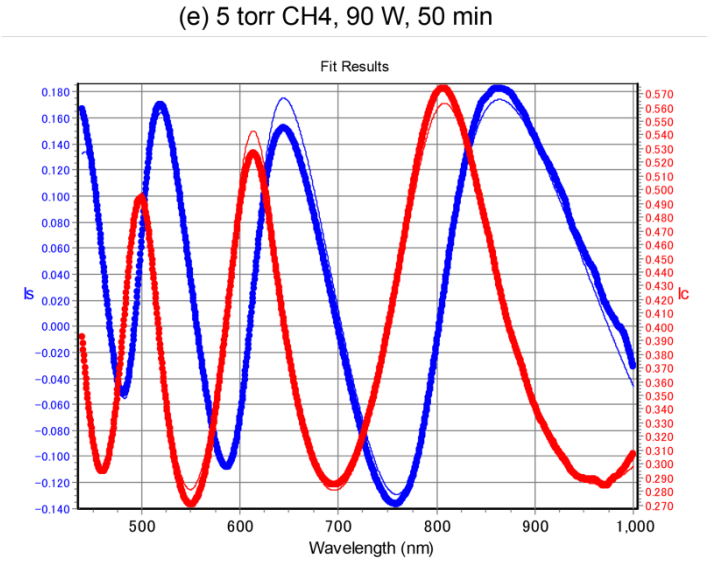

Figure 1.13. Measurement results of ellipsometry (thick lines) and model results (thin lines) of the sample produced in 5 torr of CH_4 and with a power of 90 W. (a) Results after 10 minutes of total irradiation time. Film thickness is 186.8 ± 0.07 nm and $\chi^2 = 0.085$. (b) Results after 20 minutes of total irradiation time. Film thickness is 375.3 ± 0.1 nm and $\chi^2 = 0.059$. (c) Results after 30 minutes of total irradiation time. Film thickness is 557.7 ± 0.2 nm and $\chi^2 = 0.16$. (d) Results after 40 minutes of total irradiation time. Film thickness is 736.5 ± 0.4 nm and $\chi^2 = 0.53$. (e) Results after 50 minutes of total irradiation time. Film thickness is 937.1 ± 0.5 nm and $\chi^2 = 0.75$.

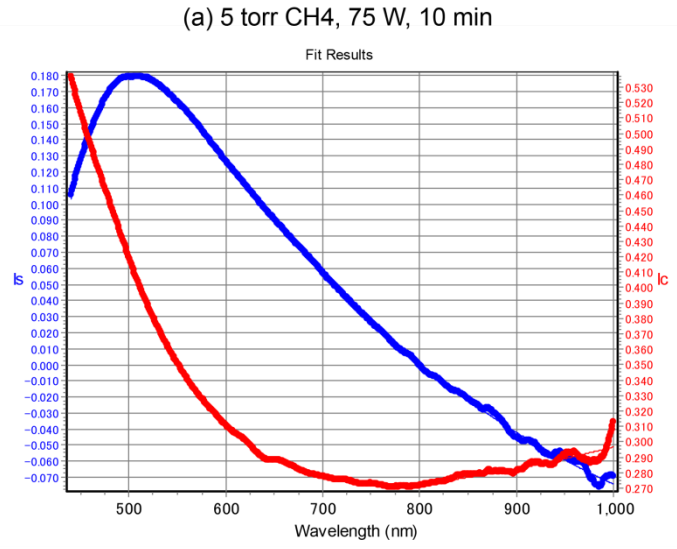

Figure 1.14. Measurement results of ellipsometry (thick lines) and model results (thin lines) of the sample produced in 5 torr of CH_4 and with a power of 75 W. Results are obtained after 10 minutes of total irradiation time. Film thickness is 153.5 ± 0.07 nm and $\chi^2 = 0.027$.

(a) 5 torr CH4, 60 W, 10 min

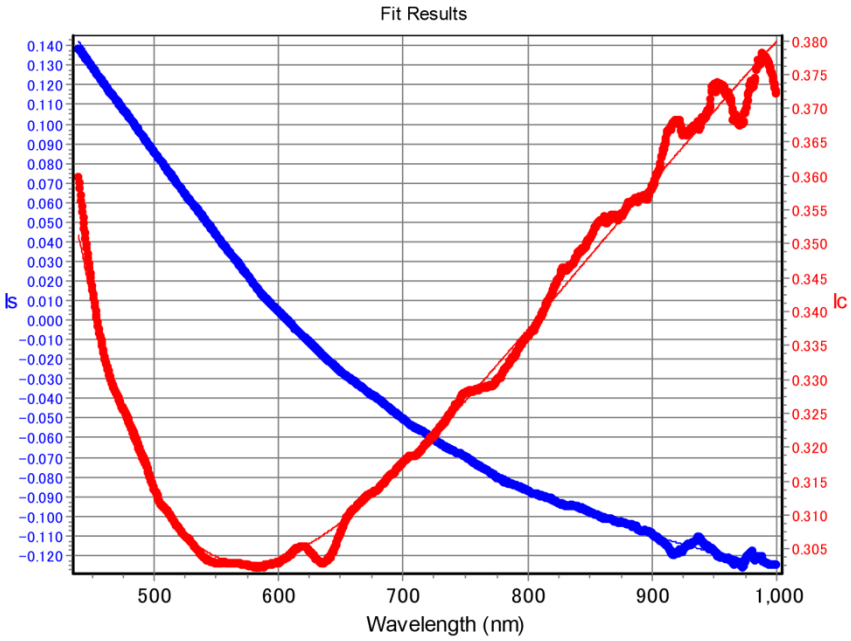

(b) 5 torr CH4, 60 W, 20 min

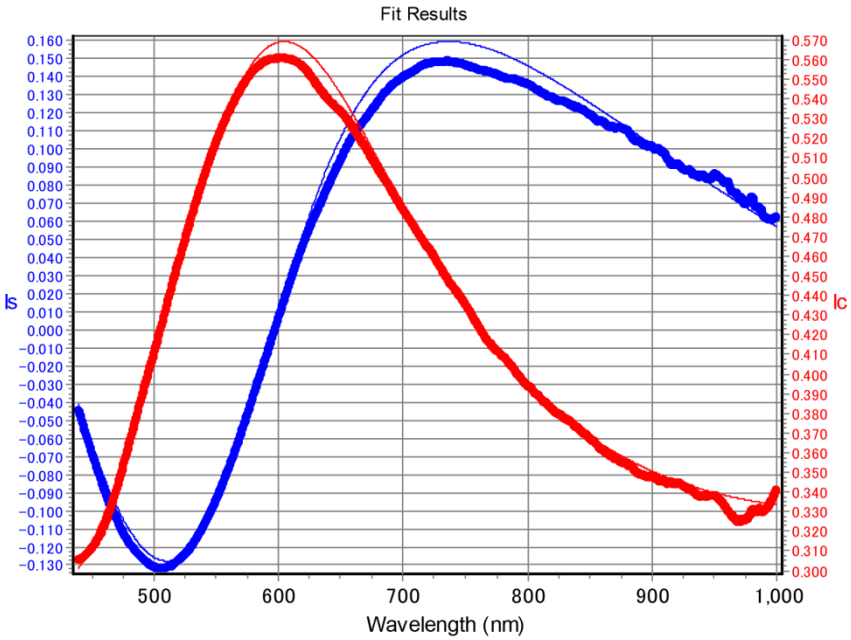

Figure 1.15. – *Continuted*.

(c) 5 torr CH4, 60 W, 30 min

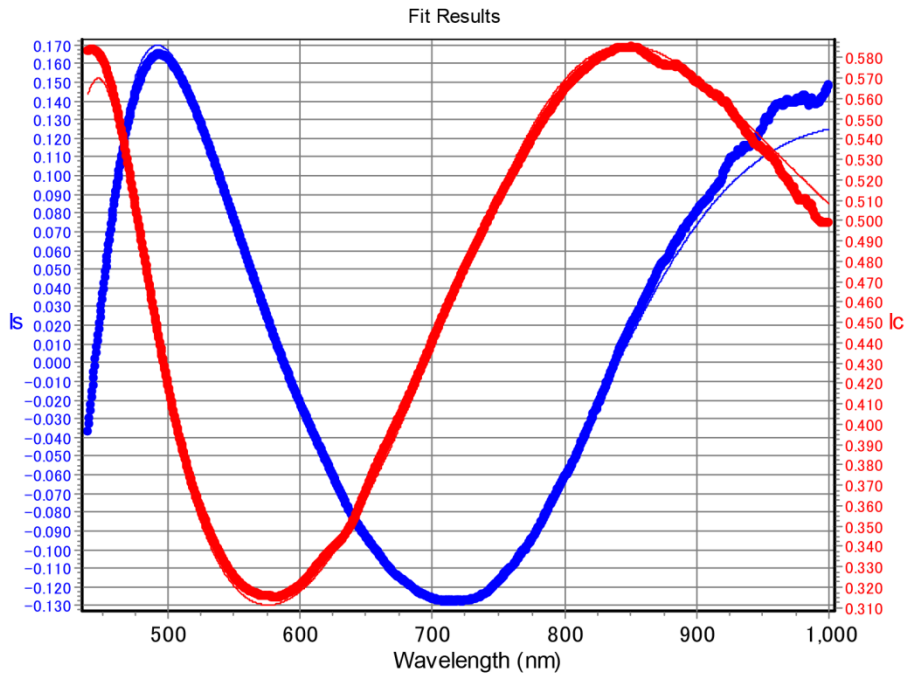

(d) 5 torr CH4, 60 W, 40 min

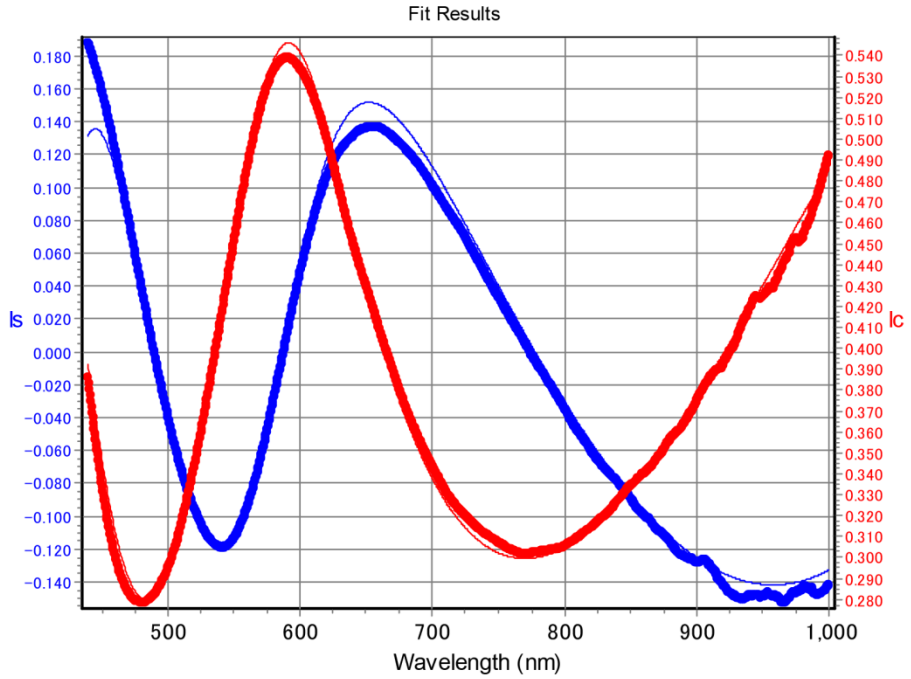

Figure 1.15. – *Continuted*.

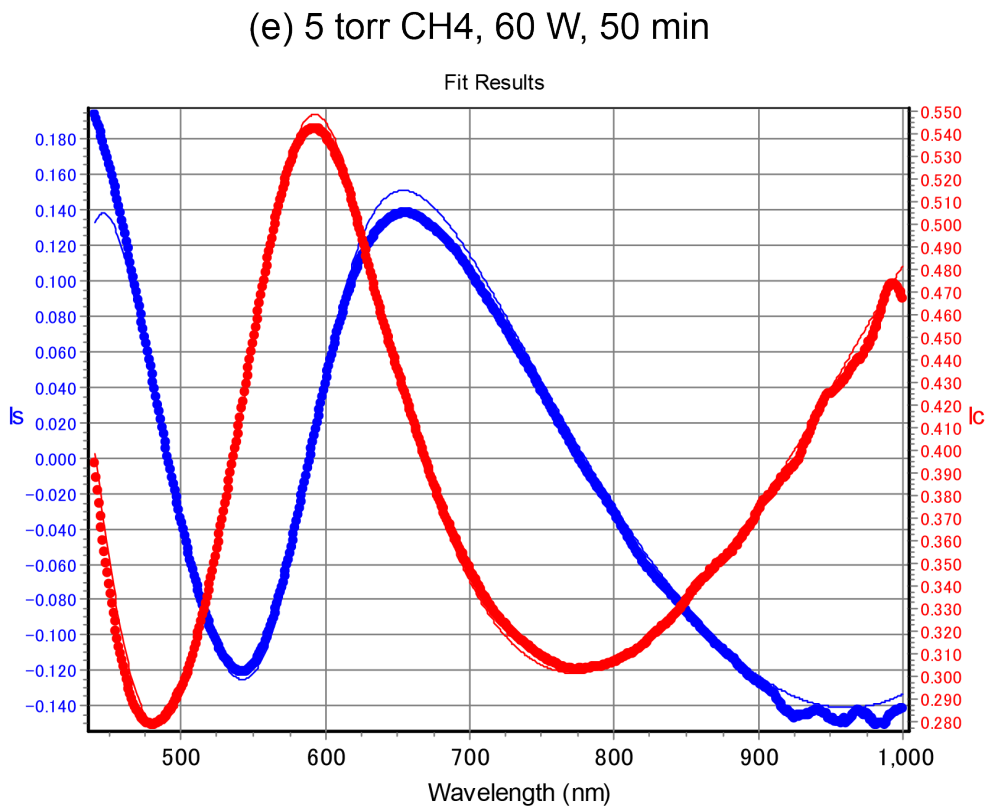

Figure 1.15. Measurement results of ellipsometry (thick lines) and model results (thin lines) of the sample produced in 5 torr of CH_4 and with a power of 60 W. (a) Results after 10 minutes of total irradiation time. Film thickness is 118.7 ± 0.08 nm and $\chi^2 = 0.33$. (b) Results after 20 minutes of total irradiation time. Film thickness is 232.5 ± 0.1 nm and $\chi^2 = 0.33$. (c) Results after 30 minutes of total irradiation time. Film thickness is 348.0 ± 0.3 nm and $\chi^2 = 0.36$. (d) Results after 40 minutes of total irradiation time. Film thickness is 451.7 ± 0.2 nm and $\chi^2 = 0.40$. (e) Results after 50 minutes of total irradiation time. Film thickness is 453.8 ± 0.3 nm and $\chi^2 = 0.38$.

(a) 5 torr CH4, 40 W, 10 min

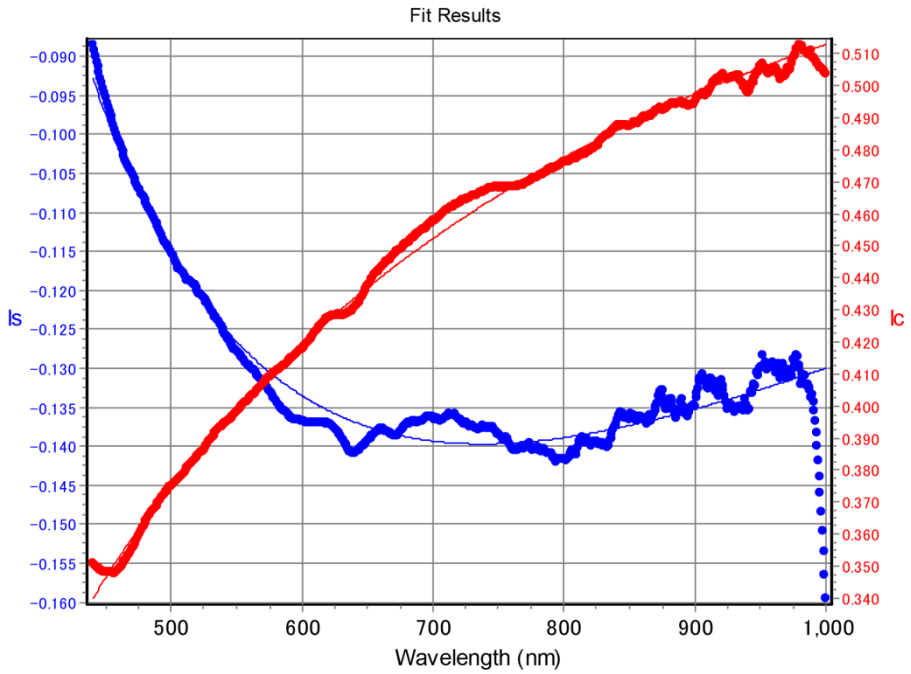

(b) 5 torr CH4, 40 W, 20 min

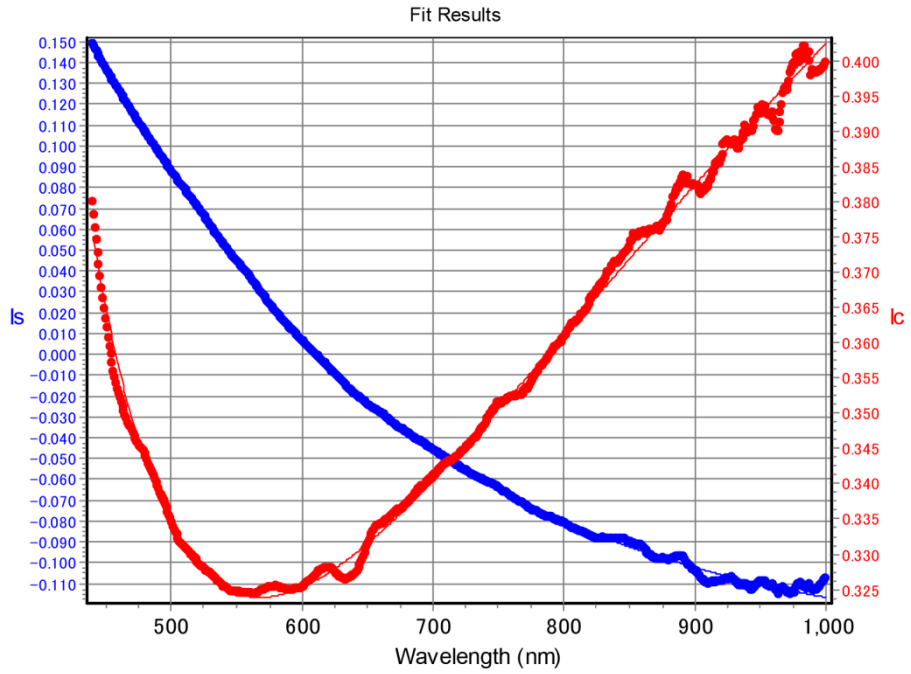

Figure 1.16. – *Continuted*.

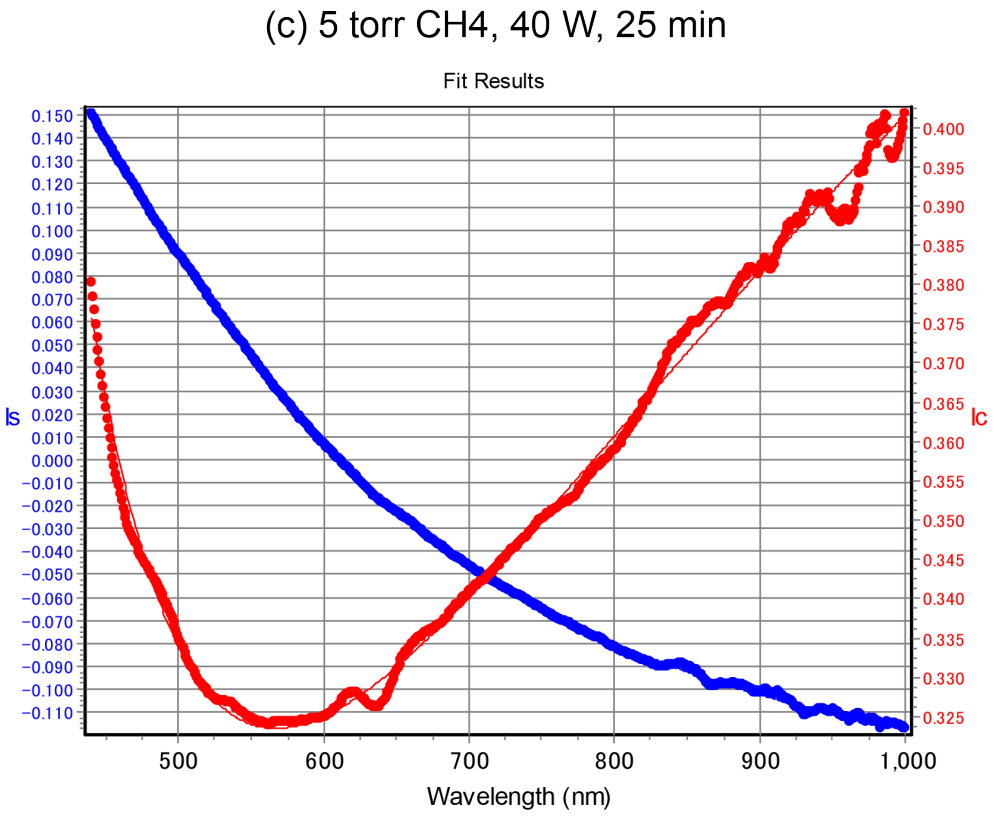

Figure 1.16. Measurement results of ellipsometry (thick lines) and model results (thin lines) of the sample produced in 5 torr of CH_4 and with a power of 40 W. (a) Results after 10 minutes of total irradiation time. Film thickness is 88.8 ± 0.5 nm and $\chi^2 = 0.062$. (b) Results after 20 minutes of total irradiation time. Film thickness is 120.7 ± 0.1 nm and $\chi^2 = 0.018$. (c) Results after 25 minutes of total irradiation time. Film thickness is 119.4 ± 0.2 nm and $\chi^2 = 0.016$.

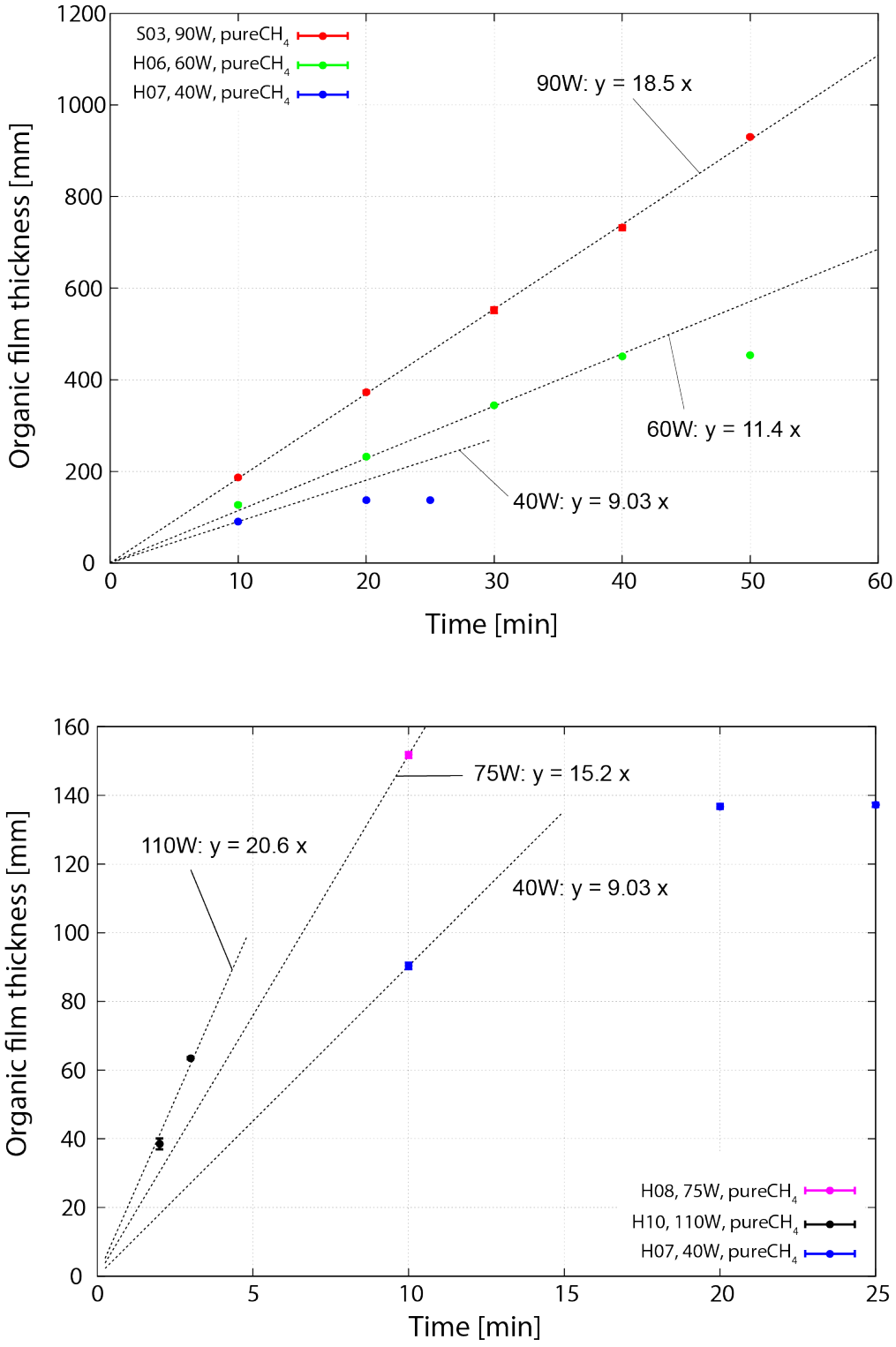

Figure 1.17. Time evolutions of organic film thickness measured with the spectroscopic ellipsometer.

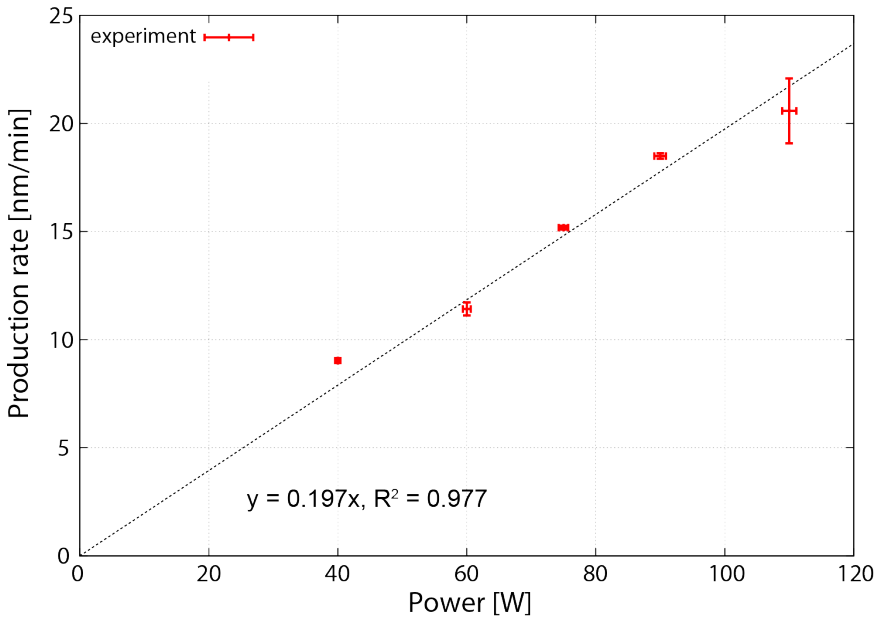

Figure 1.18. Aerosol production rate with different power. Production rates were measured as the time evolutions of organic film thickness. Also shown is a linear regression line.

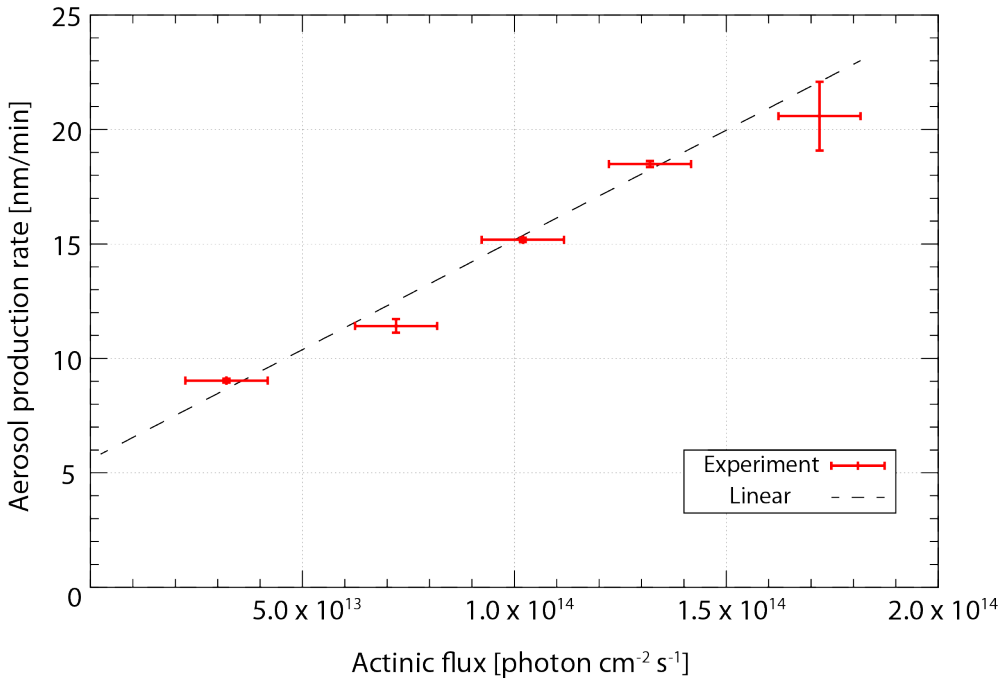

Figure 1.19. Aerosol production rate with different actinic flux. The actinic fluxes were derived from the linear regression function shown in Figure 1.8. Also shown is a linear regression line ($y = 9.6\times10^{-14}\,x + 5.6$, $R^2 = 9.87$).

1.3.3 Organic aerosol production rate as a function of CH_4/CO_2 ratio

We measured the tholin production rates for different initial CH_4/CO_2 gas ratios in the reaction cell, in order to put a constraint on the limiting reactions for particle formation in CH_4-CO_2-containing atmospheres, such as early Earth (e.g., Pavlov et al., 2001; Haqq-Misra et al., 2008). CH_4 gas (purity 99.999%, Japan Fine Products Corporation) and CO_2 gas (purity 99.999%, Taiyo Nippon Sanso Corporation) were introduced through the mass flow controllers into the reaction cell (Fig. 2.1). We performed experiments, varying the initial CH_4/CO_2 gas ratio in the reaction cell from 0.4 to 9. The reactant gas was irradiated with the hydrogen/helium lamp with a RF power of 90 W at 13.56 MHz. The time evolutions of the produced tholin thickness were directly measured with the spectroscopic ellipsometer. A part of the reactant and/or product gases were introduced to the QMS, and their mass spectra were measured.

Figure 1.20 – Figure 1.22 show typical results by ellipsometry and model results. For the experiments with $CH_4/CO_2 = 9$, 2.6 and 1.9, we used the same optical model described in Section 1.3.2 for the data analysis (i.e., two layers model). The time evolutions of tholin thickness for the experimental runs with $CH_4/CO_2 = 9$, 2.6 and 1.9 are shown in from Figure 1.25 to Figure 1.27. The results of time variations in tholin thickness are well fitted with second-order functions passing through the origin of the coordinate axes (Figure 1.25 to Figure 1.27). We interpreted the slopes of the regression lines at $t = 0$ as aerosol production rates, as the UV flux from the lamp would be attenuated due to a growth of tholin on the MgF_2 window. The results of ellipsometry for the experiments of $CH_4/CO_2 = 1$ and 0.4 are shown in Figure 1.23 and Figure 1.24, respectively. These figures show that the tholins produced at low CH_4/CO_2 ratio have distinct spectra from those formed in the experiments with high CH_4/CO_2 ratios ($CH_4/CO_2 = 9$, 2.6, 1.9). This is probably due to the thin film thickness and/or change of the complex refractive index of organic film. For the optical models of the experiments with low CH_4/CO_2 ratios ($CH_4/CO_2 = 1$, 0.4), we inserted a thin void layer between the MgF_2 substrate and the amorphous carbon layer to account for a backside reflection. This modification improves the model fitting significantly; however, there still remain large errors in terms of the measurement of film thickness. Thus, we estimated the upper and lower limits of the growth rate as follows. In the experiments at $CH_4/CO_2 = 1$, the time evolution of tholin thickness can be fitted using a second-order function. Because we could not significantly detect tholin at 60 and 240 minutes of irradiation time, we put a film thickness of 50 nm as upper limits at $t = 60$ and 240 minutes. The upper limit is based on the tholin thickness (about 50 nm) observed at 420 and 660 minutes of irradiation time. Because the tholin thicknesses were not be significantly different

between 420 and 660 minutes of irradiation time, the tholin growth would stop before 420 minutes of irradiation time. Thus we obtained an upper limit (0.83 nm min^{-1}) for the film growth rate, assuming that the film thickness increased linearly to 50 nm until $t = 60$ minutes. In the experiments at $CH_4/CO_2 = 0.4$, the time evolution of tholin thicknesses can be fitted using a second-order function. We consider the slope of the regression line at 0 minutes of irradiation time as an upper estimate for the growth rate. This upper estimate is almost identical when we assumed that the tholin thickness increased linearly to 210 nm until 1500 minutes of irradiation time (Figure 1.29). The lower estimate of the film growth rate was obtained by assuming that the film thickness increased linearly to 60 nm until $t = 1500$ minutes (Figure 1.29).

Figure 1.30 shows the aerosol production rates as a function of initial CH_4/CO_2 gas. Also shown are the results of Sasamori (2012), who performed the tholin formation experiments with the same hydrogen/helium lamp as the present study, and of Trainer et al. (2006), who performed the experiments using a deuterium lamp and 600 torr of gas mixtures of 0.1% of CH_4 and 0.02–0.5% of CO_2 balanced with N_2. The tholin production rates obtained by these three studies are normalized to the results of the experiment using only CH_4 as C-bearing reactant gas, i.e., the results of this study and Sasamori (2012) are normalized using the production rate obtained with 1 torr of CH_4 gas described in the section 1.3.2, while those of Trainer et al. (2006) are normalized using the production rate obtained with 600 torr of N_2 including 0.1% of CH_4. Sasamori (2012) measured the film thickness only once for each sample at the termination of the experiments so that they did not have to expose the sample to the air multiple times. However, they did not measure the tholin thickness as a function of irradiation time. They obtained the tholin production rate by calibration of the irradiation time by using time evolution of UV flux at 300 nm measured with a UV/VIS spectrometer.

Our results are consistent with the results of Sasamori (2012). The results of the present study and Sasamori (2012) show the aerosol production rate decreases monotonically with a decrease of CH_4/CO_2 ratio for the CH_4/CO_2 ratio below 1. This behavior is consistent with previous experiments using an electric discharge (Trainer et al., 2004). On the other hand, the results of Trainer et al. (2006) are different with the results of the present study. They observed the optimum production rate around unity of the CH_4/CO_2 ratio, and the production rate at $CH_4/CO_2 < 1$ seems to be higher than those of the present study. They suggested that their high aerosol production rate may be caused by incorporation of aldehydes and/or carboxylic acids into aerosol particles (Trainer et al., 2006), based on their mass spectra measurement of aerosol particles. They observed peaks at $m/z = 30$ and 44 in the mass spectra obtained from chemical analysis of aerosol particles, which could be interpolated as oxygenated fragments CH_2O^+ and COO^+. The primary differences between the present study and Trainer et al. (2006) are the total pressure of the reactant gases (This study: 5 torr, Trainer: 600 torr) and the type of spectra of UV lamps (i.e., the present study used a hydrogen/helium

lamp, whereas Trainer et al. used a deuterium lamp). The difference of the total pressure could change the chemical network for the production of hydrocarbons, because the rate coefficients of three-body reactions become greater at higher pressures. On the other hand, difference in the type of UV spectra of the lamps could affect the photolysis rates of reactant gas species, i.e., CH_4 and CO_2. We will investigate this discrepancy in the Section 1.4 by performing chemical network analysis using a one-box photochemical model.

Applying the experimental results using the equation (1.6) along with ($\beta \approx 0.03$), we obtain the aerosol production rate as 8×10^{-15} g cm^{-2} s^{-1}, or 8×10^{11} g year^{-1} on an early Earth with 0.001 of CH_4 molar fraction in the atmosphere with 1.4×10^{12} photon cm^{-2} s^{-1} of solar UV flux. The estimated organic aerosol flux on an early Earth is significantly smaller than CH_4 loss rate ($\sim 4 \times 10^{13}$ g year^{-1}) calculated by a photochemical model (Pavlov et al., 2001), suggesting only a small fraction (i.e., ~ a few %) of CH_4 injected in to the atmosphere would be converted into aerosol particles. This is contrast to the conclusions obtained by Trainer et al. (2006), which would reflect the difference between the experimental methods and conditions.

(a) 5 torr CH_4/CO_2 = 9, 90 W, 60 min

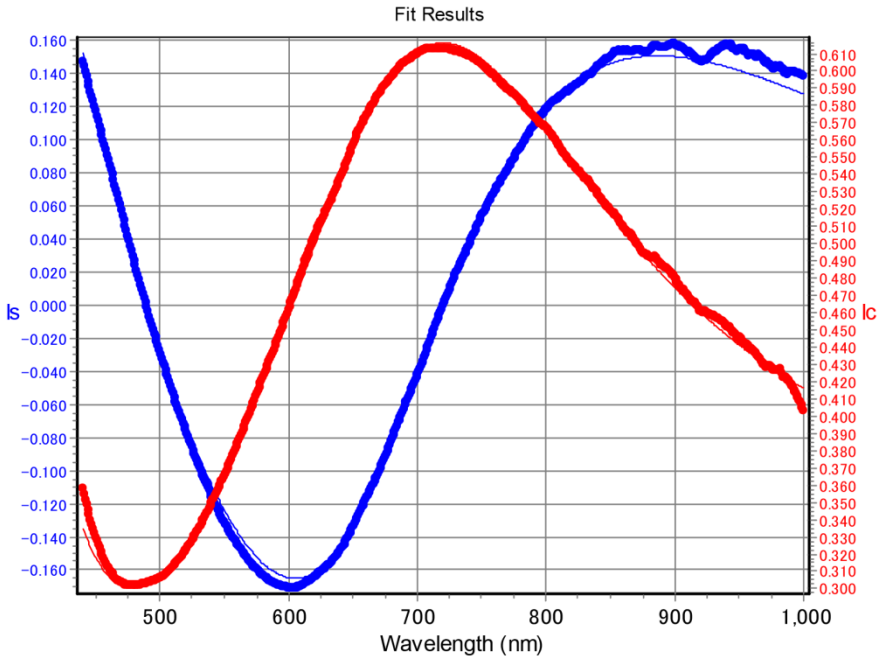

(b) 5 torr CH_4/CO_2 = 9, 90 W, 90 min

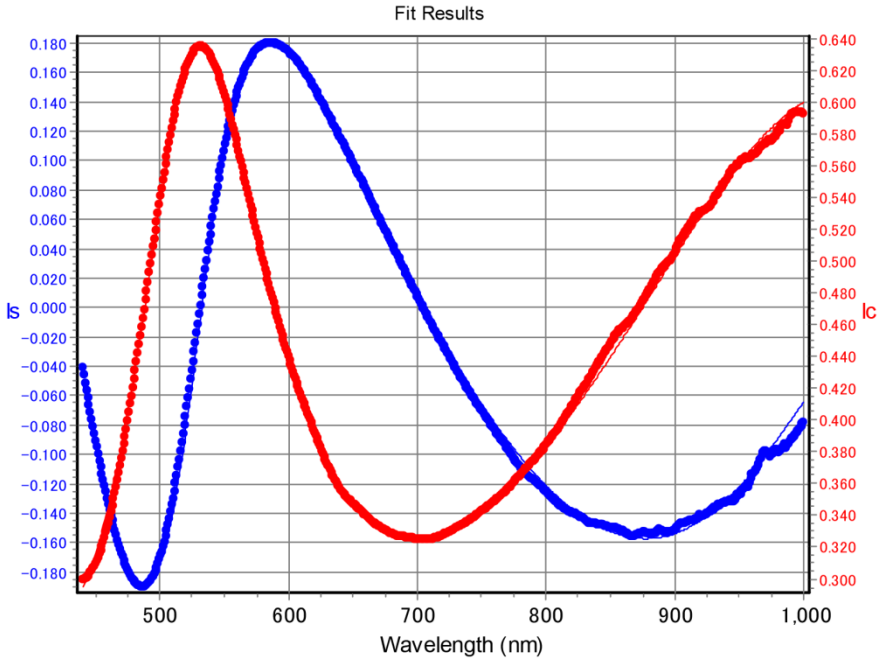

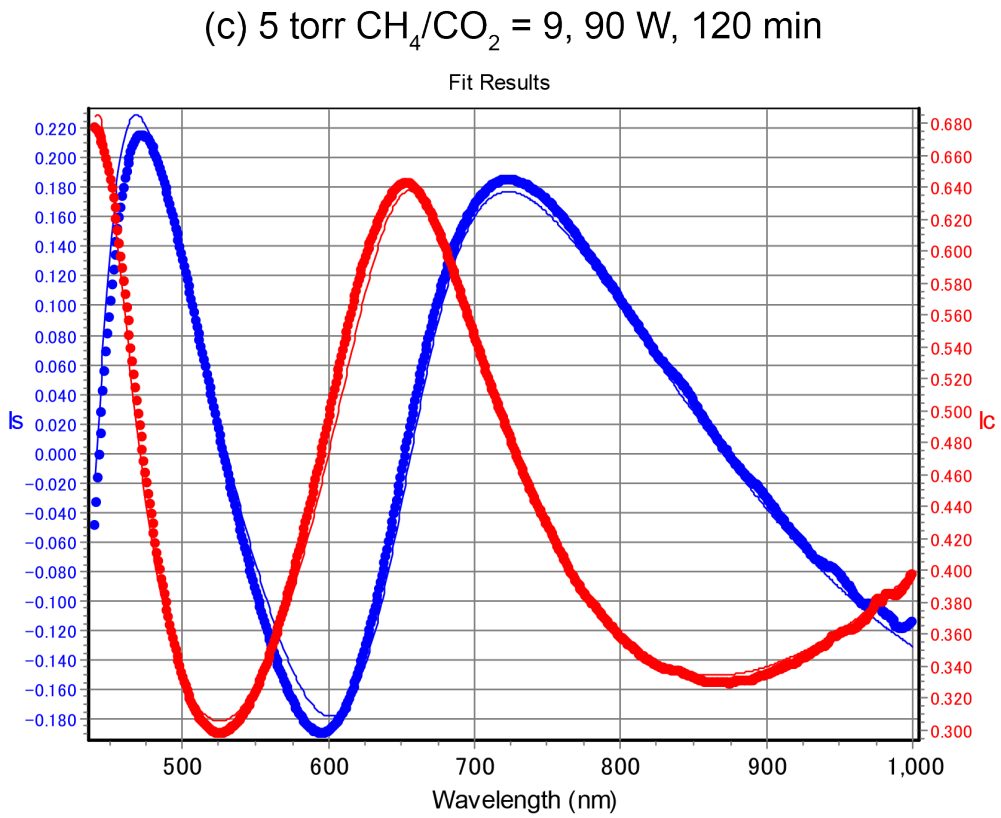

Figure 1.20. Measurement results of ellipsometry (thick lines) and model results (thin lines) of the sample produced in 5 torr of $CH_4/CO_2 = 9$ gas mixture and with a power of 90 W. (a) Results after 60 minutes of total irradiation time. Film thickness is 304.0 ± 0.2 nm and $\chi^2 = 0.17$. (b) Results after 90 minutes of total irradiation time. Film thickness is 437.6 ± 0.2 nm and $\chi^2 = 0.13$. (c) Results after 120 minutes of total irradiation time. Film thickness is 545.1 ± 0.4 nm and $\chi^2 = 0.80$.

(a) 5 torr CH_4/CO_2 = 2.6, 90 W, 60 min

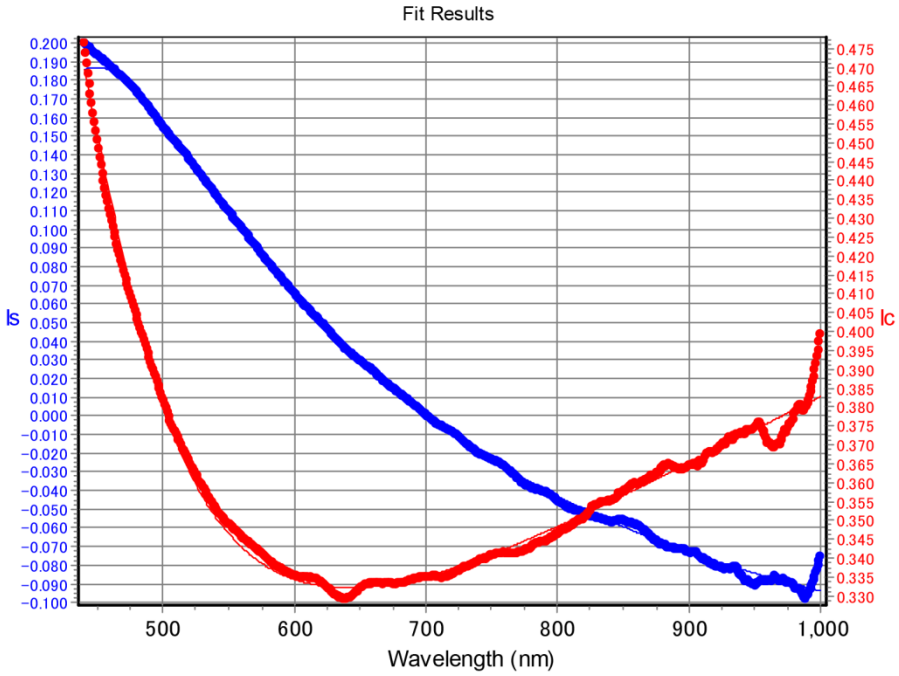

(b) 5 torr CH_4/CO_2 = 2.6, 90 W, 90 min

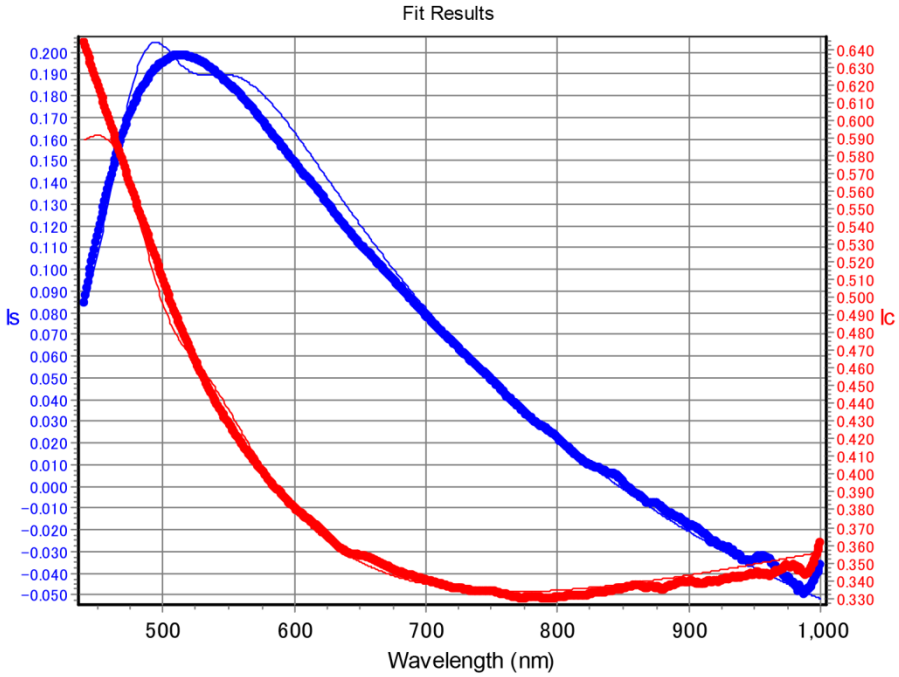

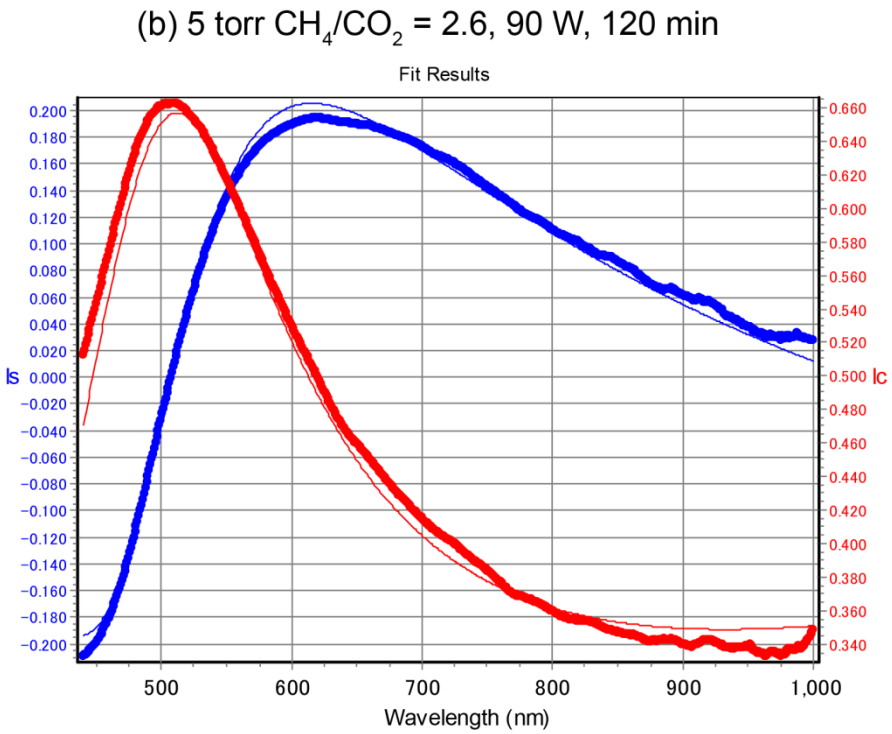

Figure 1.21. Measurement results of ellipsometry (thick lines) and model results (thin lines) of the sample produced in 5 torr of $CH_4/CO_2 = 2.6$ gas mixture and with a power of 90 W. (a) Results after 60 minutes of total irradiation time. Film thickness is 136.9 ± 0.3 nm and $\chi^2 = 0.047$. (b) Results after 90 minutes of total irradiation time. Film thickness is 166.0 ± 0.3 nm and $\chi^2 = 0.45$. (c) Results after 120 minutes of total irradiation time. Film thickness is 218.9 ± 0.3 nm and $\chi^2 = 0.75$.

(a) 5 torr CH_4/CO_2 = 1.9, 90 W, 60 min

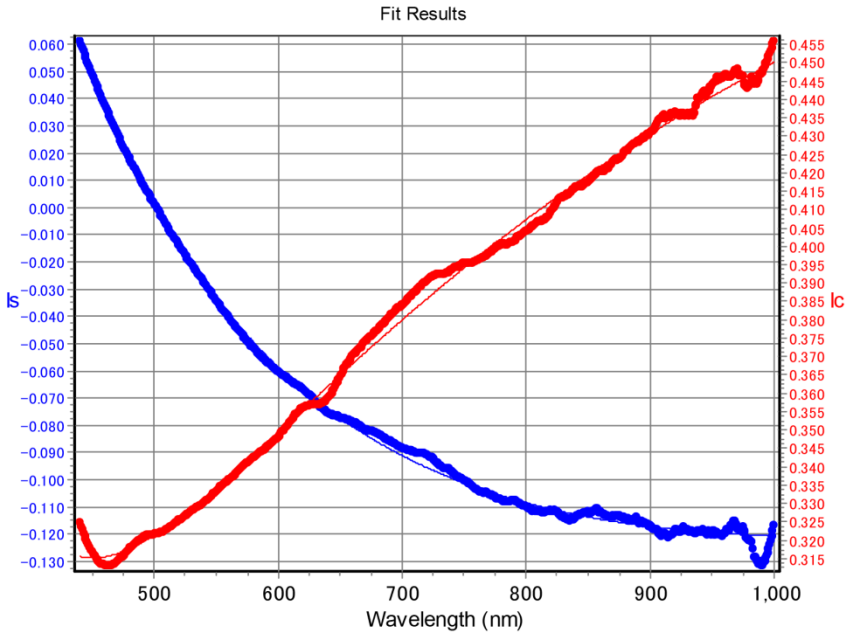

(b) 5 torr CH_4/CO_2 = 1.9, 90 W, 90 min

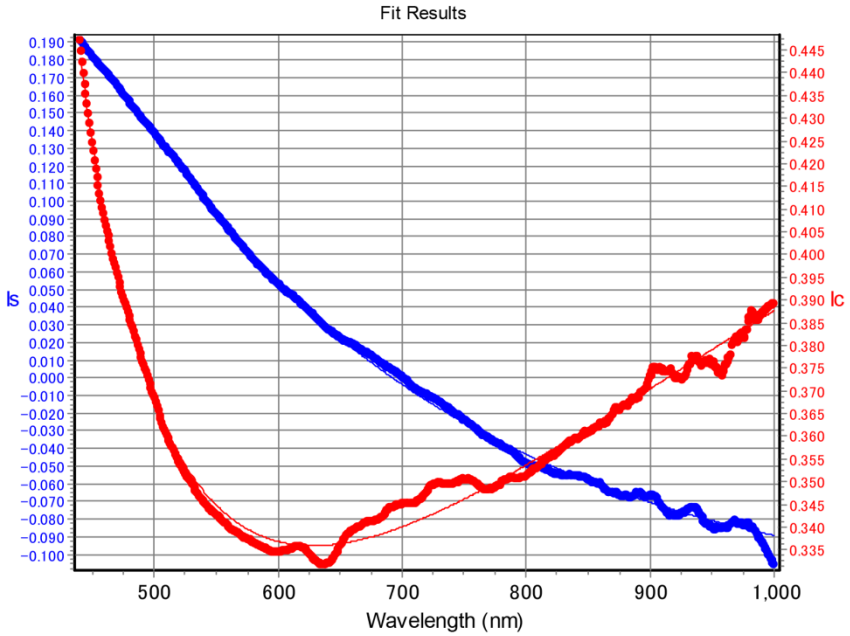

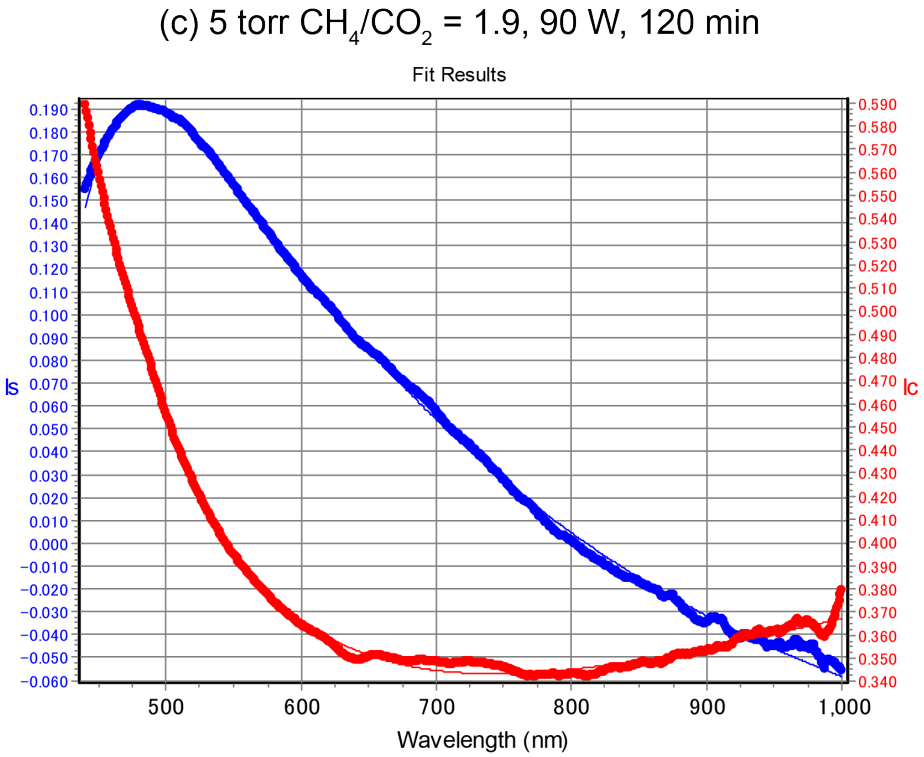

Figure 1.22. Measurement results of ellipsometry (thick lines) and model results (thin lines) of the sample produced in 5 torr of CH_4/CO_2 = 1.9 gas mixture and with a power of 90 W. (a) Results after 60 minutes of total irradiation time. Film thickness is 95.1 ± 3 nm and $\chi^2 = 0.038$. (b) Results after 90 minutes of total irradiation time. Film thickness is 136.9 ± 1.7 nm and $\chi^2 = 0.055$. (c) Results after 120 minutes of total irradiation time. Film thickness is 149.7 ± 2.5 nm and $\chi^2 = 0.049$.

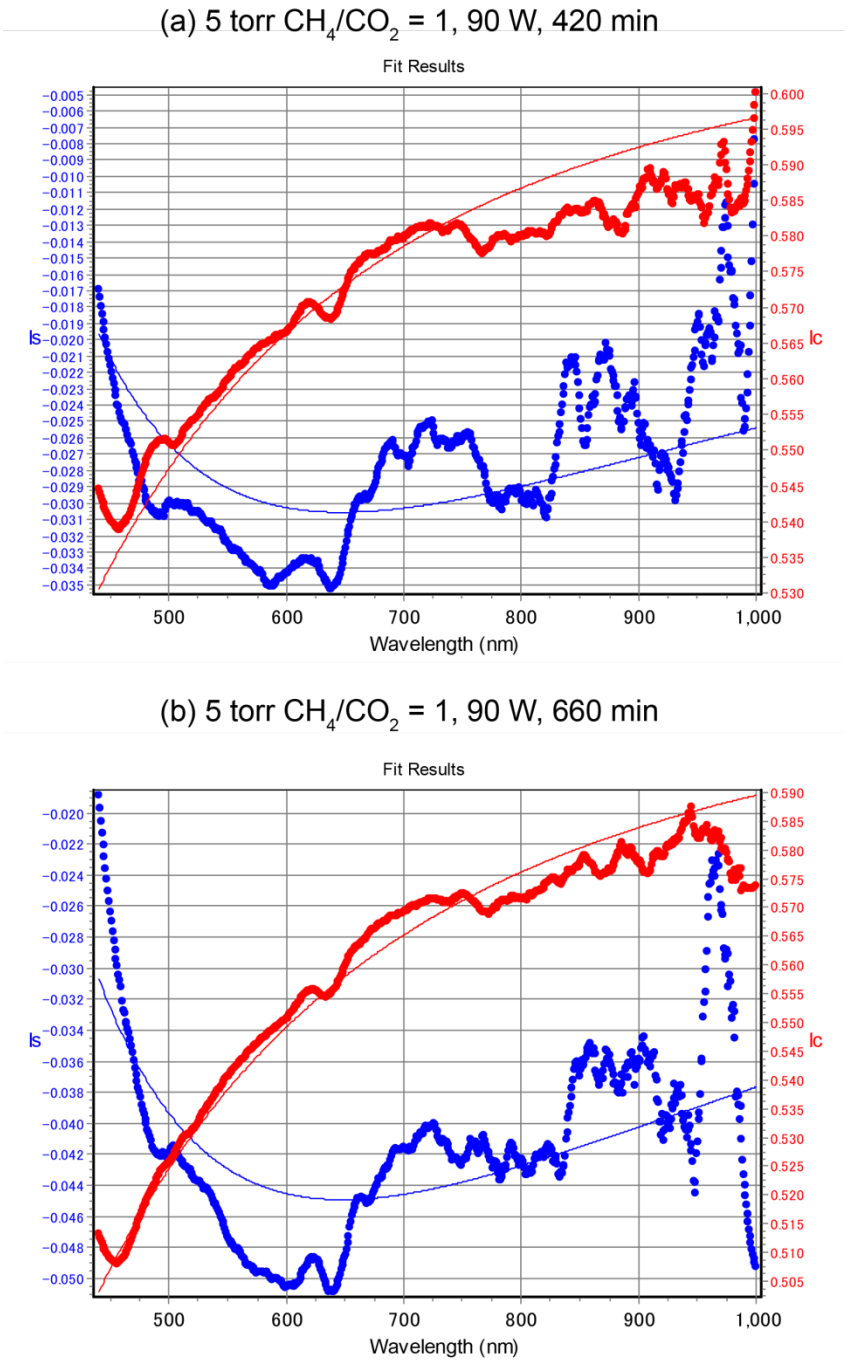

Figure 1.23. Measurement results of ellipsometry (thick lines) and model results (thin lines) of the sample produced in 5 torr of CH_4/CO_2 = 1 gas mixture and with a power of 90 W. (a) Results after 420 minutes of total irradiation time. Film thickness is 49.7 ± 21 nm and χ^2 = 0.25. (b) Results after 660 minutes of total irradiation time. Film thickness is 60.7 ± 16 nm and χ^2 = 0.21.

(a) 5 torr CH_4/CO_2 = 0.4, 90 W, 1500 min

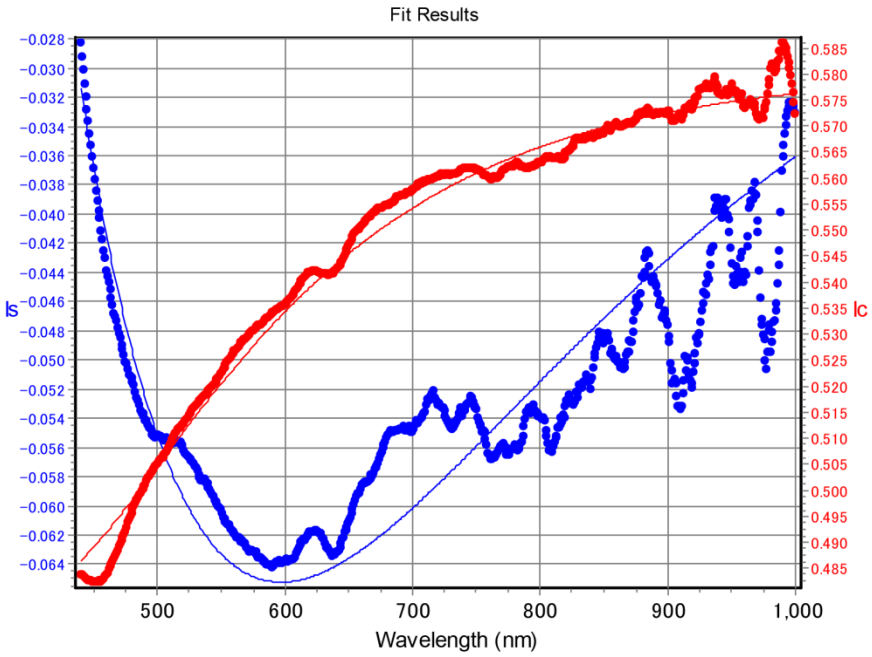

(b) 5 torr CH_4/CO_2 = 0.4, 90 W, 2451 min

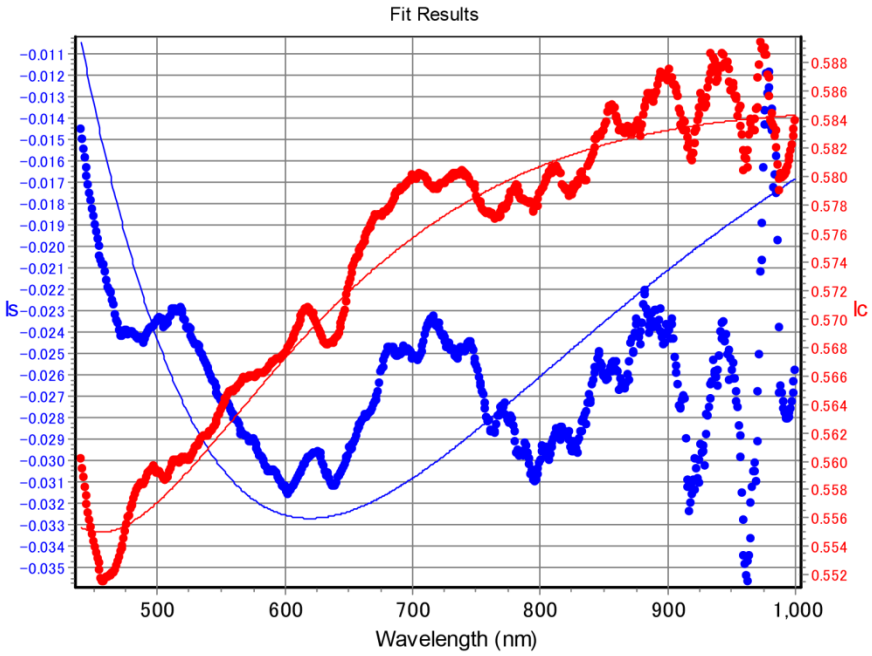

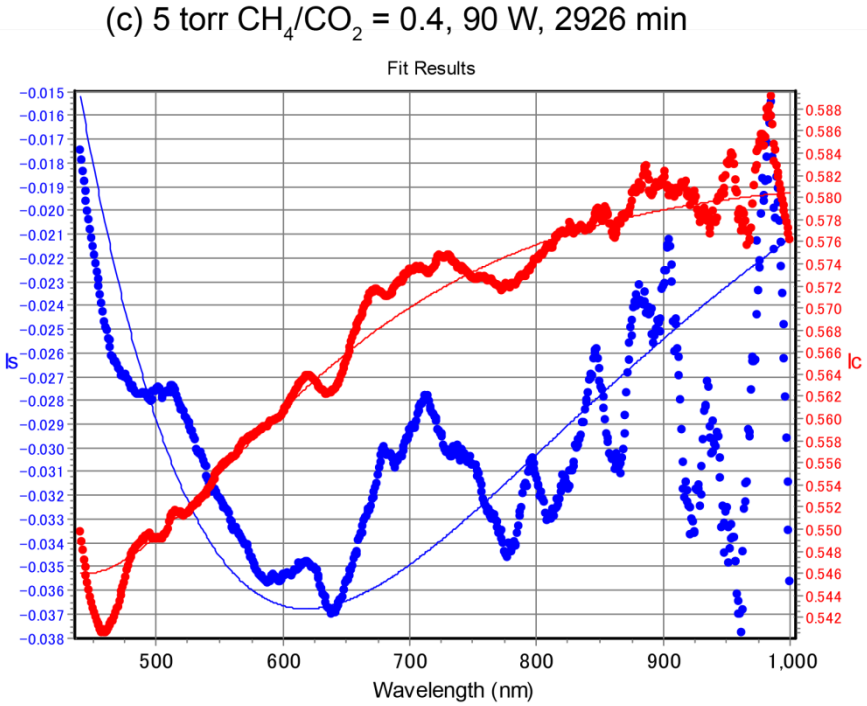

Figure 1.24. Measurement results of ellipsometry (thick lines) and model results (thin lines) of the sample produced in 5 torr of $CH_4/CO_2 = 0.4$ gas mixture and with a power of 90 W. (a) Results after 1500 minutes of total irradiation time. Film thickness is 138 ± 90 nm and $\chi^2 = 0.098$. (b) Results after 2451 minutes of total irradiation time. Film thickness is 189 ± 120 nm and $\chi^2 = 0.11$. (c) Results after 2926 minutes of total irradiation time. Film thickness is 174 ± 110 nm and $\chi^2 = 0.078$.

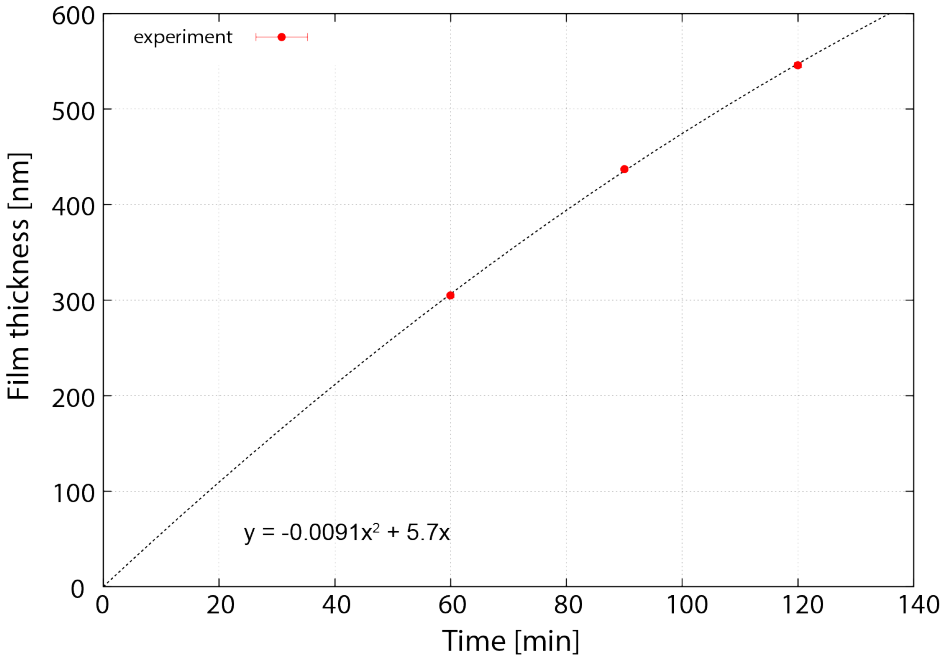

Figure 1.25. Time evolution of organic film thickness produced with 5 torr of CH_4/CO_2 gas mixture ($CH_4/CO_2 = 9$). The slope of the regression line at $t = 0$ is 5.7 [nm min^{-1}], which is interpreted as the aerosol production rate for this run.

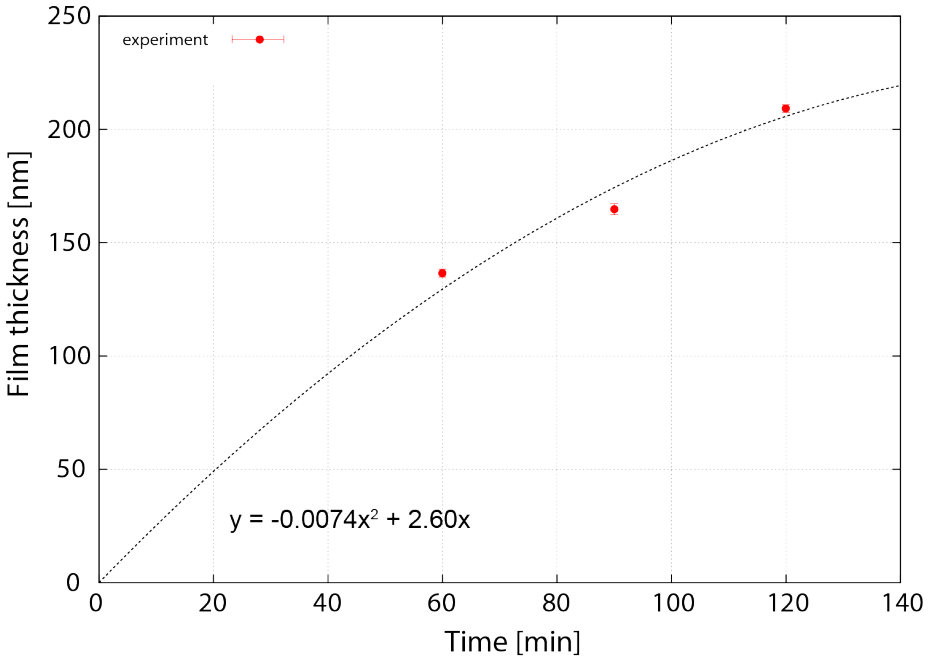

Figure 1.26. Time evolution of organic film thickness produced with 5 torr of CH_4/CO_2 gas mixture ($CH_4/CO_2 = 2.6$). The slope of the regression line at $t = 0$ is 2.6 [nm min^{-1}].

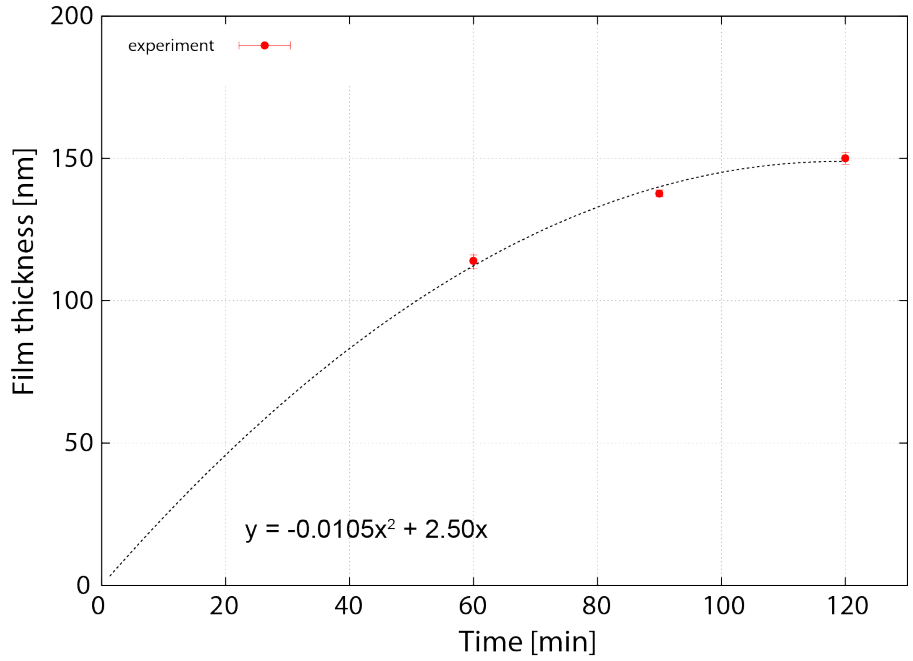

Figure 1.27. Time evolution of organic film thickness produced with 5 torr of CH_4/CO_2 gas mixture (CH_4/CO_2 = 1.9). The slope of the regression line at t = 0 is 2.5 [nm min^{-1}].

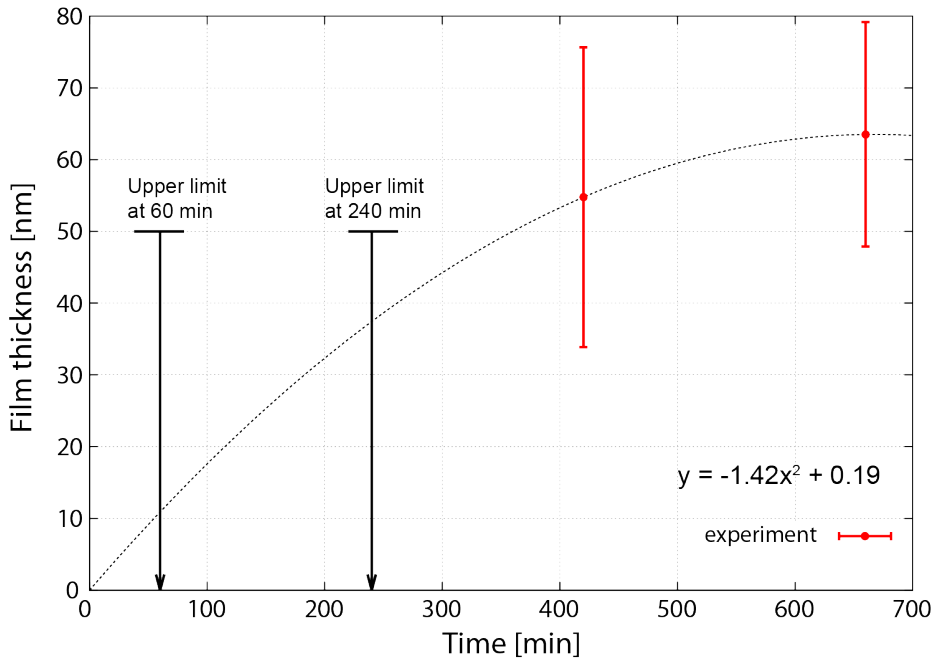

Figure 1.28. Time evolution of organic film thickness produced with 5 torr of CH_4/CO_2 gas mixture (CH_4/CO_2 = 1).

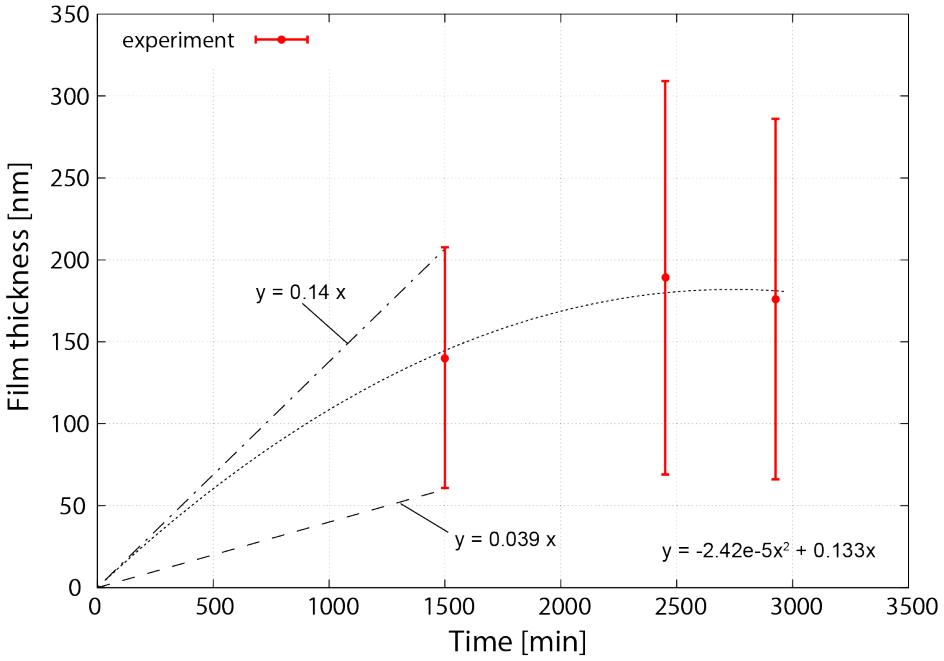

Figure 1.29. Time evolution of organic film thickness produced with 5 torr of CH_4/CO_2 gas mixture ($CH_4/CO_2 = 0.4$). The dashed line represents a lower estimate for the film growth rate, while the dash-dotted line represents an upper estimate.

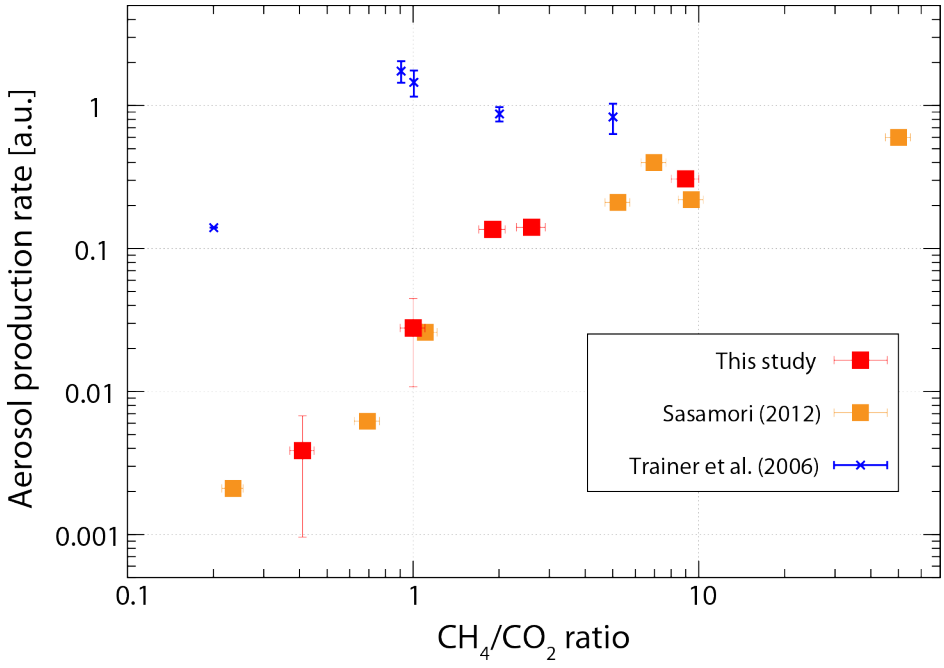

Figure 1.30. Aerosol production rate as a function of the initial CH_4/CO_2 gas ratio. The results of this study are shown by red boxes. Our results were obtained using CH_4/CO_2

gas mixture with 5 torr of total pressure and using a H_2/He lamp with a power of 90 W. Also shown are the results of Sasamori (2012), who used the same experimental apparatus with this study, and Trainer et al. (2006) who performed the experiments using a deuterium lamp and 600 torr of N_2 including 0.1% of CH_4 and 0.02 – 0.5% of CO_2. All of the production rates are normalized to that of experiment using only CH_4 as reactant gas.

1.3.4 Intermediate gas products

In order to investigate the chemical pathways in the reaction cell, we measured the abundances of intermediate gas products in the gas phase. We conducted deconvolution analysis of the mass spectra obtained by the QMS (Figure 1.1). In the section 1.4, we will perform calculations of photochemical reactions to investigate the chemical pathways in the reaction cell. The gas abundance data obtained here will also serve for validity check of the photochemical model. Previous studies have tried to explain the experimental results of gas products by CH_4 photolysis using photochemical models (Smith and Raulin, 1999; Vuitton et al., 2006), however, these studies are not capable of reproducing the experimental results (Smith and Raulin, 1999; Vuitton et al., 2006). This may be because of contamination of reactant gas by the ambient air, wall effects, or just simply uncertainty in reaction rate and/or quantum yield (Smith and Raulin, 1999; Vuitton et al., 2006). In addition, as shown in Figure 1.1, photolysis rates in the reaction cell should have a gradient along with the direction of the tube. Thus, we need to check whether the one-box photochemical model can adequately reproduce the photochemical reactions in the reaction cell, by comparing between the calculation results and measurements for intermediate gas products.

In the analyses of the QMS spectra, we performed mass deconvolution of the obtained spectra. The QMS ionizes a gas molecule with a high-temperature filament, which results in their fragmentations into gases with different m/z ratios (e.g., Adamkovics and Boerning, 2003). Also, a QMS signature at a given m/z ratio could be overlapped by fragments of multiple molecules. Thus, fragmentation patterns of each molecule must be taken into account when one needs to convert QMS intensity into the partial pressures of each molecule. Since the fragmentation pattern depends on the experimental conditions (e.g., total pressure) and on ionization efficiency of instruments, they should be experimentally determined under the relevant laboratory conditions. Figure 1.31 shows the mass spectra of standard gas species of CH_4, C_2H_2, C_2H_4, C_2H_6, CO and CO_2 measured with the QMS. All of the gas species considered in the deconvolution analyses are listed in Table 1.1. For the species whose fragmentation

patterns are not shown in Figure 1.31, their fragmentation patterns were obtained from the NIST database (http://webbook.nist.gov/chemistry/). The QMS spectrum $\boldsymbol{H}$ (m/z = 1 to m) is connected with the fragmentation pattern $\boldsymbol{R}$ (m/z = 1 to m and 1 to n species) and partial pressure $\boldsymbol{P}$ for n species, by the following equation (Adamkovics and Boering, 2003):

$$\boldsymbol{H} = \boldsymbol{R} \cdot \boldsymbol{P} \qquad (1.17)$$

where

$$\boldsymbol{H} = \begin{pmatrix} h_1 \\ h_2 \\ \vdots \\ h_m \end{pmatrix} \text{ and } \boldsymbol{P} = \begin{pmatrix} p_1 \\ p_2 \\ \vdots \\ p_n \end{pmatrix} \qquad (1.18)$$

$$\boldsymbol{R} = \begin{pmatrix} r_{11} & r_{12} & \cdots & r_{1n} \\ r_{21} & r_{22} & \cdots & r_{2n} \\ \vdots & \vdots & \ddots & \vdots \\ r_{m1} & r_{m2} & \cdots & r_{mn} \end{pmatrix} \qquad (1.19)$$

Thus,

$$\begin{pmatrix} h_1 \\ h_2 \\ \vdots \\ h_m \end{pmatrix} = \begin{pmatrix} r_{11}p_1 + r_{12}p_2 + \cdots r_{1n}p_n \\ r_{21}p_1 + r_{22}p_2 + \cdots r_{2n}p_n \\ \vdots \\ r_{m1}p_1 + r_{m2}p_2 + \cdots r_{mn}p_n \end{pmatrix} \qquad (1.20)$$

In the above equations, we assumed that the sensitivity factors (i.e., ionization efficiency) are the same among the species (CH_4, C_2H_2, C_2H_4, C_2H_6, CO and CO_2). This is based on our experimental results (not shown) that measured peak QMS signals as a function of partial pressures of each gas (CH_4, C_2H_2, C_2H_4, C_2H_6, CO and CO_2), showing a similar behavior on the partial pressures.

Figure 1.32 – Figure 1.37 show the mass spectra of gas species contained in the reaction cell in the experiments for different CH_4/CO_2 ratios. In the experiments at higher CH_4/CO_2 ratios (CH_4/CO_2 = 9 – 1.9), various high-order hydrocarbons were produced due to the UV irradiations. Their mass peaks are separated by intervals of 12, 13 and 14 amu, consistent with (-C-), (-CH-) and (-CH_2-) groups, respectively. The mass peaks at m/z = 78 and 91 are consistent with the presence of benzene and fragment ion for toluene, respectively. The remarkable detection of benzene is consistent with the previous experiments using UV light as an energy source (Trainer et al., 2006; Imanaka

and Smith, 2007) and measurements of Titan's upper atmosphere by the Cassini spacecraft (Waite et al., 2007). Figure 1.32 also shows that there is the remnant of air, which was not evacuated by the pump. We took into consideration this remnant of air in the following analysis and photochemical modeling. In the experiment at CH_4/CO_2 of 1 (Figure 1.36), the peak intensities of hydrocarbons become significantly small compared with those at higher CH_4/CO_2 ratios. In the experiment at CH_4/CO_2 of 0.4, the peaks of hydrocarbons seem to disappear, whereas the peak at m/z 30, which is probably due to the presence of H_2CO, appears in Figure 1.36.

Figure 1.38–Figure 1.43 show the results of mass deconvolution analysis (i.e., comparison of the obtained mass spectra with the synthesized spectra). These figures indicate that the obtained mass spectra for the range < 32 amu are in good agreement with the synthesized mass spectra. In the mass range from 36 to 46 amu, the spectra are mainly explained by CO and CO_2. In the mass range > 46 amu, the fitting seems to be poor because we used the fragmentation patterns from the NIST dataset.

Figure 1.44 shows the molar mixing rations of CH_4, C_2H_2, C_2H_4, C_2H_6, CO and CO_2 gases obtained by mass deconvolution. The concentrations of C_2 hydrocarbons increase with the CH_4/CO_2 ratio for the ratio less than unity, and remain almost constant for the ratio > 1 (Fig. 2.44). On the other hand, the CO concentration decreases with the CH_4/CO_2 ratio. These data will be compared with photochemical calculations in the section 1.4 to understand the formation processes of tholin in our experiments.

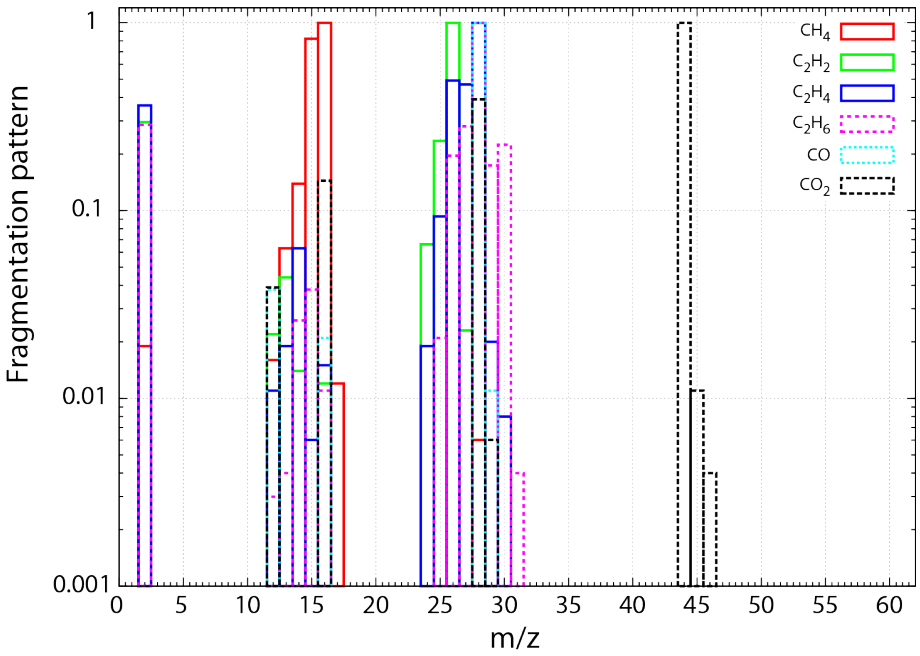

Figure 1.31. Fragmentation patterns of CH_4, C_2H_2, C_2H_4, C_2H_6, CO and CO_2 gases measured with a quadruple mass spectrometer. They were measured in 1.4 torr of total pressure in the reaction cell and in 10^{-5} mbar of the QMS pressure. C_2H_4, C_2H_6 and CO have their largest peaks at m/z = 28.

Table 1.1. Species considered in the deconvolution analysis of mass spectra. The fragmentation pattern of the species in bold were obtained experimentally under our relevant laboratory conditions, while the others were obtained from the NIST database (http://webbook.nist.gov/chemistry/)

H_2, **CH_4, C_2H_2, C_2H_4, C_2H_6,** C_3H_4, C_3H_6, C_3H_8, C_4H_2, C_4H_{10}, **CO, CO_2,** H_2O, H_2CO, CH_3OH, CH_3CHO, N_2

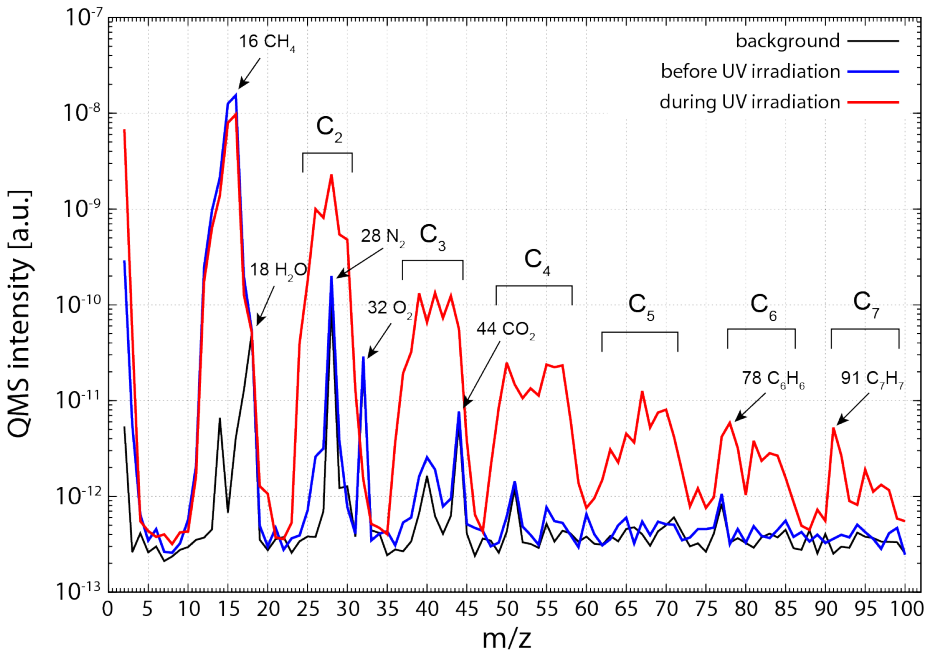

Figure 1.32. Averaged mass spectra of gases in the reaction cell using 5 torr of pure CH_4 gas measured with the QMS. The black line is background signal of QMS, the blue line is the spectra for the reactant gas before the UV irradiation. The red line is the mass spectra during the UV irradiation, showing high-order hydrocarbons are produced.

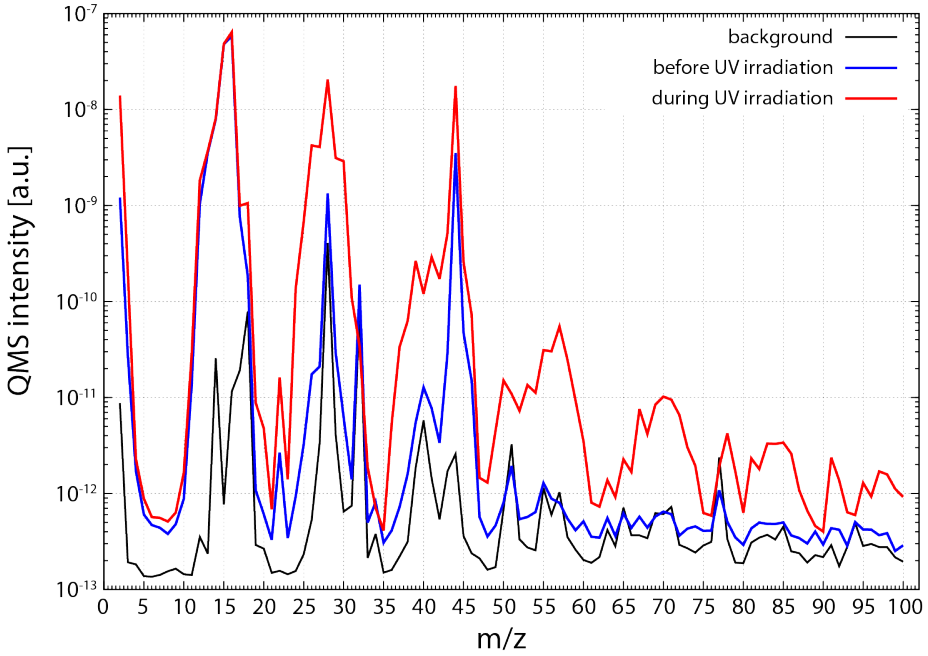

Figure 1.33. Averaged mass spectra of gases in the reaction cell using 5 torr of CH_4/CO_2 gas mixture with CH_4/CO_2 ratio of 9.

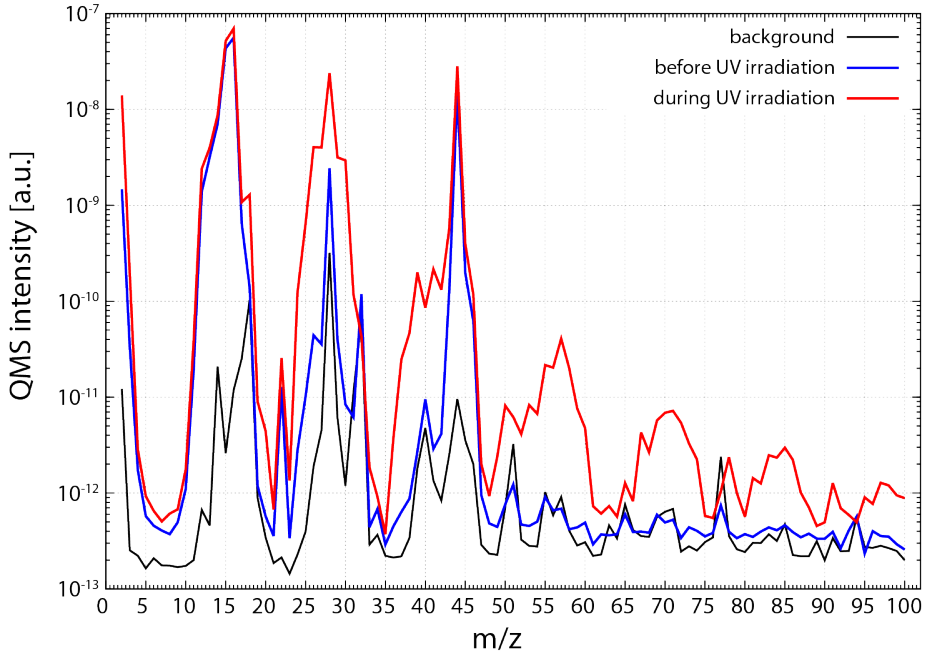

Figure 1.34. Averaged mass spectra of gases in the reaction cell using 5 torr of CH_4/CO_2 gas mixture with CH_4/CO_2 ratio of 2.6.

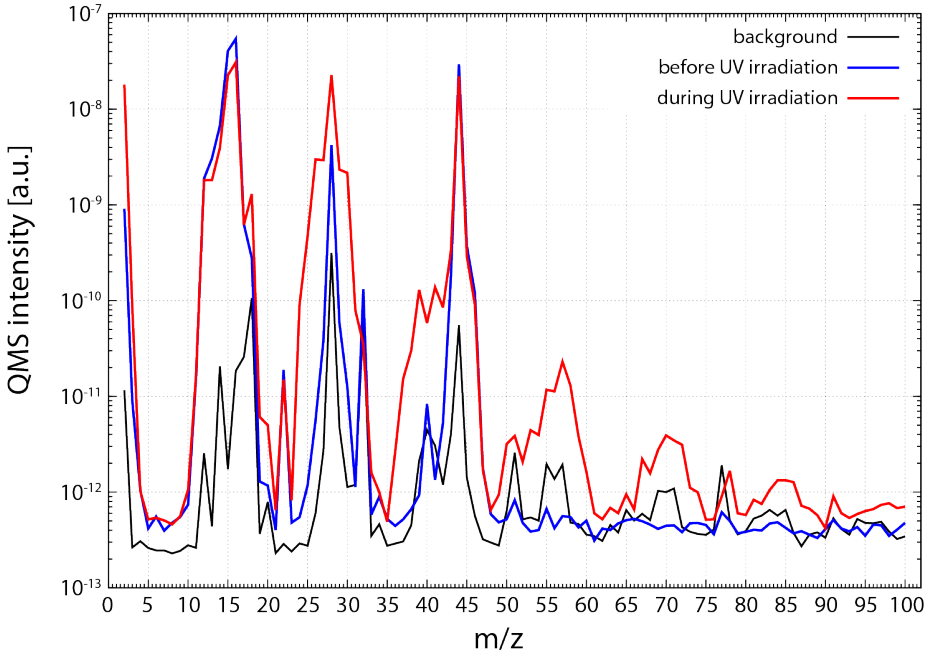

Figure 1.35. Averaged mass spectra of gases in the reaction cell using 5 torr of CH_4/CO_2 gas mixture with CH_4/CO_2 ratio of 1.9.

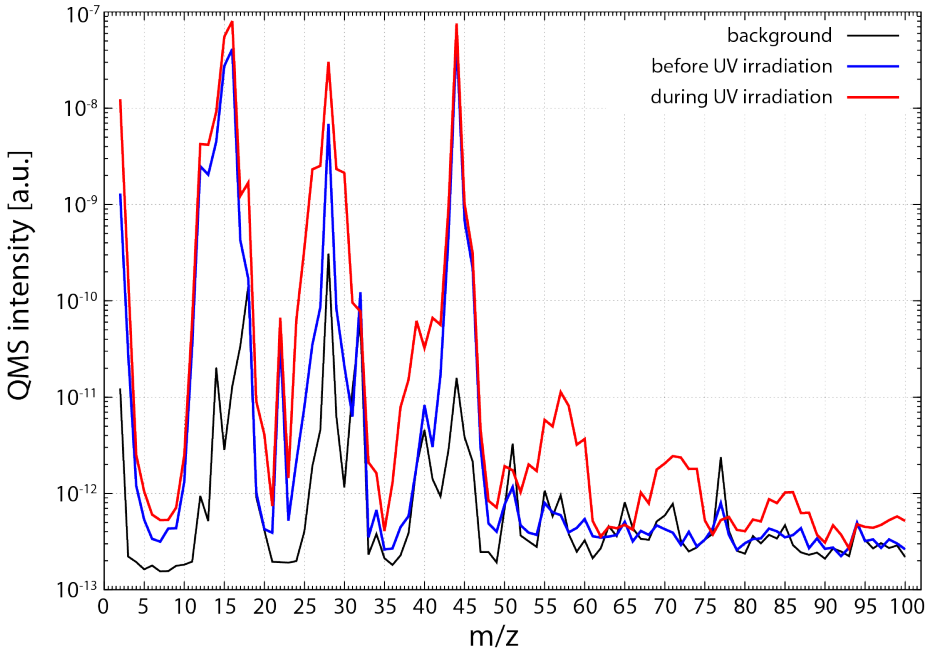

Figure 1.36. Averaged mass spectra of gases in the reaction cell using 5 torr of CH_4/CO_2 gas mixture with CH_4/CO_2 ratio of 1.

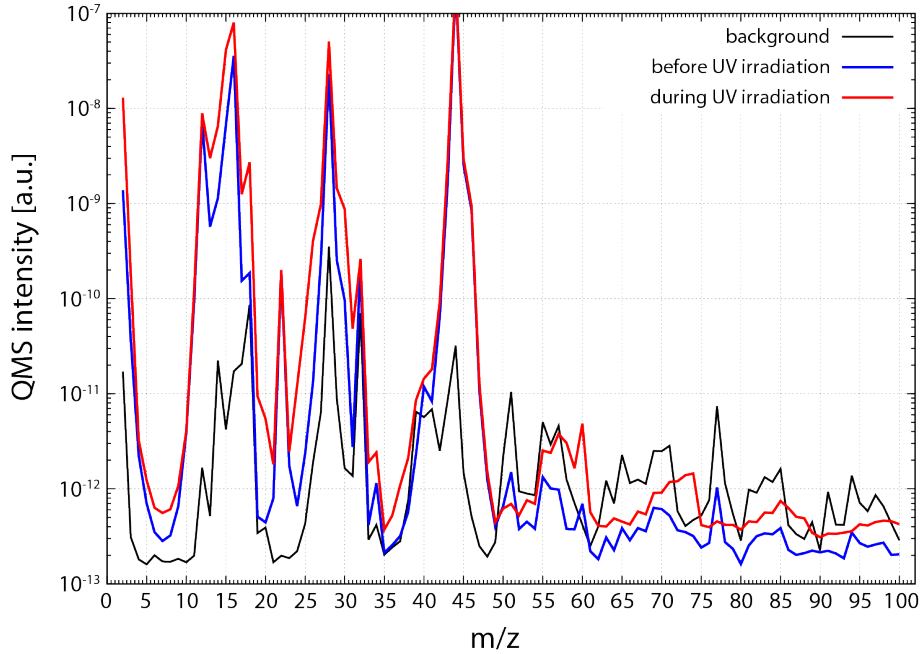

Figure 1.37. Averaged mass spectra of gases in the reaction cell using 5 torr of CH_4/CO_2 gas mixture with CH_4/CO_2 ratio of 0.4.

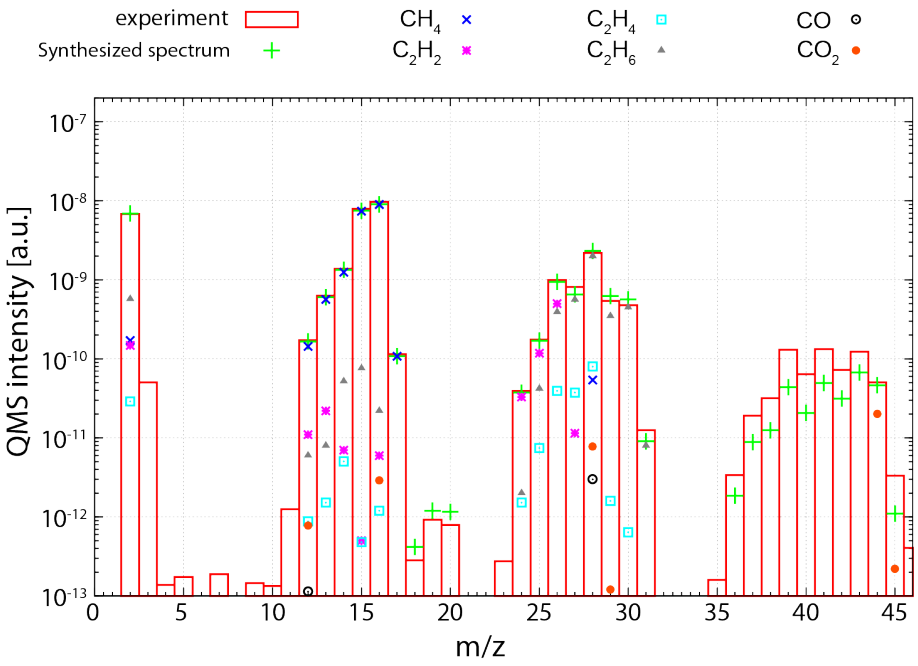

Figure 1.38. Averaged mass spectrum and its deconvolution result for the experiments with pure CH_4 gas. The synthesized spectrum includes the contribution from all of the gases considered in the analysis.

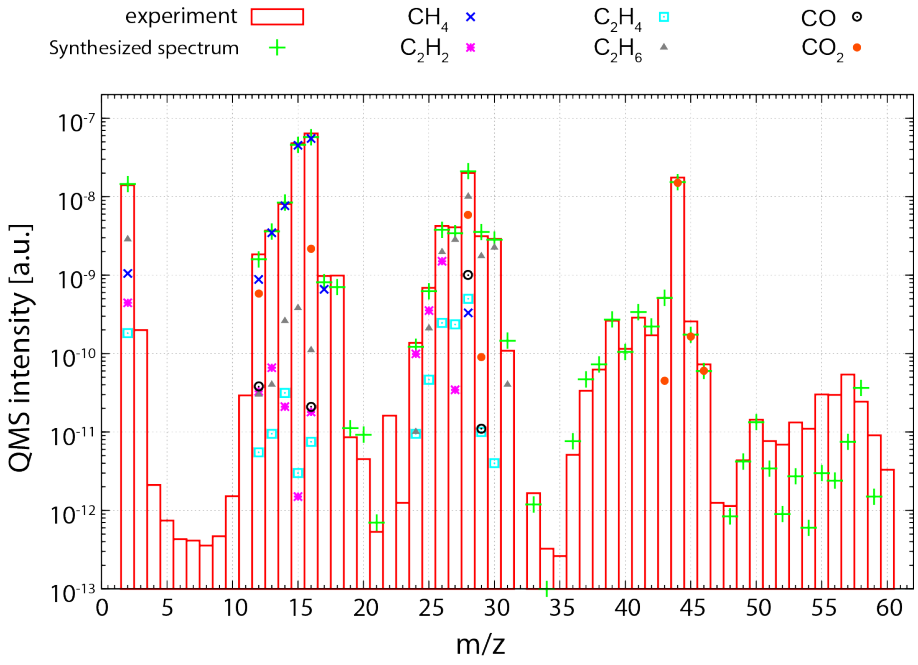

Figure 1.39. Averaged mass spectrum and its deconvolution result for the experiments with CH_4/CO_2 ratio of 9.

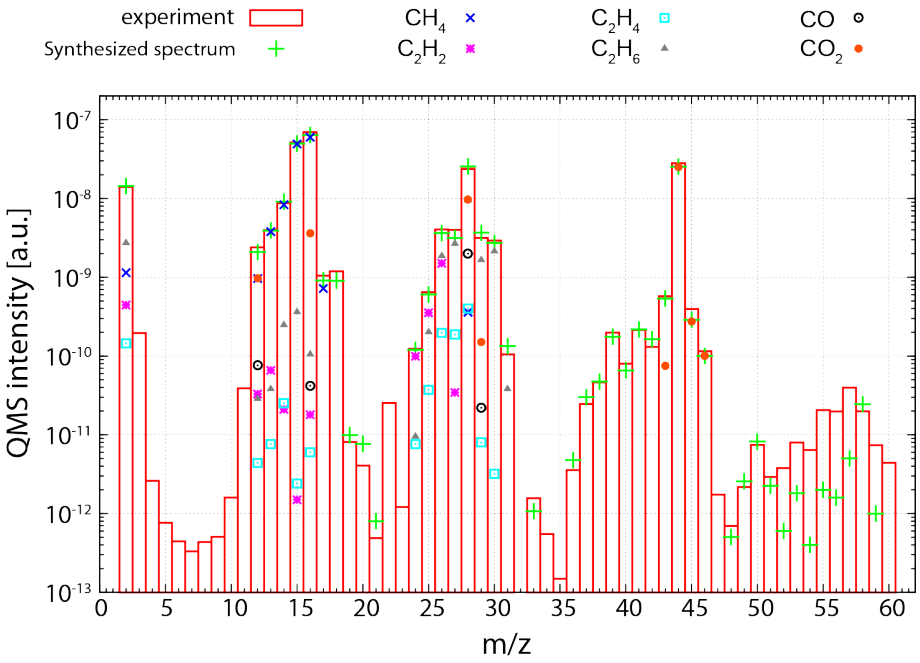

Figure 1.40. Averaged mass spectrum and its deconvolution result for the experiments with CH_4/CO_2 ratio of 2.6.

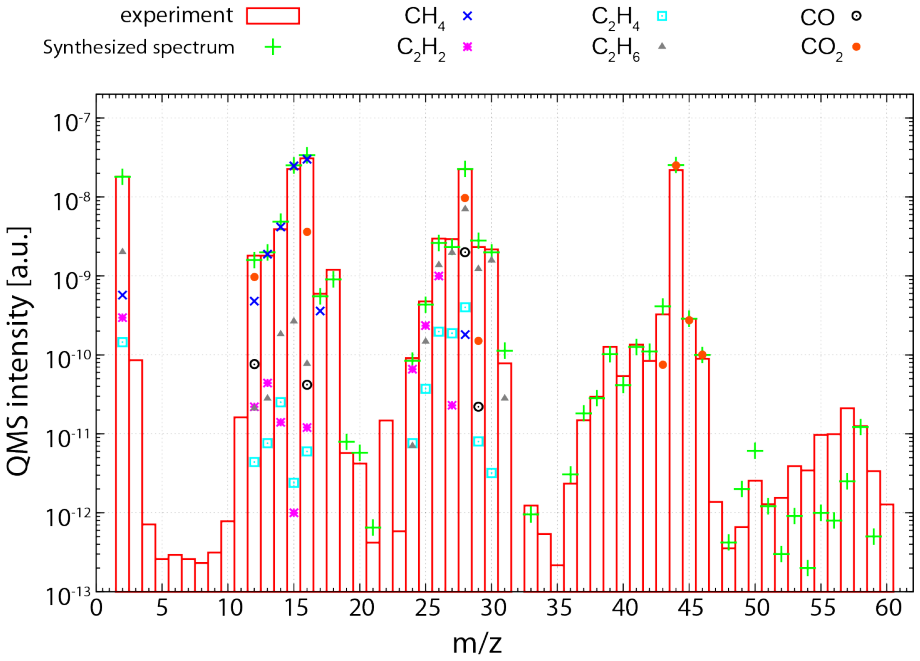

Figure 1.41. Averaged mass spectrum and its deconvolution result for the experiments with CH_4/CO_2 ratio of 1.9.

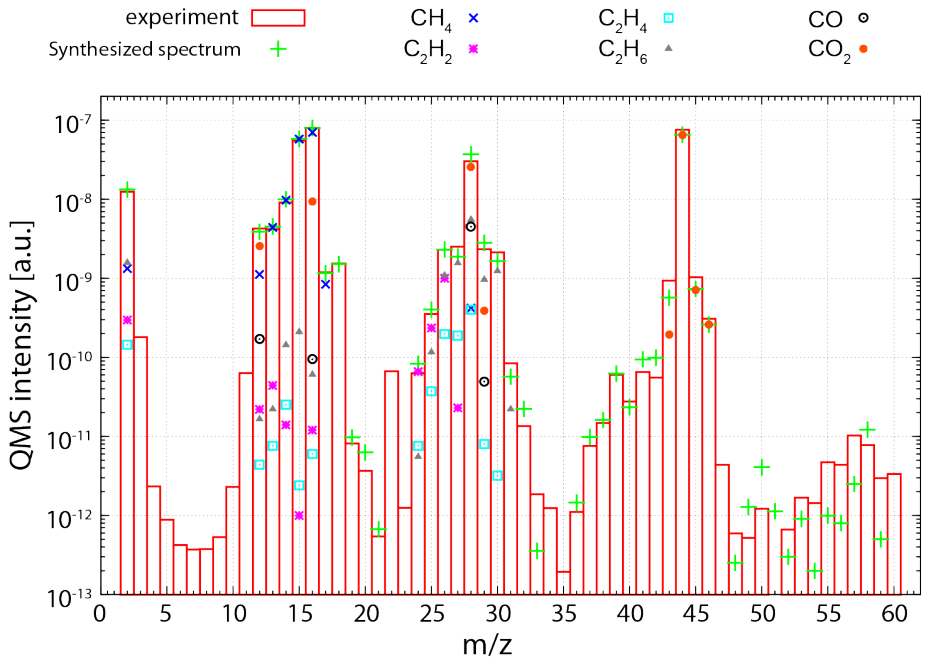

Figure 1.42. Averaged mass spectrum and its deconvolution result for the experiments with CH_4/CO_2 ratio of 1.

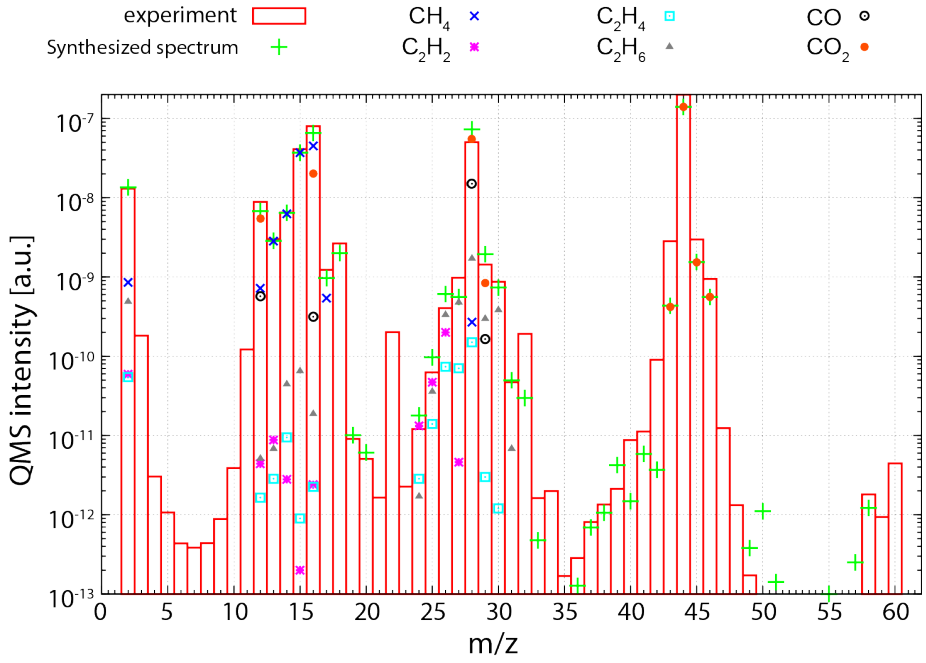

Figure 1.43. Averaged mass spectrum and its deconvolution result for the experiments with CH_4/CO_2 ratio of 0.4.

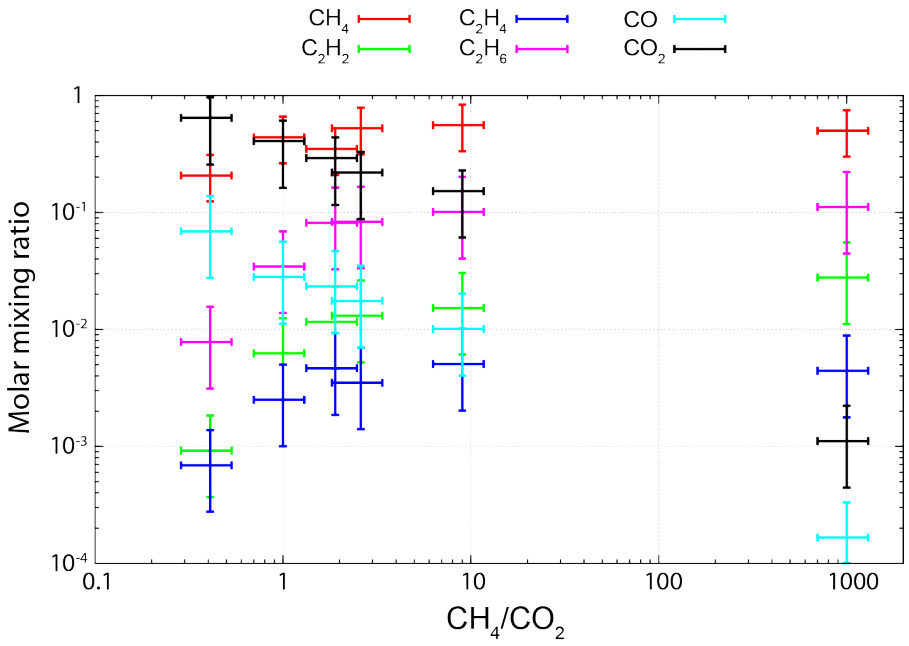

Figure 1.44. Molar mixing ratios for major gas species retrieved by deconvolution analysis of mass spectra.

1.4 Discussion: parent molecules for the formation of tholin

We compare the experimental results of the concentrations of gas molecules obtained in the section 1.3.4 with photochemical calculations in order to constrain the formation mechanism of tholin. First of all, we developed a one-box photochemical model that includes 134 species up to C_8 hydrocarbons and 791 chemical reactions. In compiling the reaction list, we used the reaction constants of hydrocarbon, nitrile, and ammonium chemistry used in the atmosphere of Titan (Hebrard et al., 2006). We also used the reaction rates of O-bearing species, such as oxides and aldehydes, based on a photochemical model about early Earth (Pavlov et al., 2001). The complete lists of species, photolysis and chemical reactions are shown in the Appendix A. The photochemical scheme contains only neutral chemistry. The basic equations and numerical procedures are described in the section 2.2. To compare our experimental results of gas species, we consider a one-box open system with a coinstantaneous inflow and outflow, similar to the experimental system. Using the equation (1.7) derived in the actinometry, the pumping efficiency of our experiments is calculated to be 0.113 s^{-1}

for f_{in} = 1.5 ml min^{-1} and 327 cm^3 of the total volume of the reaction cell. With the pumping efficiency, a typical residence time of gas species in the reaction cell is estimated as ~90 seconds. For the UV source in the one-box photochemical model, we use a total actinic flux of 2×10^{14} photon cm^{-2} s^{-1} (a RF power of 90 W at 13.56 MHz) with a UV spectrum similar to that of sun (Figure 1.3). We fixed the total pressure in the reaction cell as 5 torr and performed photochemical calculations with different initial CH_4/CO_2 gas ratio from 0.2 to 1000.

Figure 1.45 shows the calculation results of the time evolutions of CH_4, C_2H_2, C_2H_4, C_2H_6, CO and CO_2 after the start of UV irradiation. Significant changes of methane abundances can be observed 1 to 100 seconds after the UV irradiation (Fig. 1.45), which correspond to the typical residence time of gas species in the reaction cell (i.e., 90 seconds). In 100 seconds after the UV irradiation, the abundances of gas species achieve steady-states, determined by the balance between the photochemical reactions and inflow. This behavior is consistent with the experimental results of time evolutions of each species obtained by the QMS (Figure 1.7). Figure 1.46 shows the comparisons of molar mixing ratios for these gas species retrieved by mass deconvolution analysis in the experiments (see the section 1.3.4) and the calculation results obtained by the one-box photochemical model as a function of the CH_4/CO_2 ratio. The abundances calculated by the one-box photochemical model represent steady-state abundances, i.e., 10 hours after the UV irradiations. The calculation results show a good agreement with the experimental results within the error range, indicating that the chemical scheme and other model assumptions (e.g., one-box assumption without UV shielding) employed here are sufficient to simulate the photochemical reactions occurred in the reaction cell. Compared with the previous studies that compared the gas abundances between those obtained by experiments and those calculated with photochemical models (Smith and Raulin, 1999; Vuitton et al., 2006), our photochemical calculations reproduce the experiments much better than those previous studies. The previous studies suggest that H loss due to both the wall effect (Smith and Raulin, 1999) and from the contamination by O_2 inflow (Vuitton et al., 2006) brought large uncertainties to their photochemical calculations. The consistency in the experiments and calculations in the present study may suggest that these would not have occurred in our experiments.

We then investigate the parent molecules and its reactions that control the tholin production rates. Table 1.2 summarizes the polymerization reactions, which are assumed to produce aerosol monomers in previous photochemical models (Yung et al., 1994; Toublanc et al., 1995; Pavlov et al., 2001; Wilson and Atreya, 2003; Hebrard et al., 2006; Lavvas et al., 2008a, b; Krasnopolsky, 2009). These reactions are included in our one-box photochemical model. Figure 1.47 shows the steady-state molar mixing ratios of gas species as functions of initial CH_4/CO_2 gas ratio. The abundances of aromatic hydrocarbons, such as C_6H_6 and C_6H_5, and C_3H_5 decline dramatically, when the CH_4/CO_2 ratio becomes less than unity, This behavior as a function of the CH_4/CO_2

ratio are similar to those of the tholin production rate observed by the experiments. In contrary to the tholin production rate, the abundances of polyynes, such as C_4H_2, C_6H_2, C_2H, C_4H and C_6H, increase where $CH_4/CO_2 < 1$. Figure 1.48 shows the calculation results of the steady-state rates of the reactions listed in Table 1.2 as functions of initial CH_4/CO_2 ratio. Only reactions involving benzene, R515, R516 and R517 in Table 2.2, show similar dependences on the CH_4/CO_2 ratio with the tholin production rates experimentally measured. These results suggest that the polymerization reactions of benzene and its radicals are the limiting reactions for tholin production in our experimental condition. On the other hand, the steady-state rates of the other reactions in Table 1.2 are not in agreement with the experimental results of the tholin production rate. In particular, our calculation results show that the reactions involving polyynes, C_2H, C_4H, C_4H_2, C_6H_2, proceed efficiently even at low CH_4/CO_2 rations (e.g., < 1). The polymerization of polyynes is considered to be one of the major processes for the formation of organic aerosols in Titan's atmosphere. Thus, these results indicate that the polymerization of polyynes would not limit the formation of tholin in our experiments. This further implies that the production rate of monomers in planetary atmospheres would significantly be overestimated when the polymerization of polyynes are included the formation of monomers in the atmosphere with the CH_4/CO_2 ratio less than unity.

Figure 1.49 shows the schematic diagram of primary chemical reactions in gas mixtures at high CH_4/CO_2 ratios toward the formation of tholin. Photolysis of CH_4 produces two major radicals, CH_3 and $^1CH_2$. The former further produces C_2H_6. Photolysis of C_2H_6 accounts for about 40% of C_2H_2 production. Although most of the C_2H_2 produced is lost to form C_3 species, a small fraction (~ 1%) of C_2H_2 is transformed into C_4H_2 through the reaction with C_2H. The production of C_4H_2 is an important step to produce benzene under our experimental conditions because most of the C_6H_4, a precursor molecule of benzene, is produced from C_4H_2 via the reaction with C_2H_3. C_6H_4 produces phenyl radical, C_6H_5, which combines with H to form benzene. Aerosol monomers are considered to be produced from further polymerization of C_6H_6 and C_6H_5. The other hydrocarbons that do not form C_6H_6 or C_6H_5 become C_3 species or C_4H_{10} and are finally removed from the reaction cell in our experiments. Wilson and Atreya (2004) suggest that a termolecular reaction (R413: $C_3H_3 + C_3H_3 + M \rightarrow C_6H_6 + M$) plays a major role to produce benzene, however, the termolecular reaction is not important under our experimental conditions, accounting for only 0.1% of the total benzene production, because of the low abundance of C_3H_3. Wilson and Atreya (2004) also suggested a minor chemical path for benzene (R506: $C_4H_5 + C_2H_2 \rightarrow C_6H_6 + H$). This reaction accounts for about 4% of the total benzene production based on our calculations.

Figure 1.50 shows the tholin production rates obtained in our experiments and the calculation results of the steady-state rates of some key reactions for the formation of tholin. "Benzene" in this figure shows the sum of reaction rates of R515, 516 and

R517, showing a good agreement with the experimental results of tholin production rate. On the other hand, the reaction rates of polymerization of polyynes, R314 and R468, show poor agreements with the experimental results. In the section 1.3.2, we found that the aerosol production rate is a linear function of irradiated UV flux, which could be explained by the mechanism II proposed by Trainer et al. (2006) (see the section 1.1). By combining the knowledge obtained by the experiments of tholin production rate as functions of UV flux and CH_4/CO_2 ratio, tholin production mechanism can be described as the following simple mechanism:

$$CH_4 + h\nu \rightarrow C_6H_6 \text{ or } C_6H_5 \qquad (1.21)$$

$$C_6H_6 \text{ or } C_6H_5 + C_6H_6 \text{ or } C_2H_2 \rightarrow \text{aerosol particles} \qquad (1.22)$$

$$C_6H_6 \text{ or } C_6H_5 + CH_4 \rightarrow \text{nonaerosol particles} \qquad (1.23)$$

The equation (1.21) shows that the photolysis of CH_4 and subsequent photochemical reactions produce benzene and its radical C_6H_5 which act as intermediate species for the aerosol production. C_6H_5 is produced by the photolysis of benzene or by polymerization of light-molecular-weight hydrocarbons. The equation (1.22) represents that the polymerization reactions of benzene with C_6H_5 or the other hydrocarbon species C_2H_2 produce aerosol particles. Under the conditions of very high CH_4 concentrations, the tholin production is suppressed, as shown in the equation (1.23). This is probably due to the presence of excess H_2 gas in the reaction system, since the removal of H_2 is necessary for the hydrocarbon polymerization reactions (e.g., Trainer et al., 2006; Sekine et al., 2008a, b; DeWitt et al., 2009). In this case, the hydrocarbon products would recycle back to CH_4 or other saturated hydrocarbons, such as C_2H_6 and C_3H_8, which are relatively stable in the gas phase and do not contribute to aerosol production.

We also performed photochemical calculations simulating the experimental conditions of Trainer et al. (2006) in order to investigate the cause of discrepancy between our results and theirs. We used the same photochemical reaction scheme described above and changed some of the model parameters, such as UV spectrum and pressure. For the UV source, we used the deuterium lamp spectrum shown in Figure 2.4. The pumping efficiency of their experiments is set to be 3.2×10^{-3} s^{-1} for $f_{in} = 60$ ml min^{-1} and 416 cm^3 of the total volume of the reaction cell (S.M. Horst, private communication, 2012). With the pumping efficiency, a typical residence time of gas species in the reaction cell is estimated as ~320 seconds.

Figure 1.51 shows the comparison of the tholin production rates obtained by the experiments of Trainer et al. (2006) and calculation results of reaction rates calculated by our one-box photochemical model simulating their experimental

conditions. We found that, contrary to their experimental results, the abundances of hydrocarbons and hydrocarbon reaction rates decrease drastically below unity of the CH_4/CO_2 ratio. Their decrease rates are much steeper than those of the present study. This is because, in their experiments, oxidative photochemical reactions dominate the chemical network at the CH_4/CO_2 ratio less than unity. Table 1.5 is a comparison of the photochemical calculation results of the ratio of oxidants to reductants at $CH_4/CO_2 = 0.2$. These results show that the ratios of oxidants to reductants under the experimental conditions of Trainer et al. (2006) are about one order of magnitude higher than those under our experimental conditions. This would significantly affect the chemical network, such as the increase of oxidation rate of C_2H_2. Nevertheless, Trainer et al. (2006) observed high levels of tholin production rate below unity of CH_4/CO_2. At this stage, we cannot conclude the photochemical reactions that are responsible for the formation of tholin in the experiments performed by Trainer et al. (2006).

There are two possible causes to explain the discrepancy between experimental results and photochemical calculations under the experimental conditions of Trainer et al. (2006). The first explanation is that oxygen species were incorporated to aerosol production below unity of CH_4/CO_2. As they observed possible peaks of oxygenated fragments of CH_2O^+ and COO^+ in the mass spectra of aerosol particles, incorporation of O-bearing species into the tholin would increase the tholin production rate at lower CH_4/CO_2 ratios. The other explanation is that nitrogen was incorporated into aerosol production in the experiments by Trainer et al. (2006). Since they have used a deuterium lamp which is not supposed to dissociate N_2 molecule, nitrogen chemistry has not been thought to participate in the tholin production. However, their more recent study observed a significant amount of nitrogen was incorporated in the aerosol particles (Trainer et al., 2012). Although they suggested that reaction of N_2 with CH radicals may be responsible for the production of CN, the formation rate and mechanism of this reaction remains uncertain. If this was the case, their chemical reactions would be very different with ours, because our photochemical model does not include such a reaction.

(a) CH_4/CO_2 = 1000

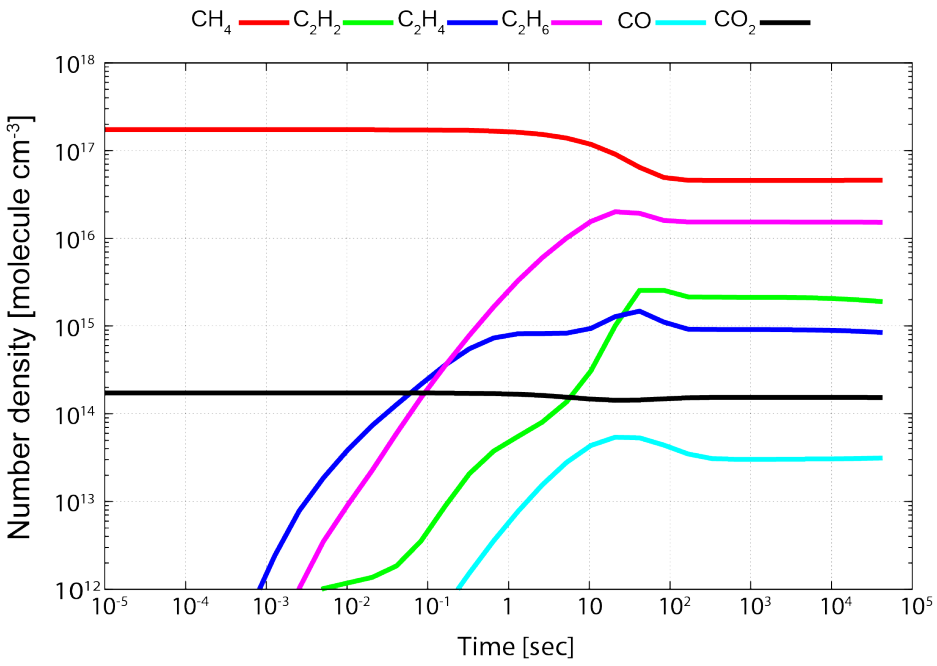

(b) CH_4/CO_2 = 10

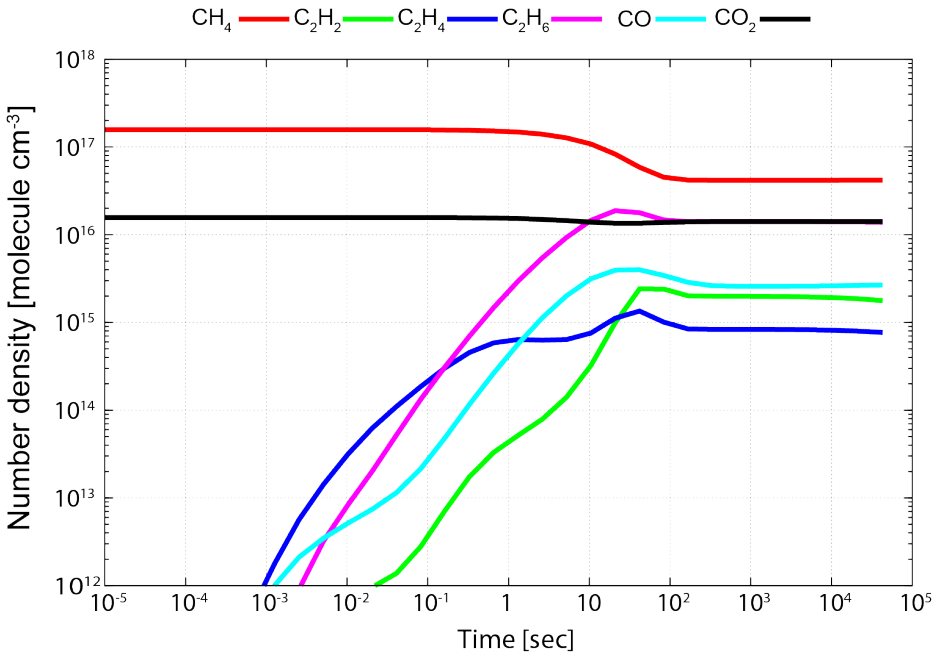

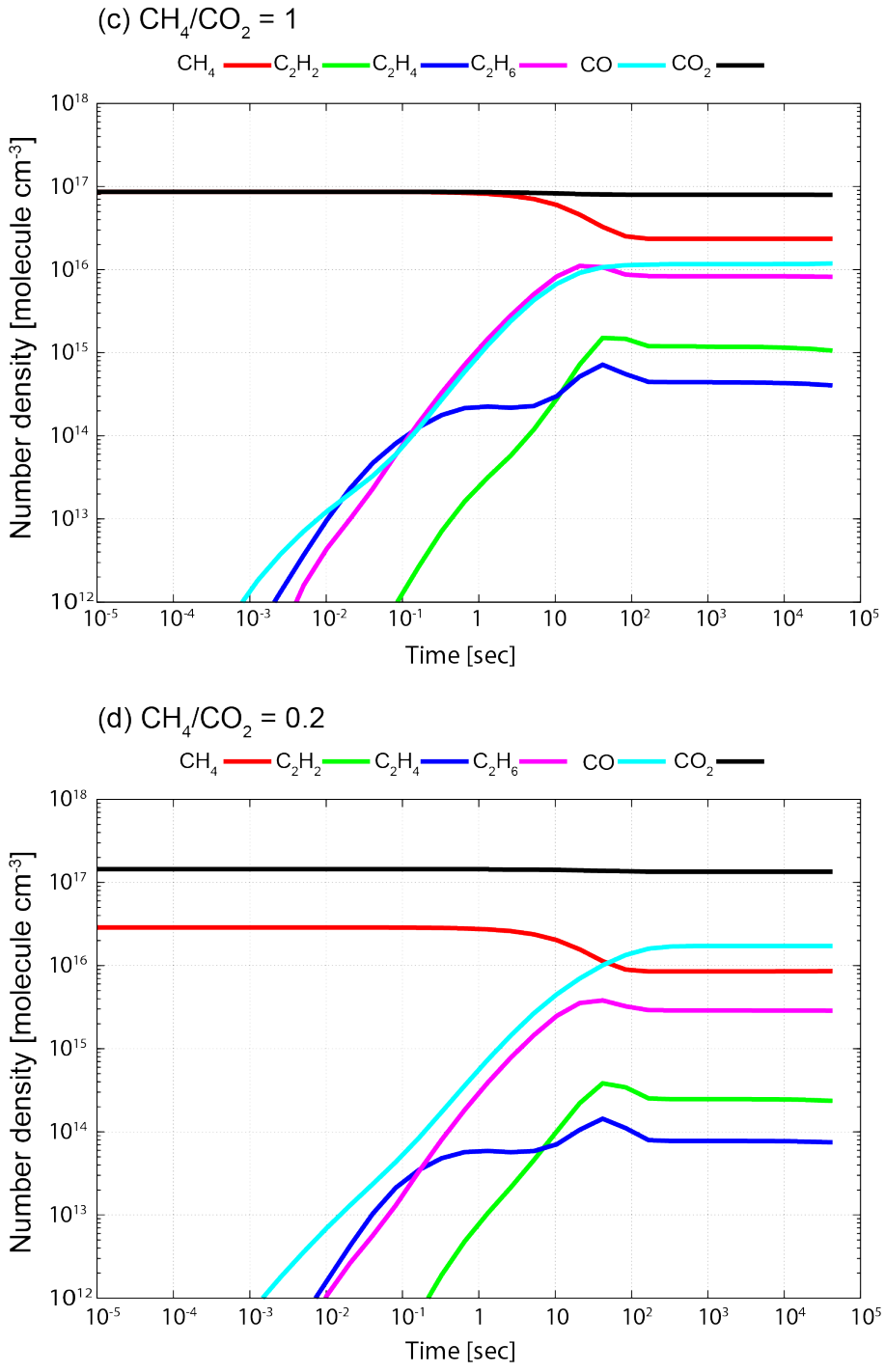

Figure 1.45. One-box photochemical calculation results for the time evolutions of major gas species. The model simulates the aerosol experiments using the H_2/He lamp with 90 W. The total pressures are fixed to be 5 torr. The pumping efficiency is set to be 0.011 s^{-1}, resulting in a typical residence time of 90 seconds. (a) $CH_4/CO_2 = 1000$, (b) $CH_4/CO_2 = 10$, (c) $CH_4/CO_2 = 1$, (d) $CH_4/CO_2 = 0.2$.

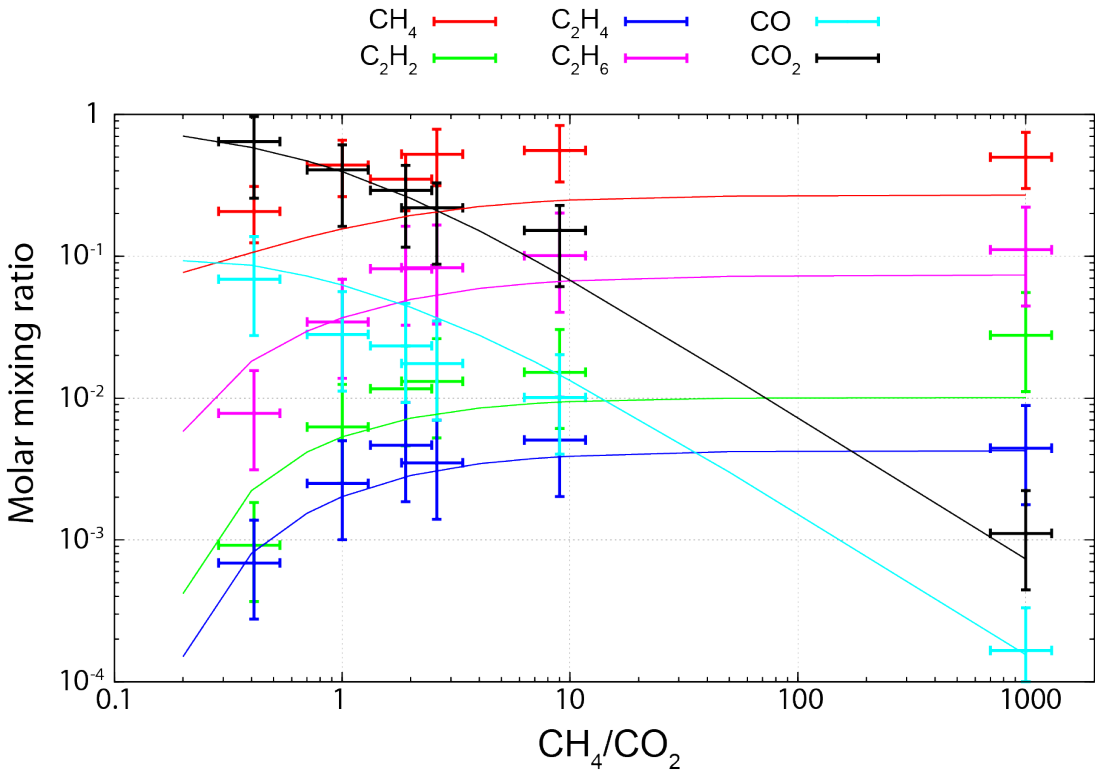

Figure 1.46. Molar mixing ratios for major gas species retrieved by deconvolution analysis of mass spectra and calculated by the one-box photochemical model. The abundances calculated by the one-box photochemical model represent steady-state abundances 10 hours after the UV irradiation. The model calculations agree well with the experimental results within the error range, indicating that the chemical scheme and other model assumptions (e.g., one-box assumption without UV shielding) employed in the one-box photochemical model are sufficient to simulate the photochemical reactions in the reaction cell.

Table 1.2. Hydrocarbon reactions assumed to produce aerosol monomers. These reactions are included in our one-box photochemical model. Also shown are the previous photochemical models which assumed these reactions for the calculation of aerosol production. See appendix A for the reaction rates.

Reaction		**Previous models**
R205	$C + C_4H_6 \rightarrow C_3H_3 + C_2H_3$	Lavvas et al. (2008a,b)
R219	$CH + C_4H_8 \rightarrow C_5H_8 + H$	Lavvas et al. (2008a,b), Wilson and Atreya (2004)
R310	$C_2 + C_6H_6 \rightarrow SOOT$	Hebrard et al. (2006)
R314	$C_2H + C_2H_2 \rightarrow C_4H_2 + H$	Pavlov et al. (2001)
R322	$C_2H + CH_2CCH_2 \rightarrow C_5H_4$	Pavlov et al. (2001)
R337	$C_2H + C_6H_6 \rightarrow SOOT$	Wilson and Atreya (2004), Hebrard et al. (2006)
R338	$C_2H + C_8H_2 \rightarrow SOOT + H$	Yung et al. (1984), Toublanc et al. (1995), Wilson and Atreya (2004), Hebrard et al. (2006) , Krasnopolsky (2009, 2010)
R468	$C_4H + C_6H_2 \rightarrow SOOT + H$	Yung et al. (1984), Toublanc et al. (1995), Wilson and Atreya (2004), Hebrard et al. (2006), Lavvas et al. (2008a,b), Krasnopolsky (2009, 2010)
R469	$C_4H + C_8H_2 \rightarrow SOOT + H$	Yung et al. (1984), Toublanc et al. (1995), Wilson and Atreya (2004), Hebrard et al. (2006) , Krasnopolsky (2009, 2010)
R511	$C_6H + C_4H_2 \rightarrow SOOT + H$	Yung et al. (1984), Toublanc et al. (1995), Wilson and Atreya (2004), Hebrard et al. (2006) , Lavvas et al. (2008a,b)
R512	$C_6H + C_6H_2 \rightarrow SOOT + H$	Yung et al. (1984), Toublanc et al. (1995), Wilson and Atreya (2004), Hebrard et al. (2006) , Lavvas et al. (2008a,b) , Krasnopolsky (2009, 2010)
R513	$C_6H + C_8H_2 \rightarrow SOOT + H$	Yung et al. (1984), Toublanc et al. (1995), Wilson and Atreya (2004), Hebrard et al. (2006) , Krasnopolsky (2009, 2010)
R515	$C_6H_5 + C_2H_2 \rightarrow SOOT + H$	Wilson and Atreya (2004), Hebrard et al.

		(2006) , Lavvas et al. (2008a,b) , Krasnopolsky (2009, 2010)
R516	$C_6H_5 + C_2H_2 \rightarrow SOOT$	Wilson and Atreya (2004), Hebrard et al. (2006) , Lavvas et al. (2008a,b) , Krasnopolsky (2009, 2010)
R517	$C_6H_5 + C_6H_6 \rightarrow SOOT + H$	Wilson and Atreya (2004), Hebrard et al. (2006) , Krasnopolsky (2009, 2010)
R661	$O(^3P) + C_3H_3 \rightarrow SOOT + H$	Wilson and Atreya (2004), Hebrard et al. (2006)
R662	$O(^3P) + C_3H_5 \rightarrow SOOT + H$	Hebrard et al. (2006)
R783	$CH_2OH + C_2H_4 \rightarrow SOOT$	Hebrard et al. (2006)
R814	$CH_3CO + C_2H_3 \rightarrow SOOT + CH_3$	Hebrard et al. (2006)

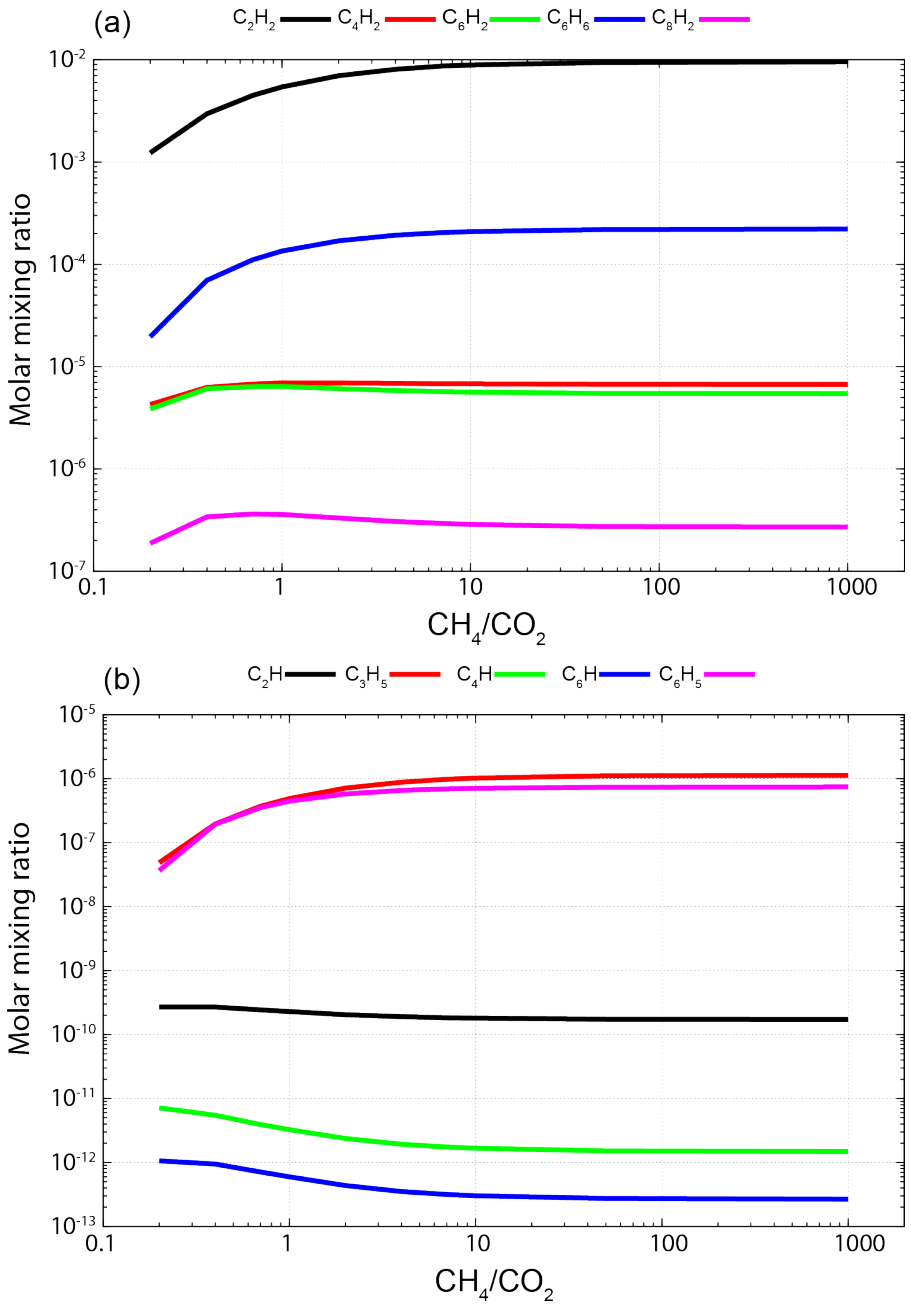

Figure 1.47. Steady-state molar mixing ratios of gas species as functions of initial CH_4/CO_2 gas ratio. The abundances of C_6H_6, C_6H_5 and C_3H_5 drop quickly where $CH_4/CO_2 < 1$, showing similar behavior with the aerosol production rate obtained by the experiments. On the other hand, the abundances of C_4H_2, C_6H_2, C_2H, C_4H and C_6H increase where $CH_4/CO_2 < 1$, contrary to the aerosol production rates.

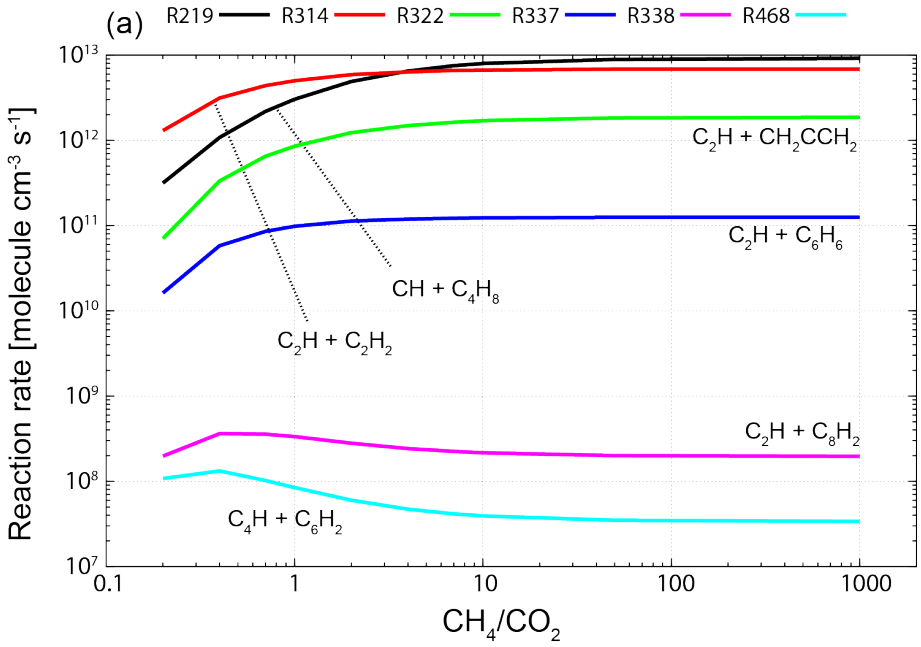
(a)
R219
R314
R322
R337
R338
R468
Reaction rate [molecule cm-3 s-1]
CH4/CO2
C2H + CH2CCH2
C2H + C6H6
CH + C4H8
C2H + C2H2
C2H + C8H2
C4H + C6H2

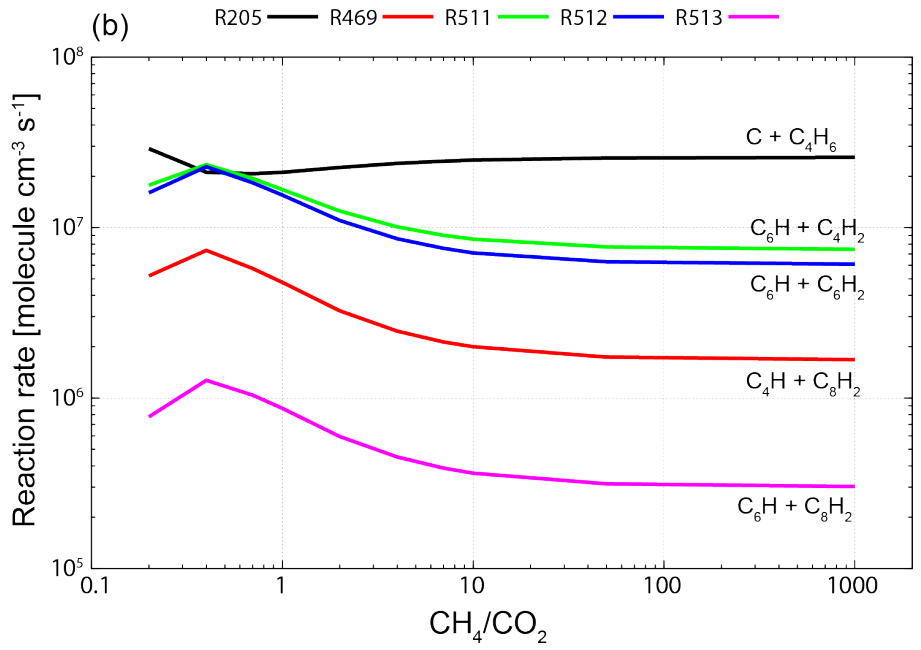
(b)
R205
R469
R511
R512
R513
Reaction rate [molecule cm-3 s-1]
CH4/CO2
C + C4H6
C6H + C4H2
C6H + C6H2
C4H + C8H2
C6H + C8H2

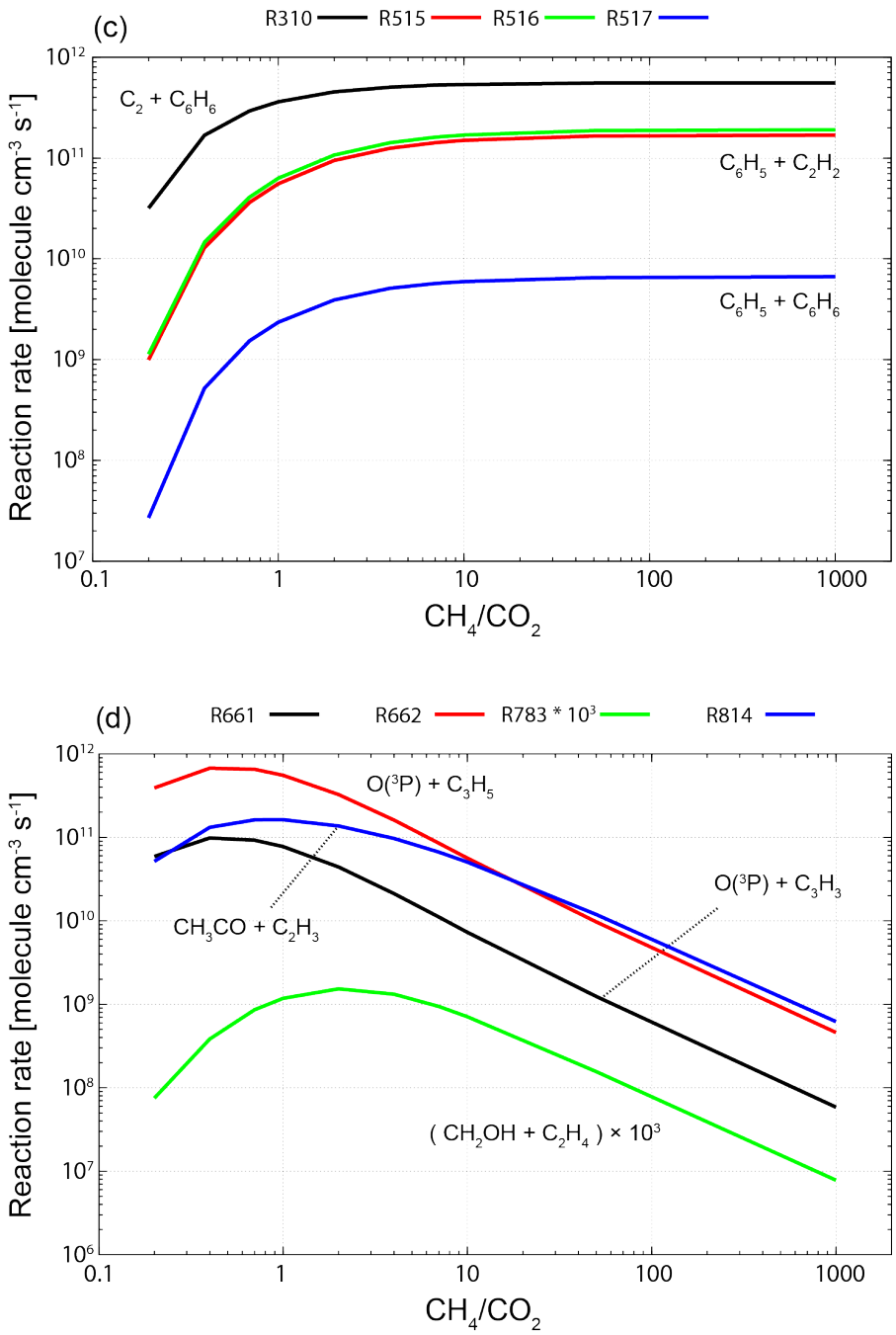

Figure 1.48. Reaction rates as functions of initial CH_4/CO_2 ratio 10 hours after the UV irradiation, calculated with the one-box photochemical model. (a) Polymerization reactions of CH, C_2H and C_4H. (b) Polymerization reactions of C, C_4H_2, C_6H_2 and C_8H_2. (c) Polymerization reactions of C_6H_5 and C_6H_6, showing similar dependence on CH_4/CO_2 ratio with the aerosol production rate obtained by the experiments. (d) Reactions involving oxygen species.

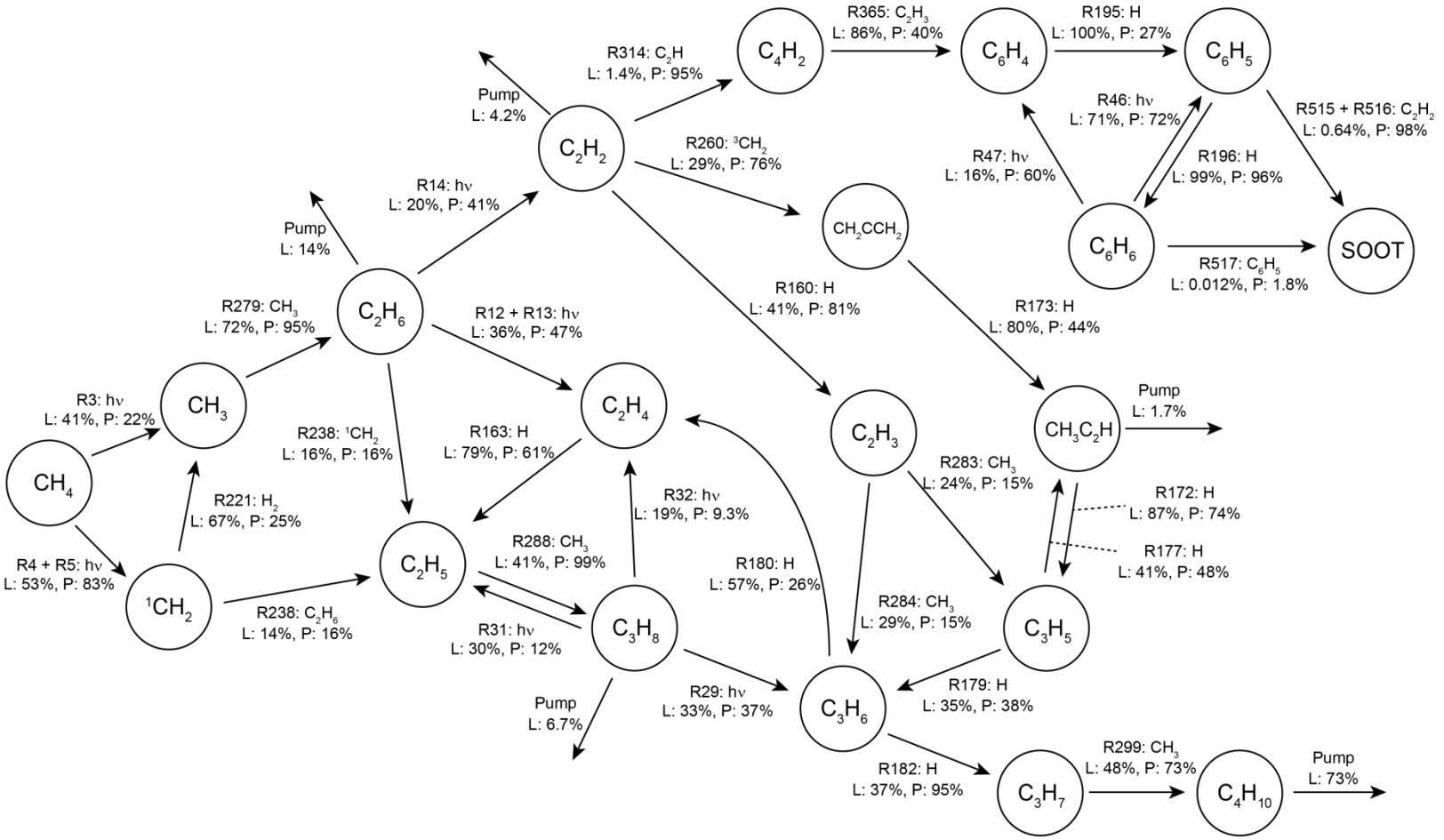

Figure 1.49. Schematic of hydrocarbon chemistry for the experimental condition with $CH_4/CO_2 = 1000$. L means the fraction of the reaction rate to the total photochemical loss rate of the reactant, while P means the fraction of the reaction rate to the total photochemical production rate of the product. For example, R3 accounts for 41% of the total photochemical loss rate of CH_4 and accounts for 22% of the total photochemical production rate of CH_3.

Table 1.3. Reaction rates of the primary reactions in molecule cm^{-3} s^{-1}.

	CH_4/CO_2 ratio	1000	1	0.2
R3	$CH_4 + h\nu \rightarrow CH_3 + H$	7.15×10^{14}	3.68×10^{14}	1.34×10^{14}
R4	$CH_4 + h\nu \rightarrow {}^1CH_2 + H + H$	9.60×10^{13}	4.94×10^{13}	1.79×10^{13}
R5	$CH_4 + h\nu \rightarrow {}^1CH_2 + H_2$	9.30×10^{14}	4.77×10^{14}	1.73×10^{14}
R12	$C_2H_6 + h\nu \rightarrow C_2H_4 + H_2$	1.62×10^{14}	8.75×10^{13}	3.05×10^{13}
R13	$C_2H_6 + h\nu \rightarrow C_2H_4 + H + H$	2.31×10^{14}	1.25×10^{14}	4.36×10^{13}
R14	$C_2H_6 + h\nu \rightarrow C_2H_2 + H_2 + H_2$	2.13×10^{14}	1.16×10^{14}	4.03×10^{13}
R29	$C_3H_8 + h\nu \rightarrow C_3H_6 + H_2$	1.39×10^{14}	6.00×10^{13}	7.80×10^{12}
R31	$C_3H_8 + h\nu \rightarrow C_2H_5 + CH_3$	1.26×10^{14}	5.45×10^{13}	7.05×10^{12}
R32	$C_3H_8 + h\nu \rightarrow C_2H_4 + CH_4$	7.85×10^{13}	3.40×10^{13}	4.43×10^{12}
R46	$C_6H_6 + h\nu \rightarrow C_6H_5 + H$	4.06×10^{13}	2.43×10^{13}	3.46×10^{12}
R47	$C_6H_6 + h\nu \rightarrow C_6H_4 + H_2$	9.20×10^{12}	5.50×10^{12}	7.85×10^{11}
R160	$H + C_2H_2 + M \rightarrow C_2H_3$	2.04×10^{14}	1.21×10^{14}	4.47×10^{13}
R163	$H + C_2H_4 + M \rightarrow C_2H_5$	6.65×10^{14}	3.38×10^{14}	1.05×10^{14}
R164	$H + C_2H_5 \rightarrow CH_3 + CH_3$	4.86×10^{14}	2.96×10^{14}	1.22×10^{14}
R172	$H + CH_3C_2H + M \rightarrow C_3H_5$	3.04×10^{14}	1.27×10^{14}	2.21×10^{13}
R173	$H + CH_2CCH_2 \rightarrow CH_3C_2H + H$	1.53×10^{14}	5.60×10^{13}	7.50×10^{12}
R177	$H + C_3H_5 \rightarrow CH_3C_2H + H_2$	1.69×10^{14}	7.50×10^{13}	1.37×10^{13}
R179	$H + C_3H_5 + M \rightarrow C_3H_6$	1.45×10^{14}	6.45×10^{13}	1.18×10^{13}
R180	$H + C_3H_6 \rightarrow CH_3 + C_2H_4$	2.16×10^{14}	9.85×10^{13}	1.87×10^{13}
R182	$H + C_3H_6 + M \rightarrow C_3H_7$	1.40×10^{14}	6.40×10^{13}	1.17×10^{13}
R195	$H + C_6H_4 + M \rightarrow C_6H_5$	1.54×10^{13}	9.90×10^{12}	1.72×10^{12}
R196	$H + C_6H_5 + M \rightarrow C_6H_6$	5.55×10^{13}	3.41×10^{13}	5.20×10^{12}
R221	${}^1CH_2 + H_2 \rightarrow CH_3 + H$	8.25×10^{14}	4.26×10^{14}	4.61×10^{14}
R238	${}^1CH_2 + C_2H_6 \rightarrow C_2H_5 + CH_3$	1.75×10^{14}	9.15×10^{13}	2.92×10^{13}
R260	${}^3CH_2 + C_2H_2 \rightarrow CH_2CCH_2$	1.45×10^{14}	4.80×10^{13}	4.88×10^{12}
R279	$CH_3 + CH_3 + M \rightarrow C_2H_6$	1.19×10^{15}	6.50×10^{14}	2.31×10^{14}
R283	$CH_3 + C_2H_3 \rightarrow C_3H_5 + H$	6.10×10^{13}	3.10×10^{13}	6.20×10^{12}
R284	$CH_3 + C_2H_3 + M \rightarrow C_3H_6$	5.75×10^{13}	2.94×10^{13}	5.85×10^{12}
R288	$CH_3 + C_2H_5 + M \rightarrow C_3H_8$	4.45×10^{14}	1.93×10^{14}	2.50×10^{13}
R299	$CH_3 + C_3H_7 + M \rightarrow C_4H_{10}$	7.10×10^{13}	3.00×10^{13}	2.95×10^{12}
R314	$C_2H + C_2H_2 \rightarrow C_4H_2 + H$	6.85×10^{12}	5.00×10^{12}	1.30×10^{12}
R365	$C_2H_3 + C_4H_2 \rightarrow C_6H_4 + H$	6.20×10^{12}	4.35×10^{12}	8.80×10^{11}
R515	$C_6H_5 + C_2H_2 \rightarrow SOOT + H$	1.69×10^{11}	5.55×10^{10}	9.95×10^{8}
R516	$C_6H_5 + C_2H_2 + M \rightarrow SOOT$	1.91×10^{11}	6.30×10^{10}	1.13×10^{9}
R517	$C_6H_5 + C_6H_5 \rightarrow SOOT + H$	6.65×10^{9}	2.35×10^{9}	2.69×10^{7}
R652	$O({}^3P) + C_2H_3 \rightarrow CH_2CO + H$	2.10×10^{8}	4.10×10^{11}	9.95×10^{11}

Table 1.4. Production or loss rates for some species in molecule cm^{-3} s^{-1}. These reaction rates are for pure photochemical production and loss rates, not including the influx and loss rate by pump. The species without "loss" or "production" are in equilibrium between photochemical production and loss and the contributions of the loss by pump are less than 1% to the total loss rate.

CH_4/CO_2 ratio	1000	1	0.2
$^1CH_2$	1.24×10^{15}	6.35×10^{14}	2.27×10^{14}
CH_3	3.31×10^{15}	1.79×10^{15}	6.55×10^{14}
CH_4 loss	1.93×10^{15}	1.01×10^{15}	3.69×10^{14}
C_2H_2 loss	4.98×10^{14}	2.69×10^{14}	8.15×10^{13}
C_2H_3	2.52×10^{14}	1.41×10^{14}	4.78×10^{13}
C_2H_4	8.40×10^{14}	4.50×10^{14}	1.43×10^{14}
C_2H_5	1.09×10^{15}	5.60×10^{14}	1.64×10^{14}
C_2H_6 loss	1.08×10^{15}	6.00×10^{14}	2.11×10^{14}
CH_2CCH_2	1.92×10^{14}	7.05×10^{13}	9.35×10^{12}
CH_3C_2H loss	3.48×10^{14}	1.46×10^{14}	2.43×10^{13}
C_3H_5	4.09×10^{14}	1.75×10^{14}	3.04×10^{13}
C_3H_6	3.77×10^{14}	1.72×10^{14}	3.13×10^{13}
C_3H_7	1.47×10^{14}	6.80×10^{13}	1.23×10^{13}
C_3H_8 loss	4.20×10^{14}	1.83×10^{14}	2.40×10^{13}
C_4H_2	7.20×10^{12}	5.40×10^{12}	1.59×10^{12}
C_4H_{10} loss	2.66×10^{13}	1.28×10^{13}	1.22×10^{12}
C_4H_{10} production	9.75×10^{13}	3.91×10^{13}	3.39×10^{12}
C_6H_4	1.54×10^{13}	9.90×10^{12}	1.72×10^{12}
C_6H_5	5.60×10^{13}	3.43×10^{13}	5.20×10^{12}
C_6H_6	5.75×10^{13}	3.48×10^{13}	5.20×10^{12}
SOOT production	3.66×10^{11}	1.21×10^{11}	2.15×10^{9}

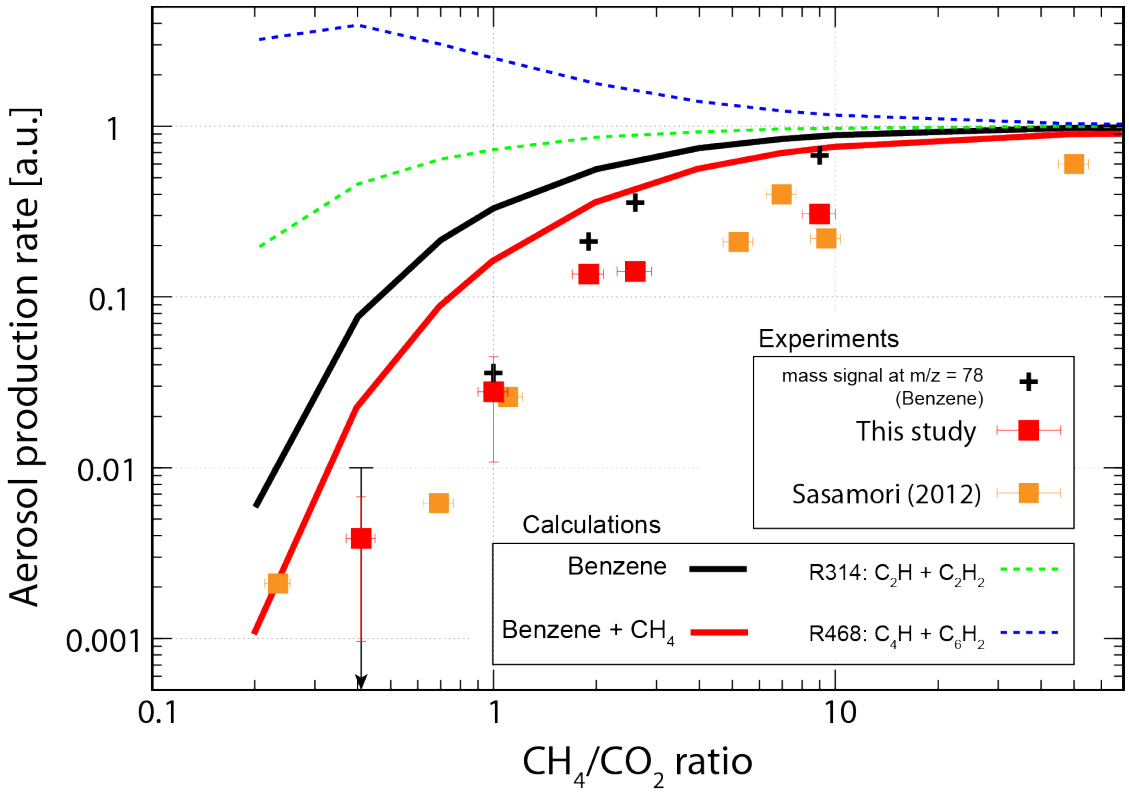

Figure 1.50. Aerosol production rates obtained by the experiments and reaction rates calculated by the one-box photochemical model. Experimental results are normalized to those using only CH_4 as reactant gas, while calculation results are normalized to the results at $CH_4/CO_2 = 1000$. "Benzene" is the sum of reaction rates of R515, 516 and R517. "Benzene + CH_4" is the product of "Benzene" and the methane mixing ratio. On the other hand, R314 and R468 are the typical reactions assumed to contribute aerosol production in previous photochemical models, showing poor agreement with the experimental results. Also shown is the QMS signal intensity at m/z = 78 when the steady-state normalized to the pure CH_4 experiment, which shows good agreement with the aerosol production rate observed in this experiment. Since the molecular mass of benzene is 78, QMS signal at m/z = 78 may represent the abundance of benzene gas. The black arrow at $CH_4/CO_2 = 0.4$ stands for the upper limit of the QMS signal at m/z = 78.

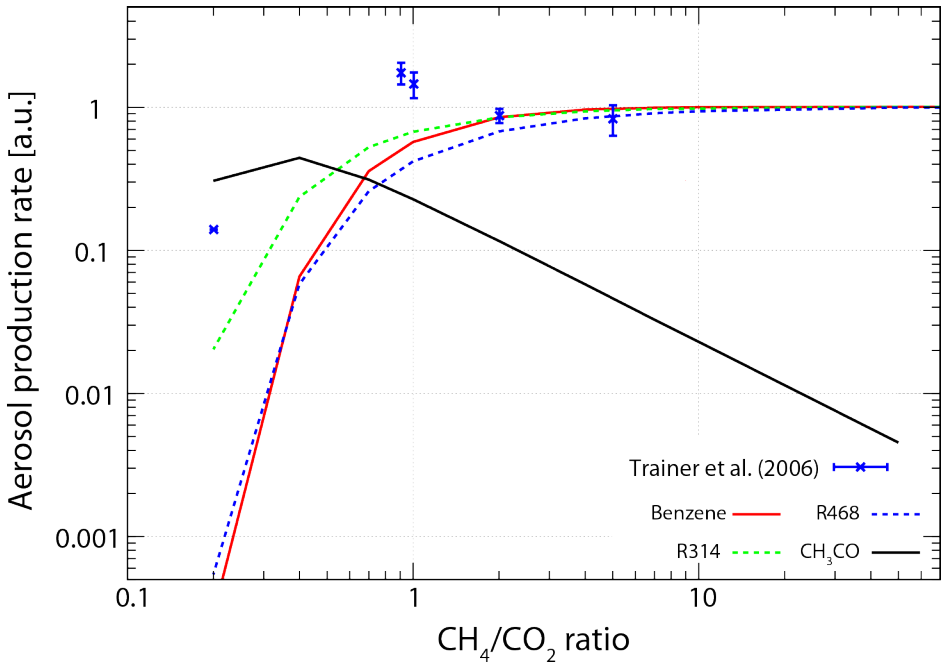

Figure 1.51. Aerosol production rates obtained by Trainer et al. (2006) and reaction rates calculated by our one-box photochemical model simulating their experimental conditions. Experimental results are normalized to those using only CH_4 as reactant gas, while calculation results are normalized to the results at $CH_4/CO_2 = 1000$. "Benzene" is the sum of reaction rates of R515, 516 and R517. Also shown is a scaled abundance of CH_3CO ([CH_3CO] in molecule cm^{-3} divided by 3×10^{10}).

Table 1.5. Photochemical calculation results at $CH_4/CO_2 = 0.2$, using the experimental conditions of this study and those of Trainer et al. (2006).

	This study	Trainer et al. (2006)
O_2/CH_4 [a]	2.77×10^{-5}	6.58×10^{-4}
$O(^3P)/CH_3$ [b]	0.538	6.16
C_2H_2 oxidation by O and OH [c]	35.3%	68.1%

[a] Ratio of O_2 abundance to CH_4 abundance after 10 hours UV irradiation. This represents a typical ratio between a major oxidizing gas and a major reducing gas.

[b] Ratio of $O(^3P)$ abundance to CH_3 abundance after 10 hours UV irradiation. This represents a typical ratio between a oxidizing radical and a reducing radical.

[c] Percentage of the C_2H_2 oxidation rate by O and OH radicals as compared to the total loss rate of C_2H_2.

1.5 Future work

Our results of photochemical calculations and gas analysis of the experiments show that benzene is the key parent molecule for the formation of aerosol particles (Figure 1.50). Although our results of mass spectra of the gas-phase products show the amount of benzene decreases with CH_4/CO_2 ratio of the initial gas mixture (Figure 1.50), its quantitative amount of production is not obtained in the present study. Furthermore, our results predict that the produced aerosols consist of polyaromatic hydrocarbons, given that benzene is the major building materials. The chemical structure of the aerosols, however, is not investigated.

In order to provide a further constraint of the aerosol production mechanism, gas chromatography-mass spectrometry (GC-MS) would be required to quantify the production of benzene in the gas-phase product (Thompson et al., 1991; Imanaka et al., 2004). Our results suggest that addition of gaseous benzene to the reactant gas mixture would yield higher aerosol production rate. In fact, Trainer et al. (2013) report that by adding 10 ppmv of benzene to 0.1% CH_4 in N_2, the aerosol production rate due to FUV irradiations is more than 100-fold compared with the same experiment without benzene in the initial gas mixture. These results strongly support our conclusions that benzene is the predominant parent molecule for aerosol formation. More systematic laboratory experiments and comparison with photochemical calculations are required to investigate the sensitivity of benzene concentration to aerosol, which is important to create a clearer view of the organic aerosol production by FUV irradiation.

It would be necessary to conduct infrared and Raman spectroscopy, which can identify the presence of aromatic rings and other functional groups, to investigate the chemical structure of the produced aerosols (Khare et al., 2002; Tran et al., 2003; Imanaka et al., 2004; Sekine et al., 2008a). Pyrolysis GCMS of aerosols would also provide information on the chemical structure of aerosols (Khare et al., 1984b; Ehrenfreund et al., 1995; Coll et al., 1999; Imanaka et al., 2004). Moreover, efficiency of incorporation of benzene into aerosols can be investigated quantitatively by a combination of isotopic labeling technique for benzene, i.e., $^{13}C_6H_6$, and isotopic analysis of carbon ($^{13}C/^{12}C$) in the produced aerosols. Elemental analyses of aerosol particles, including pyrolysis (Khare et al., 1984b; Ehrenfreund et al., 1995; Coll et al., 1999; Imanaka et al., 2004), X-ray photoelectron spectroscopy (XPS) (Tran et al., 2003) and secondary ion mass spectrometry (SIMS) (Imanaka et al., 2004; Sekine et al., 2008a), to investigate the C/H ratio, as well as C/O and C/N ratios, would be useful to provide further constraints on the aerosol production mechanism.

1.6 Conclusions

We have conducted laboratory experiments and photochemical calculations in order to discuss the parent molecules and chemical reactions that control the tholin production rate. We measured the dependences of tholin production rate on actinic UV flux and CH_4/CO_2 ratio. We found that the tholin production rate is a linear function of irradiated UV flux, which suggests that the tholin production is limited by polymerization reactions between intermediate products produced from the photochemistry of CH_4 (i.e., mechanism II), not by photolysis of the intermediate products (i.e., mechanism I). We also found that the tholin production rate decreases gradually with a decrease of CH_4/CO_2 ratio where CH_4/CO_2 ratio is greater than unity. On the other hand, the production rate decline dramatically as a decrease in CH_4/CO_2 ratio when the CH_4/CO_2 ratio become lower than unity. Our photochemical calculations show that the behavior of tholin production rate as a function of CH_4/CO_2 ratio is in a good agreement with those of polymerization of benzene. These results suggest that benzene is the key parent molecule that controls the tholin production. On the other hand, polymerization reactions of polyynes do not contribute remarkably to the tholin production, contrary to the assumptions of previous studies.

Chapter 2. Organic aerosol layers on Titan and early Earth: Influence on the radiation fields.

2.1 Introduction

Physical processes, the radiative transfer and microphysical processes, and chemical processes, photochemical and ion reactions, in planetary atmospheres are mutually dependent on each other. In particular, organic aerosols would be formed in CH_4-containing, reducing atmospheres via photochemical reactions (e.g., Yung et al, 1984; Wilson and Atreya, 2004; Lavvas et al., 2008a, b; Krasnopolsky 2009; Trainer et al., 2006; Pavlov et al., 2001), and would determine the atmospheric structure and surface temperature through the radiative transfer processes (e.g., McKay et al., 1989; Toon et al., 1992; Pavlov et al., 2001; Wolf and Toon, 2010). The atmospheric structure and radiative processes in turn would affect the efficiency of photochemical reactions. Thus, self-consistent coupling of the photochemistry, microphysics, and radiative transfer processes could provide significant implications to the climatic stability and evolution of both planets and satellites that have reducing atmospheres, such as Titan, early Earth and exoplanets (e.g., Pavlov et al., 2001; Lavvas et al., 2008a, b; Miller-Ricci Kempton et al., 2012). Many of the previous studies, however, discuss the physical and chemical processes independently due to a large uncertainty in the formation mechanism and parent molecules of organic aerosols in the atmospheres.

In Chapter 1, we investigate the formation mechanism and parent molecules of organic aerosol analogues, called tholin, based on both laboratory experiments and photochemical reaction models. We found that polymerization of aromatic hydrocarbons, benzene, is the reactions that control the formation of tholin under our experimental conditions. In this chapter, we calculate the formation of monomers of organic aerosols using a one-dimensional photochemical model based on the above experimental results. Then, the growth and coagulation of monomers in the atmosphere is calculated with a microphysical model. Finally, the self-consistent atmospheric composition and structure are obtained by coupling photochemical, microphysical, and radiative transfer models. Based on the results, we discuss the primary energy source for the formation organic aerosol layers in Titan's atmosphere. Furthermore, the climatic stability and the role of organic aerosols in early Earth's atmosphere are examined.

In Titan's atmosphere, the primary energy source for the formation organic aerosols remains poorly understood (see General Introduction). It has been suggested that the organic aerosols are produced by irradiations of solar UV light and high-energy electrons from Saturn's magnetosphere (e.g., Yung et al., 1984; Khare et al., 1984a; Wilson and Atreya, 2003; 2004; Lavvas et al., 2008a, b; Krasnopolsky 2009). Given that the aerosols formed by different energy sources would have different optical properties, determining the primary energy source is important for understanding not only the organic chemistry occurred in Titan's atmosphere but also the long term evolution and stability of the atmosphere and surface environments (see General Introduction). We

performed laboratory experiments using a UV lamp to determine the parent molecules and reactions that control tholin production by far UV (FUV) irradiations. In this chapter, we calculate the number density and profile of organic aerosol layers formed by solar FUV irradiations, using the self-consistent coupling model of photochemistry, microphysics, and radiative transfer processes. By comparing the obtained aerosol profiles formed by EUV with the observations of aerosols in Titan's atmosphere, we discuss whether solar EUV can account for the observations.

Why early Earth was habitable remains debated for many years (Pollack, 1979; 1991; Crowley, 1983; Barron, 1984; Kasting and Grinspoon, 1991; Kasting 1993; Rampino and Caldeira, 1994; Nisbet and Sleep, 2001; Kasting and Catling, 2003; Zahnle et al., 2007; Güdel, 2007; Shaw, 2008; Nisbet and Fowler, 2011; Feulner et al., 2012). In order to account for, so called, the early faint Sun paradox (see General Introduction), an enhanced greenhouse effect would be needed (e.g., Sagan and Mullen, 1972; Owen et al., 1979; Haqq-Misra et al., 2008). Ammonia has been suggested as a solution to the early faint Sun paradox (Sagan and Mullen, 1972). Adding only a trace level of ammonia (~10 ppmv) to the atmosphere could have kept an early Earth from freezing (Sagan and Mullen, 1972; Kuhn and Atreya, 1979). On early Earth, ammonia could be supplied into the atmosphere by the hydrolysis of HCN produced by photochemical reactions of N_2 and CH_4 (Zahnle, 1986; Tian et al., 2011). Photochemical models, however, suggest that ammonia is easily dissociated by solar UV light. Without shielding of UV light, ammonia supply rates could not have supported an ammonia mixing ratio above 10^{-8} (Kasting, 1982). A thick CO_2 atmosphere has been suggested to solve the early faint sun paradox (Owen et al., 1979). The previous studies suggest that at least 0.1 bar of CO_2 partial pressures are necessary to keep the surface temperature from freezing at >2.5 Gyr ago (Owen et al., 1979; Kasting et al., 1984; Kiehl and Dickinson, 1987; von Paris et al., 2008). Geochemical records, however, suggest that the CO_2 partial pressures would have been low (i.e., ~0.003–0.03 bar), insufficient to support warm environments on early Earth at ~3.5–2.5 Gyr ago (Rye et al., 1995; Sheldon, 2006; Driese et al., 2011).

In order to account for the early faint Sun paradox, Sagan and Chyba (1997) propose that optically thick organic haze layers yield a strong indirect greenhouse effect on an early Earth by protecting ammonia. Before the rise of atmospheric O_2 at ~2.5 Gyr ago, biological supply of CH_4 would have resulted in high CH_4 mixing ratio (e.g., the order of 10^{-3} bar) in the atmosphere (Hunten, 1973b; Walker, 1977; Holland 1978; Kasting and Brown, 1998). On the other hand, atmospheric CO_2 levels would have been comparable to that of CH_4 (on the order of 10^{-3}–10^{-2} bar) (Rye et al., 1995; Sheldon, 2006; Driese et al., 2011). In such an atmosphere, organic aerosol production would have been driven by solar FUV irradiations (Sagan and Chyba, 1997; Pavlov et al., 2001; Trainer et al., 2006; Wolf and Toon, 2010). The organic aerosol layers could have possessed an UV shielding effect of organic aerosol layers which protects

ultraviolet-labile greenhouse gases, such as ammonia, from UV photolysis (Sagan and Chyba, 1997). On the other hand, the other radiative transfer model shows that, the organic aerosol layer also has a strong anti-greenhouse effect due to its optical thickness at the visible wavelengths (Pavlov et al., 2001), offsetting the greenhouse effects of methane, ethane and carbon dioxide (Haqq-Misra et al., 2008). As described in General Introduction, the production rates of organic aerosols in a CH_4-CO_2-containing atmosphere are largely uncertain. This results in a large uncertainty to estimate the indirect greenhouse and anti-greenhouse effect of organic aerosol layers.

In Chapter 1, we measured the tholin production rate for a wide range of CH_4/CO_2 ratio in the laboratory experiments. Our results show that the tholin production rate drastically decreases at $CH_4/CO_2 < 1$ with increasing CO_2 concentration. We found that the behavior of tholin production as a function of CH_4/CO_2 ratio is good agreement with the polymerization rates of benzene in the gas phase, suggesting that these reactions control the tholin production in gas mixtures of CH_4 and CO_2. In this chapter, we calculate the vertical profile of production of monomers for wide range of CH_4/CO_2 ratio of the atmosphere based on our findings that polymerization of benzene results in the formation of aerosol monomers. Then, we evaluate the indirect greenhouse and anti-greenhouse effect for a given atmospheric composition by calculating both the growth and coagulation of monomers and radiative transfer of solar light.

In the section 2.2, we describe numerical scheme and validation of a one-dimensional photochemical model developed by the present study. In the section 2.3, the microphysical and radiative transfer models used in the present study are described. Finally, we investigate the influence of organic aerosols on the radiative transfer process in Titan and early Earth using the coupled photochemical/ microphysical/radiative transfer model in the section 2.4.

2.2 Development of a one dimensional photochemical model

2.2.1 General equations of a photochemical model

We have developed a one-dimensional photochemical model of planetary atmospheres (e.g., Toublanc et al., 1995; Wilson and Atreya, 2004; Lavvas et al., 2008a, b). Our photochemical model describes the time evolution of number density of gas specie as well as its equilibrium abundance. The model includes, eddy and molecular diffusion, condensation of gas, escape or influx from the top of atmosphere, degassing from the surface and deposition to the surface. The one-dimensional time dependent continuity equation in spherical geometry for atmospheric constituent i at altitude j is described as (e.g., Toublanc et al., 1995; Wilson and Atreya, 2004; Lavvas et al., 2008a, b),

$$\frac{\partial n_{i,j}}{\partial t} = -\frac{1}{r^2}\frac{\partial\left(r^2\Phi_{i,j}\right)}{\partial r} + P_{i,j} - L_{i,j} - L^c_{i,j} \qquad (2.1)$$

where $n_{i,j}$ is the number density of specie i at altitude j, $\Phi_{i,j}$ is the vertical diffusive flux, $P_{i,j}$ and $L_{i,j}$ are production (photochemistry) and loss (photochemistry, surface deposition, escape) term, respectively. $L^c_{i,j}$ is the condensation loss term. The vertical flux can be written as (Banks and Kockarts, 1973),

$$\begin{aligned}\Phi_{i,j} &= -D_{i,j}\left[\frac{1}{n_{i,j}}\frac{\partial n_{i,j}}{\partial r} + \frac{1}{H_{i,j}} + \left(1+\alpha_{T,i}\right)\frac{1}{T_j}\frac{\partial T_j}{\partial r}\right]n_{i,j} \\ &\quad - K_j\left[\frac{1}{n_{i,j}}\frac{\partial n_{i,j}}{\partial r} + \frac{1}{H_{i,j}} + \frac{1}{T_j}\frac{\partial T_j}{\partial r}\right]n_{i,j}\end{aligned} \qquad (2.2)$$

where $D_{i,j}$ and K_j are the molecular and eddy diffusion coefficient, respectively. H_j is the mean atmospheric scale height at altitude j, and $H_{i,j}$ is also the atmospheric scale height at each altitude j but for each specie i. $a_{T,i}$ is the thermal diffusion coefficient for specie i and T_j is the temperature at altitude j. This system of equations is finite differenced and solved as described in the section 2.2.2. As well as many previous photochemical models, our model contains several physical and chemical processes in the planetary atmosphere that is photodissociation, chemical production and loss, vertical transport by eddy and molecular diffusion, loss due to condensation, surface deposition and escape at the top of atmosphere. A photolysis rate J_i for ith specie at altitude z is calculated as follows (e.g., Jacob, 1999):

$$J_i(z) = \int_{\lambda} q_i(\lambda)\sigma_i(\lambda)\, I(\lambda, z)d\lambda \qquad (2.3)$$

where q_i is the quantum yield, σ_i is the absorption cross section and I is the actinic flux, which is the number of photons crossing the unit horizontal area per unit time from any direction. The actinic flux $I(\lambda, z)$ at altitude z is absorbed by gas species as follows (e.g., Jacob, 1999),

$$I(\lambda, z) = I(\lambda, z_{\mathrm{TOA}})\exp\left(-\frac{\delta(\lambda, z)}{\cos\theta}\right) \qquad (2.4)$$

where θ is the solar zenith angle. $\delta(\lambda, z)$ is the optical depth of the atmosphere above altitude z calculated by

$$\delta(\lambda, z) = \int_{z}^{z_{\mathrm{TOA}}} \sum_{i=1}^{P} \sigma_i(\lambda) n_i(z')dz' \qquad (2.5)$$

where p indicates the number of gas species that influence the intensity of UV light.

In a low-temperature region in the atmosphere, some gases may condense when their number densities $n_{i,j}$ exceed their saturated number densities, $n^{s}_{i,j}$ at the corresponding altitude j. There are a few expressions to describe the removal rate by the condensation process. Yung et al. (1984) and Wilson and Atreya (2004) used a simple scheme when the saturation ratio, $S_{i,j} = n_{i,j} / n^{s}_{i,j}$, exceeds unity.

$$L^{c}_{i,j} = A\frac{S_{i,j}}{1 + S_{i,j}}, \quad S_{i,j} > 1 \qquad (2.6)$$

where A is a constant in units of s^{-1}. Lavvas et al. (2008a,b) suggest the following expression for the condensation loss term in order to avoid oscillations of the solution, and to account for the heterogeneous nucleation process which could lead to rapid loss of the condensing species.

$$L^{c}_{i,j} = \mathrm{A}\left(S_{i,j} - 1\right)\frac{\exp\left(-0.5/\left(\ln\left(S_{i,j} + 1\right)\right)^{2}\right)}{\left(\ln\left(S_{i,j} + 1\right)\right)^{2}}, \quad S_{i,j} > 1 \qquad (2.7)$$

Krasnopolsky (2009) found that the loss term of Lavvas et al. (2008a,b) gives a similar result with the following expression.

$$L_{i,j}^{c} = \mathrm{A}\ln S_{i,j}, \quad S_{i,j} > 1 \qquad (2.8)$$

We used the equation (2.8) for the condensation term in (2.1) because of its mathematical simplicity, although we have found that the use of the other two expressions, (2.6) and (2.7), does not change the results significantly by comparing the results using those of (2.8). We chose $A = 10^{-7}$ s^{-1} according to Krasnopolsky (2009), however, the choice of coefficient A does not affect the results, or equilibrium abundances of gas species significantly. For early Earth calculations in section 2.2.4 and section 2.4.3, A is set to be 10^{-4} s^{-1}.

2.2.2 Finite differencing and matrix solver

The vertical flux in (2.1) can be written as,

$$\Phi_{i,j} = C_{1,i,j} n_{i,j} + C_{2,i,j} \frac{\partial n_{i,j}}{\partial r} \qquad (2.9)$$

where $C_{1,i,j}$ and $C_{2,i,j}$ can be written as follows:

$$C_{1,i,j} = -\left[\left(\frac{D_{i,j}}{H_{i,j}} + \frac{K_j}{H_j}\right) + \left(D_{i,j} + K_j\right)\frac{1}{T_j}\frac{\partial T_j}{\partial r} + \frac{\alpha_{\mathrm{T},i} D_{i,j}}{T_j}\frac{\partial T_j}{\partial r}\right] \qquad (2.10)$$

$$C_{2,i,j} = -\left(D_{i,j} + K_j\right) \qquad (2.11)$$

The divergence of the diffusion flux in (2.1) can be discretized using (2.9). Thus, the time evolution of the number density is described as,

$$\frac{\Delta n_{i,j}}{\Delta t} = -\frac{1}{r_j^2}\frac{r_{j+1/2}^2 \Phi_{i,j+1/2} - r_{j-1/2}^2 \Phi_{i,j-1/2}}{\Delta r_j} + P_{i,j} - L_{i,j} - L_{i,j}^{c} \qquad (2.12)$$

where

$$r_{j+1/2} = r_j + \frac{1}{2}\Delta r_j\,,\quad r_{j-1/2} = r_j - \frac{1}{2}\Delta r_j \tag{2.13}$$

$$\Phi_{i,j+1/2} = \frac{\Phi_{i,j} + \Phi_{i,j+1}}{2}\,,\quad \Phi_{i,j-1/2} = \frac{\Phi_{i,j} + \Phi_{i,j-1}}{2} \tag{2.14}$$

Equation (2.14) denotes the upper and lower boundary fluxes of the *j*th layer. Applying (2.9) to (2.12), we can obtain as follows;

$$\begin{aligned}\frac{\Delta n_{i,j}}{\Delta t} &= -\frac{1}{r_j^2}\frac{1}{\Delta r_j}\Bigg[r_{j+1/2}^2\left(C_{1,i,j+1/2}\,n_{i,j+1/2} + C_{2,i,j+1/2}\frac{\partial n_{i,j+1/2}}{\partial r}\right) \\ &\quad - r_{j-1/2}^2\left(C_{1,i,j-1/2}\,n_{i,j-1/2} + C_{2,i,j-1/2}\frac{\partial n_{i,j-1/2}}{\partial r}\right)\Bigg] \\ &\quad + P_{i,j} - L_{i,j} - L_{i,j}^c\end{aligned} \tag{2.15}$$

where

$$\mathrm{C}_{1,i,j+1/2} = \frac{\mathrm{C}_{1,i,j} + \mathrm{C}_{1,i,j+1}}{2}\,,\quad \mathrm{C}_{1,i,j-1/2} = \frac{\mathrm{C}_{1,i,j} + \mathrm{C}_{1,i,j-1}}{2} \tag{2.16}$$

$$\mathrm{C}_{2,i,j+1/2} = \frac{\mathrm{C}_{2,i,j} + \mathrm{C}_{2,i,j+1}}{2}\,,\quad \mathrm{C}_{2,i,j-1/2} = \frac{\mathrm{C}_{2,i,j} + \mathrm{C}_{2,i,j-1}}{2} \tag{2.17}$$

$$n_{i,j+1/2} = \frac{n_{i,j} + n_{i,j+1}}{2}\,,\quad n_{i,j-1/2} = \frac{n_{i,j} + n_{i,j-1}}{2} \tag{2.18}$$

$$\frac{\partial n_{i,j+1/2}}{\partial r} = \frac{n_{i,j+1} - n_{i,j}}{\Delta r_{j+1/2}}\,,\quad \frac{\partial n_{i,j-1/2}}{\partial r} = \frac{n_{i,j} - n_{i,j-1}}{\Delta r_{j-1/2}} \tag{2.19}$$

The central difference method is used to spatially discretize the above quantities. The atmosphere is divided into J layers of equal thickness Δr_j.

$$\Delta r_{j+1/2} = \frac{\Delta r_j + \Delta r_{j+1}}{2} = \Delta r_j\,,\quad \Delta r_{j-1/2} = \frac{\Delta r_j + \Delta r_{j-1}}{2} = \Delta r_j \tag{2.20}$$

Applying (2.18) - (2.20) to the equation (2.15), we can obtain a compact form of

(2.15) as,

$$\frac{\partial n_{i,j}}{\partial t} = \alpha_{i,j} n_{i,j-1} + \beta_{i,j} n_{i,j} + \gamma_{i,j} n_{i,j+1} + P_{i,j} - L_{i,j} - L^c_{i,j} \qquad (2.21)$$

where

$$\alpha_{i,j} = -\left(\frac{r_{j-1/2}}{r_j}\right)^2 \frac{1}{\Delta r_j}\left(-\frac{\mathrm{C}_{1,i,j-1/2}}{2} + \frac{\mathrm{C}_{2,i,j-1/2}}{\Delta r_j}\right) \qquad (2.22)$$

$$\begin{aligned}\beta_{i,j} &= -\frac{1}{r_j^2}\frac{1}{\Delta r_j}\left(\frac{1}{2} r_{j+1/2}^2 \mathrm{C}_{1,i,j+1/2} - \frac{1}{2} r_{j-1/2}^2 \mathrm{C}_{1,i,j-1/2}\right. \\ &\left. - \frac{1}{\Delta r_j} r_{j+1/2}^2 \mathrm{C}_{2,i,j+1/2} - \frac{1}{\Delta r_j} r_{j-1/2}^2 \mathrm{C}_{2,i,j-1/2}\right)\end{aligned} \qquad (2.23)$$

$$\gamma_{i,j} = -\left(\frac{r_{j+1/2}}{r_j}\right)^2 \frac{1}{\Delta r_j}\left(\frac{\mathrm{C}_{1,i,j+1/2}}{2} + \frac{\mathrm{C}_{2,i,j+1/2}}{\Delta r_j}\right) \qquad (2.24)$$

At the upper and lower boundaries, we can obtain general forms for the continuity equation including inward/outward flux as follows;
At the top of atmosphere for $j = J$, the equation (2.12) is written as,

$$\begin{aligned}\frac{\Delta n_{i,J}}{\Delta t} &= -\frac{1}{r_J^2}\frac{r_{J+1/2}^2 \Phi_{i,J+1/2} - r_{J-1/2}^2 \Phi_{i,J-1/2}}{\Delta r_J} \\ &+ P_{i,J} - L_{i,J} - L^c_{i,J}\end{aligned} \qquad (2.25)$$

where $\Phi_{i,J+1/2}$ is the boundary flux for the *i*th specie at the top of atmosphere. The above equation can be written in a similar form with (2.21) as,

$$
\begin{aligned}
&\frac{\Delta n_{i,J}}{\Delta t} \\
&= \left(\frac{r_{J+1/2}}{r_J}\right)^2 \frac{1}{\Delta r_J}\Big(C_{1,i,J-1/2}\, n_{i,J-1/2} \\
&+ C_{2,i,J-1/2}\frac{\partial n_{i,J-1/2}}{\partial r}\Big) - \left(\frac{r_{J+1/2}}{r_J}\right)^2 \frac{1}{\Delta r_J}\Phi_{i,J+1/2} \\
&\qquad + P_{i,J} - L_{i,J} - L^c_{i,J} \\
&= \left(\frac{r_{J+1/2}}{r_J}\right)^2 \frac{1}{\Delta r_J}\left[C_{1,i,J-1/2}\frac{n_{i,J-1}+n_{i,J}}{2}\right. \\
&\left. + C_{2,i,J-1/2}\frac{n_{i,J}-n_{i,J-1}}{\Delta r_J}\right] - \left(\frac{r_{J+1/2}}{r_J}\right)^2 \frac{1}{\Delta r_J}\Phi_{i,J+1/2} \\
&\qquad + P_{i,J} - L_{i,J} - L^c_{i,J} \\
&= \alpha_{i,J} n_{i,J-1} + \beta_{i,J} n_{i,J} - \left(\frac{r_{J+1/2}}{r_J}\right)^2 \frac{1}{\Delta r_J}\Phi_{i,J+1/2} \\
&\qquad + P_{i,J} - L_{i,J} - L^c_{i,J}
\end{aligned}
\qquad (2.26)
$$

where

$$
\alpha_{i,J} = \left(\frac{r_{J-1/2}}{r_J}\right)^2 \frac{1}{\Delta r_J}\left(\frac{C_{1,i,J-1/2}}{2} - \frac{C_{2,i,J-1/2}}{\Delta r_J}\right) \qquad (2.27)
$$

$$
\beta_{i,J} = \left(\frac{r_{J-1/2}}{r_J}\right)^2 \frac{1}{\Delta r_j}\left(\frac{C_{1,i,J-1/2}}{2} + \frac{C_{2,i,J-1/2}}{\Delta r_J}\right) \qquad (2.28)
$$

If there is no boundary flux, the equation (2.26) becomes as follows,

$$
\frac{\Delta n_{i,J}}{\Delta t} = \alpha_{i,J} n_{i,J-1} + \beta_{i,J} n_{i,J} + P_{i,J} - L_{i,J} - L^c_{i,J} \qquad (2.29)
$$

Continuity equations at the surface can be obtained by the similar derivation to that of the top of atmosphere, that is,

$$\frac{\Delta n_{i,1}}{\Delta t} = \beta_{i,1} n_{i,1} + \gamma_{i,1} n_{i,2} - \left(\frac{r_{1/2}}{r_1}\right)^2 \frac{1}{\Delta r_1} \Phi_{i,1/2} + P_{i,1} - L_{i,1} - L_{i,1}^c \qquad (2.30)$$

where

$$\beta_{i,1} = -\left(\frac{r_{3/2}}{r_1}\right)^2 \frac{1}{\Delta r_1}\left(\frac{\mathrm{C}_{1,i,3/2}}{2} - \frac{\mathrm{C}_{2,i,3/2}}{\Delta r_1}\right) \qquad (2.31)$$

$$\gamma_{i,1} = -\left(\frac{r_{3/2}}{r_1}\right)^2 \frac{1}{\Delta r_1}\left(\frac{\mathrm{C}_{1,i,3/2}}{2} + \frac{\mathrm{C}_{2,i,3/2}}{\Delta r_1}\right) \qquad (2.32)$$

The differential equations (2.21) contain $IJ = I \times J$ nonlinear equations. These nonlinear equations are stiff because of the great variety of the characteristic time scale of the number densities of each species (e.g., Toublanc et al., 1995). To solve this set of nonlinear equations, the set is calculated as following procedure:
First, the continuity equations (2.21) are written as,

$$\frac{\partial n_{i,j}}{\partial t} = H\left(n_{1,j}, n_{2,j}, n_{3,j}, \ldots, n_{i,j}, \ldots, n_{I,j};\ n_{i,j-1}\ ;\ n_{i,j+1}; t\right) \qquad (2.33)$$

with

$$H = \alpha_{i,j} n_{i,j-1} + \beta_{i,j} n_{i,j} + \gamma_{i,j} n_{i,j+1} + P_{i,j} - L_{i,j} - L_{i,j}^c \qquad (2.34)$$

Then all the number density $n_{i,j}$ is compiled into a vector $\boldsymbol{n}$ of which dimension is $IJ = I \times J$ and the species are numbered from the surface to the top of atmosphere as,

$$\boldsymbol{n}(t) = \left\{n_{1,1}, n_{1,2}, \ldots, n_{1,J}, n_{2,1}, n_{2,2} \ldots, n_{2,J}, \ldots, n_{I,1}, n_{I,2}, \ldots, n_{I,J}\right\} \qquad (2.35)$$

Since each number density is a function of time, the vector $\boldsymbol{n}$ is also a function of time. The set of continuity equations are written as follows.

$$\frac{\partial \boldsymbol{n}(t)}{\partial t} = H\left(\boldsymbol{n}(t)\right) \qquad (2.36)$$

In order to solve the set of equations, we used the Crank-Nicholson method, which is a

useful implicit method for solving stiff equations and gives second-order convergence in time (e.g., Toublanc et al., 1995). Applying the Crank-Nicholson method to equation (2.36), we obtain,

$$\frac{\boldsymbol{n}(t_{m+1}) - \boldsymbol{n}(t_m)}{\Delta t_m} = \frac{H\big(\boldsymbol{n}(t_{m+1})\big) + H\big(\boldsymbol{n}(t_m)\big)}{2} \qquad (2.37)$$

where m is the time step at a time t_m and $m + 1$ is the next time step. Equation (2.37) can be linearized as,

$$F\big(\boldsymbol{n}(t_{m+1})\big) = \frac{\boldsymbol{n}(t_{m+1}) - \boldsymbol{n}(t_m)}{\Delta t_m} - \frac{H\big(\boldsymbol{n}(t_{m+1})\big) + H\big(\boldsymbol{n}(t_m)\big)}{2} = 0 \qquad (2.38)$$

In order to calculate $\boldsymbol{n}(t_{m+1})$, the Newton-Raphson method was used as follows:
First, we consider a certain number density $\boldsymbol{n}_1(t_{m+1})$ as an approximate solution of the equation (2.38). Then, the equation was approximated by first-order Taylor series in a neighborhood of $\boldsymbol{n}_1(t_{m+1})$ as,

$$F\big(\boldsymbol{n}(t_{m+1})\big) = F\big(\boldsymbol{n}_1(t_{m+1})\big) + \frac{\partial F\big(\boldsymbol{n}_1(t_{m+1})\big)}{\partial \boldsymbol{n}_1(t_{m+1})} d\boldsymbol{n}_1(t_{m+1}) = 0 \qquad (2.39)$$

where $\partial F\big(\boldsymbol{n}_1(t_{m+1})\big)/\partial \boldsymbol{n}_1(t_{m+1})$ is the jacobian matrix and $d\boldsymbol{n}_1(t_{m+1})$ is calculated by solving the following system of linear equations.

$$\frac{\partial F\big(\boldsymbol{n}_1(t_{m+1})\big)}{\partial \boldsymbol{n}_1(t_{m+1})} d\boldsymbol{n}_1(t_{m+1}) = -F\big(\boldsymbol{n}_1(t_{m+1})\big) \qquad (2.40)$$

By substituting (2.38) into (2.40), we obtain a detailed description of the equation (2.40),

$$\left[\frac{1}{\Delta t_m} - \frac{1}{2}\frac{\partial H\big(\boldsymbol{n}_1(t_{m+1})\big)}{\partial \boldsymbol{n}_1(t_{m+1})}\right] d\boldsymbol{n}_1(t_{m+1}) = -\frac{\boldsymbol{n}(t_{m+1}) - \boldsymbol{n}(t_m)}{\Delta t_m} + \frac{H\big(\boldsymbol{n}_1(t_{m+1})\big) + H\big(\boldsymbol{n}(t_m)\big)}{2} \qquad (2.41)$$

This system of IJ linear equations becomes a band matrix and we solve the matrix by LU decomposition method with partial pivoting. $d\boldsymbol{n}_1(t_{m+1})$ is calculated as,

$$d\boldsymbol{n}_1(t_{m+1}) = \boldsymbol{n}_2(t_{m+1}) - \boldsymbol{n}_1(t_{m+1}) \quad (2.42)$$

where $\boldsymbol{n}_2(t_{m+1})$ is the solution after one iteration. Thus, we can obtain the approximate solution after one iteration as,

$$\boldsymbol{n}_2(t_{m+1}) = \boldsymbol{n}_1(t_{m+1}) + d\boldsymbol{n}_1(t_{m+1}) \quad (2.43)$$

By replacing $\boldsymbol{n}_1(t_{m+1})$ with $\boldsymbol{n}_2(t_{m+1})$ and repeating the above iteration process, the approximate solution $\boldsymbol{n}_k(t_{m+1})$ after k iterations approaches the true solution. We repeat these iteration calculations until the solution converge and the errors are negligible. The convergence condition is satisfied when the following inequalities are hold for all species and all altitudes.

$$\left|\frac{d\boldsymbol{n}_k(t_{m+1})}{\boldsymbol{n}_k(t_{m+1})}\right| < \varepsilon \quad (2.44)$$

We set ε to be 10^{-4} in our model.

The photochemical model we developed can be basically applied to a wide variety of neutral photochemistry in planetary atmospheres by considering a proper chemical reaction set. We have applied our model to Titan's atmosphere on present-day and an early Earth atmosphere in order to check the validity of the photochemical model by comparing with results of previous studies (Toublanc et al., 1995; Krasnopolsky, 2009; Pavlov et al., 2001).

2.2.3 Validation of the photochemical model based on Titan's atmosphere

There are several one-dimensional photochemical models for the current Titan's atmosphere (Yung et al., 1984; Yung 1987; Toublanc et al., 1995; Lara et al., 1996; Wilson and Atreya, 2004; Lavvas et al., 2008a, b; Krasnopolsky, 2009; 2010). Although the neutral photochemistry in Titan's atmosphere was studied before the arrival of Voyager I and II (Strobel, 1974; Allen et al., 1980), the first detailed photochemical model was developed by Yung et al. (1984) with further improvements by Yung (1987) to account for the gas abundances observed by the Voyagers. Their model described the basic photochemical processes of simple hydrocarbons and nitriles occurring in Titan's lower and middle atmosphere. Toublanc et al. (1995) developed a photochemical model based on more recent experimental data and analysis of observations provided by the Voyager spacecraft and ground-based observations. Their model used a Monte Carlo calculation for the attenuation of solar radiation through the stratospheric atmospheric layer, although their results of the attenuation of solar radiation were significantly different with those of other later photochemical models (Wilson and Atreya, 2004; Krasnopolsky, 2009). Lara et al. (1996) included water influx from the top of atmosphere due to ablation of microcomets and also considered the dissociation of molecular nitrogen in the lower atmosphere by galactic cosmic ray. Wilson and Atreya (2004), which is the last model developed before the arrival of Cassini to Titan, includes ionospheric chemistry in Titan's upper atmosphere. After the arrival of Cassini, Lavvas et al. (2008a, 2008b) coupled Titan's neutral photochemical model with radiative transfer model and microphysical model of organic haze. However, their photochemical scheme does not include oxygen species, and there are significant uncertainty in aerosol production processes (see General Introduction). Krasnopolsky (2009, 2010) developed a coupled neutral and ion chemistry for Titan's atmosphere in order to account for the significant production of high-molecular-weight hydrocarbons in the upper atmosphere, observed by the Cassini spacecraft.

We have developed a one dimensional photochemical model for current Titan's atmosphere. Our chemical scheme is identical to that of Toublanc et al. (1995). We chose their chemical scheme because they did not group the reactive species together (i.e., the family method) but solve for each species individually. The family method generally improves the numerical stability and results faster computation time. It needs, however, more complex calculation code and elaborate treatment of the choice of species and chemical reactions considered. Our model contains H, C, N and O chemistry with 249 reactions and 62 species. The chemical species calculated are listed in Table 2.1. We consider both ground-state and excited-state for some of the important radicals: $^3CH_2$, C_4H_2, N(^{4}S), O(^{3}P) are the ground-state species, while $^1CH_2$, $C_4H_2^*$,

$N(^2D)$, $O(^1D)$ are the excited-state species. Condensable species are bold in Table 2.1. Most of the saturated vapor pressures are from Krasnopolsky (2009), while the saturated vapor pressure of CH_3C_2H is from Lara et al. (1996) and those of CH_2CCH_2, CH_3OH, H_2CO and CH_2CO are from NIST Chemistry Webbook (CH_2CCH_2, allene: Stull (1947), CH_3OH, methyl alcohol: Ambrose and Sprake (1970), H_2CO, formaldehyde: Spence and Wild (1935), CH_2CO, ketene: Reuben (1969)). Based on Toublanc et al. (1995), the model atmosphere extends from the surface to 1250 km with equally divided 126 layers, thus each atmospheric layer has a thickness of 10 km. The altitude profiles of pressure and temperature used are shown in Figure 2.1 and Figure 2.2, respectively. The pressure profile was that of the recommended model of Yelle et al. (1997) at the beginning of the calculation and then calculated based on hydrostatic equilibrium. The eddy diffusion coefficient determines the vertical transport in the lower and middle atmosphere. There is a wide variety of eddy diffusion profiles used among previous photochemical models. We used the eddy diffusion coefficient profile given by Yelle et al. (2008), which is based upon recent Cassini's observation of vertical profiles of CH_4 and ^{40}Ar abundances in the upper atmosphere, although the tropospheric value was fixed according to the previous photochemical models (Yung et al., 1984; Toublanc et al., 1995; Wilson and Atreya, 2004; Lavvas et al., 2008a, 2008b; Krasnopolsky, 2009) (Figure 2.3). The molecular diffusion coefficients for some of the species were calculated with their binary diffusion coefficients experimentally measured. Their calculations are based on Lavvas et al. (2008a):

$$D_{i,j} = A_i \frac{T^s}{M_j} \qquad (2.45)$$

where A_i and s are parameters given in Table 2.2 and M_j is the total number density at altitude j. The altitude profiles of molecular diffusion coefficients calculated are shown in Figure 2.3. For the rest of the species whose binary coefficients are unknown, the molecular diffusion coefficients are calculated based on Banks and Kockarts (1973):

$$D_{i,j} = 1.52 \times 18^{18} \left(\frac{1}{m_i} + \frac{1}{m_j}\right)^{1/2} \frac{T^{1/2}}{M_j} \quad \mathrm{cm^2 s^{-1}} \qquad (2.46)$$

where m_i is the molecular weight of ith specie and m_j is the mean molecular weight at altitude j. With the above eddy and molecular eddy diffusion coefficients, the homopause which is the boundary between homosphere and heterosphere locates around 750 km in height as shown in Figure 2.3. Below the homopause (i.e., homosphere), vertical transport is governed by eddy diffusion and the gas species are homogeneously mixed regardless of their molecular weights. On the other hand, above

the homopause (i.e., heterosphere), molecular diffusion dominates the vertical transport and each gas specie obey its hydrostatic equilibrium profile depending on the scale height (i.e., molecular weight). Thus diffusive equilibrium or gravity separation will occur in the heterosphere. Figure 2.4 shows the unattenuated solar ultraviolet flux used in our photochemical model. The data are from Mount and Rottman (1983), suitable for moderate solar activity, and rescaled to the Sun-Titan distance in the photochemical model. The solar zenith angle is set to be 30°, which is equivalent to a global daytime average condition for optically thick absorption. The wavelength range of UV radiation field is from 115 to 315 nm with a wavelength resolution of 1 nm. Photodissociation is included for 28 species, i.e., CH_3, CH_4, C_2H_2, C_2H_4, C_2H_6, C_3H_3, CH_2CCH_2, CH_3C_2H, C_3H_6, C_3H_8, C_4H_2, C_4H_4, C_4H_6, C_6H_2, C_8H_2, HCN, HC_3N, C_2N_2, C_4N_2, H_2O, CO, HCO, H_2CO, CH_2CO, CO_2, CH_3CN, C_2H_3CN and N_2. Their references of the absorption cross sections are shown in Table 2.3. The absorption cross sections shown in the references are interpolated or extrapolated to suite for the wavelength resolution we used. When there are a few cross sections available at different temperatures, we used the ones obtained at the lowest temperature, in order to simulate low-temperature conditions in Titan's atmosphere. In the lower atmosphere, the solar UV radiation field is attenuated by aerosol absorption in addition to molecular absorption. In order to include the attenuation effect by aerosols, we used the transmission factor given by Yung et al. (1984) as follows;

$$\begin{aligned} Tm(z) &= e^{-(240-z)/Ha}, \quad 45 < z < 240 \text{ km} \\ Tm(z) &= 1 \qquad\qquad , \quad z > 240 \text{ km} \end{aligned} \qquad (2.47)$$

where Ha = 50 km is the scale height for aerosol absorption. The transmission factor is consistent with a previous observation (Caldwell et al., 1981) and an aerosol model for Titan (Pollack et al., 1980). The haze transmission factor given by Yung et al. (1984) is a crude approximation. Nevertheless, it is consistent with a recent model including more elaborate Mie scattering calculation due to aggregates or organic aerosols (Krasnopolsky, 2009). Initial gas mixing ratios are assigned for some of the species as shown in Table 2.4, which are based on observational data (Coustenis et al., 1989; 1991). They have homogeneous altitude profile at any altitude at the beginning of the calculation.

Table 2.1. Species calculated in the Titan model.[a, b]

H, H_2, $^3CH_2$, $^1CH_2$, CH_3, **CH_4**, C_2, C_2H, **C_2H_2**, C_2H_3, **C_2H_4**, C_2H_5, **C_2H_6**, C_3H_2, C_3H_3, **CH_2CCH_2**, **CH_3C_2H**, C_3H_5, C_3H_6, C_3H_7, **C_3H_8**, C_4H, **C_4H_2**, $C_4H_2^*$, C_4H_3, **C_4H_4**, **C_4H_6**, **C_4H_{10}**, C_6H, C_6H_2, C_8H_2, N(^{4}S), N(^{2}D), N_2, NH, CN, C_3N, **HCN**, H_2CN, CHCN, **CH_3CN**, **HC_3N**, **C_2H_3CN**, **C_2N_2**, C_4N_2, O(^{3}P), O(^{1}D), OH, CO, **H_2O**, HCO, **CO_2**, **H_2CO**, CH_3O, **CH_3OH**, **CH_2CO**, CH_2OH, HC_2N_2, H_2C_3N, SOOT

[a] $^3CH_2$, C_4H_2, N(^{4}S), O(^{3}P) are the ground-state species, while $^1CH_2$, $C_4H_2^*$, N(^{2}D), O(^{1}D) are the excited-state species.

[b] Condensable species are bold. Most of the saturated vapor pressures are from Krasnopolsky (2009). The saturated vapor pressure of CH_3C_2H is from Lara et al. (1996), while those of CH_2CCH_2, CH_3OH, H_2CO and CH_2CO are from NIST Chemistry Webbook (CH_2CCH_2, allene: Stull (1947), CH_3OH, methyl alcohol: Ambrose and Sprake (1970), H_2CO, formaldehyde: Spence and Wild (1935), CH_2CO, ketene: Reuben (1969)).

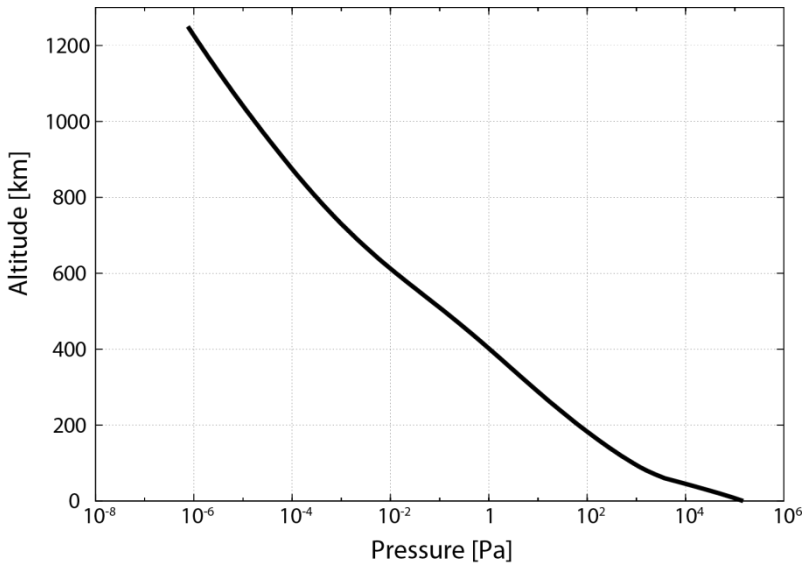

Figure 2.1. Pressure profile of the standard Titan model. This profile was calculated based on hydrostatic equilibrium, although the initial profile at the beginning of the calculation was assumed to be that of the recommended model of Yelle et al. (1997).

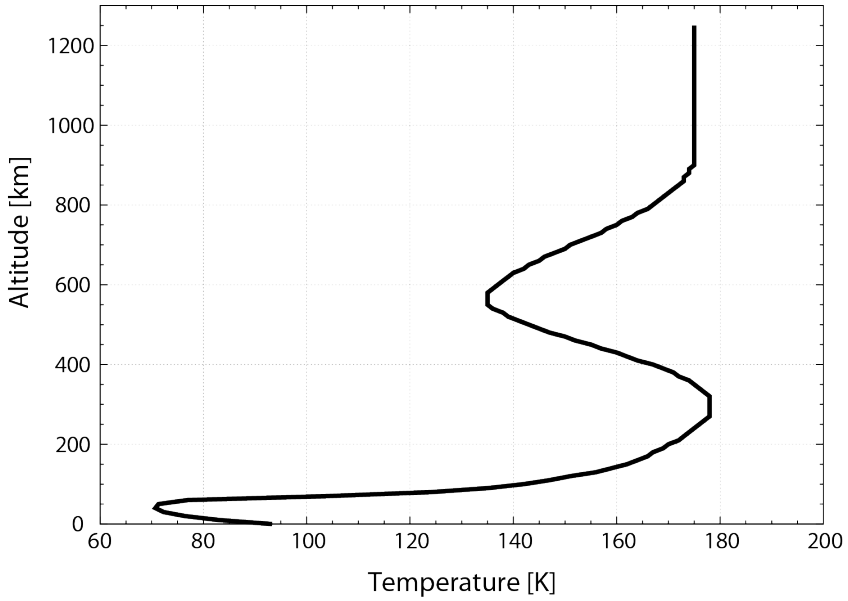

Figure 2.2. Temperature profile of the standard Titan model, which is based on the recommended model of Yelle et al. (1997).

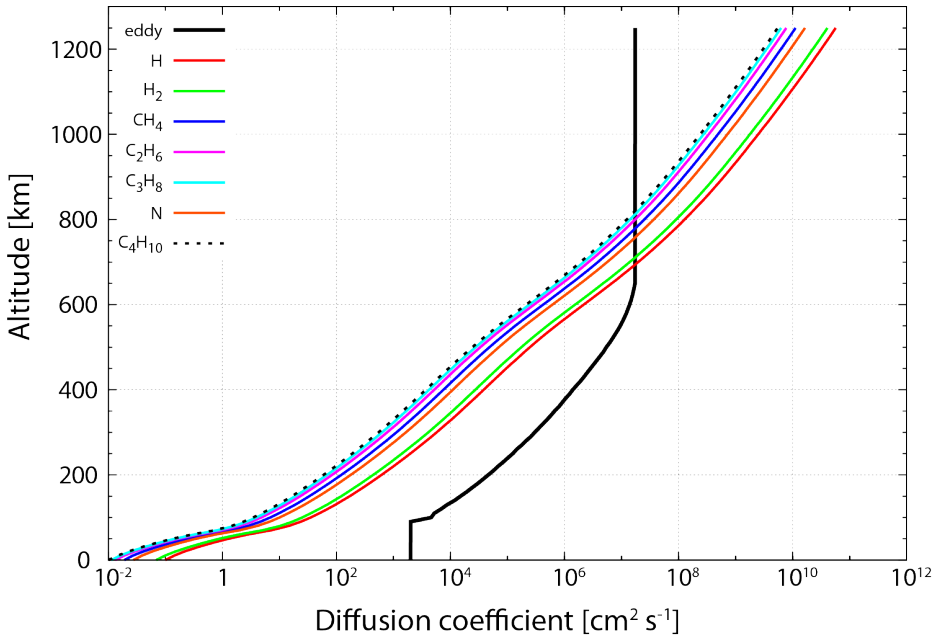

Figure 2.3. Eddy and molecular diffusion coefficients of the standard Titan model. The eddy diffusion coefficient above the troposphere is from Yelle et al. (2008), while that in the troposphere is fixed similarly to previous photochemical models (Yung et al., 1984; Toublanc et al., 1995; Wilson and Atreya, 2004; Lavvas et al., 2008a, 2008b; Krasnopolsky, 2009). The molecular diffusion coefficients are calculated based on Lavvas et al. (2008a). The equations are given in (2.45) and (2.46) and their parameters are given in Table 2.2.

Table 2.2. Binary diffusion coefficients used in the photochemical model.

Pair	$A \times 10^{17}$ cm^{2}s^{-1}	s	References
$H - N_2$	4.87	0.698	Banks and Kockarts (1973)
$H_2 - N_2$	2.80	0.740	Banks and Kockarts (1973)
$N - N_2$	0.969	0.770	Mason and Marreno (1970)
$CH_4 - N_2$	0.734	0.750	Banks and Kockarts (1973)
$C_2H_6 - N_2$	0.561	0.730	Wakeham and Slater (1973)
$C_3H_8 - N_2$	0.653	0.660	Wakeham and Slater (1973)
$C_4H_{10} - N_2$	0.734	0.610	Wakeham and Slater (1973)

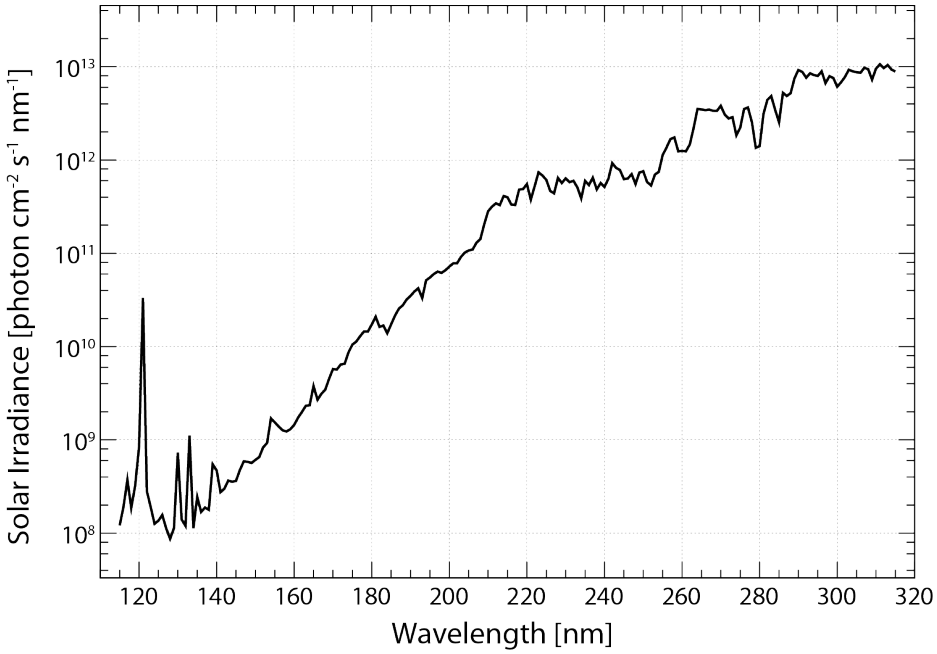

Figure 2.4. Solar ultraviolet spectrum used in the photochemical model. The data are from a rocket observation on May 17, 1982 by Mount and Rottman (1983), suitable for moderate solar activity.

Table 2.3. References of the absorption cross sections used in the photochemical model.[a]

Species	References
CH_3	Parks et al. (1973)
CH_4	Ditchburn (1955), Sun and Weissler (1955), Mount and Moos (1978)
C_2H_2	Benilan et al. (2000), Wu et al. (2001)
C_2H_4	Zelikoff and Watanabe (1953), Schoen (1962)
C_2H_6	Okabe and Becker (1963), Lombos et al. (1967), Mount and Moos (1978)
C_3H_3	Estimated by Toublanc et al. (1995)
CH_2CCH_2	Estimated by Toublanc et al. (1995)
CH_3C_2H	Ho et al. (1998), Fahr and Nayak (1996)
C_3H_6	Samson et al. (1962), Fahr and Nayak (1996)
C_3H_8	Au et al. (1993)
C_4H_2	Kloster-Jensen et al. (1974), Okabe (1981), Fahr and Nayak (1994)
C_4H_4	Estimated to be the same as C_4H_6 by Toublanc et al. (1995)
C_4H_6	Fahr and Nayak (1996)
C_6H_2	Kloster-Jensen et al. (1974), Benilan et al. (1995)
C_8H_2	Estimated to be the same as C_6H_2 by Toublanc et al. (1995)
N_2	Bertrand et al. (1975)
HCN	West and Berry (1974), SwRI[b]
HC_3N	Ferradaz et al. (2009)
C_2N_2	Nuth and Glicker (1982), LISA-unpubl (1999)[c]
C_4N_2	Connors et al. (1974), Benilan et al. (1996)
H_2O	Watanabe and Zelikoff (1953)
CO	Chan et al. (1993)
HCO	Estimated to be the same as $\sigma_{H2O} \times 10^4$ by Toublanc et al. (1995)
H_2CO	Estimated to be the same as $\sigma_{H2O} \times 10$ by Toublanc et al. (1995)
CH_2CO	Estimated to be the same as $\sigma_{H2O} \times 10^2$ by Toublanc et al. (1995)
CO_2	Nakata et al. (1965)
CH_3CN	Eden et al. (2003)
C_2H_3CN	Estimated to be the same as CH_3CN by Toublanc et al. (1995)

[a] When there are a few cross sections available at different temperatures, the ones obtained at the lowest temperature are used, in order to simulate Titan's cold atmosphere.

[b] Data from the Southwest Research Institute (http://phidrates.space.swri.edu/).

[c] Unpublished data from the Laboratoire Interuniversitaire des Systèmes Atmosphériques (Paris). http://losno.lisa.univ-paris-diderot.fr/services/DiffuseUVdata/

Table 2.4. Initial mixing ratios used in the standard Titan model.

Species	Molar mixing ratios
CH_4	4.4×10^{-2}
C_2H_2	2.2×10^{-6}
C_2H_4	9.0×10^{-8}
C_2H_6	1.3×10^{-5}
CH_2CCH_2	4.4×10^{-9}
CH_3C_2H	3.0×10^{-8}
C_3H_8	7.0×10^{-7}
C_4H_2	1.4×10^{-9}
C_2N_2	1.5×10^{-9}
H_2	2.0×10^{-3}
N_2	0.95
HCN	1.6×10^{-7}
HC_3N	1.5×10^{-9}
H_2O	1.0×10^{-10}
CO	4.5×10^{-5}
CO_2	1.4×10^{-8}

Boundary conditions used in our Titan's photochemical model are shown in Table 2.5. $N(^4S)$ and $N(^2D)$ atoms flow from the top of atmosphere as a result of dissociation of molecular nitrogen by energetic particles or extreme ultraviolet radiation (e.g., Wilson and Atreya, 2004; Krasnopolsky, 2009).

$$N_2 + e^- \rightarrow N(^4S) + N(^2D) + e^-$$

The $N(^4S)$ influx in the present study is based on Toublanc et al. (1995), but the $N(^2D)$ influx used is significantly lower than that of Toublanc et al. (1995). This is because, as argued in Krasnopolsky (2009), Toublanc et al. (1995) erroneously overestimated the production of atomic nitrogen by extreme ultraviolet. Toublanc et al. (1995) assumed that the dissociation of molecular nitrogen occurs by extreme ultraviolet radiation for wavelengths less than 80 nm:

$$N_2 + h\nu\,(\lambda < 80 \text{ nm}) \rightarrow 2N(^2D)$$

However, the actual processes are

$$N_2 + h\nu\,(\lambda < 80\ \text{nm}) \rightarrow N_2^+ + e^-$$

$$N_2^+ + CH_4 \rightarrow CH_3^+ + H + N_2$$

with no production of atomic nitrogen (Krasnopolsky, 2009). The H_2O influx from the top of atmosphere is based on an estimate of the mass of infalling micrometeorites proposed by Samuelson et al. (1983), which assumed that Titan's flux of micrometeorites is the same as that of Earth. Unlike Toublanc et al. (1995), we introduced an escape flux of CH_4 from the top of atmosphere, because they overestimated the mixing ratio of methane in the heterosphere (z > 900 km). The escape flux of CH_4 used in our model is close to recent estimates considering slow hydrodynamic escape (e.g., Yelle et al., 2008; Lavvas et al., 2008a; 2008b; Strobel 2008; 2009; Krasnopolsky 2009). We chose the escape velocities of H and H_2 in order to fit the observational data. The choice of the escape velocities of H and H_2 will be discussed in the section 2.2.3. The surface mixing ratios of N_2, CH_4 and CO are fixed, while the fluxes of the other species are assumed to be zero both at the surface and at the top of atmosphere as Toublanc et al. (1995). Our photochemical calculation was initiated with a time step of 10^{-7} sec, and the time step was automatically adjusted after each calculation. The calculation was done at least 10^6 years to achieve photochemical equilibrium at each altitude.

Table 2.5. Boundary conditions assumed in the standard Titan model.

Influx at the top of atmosphere	
$N(^4S)$	7.0×10^7 molecule cm^{-2} s^{-1}
$N(^2D)$	1.4×10^8 molecule cm^{-2} s^{-1}
H_2O	1.5×10^6 molecule cm^{-2} s^{-1}
Escape at the top of atmosphere	
H	1.25×10^4 cm s^{-1}
H_2	5.00×10^2 cm s^{-1}
CH_4	2.2×10^9 molecule cm^{-2} s^{-1}
Fixed surface mixing ratio	
N_2	0.95
CH_4	4.4×10^{-2}
CO	4.5×10^{-5}
Zero fluxes at the surface and top of atmosphere for the other species	

Since our chemical scheme is identical to that of Toublanc et al. (1995), we compare our results with those of Toublanc et al. (1995). The major differences between our model and that of Toublanc et al. (1995) are the absorption cross sections, UV attenuation by aerosols layers, eddy diffusion coefficient profile and the boundary conditions ($N(^2D)$ influx, H and H_2 escape velocity and introduction of CH_4 escape). We also compare our results with the vertical profiles of some gas species given by a recent photochemical model (Krasnopolsky, 2009), which includes ion chemistry in the upper atmosphere, to discuss how the ionosphere affect the neutral chemistry in current Titan's atmosphere. The altitude profiles of the mixing ratios calculated by the photochemical models are also compared with various observation data. In the following figures (from Figure 2.5 to Figure 2.9), Cassini Ion and Neutral Mass Spectrometer (INMS) data are from Waite et al. (2005; 2007), Yelle et al. (2008) and Cui et al. (2008). For the rest of the observation data, the references are shown in the figures or in the captions.

In summary, despite some differences among the models, our photochemical model basically can reproduce the observations and the results of the previous models. The differences in the profiles of gas species caused mainly by (1) the absence of ion chemistry in the ionosphere in our model and (2) less absorption of UV light by organic aerosols in Toublanc et al. (1995). The followings are the detailed comparisons of our model results with the observations and those of the previous models.

Figure 2.5 shows the calculation results of profiles CH_4 and H_2 mixing ratios compared with the observational data and the results of the previous studies (Toublanc et al., 1995; Krasnopolsky, 2009; Samuelson et al., 1981; Courtin et al., 1995; Waite et al., 2005; 2007, Yelle et al., 2008; Cui et al., 2008). Our CH_4 profile is close to the observations and the calculation by Krasnopolsky (2009). Our CH_4 mixing ratio is lower than those of Toublanc et al. (1995) in the heterosphere (z > 900 km) and Krasnopolsky (2009). This is because of the methane escape from the top of atmosphere, which was not considered in Toublanc et al. (1995). A slow escape of methane from Titan has been suggested by Cassini's observations, and our escape flux of methane is consistent with the recent studies, which include escape of methane (Yelle et al., 2008; Lavvas et al., 2008a; 2008b; Strobel 2008; 2009; Krasnopolsky 2009). The H_2 mixing ratio calculated by our model seems to be consistent with the observations (Figure 2.5). The escape flux of H_2 (2.8×10^9 cm^{-2} s^{-1}) in our model is about ~3–4 times lower than those of Toublanc et al. (1995), 1.0×10^{10} cm^{-2} s^{-1}, and of Krasnopolsky (2009), 1.2×10^{10} cm^{-2} s^{-1}. This is because we used relatively low H_2 escape velocity, assuming Jeans escape of H_2. The use of Jeans escape flux for H_2 escape would result in an underestimate of H_2 mixing ratio similar to Toublanc et al. (1995). Krasnopolsky (2009) obtains a H_2 profile and escape flux consistent with the observations, even though they assumed a similar escape velocity with the present study and Toublanc et al. (1995). This discrepancy is probably because Krasnopolsky (2009) takes into account the

ionospheric chemistry, i.e., CH_4 is destroyed by energetic particles or ions in the upper atmosphere, yielding a significant amount of H_2 and hydrocarbons. The H_2 produced by ion chemistry contributes to the influx of H_2 that compensates the H_2 loss by escape.

Figure 2.6 shows the calculation results of altitude profile of C_2H_2 compared with the observations and previous models (Toublanc et al., 1995; Krasnopolosky, 2009). Our results are consistent with the observation at altitude of ~400–800 km, but are lower than the observations at altitude of >800 km (Fig. 2.6). The discrepancy in C_2H_2 production at higher altitudes is occurred probably because we do not take into account ion chemistry occurred at altitude >800 km. Our results are also significantly lower than the results of the previous models (Toublanc et al., 1995; Krasnopolsky, 2009). The production of C_2H_2 is mainly caused by both the photolysis of C_2H_4 and reaction between $^3CH_2$ radicals.

$$^3CH_2 + {}^3CH_2 \rightarrow C_2H_2 + H_2$$

As shown in Figure 2.13 below, our $^3CH_2$ mixing ratio is significantly lower than that of Toublanc et al. (1995) below the altitude of 600 km, which results in a lower production of C_2H_2 in the middle atmosphere. In addition, as shown in Figure 2.7, Toublanc et al. (1995) overestimated the C_2H_4 mixing ratio above 800 km compared with the results of the present study and of Krasnopolsky (2009). The discrepancy of $^3CH_2$ abundance below altitude of 600 km between our results and that of Toublanc et al. (1995) probably originates from the UV transmission factor by organic aerosol layers. Since more photons can penetrate to the lower atmosphere in Toublanc et al. (1995) compared with our model and Krasnopolsky (2009), they can contribute to a more efficient photolysis of CH_4 and other hydrocarbons, yielding a more efficient production of $^3CH_2$. The discrepancy between our results and that of Krasnopolsky (2009) could originate from the ionospheric chemistry, since Krasnopolsky (2009) showed that about 15% out of the total C_2H_2 production is driven by nitrile plus ion reactions above 1000 km, which are not considered in our model.

Our C_2H_4 and C_2H_6 profiles, shown in Figure 2.7 and Figure 2.8 respectively, are consistent with the observations and the calculation results by Krasnopolsky (2009), whereas Toublanc et al. (1995) underestimated C_2H_6 mixing ratio significantly in the upper atmosphere. The reason of this discrepancy is not clear, because their altitude profile of CH_3 radical, which are the main source of C_2H_6, is close to ours (Figure 2.13).

$$CH_3 + CH_3 + M \rightarrow C_2H_6 + M$$

However, since they did not mention C_2H_6 cross section used in their paper, the

difference in the cross section possibly causes the discrepancy in photolysis rate of C_2H_6.

Figure 2.9 shows the results of altitude profiles of CH_3C_2H and C_3H_8 compared with the observations and the previous model results (Toublanc et al., 1995; Krasnopolsky, 2009). Our CH_3C_2H profile is close to that of Toublanc et al. (1995). Although our C_3H_8 profile in the lower atmosphere is consistent with the observations, the profile in the upper atmosphere is about one order of magnitude lower than those of Toublanc et al. (1995) and Krasnopolsky (2009), and the observations. This may be caused by the overestimated the photolysis rate of C_2H_6 by Toublanc et al. (1995) mentioned above. Since C_3H_8 is primary produced by the reaction between C_2H_5 and CH_3 in the chemical scheme of Toublanc et al. (1995),

$$C_2H_5 + CH_3 + M \rightarrow C_3H_8 + M$$

Enhanced photolysis rate of C_2H_6 could result in an increased mixing ratio of C_2H_5, which results in an increased mixing ratio of C_3H_8 in Toublanc's model.

Figure 2.10 and Figure 2.11 show the altitude profiles of HCN and HC_3N, respectively, compared with the observations and the previous models (Toublanc et al., 1995; Krasnopolsky, 2009). Our HCN profile shows good agreement with the previous model results and the observations (Figure 2.10). HC_3N profile by our model shown in Figure 2.11 is also consistent with the previous models and the observations. However, its mixing ratio is underestimated in the upper atmosphere probably due to the lack of ionospheric chemistry. In addition, we consider smaller $N(^2D)$ influx at the top of atmosphere than that of Toublanc et al. (1995).

Figure 2.12 shows the mixing ratios of oxygen species obtained by our models with those of the previous models and the observations. Our CO abundance at the surface was fixed to the observed mixing ratio by the Cassini Composite Infrared Spectrometer (Flasar et al., 2005; de Kok et al., 2007). Toublanc et al. (1995) fixed their CO mixing ratio at the surface to the observations in the stratosphere by Marten et al. (1988) using a ground-based radiotelescope, but this value is now considered to be too low because the telescope parameters were not well understood at the time of their analysis (Hidayat et al., 1998). Furthermore, the low CO mixing ratio in the stratosphere observed by Marten et al. (1988) contradicts with the recent Cassini observations (Flasar et al., 2005; de Kok et al., 2007). The low CO mixing ratio in Toublanc et al. (1995) results in significantly low levels of CO_2 mixing ratio compared with the observations (The CO_2 mixing ratio calculated by Toublanc et al. (1995) is $<10^{-9}$). In the chemical scheme of Toublanc et al. (1995), CO_2 is produced via the following reactions involving the reaction between OH and CO:

$$H_2O + h\nu \rightarrow OH + H$$

$$OH + CH_3 \rightarrow CO + 2H_2$$

$$OH + CO \rightarrow CO_2 + H$$

Our CO_2 mixing ratio agrees well with that of Krasnopolsky et al. (2009) and Cassini's observations (Coustenis et al., 2007) in the lower atmosphere. Above altitude of 300 km, our CO_2 mixing ratio is about one order of magnitude lower than that of Krasnopolsky et al. (2009), although there is no observational data to compare. The altitude profile of H_2O mixing ratio is largely dependent on the H_2O influx from the top of atmosphere. Our H_2O profile agrees with the observation by Coustenis et al. (1998) and is close to those of Toublanc et al. (1995) and Krasnopolsky (2009), since these three photochemical models used similar H_2O influx.

Figure 2.13 shows the comparisons of profiles of some major radical species among the models. Our results are generally consistent with those of Toublanc et al. (1995) except for the mixing ratio of $^3CH_2$ in the lower atmosphere. The larger mixing ratio of $^3CH_2$ of Toublanc et al. (1995) in the lower atmosphere is probably due to less UV absorption by organic aerosols in Toublanc et al. (1995). Toublanc et al. (1995) calculated the transfer of solar radiation using a Monte Carlo scheme; however, their attenuation effect by organic aerosols in the lower atmosphere is much less than other models (Yung et al., 1984; Wilson and Atreya, 2004; Krasnopolsky, 2009). The less UV absorption could increase photolysis rate of methane, resulting in a increasesd mixing ratio of $^3CH_2$ in Toublanc et al. (1995).

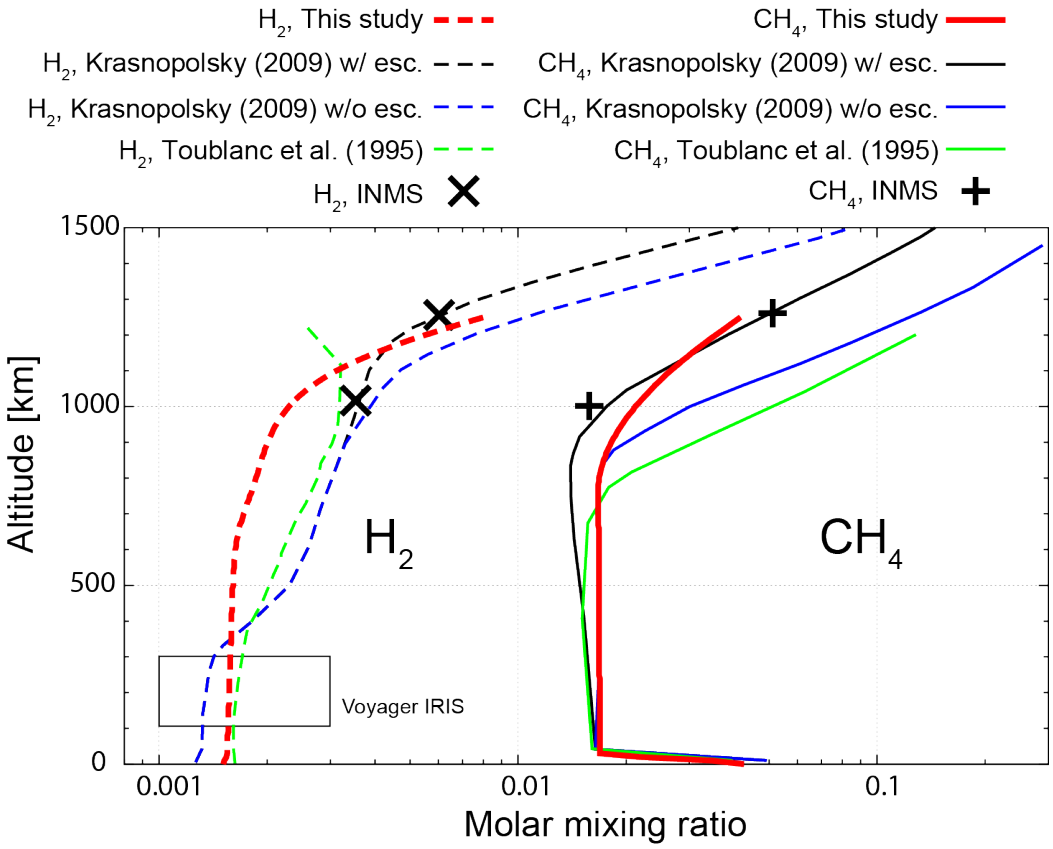

Figure 2.5. Mixing ratios of CH_4 and H_2 calculated by our standard Titan model, Krasnopolsky (2009) and Toublanc et al. (1995). The rectangle shows the H_2 mixing ratio observed by the Voyager IRIS (Samuelson et al., 1981; Courtin et al., 1995).

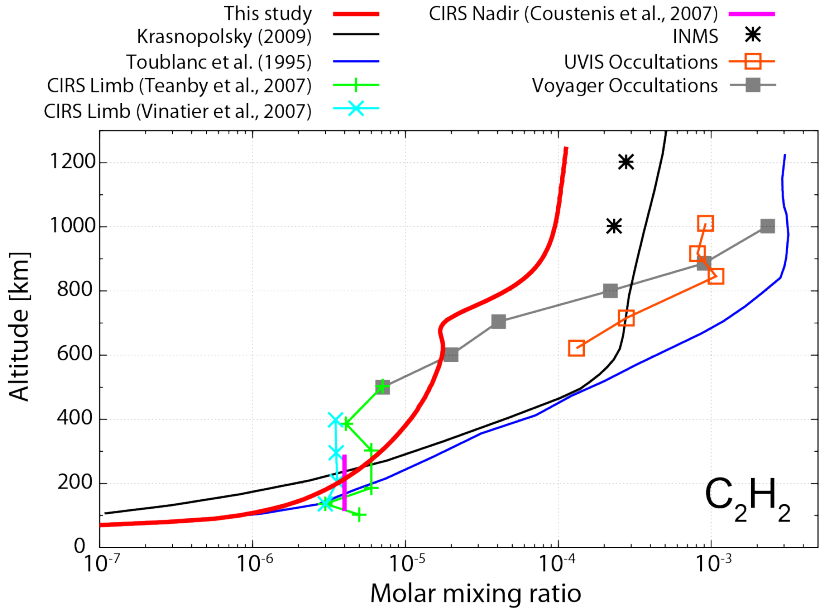

Figure 2.6. Mixing ratio of C_2H_2 calculated by our standard Titan model, Krasnopolsky

(2009) and Toublanc et al. (1995). Observation data by Cassini UVIS Occultations (Shemansky et al., 2005) and Voyager Occultations (Vervack et al., 2004) are also shown.

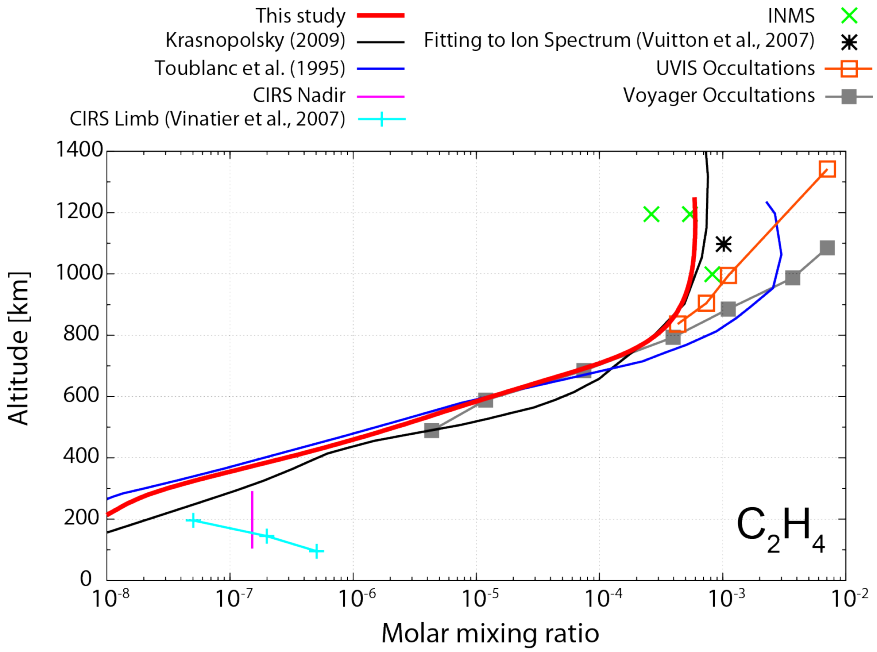

Figure 2.7. Mixing ratio of C_2H_4 calculated by our standard Titan model, Krasnopolsky (2009) and Toublanc et al. (1995). Cassini Nadir stands for the observation data by Coustenis et al. (2007). Observation data by Cassini UVIS Occultations (Shemansky et al., 2005) and Voyager Occultations (Vervack et al., 2004) are also shown.

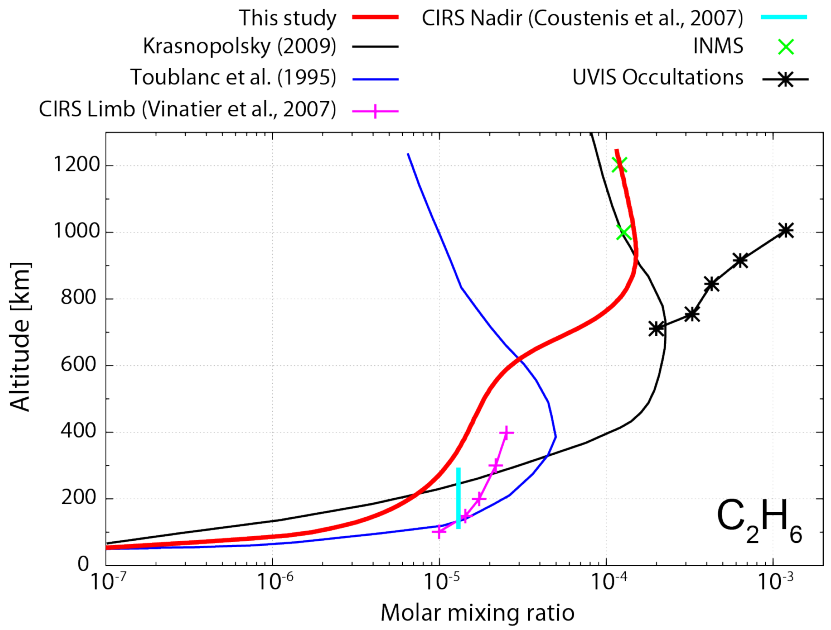

Figure 2.8. Mixing ratio of C_2H_6 calculated by our standard Titan model, Krasnopolsky (2009) and Toublanc et al. (1995). The observation data of Cassini UVIS Occultations are from Shemansky et al. (2005).

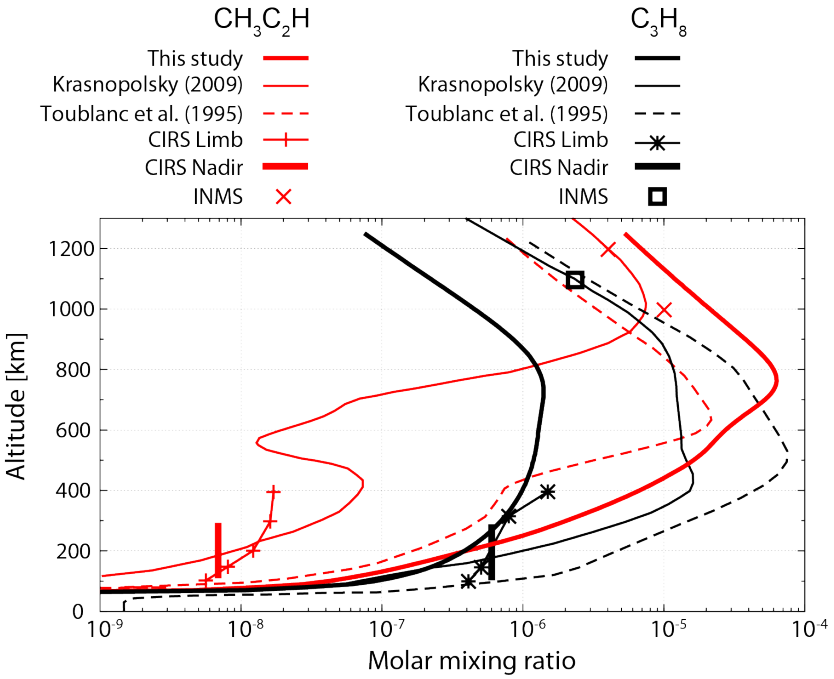

Figure 2.9. Mixing ratios of CH_3C_2H and C_3H_8 calculated by our standard Titan model, Krasnopolsky (2009) and Toublanc et al. (1995). CIRS Limb and CIRS Nadir stand for the observation data by Vinatier et al. (2007) and Coustenis et al. (2007), respectively.

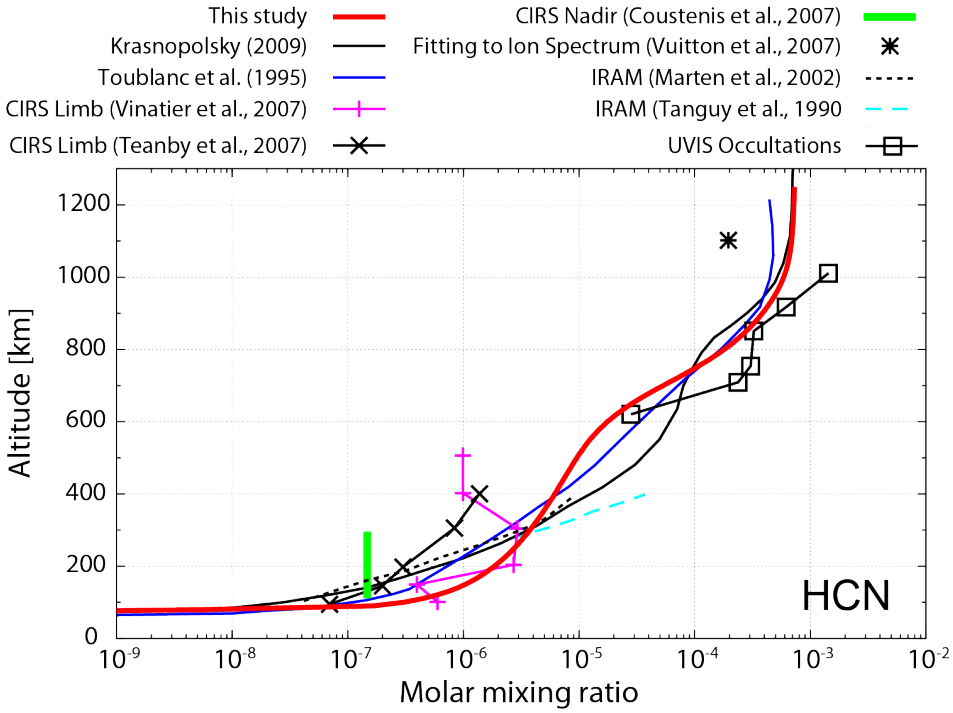

Figure 2.10. Mixing ratios of HCN, calculated by our standard Titan model, Krasnopolsky (2009) and Toublanc et al. (1995). The observation data of UVIS Occultations are from Shemansky et al. (2005).

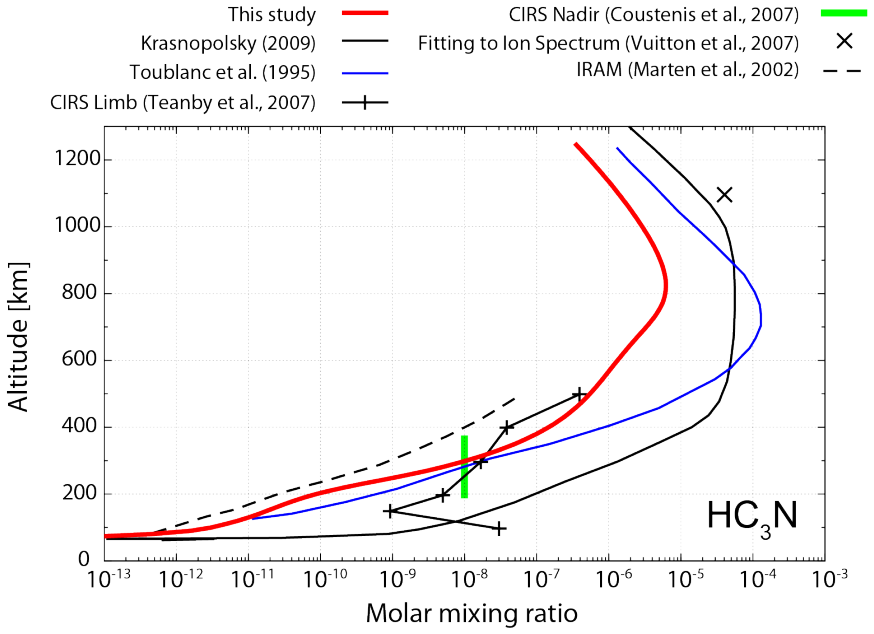

Figure 2.11. Mixing ratios of HC_3N, calculated by our standard Titan model, Krasnopolsky (2009) and Toublanc et al. (1995).

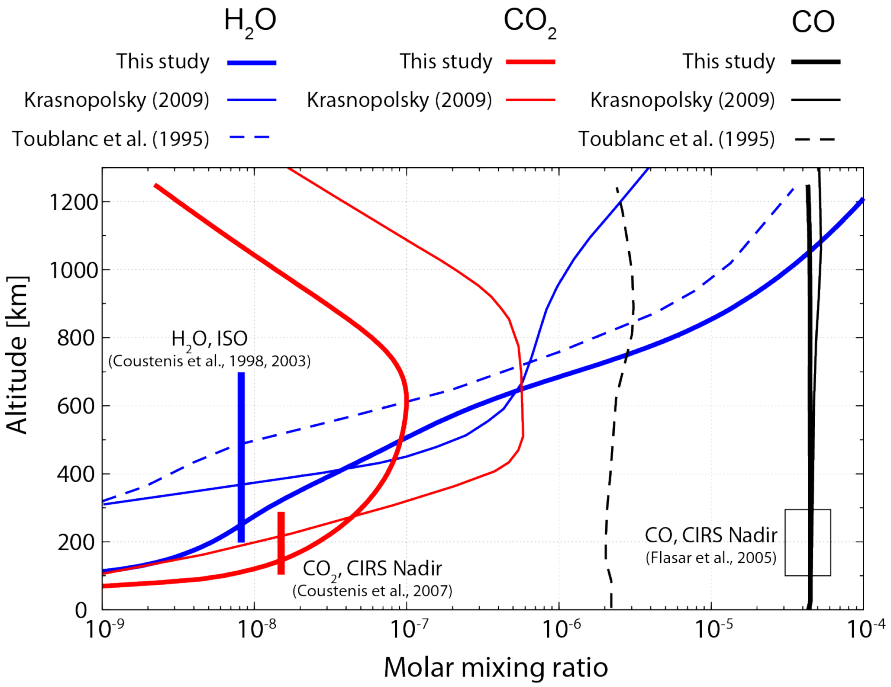

Figure 2.12. Mixing ratios of oxygen species calculated by our standard Titan model, Krasnopolsky (2009) and Toublanc et al. (1995). The CO_2 mixing ratio calculated by Toublanc et al. (1995) is below 10^{-9} at all altitudes thus beyond the range of this figure.

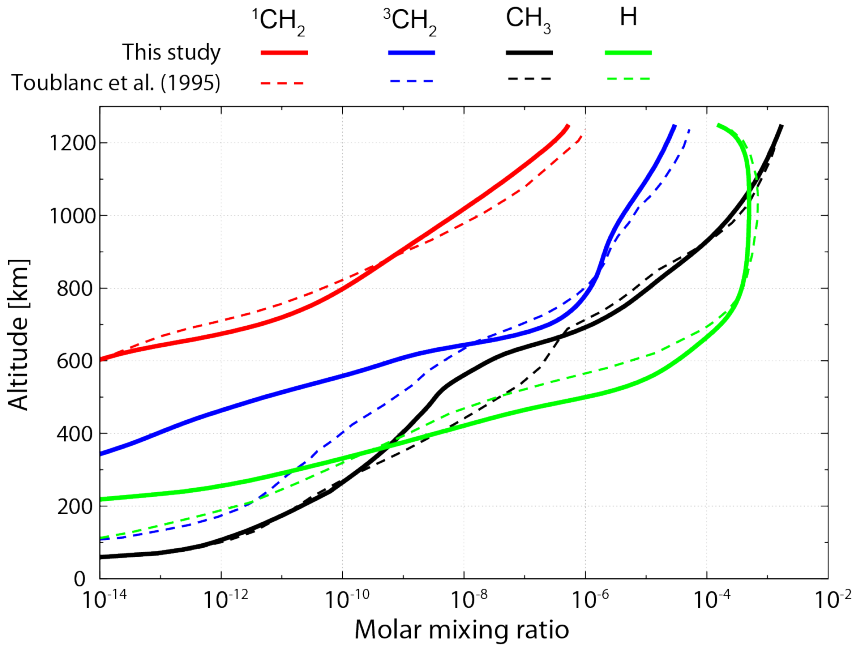

Figure 2.13. Mixing ratios of radicals calculated by our standard Titan model and Toublanc et al. (1995).

2.2.4 Validation of the photochemical model based on an Early Earth atmosphere

A number of photochemical models have been developed to study the atmospheric composition of early Earth (e.g., Kasting et al., 1979; Kasting and Donahue, 1980; Kasting and Walker, 1981; Kasting, 1982; Kasting et al., 1983; Zahnle, 1986; Kasting, 1990; Pavlov et al., 2001; Tian et al., 2011). Pavlov et al. (2001) first investigate the organic aerosol production and its influence on the radiative transfer on an early Earth, by using a microphysical, photochemical and radiative transfer models. Those three models are, however, not coupled each other but independently calculated (Pavlov et al., 2001). Since the chemical scheme of Pavlov et al. (2001) is comprehensive enough to calculate oxygen, ammonia, HO_x, NO_x, sulfur and low-order hydrocarbon families (up to C_4), we adopted their chemical scheme to check the validity of our photochemical model.

The photochemical model contains H, C, N, O, and S chemistry (337 reactions and 69 species), which is identical with Pavlov et al. (2001). The model atmosphere extends from the surface to 100 km altitude with equally divided 51 layers. Thus, each atmospheric layer has a thickness of 2 km. The time dependent one dimensional continuity equation was solved for each reactive species including condensation of H_2O and transport by eddy and molecular diffusion. The details of finite differencing and matrix solver for the continuity-diffusion equation in spherical coordinates are shown in the section 2.2.2. Calculations were carried out at 1 bar of surface pressure and 275 K of surface temperature. Figure 2.14a shows the altitude profile of temperature and initial pressure profile. The temperature is fixed throughout the calculation, while the pressure is calculated based on hydrostatic equilibrium. The temperature profile was taken from Tian et al. (2011), which corresponds to a simplified temperature profile for a weakly reducing Archean atmosphere, in which a temperature increase does not occur above the tropopause due to the lack of ozone layer. The troposphere was fixed to saturate with H_2O vapor. Above the tropopause, water vapor is calculated by solving the combined equations of photochemistry and transport. Eddy coefficients were obtained from the current terrestrial values (Massie and Hunten, 1981), shown in Figure 2.14b. Our model calculates the UV radiation field considering molecular absorption via photolysis reactions. The wavelength range of UV radiation field is from 115 to 315 nm with a wavelength resolution of 1 nm. Because our model does not calculate Rayleigh scattering at the present time, and because the optical depth of Earth's atmosphere due to Rayleigh scattering at 310 nm is about unity (Yung and DeMore, 1999), photolysis rates near the surface could be overestimated by a factor of ~3. This will give us upper estimates of the destruction rates of photolytic species and lower estimates of the abundances near the surface for photolytic species. For the spectrum of the incoming

UV flux from the sun, the current solar UV spectrum (Mount and Rottman, 1983: Figure 2.4) was used but the solar luminosity was set to 80% of its present value to account for a young Sun at ~2.8 billion years ago (Gough, 1981). The solar zenith angle was set to 30° and the solar UV flux at the top of atmosphere was halved to account for mid-latitude daily average.

Boundary conditions in photochemical calculations are one of the important factors to determine atmospheric compositions. At the top of atmosphere, escape of H and H_2 was simulated by assuming a diffusion-limited escape (Hunten, 1973a; 1973b). The diffusion-limited escape flux ϕ_i^l for specie *i* at the top of atmosphere is expressed as follows;

$$\phi_i^l = D_i \left(\frac{1}{H_{\text{avg}}} - \frac{1}{H_i} \right) n_i \qquad (2.48)$$

where D_i is the diffusion coefficient, H_i is the scale height, n_i is the number density of specie *i* and H_{avg} is the mean scale height. Since the diffusion-limited escape provides only an upper limit on the escape rate, the mixing ratios of H and H_2 could be underestimated, especially for a low-temperature exosphere. The low-temperature exosphere is likely under low-O_2 and high-CO_2 conditions, such as current Mars and Venus (e.g., Yung and DeMore, 1999). The lower boundary conditions used are tabulated in Table 2.6. The lower boundary conditions are adopted from the previous photochemical models of early Earth's atmosphere (Pavlov et al., 2001; Zerkle et al., 2012). These values are based on the deposition and rain out velocity from Slinn et al. (1978) and Lee and Schwartz (1981), respectively. Mixing ratios of five major species (N_2, H_2O, SO_2, NH_3, CO_2) at the surface are fixed, in which that of CO_2 was chosen as a free parameter. This procedure, fixing the surface mixing ratios and calculating their corresponding degassing fluxes, speeds up model convergence (e.g., Kasting, 1990). NO is deposited slowly to the surface but also produced by lightning production of oxidants (Kasting, 1990). The deposition velocity of CO was chosen to be 2.0×10^{-7} cm s^{-1}, which is close to an upper estimate of abiotic uptake of atmospheric CO by the ocean (Kasting, 1990; Kharecha et al., 2005). The deposition velocity of H_2 was chosen in order to preserve the atmospheric hydrogen budget, which physically represents the flow of electrons (or protons) of the system (See the appendix 1 of Kharecha et al., 2005).

The calculation was carried out at least for 2×10^7 years to achieve chemical equilibrium. It was initiated with a time step of 1×10^{-7} second, and an automatic adjustment of the time step was done after each calculation.

Figure 2.15 shows the mixing ratio profiles of some major gas species for the calculation with $f_{\text{CH}_4} = 1000$ ppmv, $f_{\text{CO}_2} = 2500$ ppmv, which is the same as Pavlov

et al. (2001). Pavlov et al. (2001) argue that CH_4 mixing ratios of the order of 10^{-3} would be possible if CH_4 outgassing rate by methanogens (the reaction is (2.49)) exceed the burial rate of organic carbon.

$$CO_2 + 4H_2 \rightarrow CH_4 + 2H_2O \qquad (2.49)$$

The mixing ratio profiles of our model are generally consistent with those of Pavlov et al. (2001). CO is the second most abundant gas as the primary byproduct of the methane oxidation in the atmosphere by OH and other oxidants. The mixing ratio of CO_2 in our model decreases with an increase in altitude due to the photolysis of CO_2, whereas Pavlov et al. (2001) fixed the CO_2 mixing ratio at all altitudes. The photolysis of methane occurs above ~60 km altitude, resulting in increases in H_2, C_2H_2, C_2H_4 mixing ratios at these altitudes. The mixing ratio of H_2 in the lower atmosphere is decreased because of the H_2 deposition at the surface as the conservation of the hydrogen budget, which is physically caused by the consumption of H_2 by methanogens as described in the equation (2.49). Without such biological consumptions, the hydrogen mixing ratio would be as high as 10^{-3}, which is determined by the balance between volcanic outgassing and the diffusion-limited escape (Kasting and Brown, 1998). Our mixing ratio of H_2O at the tropopause is about one order of magnitude lower than that of Pavlov et al. (2001) because the H_2O mixing ratio below the tropopause is very sensitive to the tropopause temperature, which in our model is lower than that of Pavlov et al. (2001). Because a later radiative transfer model revealed that Pavlov et al. (2001) erroneously overestimated the greenhouse effect of methane, resulting in a high tropospheric temperature (Haqq-Misra et al., 2008), it may be appropriate to use our value for the tropopause temperature. O_2 is produced abiotically by the photolysis of carbon dioxide and water vapor through the following reactions (Kasting et al., 1979):

$$CO_2 + h\nu \rightarrow CO + O$$

$$H_2O + h\nu \rightarrow OH + O$$

$$CO + OH \rightarrow CO_2 + H\uparrow$$

$$O + O \rightarrow O_2$$

$$\text{(Net) } CO_2 + 2H_2O \rightarrow CO_2 + O_2 + 4H\uparrow$$

In the troposphere, atomic oxygen is removed by other reducing gases thus the O_2 mixing ratio is maintained as significantly low values at the surface.

Figure 2.16 shows the altitude profiles of two aerosol monomer production reactions assumed in the chemical scheme of Pavlov et al. (2001); that is formation of C_4H_2 and C_5H_4. The monomer production rate reaches its greatest value at around altitude of 70 km corresponding to the peak of methane photolysis. Since Pavlov et al. (2001) provide neither the production rates of those two chemical reactions nor monomer production rate, we cannot directly compare our results with their results. However, our peak altitude of the reaction rate is consistent with the peak altitude of particle number density of Pavlov et al. (2001). The column monomer production rate is 1×10^{9} cm^{-2} s^{-1}, or 8×10^{-14} g cm^{-2} s^{-1}, indicating that the production of C_4H_2 and C_5H_4 accounts for only 5% of the methane loss (Figure 2.17) (CH_4 + CH: ~2×10^{9} cm^{-2} s^{-1} for $f_{CH_4}=10^{-3}$). The column monomer production rate calculated is one order of magnitude larger than the experimentally estimated rate, 8×10^{-15} g cm^{-2} s^{-1}, in the section 1.3.3 of this thesis. These results suggest that Pavlov et al. (2001) overestimates the monomer production rate in early Earth's atmosphere. This is because we show that the monomer production would be controlled by polymerization of aromatic hydrocarbons, such as benzene, not polyynes and other hydrocarbons. Overall, our photochemical model can satisfactory reproduce the profiles of simple organic and inorganic gas species obtained by the previous calculations (Pavlov et al., 2001).

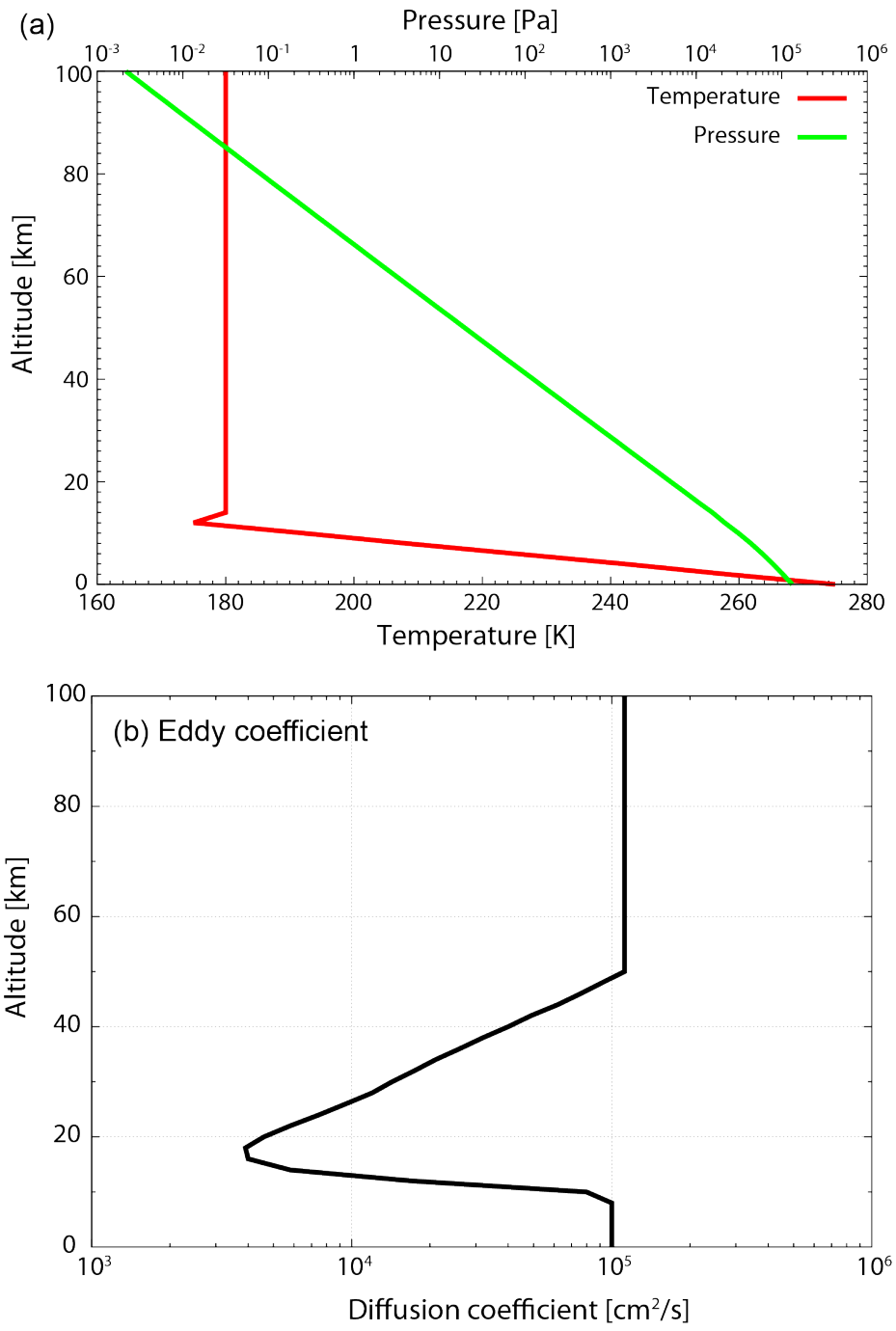

Figure 2.14. (a) Temperature and pressure profiles used in the photochemical model for an early Earth. Temperature profile is based on Tian et al. (2011) which corresponds to a simplified temperature profile for a weakly reducing Archean atmosphere that does not have a temperature increase above the tropopause due to the lack of ozone layer. (b) Eddy diffusion coefficient adopted from the current terrestrial value (Massie and Hunten, 1981)

Table 2.6. Lower boundary conditions for the early Earth model [a].

Fixed mixing ratios	N_2: 1.0 bar, H_2O: 1.0×10^{-8}, SO_2: 1.0×10^{-11}, NH_3: 1.0×10^{-10}, CO_2, 2.5×10^{-3}
0.2 cm s^{-1}	H_2O_2, H_2CO, HNO_3
1.0 cm s^{-1}	H, O(^{3}P), OH, HCO, CH_3, HNO, HO_2, HSO, H_2SO_4
No flux	N, H_2, O(^{1}D), O_2, O_3, C, C_2, CH, $^1CH_2$, $^3CH_2$, C_2H, C_2H_2, C_2H_3, C_2H_4, C_2H_5, C_2H_6, C_3H_2, C_3H_3, C_3H_5, C_3H_6, C_3H_7, C_3H_8, CH_2CCH_2, CH_3C_2H, CH_2CO, CH_3CHO, CH_3CO, CH_3O, C_2H_2OH, C_2H_4OH, C_2H_5CHO, NH, NH_2^*, HNO_2, S_2, $^1SO_2$, $^3SO_2$, HSO_3, SO_3, S_3, S_4
Others	NO_2: 3.0×10^{-3} cm s^{-1}, CO: 2.0×10^{-7} cm s^{-1}, NO: 3.0×10^{-4} cm s^{-1} (deposition), 1.0×10^{9} molecules cm^{-2} s^{-1} (lightning production) CH_4: 6.0×10^{10} cm^{-3} s^{-1} (outgassing) H_2: deposition velocity based on the atmospheric hydrogen budget (Kharecha et al., 2005)

[a] Most of the deposition velocities are similar with previous early Earth model (Pavlov et al., 2001; Zerkle et al., 2012) which adopted deposition and rain out velocity from Slinn et al. (1978) and Lee and Schwartz (1981), respectively.

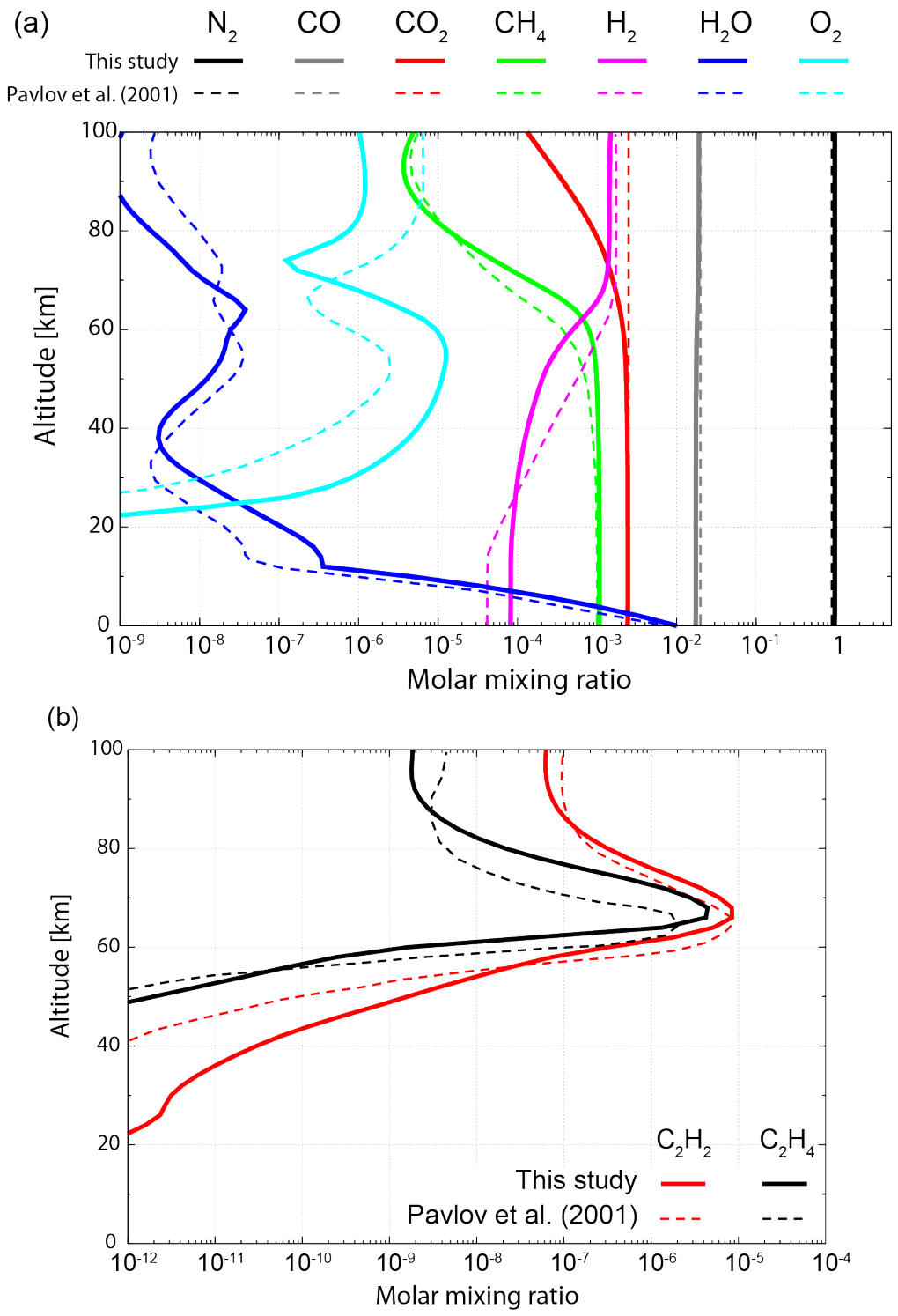

Figure 2.15. (a) Altitude profiles for major gas species calculated by our early Earth model and Pavlov et al. (2001) with $f_{CH_4} = 1000$ ppmv, $f_{CO_2} = 2500$ ppmv. Note that CO_2 profile of Pavlov et al. (2001) is not calculated but fixed. (b) Altitude profiles of C_2H_2 and C_2H_6.

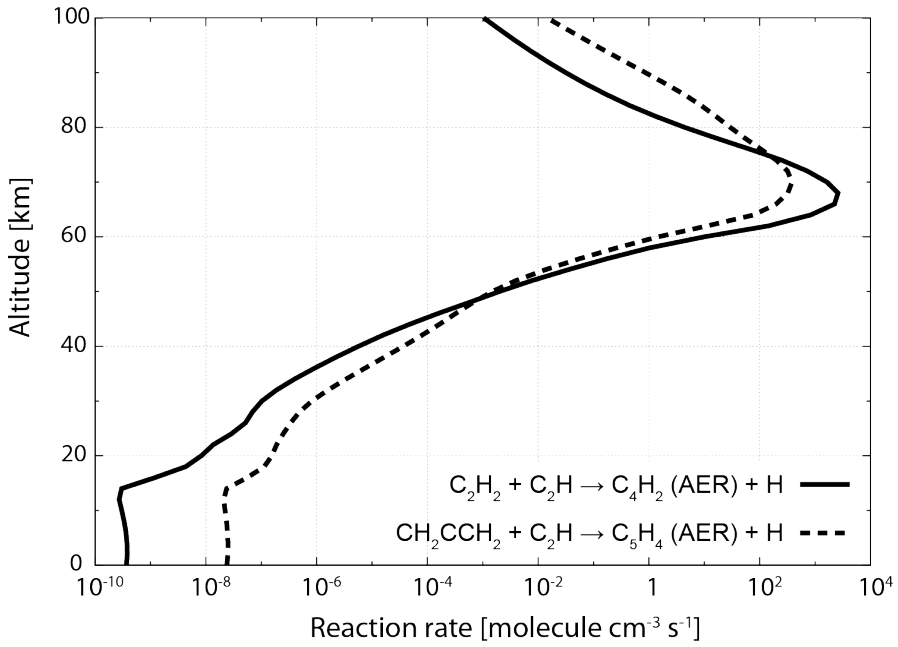

Figure 2.16. Reaction rates of aerosol monomer production reactions assumed in the chemical scheme of Pavlov et al. (2001), calculated by our photochemical model. The column monomer production rate is 1×10^9 cm^{-2} s^{-1}, or 8×10^{-14} g cm^{-2} s^{-1}.

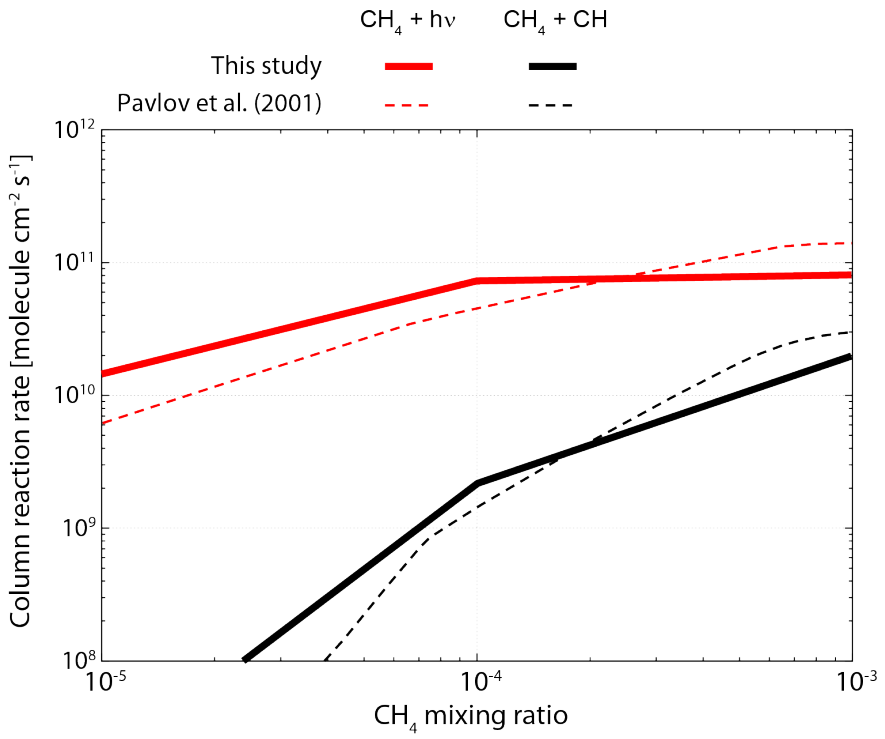

Figure 2.17. Photochemical processes contributing to the methane loss calculated by our model and Pavlov et al. (2001).

2.3 Microphysical/Radiative transfer model

To investigate the microphysical and radiative transfer processes, we use the Community Aerosol and Radiation Model for Atmospheres (CARMA), which has been developed previously (e.g., Turco et al., 1979; Toon et al., 1979; 1980; 1988; 1992; Barth and Toon, 2003; 2004). The model is briefly described in the subsection. The validation of the model was conducted by comparing with the previous results of the organic aerosol profile in Titan's atmosphere.

2.3.1 Model description

The microphysical model solves one dimensional continuity equations (e.g., Seinfeld and Pandis, 2006; Pruppacher and Klett, 2010). The equation (2.50) states that the time evolution of the number density of particles having volume v, at altitude z, at time t is equal to the sum of the gradient of the sedimentation flux using fall velocity V_{fall}; the gradient of the diffusion flux with diffusion coefficient K_{diff}; the production rate of particles of volume v by the coagulation of smaller particles at a rate determined by the coagulation kernel K_{coag}; the loss rate of particles of volume v by coagulation with all the other particles; the aerosol monomer production rate P, which should be determined by photochemistry, and the loss rate due rainfall at a rate given by L_{rain}. n_{gas} is the number density of gas species.

$$\begin{aligned}\frac{\partial n(v)}{\partial t} &= -\frac{\partial}{\partial z}(nV_{\mathrm{fall}}) - n_{\mathrm{gas}}K_{\mathrm{diff}}\frac{\partial\left[n(v)/n_{\mathrm{gas}}\right]}{\partial z} \\ &+ \frac{1}{2}\int_0^v K_{\mathrm{coag}}(v',\, v-v')n(v')n(v-v')dv' \\ &- \int_0^\infty K_{\mathrm{coag}}(v',\, v)n(v')dv' + P(v) - L_{\mathrm{rain}}(v)\end{aligned} \qquad (2.50)$$

Aerosol particles coagulate because of their Brownian motion or as result of their motion produced by hydrodynamic, electrical, gravitational, or other forces (e.g., Seinfeld and Pandis, 2006; Pruppacher and Klett, 2010). The coagulation kernel by Brownian motion is given by

$$K_{\text{coag, Br}} = 2\pi\left(D_{\text{p1}} + D_{\text{p2}}\right)(D_1 + D_2)\beta \qquad (2.51)$$

where $D_{\text{p}i}$ is the diameter of the ith particle and D_i is the diffusivity. The factor β is a correction factor suggested by Fuchs (1964) for when the mean free path of the aerosol particle is comparable to the radius of the absorbing particle. Toon et al. (1980) found that Brownian coagulation is the dominant coagulation process for organic aerosols in Titan's atmosphere. On the other hand, for Titan's cloud particles, Brownian coagulation is not important due to their low number density and large size (Barth and Toon, 2003). The Brownian coagulation, often referred to as thermal coagulation, would produce various particles with different diameters. Coagulation from gravitational settling then takes place when larger particles fall faster than smaller particles, catching up with the smaller particles, and collide with them (Seinfeld and Pandis, 2006). The coagulation kernel by the gravitational settling is given by (e.g., Seinfeld and Pandis, 2006; Pruppacher and Klett, 2010)

$$K_{\text{coag, GS}} = \frac{4}{\pi}\left(D_{\text{p1}} + D_{\text{p2}}\right)^2 (v_{\text{t1}} - v_{\text{t2}})E\left(D_{\text{p1}}, D_{\text{p2}}\right) \qquad (2.52)$$

where v_{t1} and v_{t2} are the terminal settling velocities for the large and small particles, respectively. E is the collision efficiency as a function of particle sizes. Gravitational coagulation can be neglected for submicrometer particles but becomes significant for particle diameters larger than a few micrometers (Seinfeld and Pandis, 2006). The coagulation processes can be affected by external forces, such as Coulomb forces. This effect can be described by adding a correction factor W:

$$K'_{\text{coag}} = \frac{K_{\text{coag}}}{W} \qquad (2.53)$$

where the correction factor is a result of the interparticle force as a function of the potential of external force Φ:

$$W = \left(R_{\text{p1}} + R_{\text{p2}}\right)\int_{R_{\text{p1}}+R_{\text{p2}}}^{\infty} \frac{1}{x^2}\exp\left(\frac{\Phi(x)}{kT}\right)dx \qquad (2.54)$$

in which $R_{\text{p}i}$ is the radii of ith particle, k is the Boltzmann constant and T is the temperature. The Coulomb potential is given by

$$\Phi_C = \frac{z_1 z_2 e^2}{4\pi\varepsilon_0 \varepsilon r} \quad (2.55)$$

where z_i is the electric charge of ith particle including sign, e is the elementary charge, ε_0 is the permittivity of vacuum, ε the dielectric constant of the medium and r the distance between the two particles. By substituting (2.55) into (2.54), the correction factor by Coulomb forces can be obtained by the following equations:

$$W_C = \frac{\exp(\kappa) - 1}{\kappa} \quad (2.56)$$

where

$$\kappa = \frac{z_1 z_2 e^2}{4\pi\varepsilon_0 \varepsilon \left(R_{p1} + R_{p2}\right) kT} \quad (2.57)$$

The constant κ can be interpreted as the ratio of the electrostatic potential energy to thermal energy kT. Toon et al. (1992) found that the aerosol's electrical charge in Titan's atmosphere is critical for limiting the particle size thus affecting the optical depth of organic aerosol layer. More detailed formulation regarding the coagulation kernels can be found in other literatures (e.g., Seinfeld and Pandis, 2006). The numerical algorithm of our microphysical model is described in Toon et al. (1988).

A one-dimensional radiative transfer model was used to calculate the radiation field of solar visible light. The model uses a two-stream approximation scheme for radiative transfer in inhomogeneous multiple scattering atmospheres, described in Toon et al. (1989), along with the delta-Eddington approximation (Joseph et al., 1976; Meador and Weaver, 1980). Radiative properties of aerosol layers (optical depth, single scattering albedo, asymmetry parameter) were calculated using Mie theory and incorporated into radiative transfer calculation (e.g., Liou, 2002). Therefore, the radiative transfer calculation includes absorption and scattering by aerosol particles and radiatively active gases as well as Rayleigh scattering by background gases.

2.3.2 Organic aerosol layers in Titan's atmosphere

We applied CARMA to current Titan's atmosphere for the validation of the numerical code. Most of the parameters are identical to the previous models (Toon et al., 1992; Barth and Toon, 2003). Figure 2.18 shows the aerosol monomer production rate in the atmosphere assumed in the microphysical model. The altitude profile of the monomer production rate is based on Toon et al. (1992), having the peak production at altitude of ~260 km. Toon et al. (1992) at first adopted the monomer production rate by fitting the methane destruction rate calculated by Yung et al. (1984), then adjusted the profile in order to account for Titan's geometric albedo. The total column production rate of monomer is set to be 1.22×10^{-14} g cm^{-2} s^{-1}, based on the estimate by McKay et al. (1989). Temperature and atmospheric density profiles are from the model of Lellouch and Hunten (1987). Atmospheric viscosity and thermal conductivity are from Lorenz (1993) and Stephan et al. (1987), respectively. The coagulation parameters are the same with that of Toon et al. (1992), including particle charging by galactic cosmic rays below about 400 km (Borucki et al., 1987). Rainout is not included in the model. The altitude grid extends from 0 to 1000 km in 10-km increments. The eddy diffusion coefficient for aerosol particles is the same with the revised model of Toon et al. (1992), resulting in ~100 years for a typical diffusion time scale below 100 km. Generally, micrometer-sized large particles are removed more quickly by falling than diffusion, meanwhile submicrometer-sized small particles have longer residence time (e.g., Seinfeld and Pandis, 2006). Thus, they are removed by growth to larger particles through coagulation (Toon et al., 1992). Particles are calculated as spheres. The aerosol particles are segregated into 35 bins that double in volume. The bin-mean radii range from 1.3 nm (i.e., monomer size) to 3.35 μm. The particle density is assumed to be 1 g cm^{-3}. Cloud physics in Titan's lower atmosphere (Barth and Toon, 2003; 2004) was not considered in the present calculation.

For the radiative transfer calculation, the visible spectrum is divided into 24 spectral regions, ranging from 325 nm to 2.4 μm (McKay et al., 1989). The complex refractive index for organic aerosol particles is taken from those of tholin produced by Khare et al. (1984a). Toon et al. (1992) multiplied the imaginary index of aerosol particles by 1.5 in order to reproduce Titan's geometric albedo. We adopted the same methodology. We assumed that the surface of Titan has a Lambert scattering albedo of 0.1 (McKay et al., 1989; Toon et al., 1992). Only methane absorption was considered for the gas absorption, and its absorption database is from McKay et al. (1989). We adopted the two-stream approximation method for the radiative transfer calculation. Nevertheless, this method cannot calculate the geometric albedo (Toon et al., 1977; 1989). The previous models provided additional calculations for the geometric albedo by using other schemes (e.g., McKay et al., 1989; Toon et al., 1992).

Figure 2.19 shows the altitude profile of aerosol particle density for various

particle radii calculated by our microphysical model, compared with those of the previous studies (Barth and Toon, 2003). The model was run for 500 years to achieve a steady-state distribution. The result is consistent with the previous microphysical models (e.g., Toon et al., 1992; Barth and Toon, 2003). The maximum number density locates at around 260 km altitude, corresponding to the peak of monomer production. Our model outputs a thin detached aerosol layer at around 350 km for large particles. At this altitude, the production of large particles by coagulation and the loss due to fall are almost balanced. Since the fall velocity decreases with a decrease in altitude (e.g. Hamill et al., 1977), the loss rate for large particles by particle falling exceeds the loss rate by coagulation at higher altitudes than 350 km. Thus at these altitudes, the particle densities for large particles are limited by the loss due to fall. On the other hand, at altitudes below 350 km, the loss of large particles is primary due to coagulation. Large particles are more quickly removed than particle falling at these altitudes. Then the produced large particles accumulate into lower altitudes, resulting in formation of a thick aerosol layer at around 100 km (Figure 2.19). The detached aerosol layers have been observed in Titan's atmosphere, showing seasonal changes in altitude and thickness (Tomasko and West, 2009). The detached aerosol layer appeared in our model could be consistent with the observations. However, there are other hypotheses to form the detached aerosol layers, such as global-scale dynamical motion in the atmosphere (e.g., Rannou et al., 2002; 2004), which cannot be simulated by our one dimensional model.

Figure 2.20 shows the cumulative optical depth due to aerosol layers and Rayleigh scattering calculated by our model. As discussed elsewhere (Wolf and Toon, 2010), the optical depth due to aerosol layer depends critically on the shape of aerosol particles. The optical depth by spherical aerosols shows a gradual increase toward UV region (Figure 2.20). The wavelength dependence is weak and rather flat throughout the visible region for spherical aerosols (Figure 2.20). On the other hand, the descent imager/spectral radiometer (DISR) instrument aboard the Huygens probe observed strong forward scattering of Titan's aerosol particles, resulting in a steep increase of visible optical depth toward UV region (Tomasko et al., 2008). These observations suggest Titan's aerosol particles being fractal aggregates (Tomasko et al., 2008). The optical depth of aggregated aerosols shows stronger dependence as a function of wavelength (Wolf and Toon, 2010). Thus, the sphere assumption provides a lower estimate for the aerosol optical depth.

Figure 2.21 shows the transmittance for solar FUV flux calculated in our radiative transfer model for aerosol profiles obtained by the microphysical model. The transmittance by our model is calculated by dividing the downward fluxes at 325 nm by the incident flux at 325 nm. The UV extinction effect by aerosol layers becomes evident below 200 km altitude where the thick aerosol layer starts to form, while the effect of Rayleigh scattering is weak above 100 km.

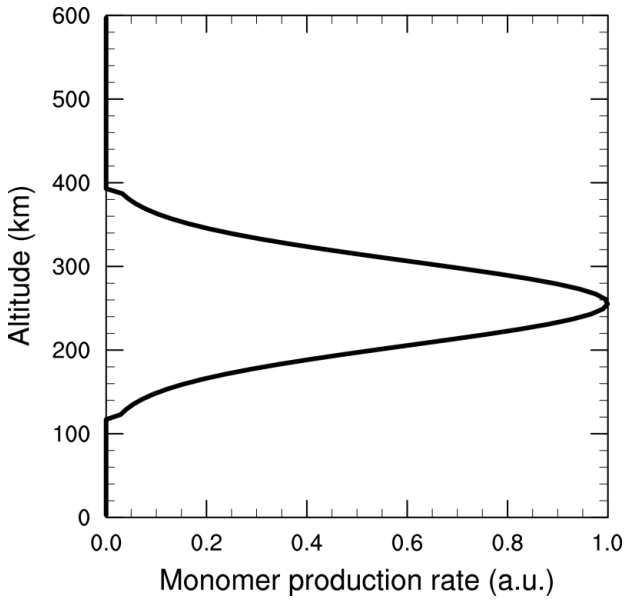

Figure 2.18. Aerosol monomer production rate based on Toon et al. (1992) and Barth and Toon (2003; 2004). Total column production rate is set to be 1.22×10^{-14} g cm^{-2} s^{-1}, or 1.33×10^{6} particle cm^{-2} s^{-1} for monomers with r = 1.3 nm and ρ = 1 g cm^{-3} (McKay et al., 1989).

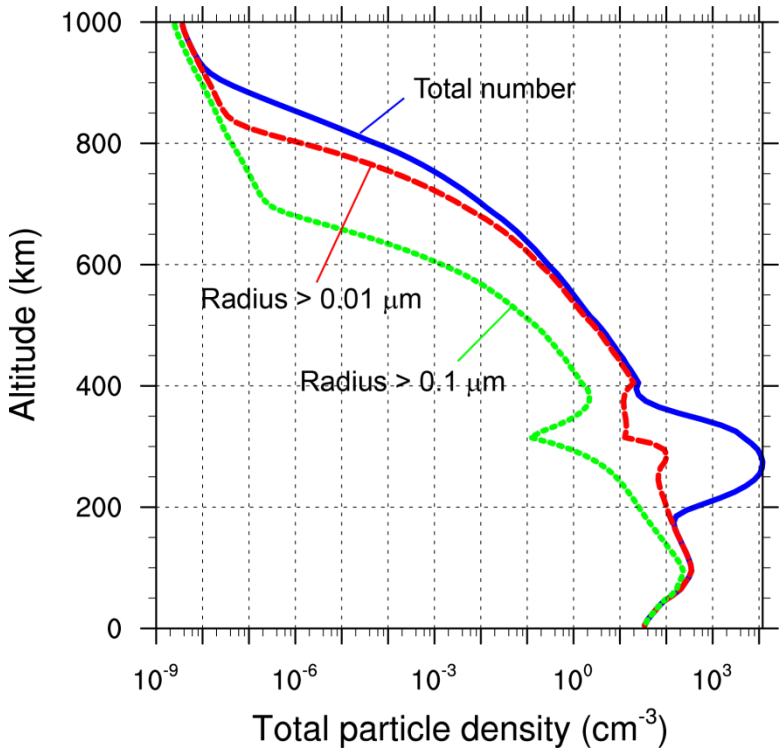

Figure 2.19. Altitude profile of aerosol particle density for various particle radii calculated by the microphysical model. The model was run for 500 years to achieve the steady-state distribution.

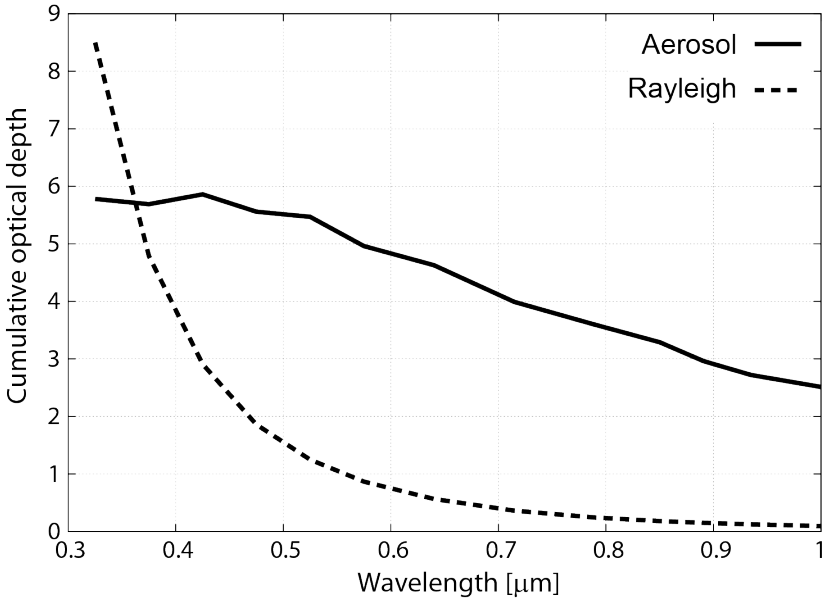

Figure 2.20. Cumulative optical depth of aerosol layer and Rayleigh scattering at Titan's surface.

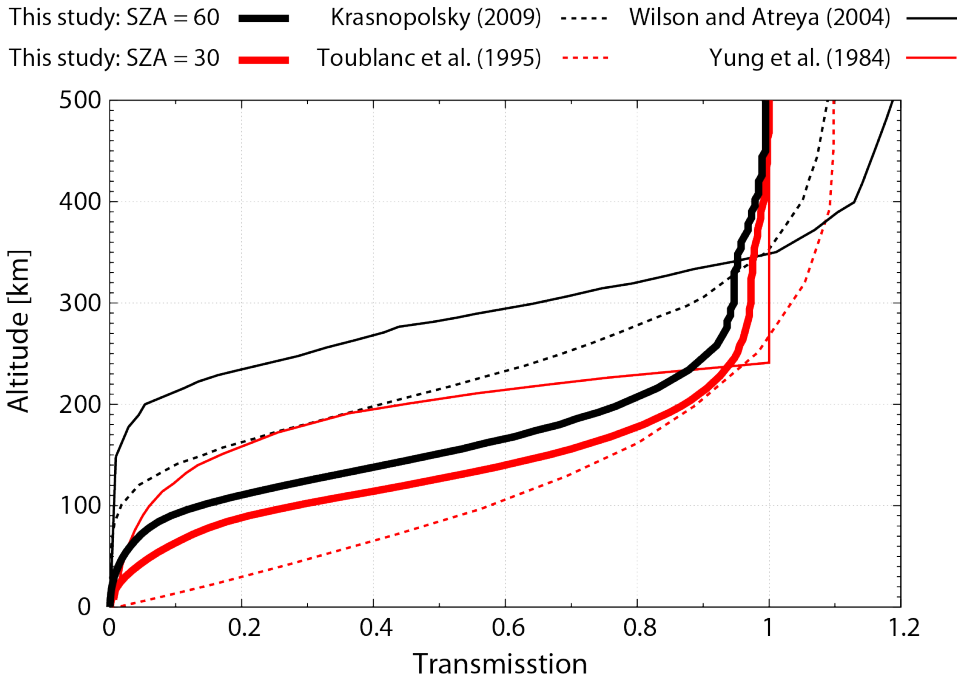

Figure 2.21. Transmittance for solar FUV flux in Titan's atmosphere. Black and red lines represent the results for the solar zenith angle (SZA) being 60° and 30°, respectively. The transmittance by our model is calculated by dividing the downward

fluxes at 325 nm by the incident flux at 325 nm. The result of Krasnopolsky (2009) is haze transmission plus reflection at 250 nm. The result of Toublanc et al. (1995) is average intensity (upward + downward) divided by the incident intensity at 300 nm. The result of Wilson and Atreya (2004) is calculated with the direct and scattered solar flux at 300 nm. The transmission factor due to aerosol absorption of Yung et al. (2004) was assumed for all UV wavelengths below 300 nm in their paper.

2.4 Application to CH_4-rich reducing atmospheres using coupled Photochemical/Microphysical/Radiative transfer model

2.4.1 Coupling of photochemical model and microphysical radiative transfer model

We couple a photochemical model to a microphysical/radiative transfer model using the monomer production reactions experimentally constrained. The chemical scheme is the same one used in the section 1.4. The monomer production reactions are the polymerization reactions of benzene (R515, R516 and R157 listed in Table 1.2). Aerosol productions by nitrile reactions, listed in Table 2.7, are also included into the model. Since the aerosol production rates calculated by photochemistry are given in molecule cm^{-3} s^{-1}, the reaction rates are first converted into a mass production rate given in g cm^{-3} s^{-1} by using the molecular weights of products. For example, in R515 (C_6H_5 + C_2H_2 → SOOT + H), the product has C_8H_7 as the stoichiometric composition, 103 g mol^{-1} was used as the molecular weight for the soot particle. The mass production rates are then converted into monomer production rates given in particle cm^{-3} s^{-1}, by assuming that the radii and density of a monomer are 1.3 nm and 1 g cm^{-3}, respectively. This procedure was done for all of the monomer production reactions at every altitude and at every time step.

We introduced the UV extinction effect by aerosol layers and Rayleigh scattering when the photolysis rate calculation, by using the transmittance at 325 nm (Figure 2.21), which is the shortest wavelength considered in the radiative transfer module of CARMA. Because of lack of gas absorption at this wavelength in our model, we can estimate the UV extinction effect by aerosols and Rayleigh scattering. The transmittance was obtained with the downward flux profile at 325 nm as described above. In the photochemical calculation, the incident solar UV flux at the all

wavelength considered (115–315 nm) was reduced by this transmittance. Despite its crudeness, the photochemical models adopted this scheme show that this scheme can reproduce the atmospheric composition of Titan (e.g., Yung et al., 1984; Lara et al., 1996). Although we believe this scheme is sufficient for the purpose of this study, a self-consistent radiative transfer calculation for the UV wavelength regions will be done in the future by the following two reasons. First, the above scheme neglects the wavelength-dependence of Rayleigh scattering and aerosol extinction. Generally, optical depths due to Rayleigh scattering and due to the extinction by fractal aerosol particles increase with a decrease in wavelength. Thus, the above scheme would underestimate the extinction by Rayleigh scattering and aerosols. This issue may not be significant at wavelengths below 200 nm, where various molecular absorptions dominate the UV attenuation (e.g., Krasnopolsky, 2009). On the other hand, at wavelengths from 200 nm to 300 nm, there are not so many absorbing gas species in this wavelength region. Thus, this issue might become important. For example, because the Rayleigh scattering cross-section is in inverse proportion to the fourth power of wavelength, we would underestimate the optical depth due to Rayleigh scattering at 200 nm by a factor of ~5. Second, the above scheme assumes that gas absorption is an independent process of the rest of the radiative transfer processes so that gas absorption does not affect scattering process. In reality, however, they interact with each other non-linearly and gas absorption does affect the scattering process. This can be understood by the following example: a single scattering albedo, ϖ, of an atmospheric layer is given by

$$\varpi = \frac{\varpi^{\mathrm{R}}\Delta\tau^{\mathrm{R}} + \varpi^{\mathrm{M}}\Delta\tau^{\mathrm{M}} + \varpi^{\mathrm{G}}\Delta\tau^{\mathrm{G}}}{\Delta\tau^{\mathrm{R}} + \Delta\tau^{\mathrm{M}} + \Delta\tau^{\mathrm{G}}} = \frac{\Delta\tau^{\mathrm{R}} + \varpi^{\mathrm{M}}\Delta\tau^{\mathrm{M}}}{\Delta\tau^{\mathrm{R}} + \Delta\tau^{\mathrm{M}} + \Delta\tau^{\mathrm{G}}} \qquad (2.58)$$

where $\Delta\tau$ is optical depth and the superscripts R, M and G stand for Rayleigh scattering by gas species, Mie scattering by particles and gas absorption, respectively. By definition, ϖ^{R} and ϖ^{G} are 1 and 0, respectively. From the equation (2.58), it is evident that the gas absorption does affect the single scattering albedo of the layer thus affect the subsequent radiative transfer calculation. This non-linear effect becomes most obvious when $\Delta\tau^{\mathrm{R}} + \Delta\tau^{\mathrm{M}} \approx \Delta\tau^{\mathrm{G}}$, i.e., the optical depth by gas absorption is comparable to the sum of the optical depths by Rayleigh and Mie scattering. When $\Delta\tau^{\mathrm{R}} + \Delta\tau^{\mathrm{M}} \ll \Delta\tau^{\mathrm{G}}$, radiative transfer is dictated by gas absorption thus this effect becomes negligible. This means that at shorter UV wavelengths, where the optical depth is dominated by gas absorption, the non-linear effect would be negligible. In summary, although there could be overestimation of the photolysis rate near 300 nm wavelength region, photolysis rate at wavelengths below 200 nm would not be affected significantly by the above assumption.

The time scales of microphysical process and photochemical process differ significantly. This means a special treatment for time stepping is needed to couple these

processes. The physical time scales of microphysics are at most 100 years (Toon et al., 1992) on Titan and a few years on early Earth (Wolf and Toon, 2010). Meanwhile, the time scale for achieving chemical equilibrium is 10^6–10^7 years on reducing atmospheres, which needs a very long time step contrary to a microphysical model. A long time step in a microphysical model would violate the mass conservation law given in (2.50). For example, particles could fall across multiple layers in a single time step. In order to avoid this problem, we limited the time step of microphysical model to be at most 10 hours. For example, when the photochemical model is running with a very long time step like 100 years, the microphysical model runs for 1 year with a 10-hour time step, which is sufficient to adjust a change of atmospheric compositions.

Table 2.7. Nitrile reactions assumed to produce aerosol monomers. These reactions are included in our one-box photochemical model. Also shown are the previous photochemical models which assumed these reactions for the calculation of aerosol production. See appendix A for the reaction rates.

Reaction		**Previous models**
R595	$CN + C_2H_3CN \rightarrow SOOT$	Hebrard et al. (2006), Lavvas et al. (2008a, b) , Krasnopolsky (2009, 2010)
R596	$CN + C_2N_2 \rightarrow SOOT$	Wilson and Atreya (2004), Hebrard et al. (2006), Lavvas et al. (2008a, b) , Krasnopolsky (2009, 2010)
R597	$CN + C_4N_2 \rightarrow SOOT$	Wilson and Atreya (2004), Hebrard et al. (2006), Lavvas et al. (2008a, b) , Krasnopolsky (2009, 2010)
R610	$H_2CN + HCN \rightarrow SOOT$	Wilson and Atreya (2004), Hebrard et al. (2006), Lavvas et al. (2008a, b), Krasnopolsky (2009, 2010)
R636	$HC_3N + C_6H_5 \rightarrow SOOT$	Wilson and Atreya (2004), Hebrard et al. (2006), Lavvas et al. (2008a, b) , Krasnopolsky (2009, 2010)

2.4.2 Application to Titan's atmosphere

In this section, we discuss the energy source for aerosol production in Titan's atmosphere and its climatic stability, based on the developed atmosphere model. Figure 2.22 shows our calculation results of the altitude profiles of reaction rate for the production of aerosol monomer. These results show that benzene polymerization reactions contribute only ~10% of the monomer production in the lower atmosphere. When aerosol monomers are produced by polymerization of benzene only, the column mass production of aerosols becomes 0.03×10^{-14} g cm^{-2} s^{-1}, which is remarkably smaller than that proposed values in Titan's atmosphere ($(0.5 - 2) \times 10^{-14}$ g cm^{-2} s^{-1}, McKay et al., 2001). These results suggest that solar EUV is not the primary energy source responsible for the formation of aerosols in Titan's atmosphere.

Another important reaction proposed for Titan's aerosol formation is polymerization of nitriles (e.g., Imanaka and Smith, 2010), which is initialized by irradiations of high energy particles and solar EUV (e.g., Waite et al., 2007; Krasnopolsky 2009). When including monomer production through nitrile polymerization reactions, the column mass production rate increases to 0.4×10^{-14} g cm^{-2} s^{-1}, which is close to the values proposed by the previous study ($(0.5 - 2) \times 10^{-14}$ g cm^{-2} s^{-1}, McKay et al., 2001). Our results show that nitrile polymerization reactions dominate the monomer production over all of the altitude (Figure 2.22). These results suggest that the aerosol production by nitrile polymerization reactions is essential to explain the observed Titan's aerosol layers. These results may be consistent with the possible inclusions of nitrogen in organic aerosol suggested by the detection of HCN and NH_3 in pyrolysis analysis of aerosols by the Huygens probe (Israel et al., 2005).

The reaction rates of nitrile polymerization reactions in the lower atmosphere, especially R610, are predominated by reactions induced by irradiations of galactic cosmic ray (GCR) (Lavvas et al., 2008b). Without the GCR flux, the reaction rates of the nitrile reactions in Figure 2.22 would decrease drastically. The reaction of R610 dominates the monomer production in the lower atmosphere around the center altitude of main aerosol layer (~300 km), while the reaction of R595 dominates the aerosol production above 300 km. Our calculation results indicate that the monomer production rate of the present study in the middle to upper atmosphere (>400 km) is significantly lower than those of the previous photochemical models (Lavvas et al., 2008b; Krasnopolsky, 2009). The discrepancy between the present study and previous photochemical models is because the previous studies take into account the polymerization of polyynes for monomer production (Lavvas et al., 2008b), whereas the present study does not consider monomer production due to polymerization of polyynes based on the laboratory experiments (section 1.4). Thus, addition of these reactions in

the upper atmosphere would enhance the abundance of benzene and nitriles, which would result in efficient monomer production. Figure 2.23 shows the number density profiles of aerosol particles for various size ranges. When we include the monomer production rate calculated by the photochemical model, this affects the distributions of small particles (r < 10 nm). On the other hand, the distribution of middle size particles (10 nm < r < 100 nm) is not significantly influenced because electrical charging on particles limit the growth for this size range (Toon et al., 1992).

Our results suggest that Titan's aerosols are largely produced by nitrile polymerization, which are initialized with dissociation of N_2 and CH_4 by irradiations of high energy particles and solar EUV. There are two major implications of our results. First is the chemical lifetime of N_2 in Titan's atmosphere. The chemical life time of N_2 is estimated on the order of 10^8 years (Wilson and Atreya, 2004), which is consistent with our calculation because we adopted N_2 destruction rate from previous estimates (Wilson and Atreya, 2004; Krasnopolsky, 2009). This implies that early Titan would have possessed abundant N_2 on the surface (e.g., ~10 times that on present-day). Nevertheless, the formation mechanism of such amount of N_2 on Titan is unclear. This is because all of the proposed mechanisms require formation of a thick proto-atmosphere associated with major rock-ice differentiation during accretion (e.g., Atreya et al., 1978; Kuramoto and Matsui, 1994), which seems to be inconsistent with a only partially differentiated interior of Titan (Iess et al., 2010). Alternatively, the rapid loss of N_2 in the current atmosphere implies that the efficient aerosol formation has taken place only in geological recent time in Titan's history. Our results show that the major fate of N_2 in photochemical reactions is HCN (56%), H_2CN (35%), HC_3N (3.5%), CHCN (2.2%), CH_3CN (3.0%) and organic aerosols (0.2%). Thus, if CH_4 is not present in the atmosphere, the chemical loss of N_2 would become very inefficient. In fact, an evolution model of Titan's interior suggests that an outgassing of CH_4 from the interior occurred only in 0.2 Gyrs ago due to initialization of crustal convection (Tobie et al., 2006).

The other implication of the present study is Titan's climatic stability in response to a change in the flux of high energy particles. For instance, given the enhanced FUV flux from Sun in the early stages of its evolution (Zahnle and Walker, 1982; Ribas et al., 2005), the aerosol production rates would have been much higher in the past than those of present-day. In addition, the flux of high energy particles depends on the magnetic field intensity of Saturn and its interactions with the solar wind. The flux of GCR also would have greatly influenced due to the solar activity and the occurrence of supernova of massive stars.

Since Titan's organic aerosol layers have an anti-greenhouse effect (McKay et al., 1989), such a variation in flux of the energy sources would have strongly influenced the surface temperature. For instance, when the flux of these energy sources increase, this would result in the formation of thick aerosol layers, which reduce the surface

temperature. This in turn would cause a decrease in the CH_4 concentration in the atmosphere, leading to a further decline in the surface temperature due to a reduction of greenhouse effects. Such a positive feedback between climate and aerosol might be dampened if the atmospheric CH_4 levels become too low to produce aerosols in the atmosphere. We suggest that Titan's climate system is very sensitive to a small change in the flux of high energy particles and/or EUV. To study the climatic instability on Titan more quantitatively, it will be important to perform self-consistent modeling of nitrile chemistry, aerosol production, and radiative transfer.

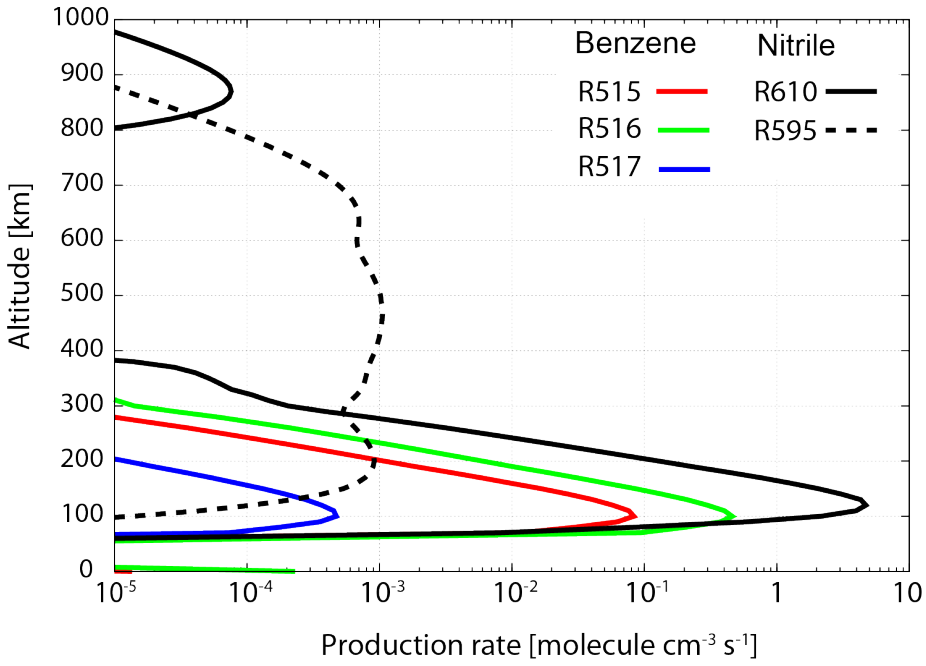

Figure 2.22. Altitude profiles of reaction rate for the production of aerosol monomer for major reactions that contribute to the monomer production. R515 & R516: $C_6H_5 + C_2H_2$, R517: $C_6H_5 + C_6H_6$, R595: $CN + C_2H_3CN$, R610: $H_2CN + HCN$. Nitrile reactions dominate the monomer production for all the altitude, although benzene polymerization reactions contribute about 10% of the monomer production in the lower atmosphere.

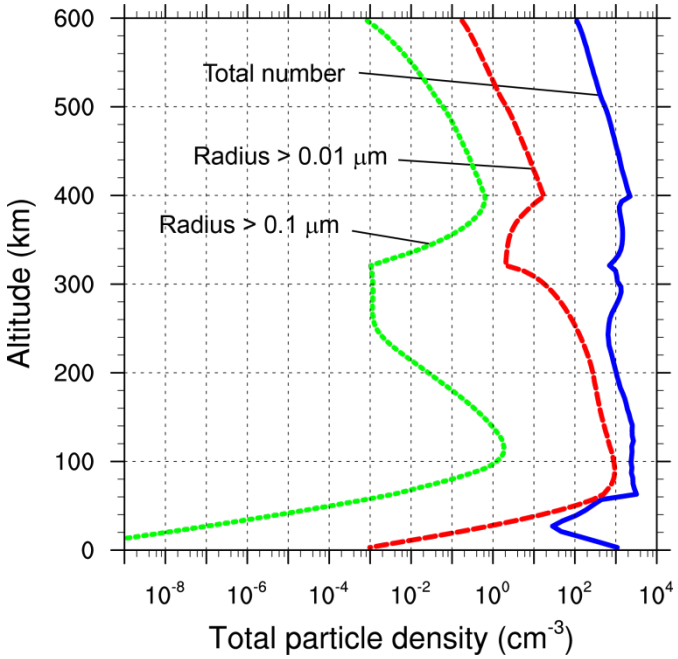

Figure 2.23. Number density profiles for various aerosol particle radii by the coupled atmospheric model.

2.4.3 Application to early Earth atmosphere

We here discuss the aerosol formation in early Earth's atmosphere and its climatic influences, based on the coupled atmosphere model developed by the present study. The calculations were performed for atmospheres with the following CH_4 and CO_2 mixing ratios: Case 1 (CH_4/CO_2=0.1, $f_{CH_4} = 250$ ppm, $f_{CO_2} = 2500$ ppm), Case 2 (CH_4/CO_2=0.4, $f_{CH_4} = 1000$ ppm, $f_{CO_2} = 2500$ ppm), Case 3 (CH_4/CO_2=1, $f_{CH_4} = 1000$ ppm, $f_{CO_2} = 1000$ ppm), Case 4 (CH_4/CO_2=10, $f_{CH_4} = 3000$ ppm, $f_{CO_2} = 300$ ppm). The rest of the parameters are same as those described in section 2.2.4. We consider that aerosol monomer productions are limited by benzene polymerization in Cases 1–4, as suggested by our experiments (see section 1.4). In Cases 3 and 4, we performed additional calculations, in which aerosol production through nitrile polymerization were included in addition to benzene polymerization. Given the uncertainty in the shape of aerosol in early Earth's atmosphere, the optical depth was calculated for two cases for a given atmospheric composition, that is, aerosols have spherical or fractal shape. The optical depth due to spherical particles is directly calculated in our radiative transfer model (see section 2.3.1); however our model cannot calculate the optical depth due to fractal particles. Thus, we used the results of Wolf and Toon (2010) to obtain the optical depth due to fractal aerosol particles (Figure 2.25). Wolf and Toon (2010) obtained a relationship of the optical depth between spherical particles and fractal particles, based on their calculation results from the microphysical model. Because the microphysical processes considered in our model are same as those of Wolf and Toon (2010), we applied this relationship given by Wolf and Toon (2010) to our calculations.

Figure 2.24 shows the cumulative optical depth of organic aerosol layers at a UV wavelength (325 nm) and a visible wavelength (575 nm). Without aerosol production through nitrile polymerization, both of the UV and visible optical depths of sphere particles are remarkably low, compared to those of the previous study (Pavlov et al., 2001). This is because the previous study includes all of polymerization reactions of hydrocarbons for aerosol monomer production (Pavlov et al., 2001); accordingly they overestimate the production rate of aerosol monomer.

In order to protect NH_3 from photolysis (i.e., to cause the indirect greenhouse effect) and to extend its chemical lifetime longer than the timescale of carbon cycle (~10^5 year: Kump, 1991), an UV optical depth due to aerosol layers is required to be in excess of ~3 (Sagan and Chyba, 1997). Our results show that UV shielding effect of fractal particles exceed unity at CH_4/CO_2 ratio > 2 (Figure 2.24). However, the organic aerosol layers, regardless of shape of aerosols, do not have sufficient UV optical depths (i.e., > 3) for $CH_4/CO_2 \leq 10$. These results suggest that the organic aerosol layers are much more optically thin in the UV wavelength than the previous estimates (e.g., Sagan

and Chyba, 1997; Wolf and Toon, 2010). This is again because the previous studies overestimate the production rate of aerosol monomers. On the basis of these calculations, we conclude that the indirect greenhouse by organic aerosols formed by solar EUV would not be able to keep early Earth warm.

It should be noted that our calculations for early Earth were performed for the modern solar FUV flux from 115 to 315 nm. The stellar evolution model and observations of young main-sequence stars, however, show that solar UV flux would have been higher in the past (e.g., Zahnle and Walker, 1982). In fact, during the first billion years of the solar system, the sun would have radiated an UV flux a few times stronger than the current UV flux (Zahnle and Walker, 1982). Given a strong UV flux from the early sun, aerosol production rate would have become high due to efficient photolysis of hydrocarbons, yielding optically thick aerosol layers. However, based on our experimental results described in section 1.3.2, aerosol production rate by FUV is only a linear function of the FUV flux. In addition, a microphysical model shows that optical depth of aerosol layers is not a linear function of the production rate but 0.6 – 0.8^{th} order function of the production rate (Wolf and Toon, 2010), which indicates the optical depth of aerosol layers is determined not only by production rate but also by other physical processes. Considering these relationships among UV flux, aerosol production rate and optical depth of aerosol layers, the optical depth of the aerosol layers formed by early sun would increase within a factor of ~2 from the results in Figure 2.24. Therefore, our conclusions of optically thin aerosol layers do not change significantly. A strong UV flux could also cause an intense heating in the upper atmosphere, where most of the photolysis reactions occur. This could enhance the chemical reaction rates. Modeling of such an Earth's upper atmosphere for evolving sun by coupling with a hydrodynamic-thermospheric model (e.g., Tian et al., 2008a; 2008b) is of particular interest for future research, not only for Earth but also for exoplanets.

Warming early Earth by greenhouse effect by H_2O, CH_4, CO_2 and C_2H_6

Our results show that the optical depth in the visible wavelength is also very low for $CH_4/CO_2 \leq 10$ (Figure 2.24), suggesting little anti-greenhouse effect due to organic aerosols formed by solar EUV. The absence of a strong anti-greenhouse effect suggests that a combination of greenhouse effects due to gas molecules, such as CH_4, C_2H_6, H_2O, and CO_2, would have played an important role to control the surface temperature. In particular, Haqq-Misra et al. (2008) proposed that C_2H_6 would be an important greenhouse gas. Nevertheless, the formation of abundance of C_2H_6 in highly CH_4-rich atmospheres also implies efficient formation of organic aerosols, which could have possessed an anti-greenhouse effect. Haqq-Misra et al. (2008) infer that the strong anti-greenhouse effect by organic aerosols could have overwhelmed the greenhouse

effect by the gas species for the atmospheres with CH_4/CO_2 ratio of > 0.1. However, our results indicate that, regardless of the particle shapes, the aerosol layers produced would have been optically thin due to low production rate of aerosol monomer. Accordingly, the greenhouse effect by C_2H_6 would have been critical to determine the surface temperature even in CH_4-rich atmospheres. The C_2H_6 mixing ratios in our model are generally consistent with those of Haqq-Misra et al. (2008). For example, Figure 2.26 shows ~1 ppm of mixing ratio of C_2H_6 for Case 4 (CH_4/CO_2=10, $f_{CH_4} = 3000$ ppm, $f_{CO_2} = 300$ ppm), which is comparable to 3.8 ppm of mixing ratio of C_2H_6 obtained by Haqq-Misra et al. (2008) (CH_4/CO_2=10, $f_{CH_4} = 1000$ ppm, $f_{CO_2} = 100$ ppm). Thus, we conclude that high abundance of C_2H_6 would have been important to keep early Earth warm, if early Earth had a CH_4-rich atmosphere.

Based on these calculation results, we then discuss the stability of climate system on early Earth with a CH_4-rich atmosphere. To discuss the climate system, understanding of feedback mechanisms in biogeochemical cycles is important. In fact, it has been poorly understood that how Earth's climate had been stabilized in a CH_4-rich atmosphere on early Earth (e.g., Pavlov et al., 2001; Kasting, 2005). For instance, Pavlov et al. (2003) proposed a possible positive feedback between CH_4 and climate. If the surface temperature increased on early Earth, the CH_4 flux injected into the atmosphere would also increase due to the enhanced methanogenic activity at higher surface temperatures (Cooney and Wise, 1975). The enhanced CH_4 flux would result in higher mixing ratios of both CH_4 and C_2H_6, leading to a further increase in surface temperature (e.g., Pavlov et al., 2003). If there were not any other competing mechanisms, this would have worked as a positive feedback, which destabilized the climate system. Pavlov et al. (2001) suggest that organic aerosol production in a CH_4-rich atmosphere would have dampened the positive feedback. They propose that an increase in CH_4 flux would have caused the formation of thick aerosol layers, which would decrease the surface temperature due to the anti-greenhouse effect. This in turn would have reduced methanogenic activity and stabilize the surface temperature (Pavlov et al., 2001).

Our calculations, however, show that the negative feedback due to organic aerosol would have been minimal, as aerosol layers produced in early Earth's atmosphere would be insufficient to cause the anti-greenhouse effect (Figure 2.24). Instead of the negative feedback due to aerosol, we propose that the silicate-carbonate feedback would have played a key role to stabilize the climate even in a CH_4-rich atmosphere, as previously proposed to stabilize a CO_2-rich early Earth (e.g., Walker et al., 1981). When the surface temperature increases, the chemical weathering rate of continents would also increase, which would decrease CO_2 partial pressures (Walker et al., 1981). A decrease in CO_2 levels would cool the surface and limit the biological activity of methanogens, which would have stabilized the climate for long-term periods.

Above we discuss the effect of organic aerosols when considering benzene

polymerization limits its production rate. This implicitly assumes that solar FUV is the predominant energy source for formation of aerosol in early Earth's atmosphere. However, as discussed below, nitrile polymerization could have occurred on early Earth as well as Titan, especially if early Earth had a weak geomagnetic field. In fact, some thermal evolution models suggest that an intensity of geomagnetic field in late Archean (3.0–2.5 Ga) could have been weaker than today (e.g., Stevenson et al., 1983), which may be consistent with paleomagnetic data (e.g., Hale, 1987; Morimoto et al., 1997; Selkin et al., 2000). In this case, efficient nitrile polymerization and aerosol formation could have caused by intense irradiations of high energy particles in the upper atmosphere.

Influence of nitrile reactions induced by high-energy particle irradiation

When including aerosol production through nitrile polymerization in our model, organic aerosol layers become optically thick (Figure 2.24). Our calculations show that UV and visible optical depths due to aerosol become moderate (~2) for spherical-shaped aerosol particles when including monomer formation by nitrile polymerization (Figure 2.24). When considering fractal-shaped particles, the UV optical depths are greatly enhanced to become ~24, which is sufficient for UV shielding of NH_3, whereas the optical depths at the visible wavelength remain moderate (Figure 2.24). These results suggest that a significant indirect greenhouse effect is caused by organic aerosol layers if nitrile polymerization leads to formation of monomers, whereas the anti-greenhouse effect by aerosol is relatively low.

Our results indicate that the optical depths of aerosol layers including nitrile polymerization depend only weakly on CH_4/CO_2 ratio of the atmosphere (Figure 2.24). This is the case because nitrile formation is not directly relevant with hydrocarbon formation, which is very sensitive to CH_4/CO_2 ratio in the atmosphere. We show the atmospheric compositions and reaction rates of the monomer production for CH_4/CO_2 of 10 in Figure 2.26–Figure 2.27. The efficient monomer production by nitrile polymerization (R595: $CN + C_2H_3CN \rightarrow SOOT$, R610: $H_2CN + HCN \rightarrow SOOT$) is sustained by high abundances of HCN and C_2H_3CN in the atmosphere. The HCN abundances calculated by our model are consistent with the results of the previous photochemical models (Zahnle 1986; Tian et al., 2011). Nitrile formation is initiated by the dissociation of N_2 in the upper atmosphere, whereas the photolysis of NH_3 in the lower atmosphere provides an additional source for formation of nitriles. Although we did not consider rainout of HCN into the ocean, HCN is not a very soluble gas at low partial pressures (Cicerone and Zellner, 1983). Figure 2.28 shows the number density profiles for various aerosol particle radii for CH_4/CO_2 of 10 including aerosol production by nitrogen polymerization. Because of a shorter residence time of organic

aerosol in early Earth's atmosphere than that in Titan's atmosphere, aerosol layers on an early Earth are composed of smaller particles than those in Titan, as suggested by the previous study (Wolf and Toon, 2010).

As similar to solar FUV flux, flux of high energy particles from young sun could have been significantly higher than that of today (Zahnle and Walker, 1982). The present calculations including nitrile reactions for the aerosol production assume a modern solar activity. This results in a globally averaged production of N atoms being 1.0×10^{10} atoms cm^{-2} s^{-1}, which is consistent with a previous estimate by Zahnle (1986) (4×10^{9} to 1.5×10^{10} atoms cm^{-2} s^{-1}). According to a stellar evolution model, during the first billion years of the solar system, the sun would have radiated a EUV/XUV flux more than 10 times the current value (Zahnle and Walker, 1982). Although the dependence of aerosol production rate on radiation dose is not clear, we can anticipate an efficient aerosol production via nitrile reactions in an Archean atmosphere due to the high levels of high-energy particle flux. Assuming that the aerosol production via nitrile reactions is a linear function of EUV/XUV flux, similar to our results of FUV experiments, the aerosol production rate with an enhanced EUV/XUV flux would be 10 times the results for the modern solar activity. Thus, even though the optical depth of aerosol layers does not increase linearly with the production rate (Wolf and Toon, 2010), the produced optical depth for early active sun would be several times the values shown in Figure 2.24.

If organic aerosols formed efficiently on early Earth through nitrile polymerization, this would strongly affect both the climate and nitrogen cycles. Our results indicate that aerosol layers formed by nitrile polymerization are optically thick in the UV wavelength sufficient to cause the indirect greenhouse (Figure 2.24). Thus, a rapid increase in intensity of the geomagnetic field would have induced a reduction of aerosol formation, leading to a dramatic decline in the surface temperature on early Earth. Indeed, the thermal evolution models show that a remarkable increase in the magnetic intensity could have occurred at ~3–2 Ga due to the formation of inner solid core and/or a change in the mantle convection style (e.g., Stevenson et al., 1983, Breuer and Spohn, 1995). We suggest that the evolution of solid Earth could have changed the atmospheric chemistry, which in turn triggered the first, large-scale glacial events in Earth's history, recorded in the sediments deposited at around 2.5–2.2 Ga (e.g., Kirschvink et al., 2000; Young et al., 2001; Bekker et al., 2004).

The nitrogen cycles under the presence of organic aerosol also have not been considered in the previous studies (e.g., Pavlov et al., 2001). As mentioned above, it has been suggested that UV shielding of NH_3 resulted in high NH_3 abundances in the troposphere (Sagan and Chyba, 1997), however the continuous source of NH_3 into the atmosphere is unknown. Our results show that HCN is also efficiently produced in the upper atmosphere (Figure 2.26). We propose that hydrolysis of the produced HCN in the ocean would have been an abiotic source of NH_3 (Zahnle 1986; Tian et al., 2011).

Therefore, nitriles might be able to have been responsible for both the source of a strong greenhouse gas (NH_3) and its protector from UV photolysis (aerosol layers). To study aerosol production mechanism through nitrile polymerization and nitrogen-carbon cycles in the atmosphere-ocean system, further laboratory experiments using EUV light source would be important in future.

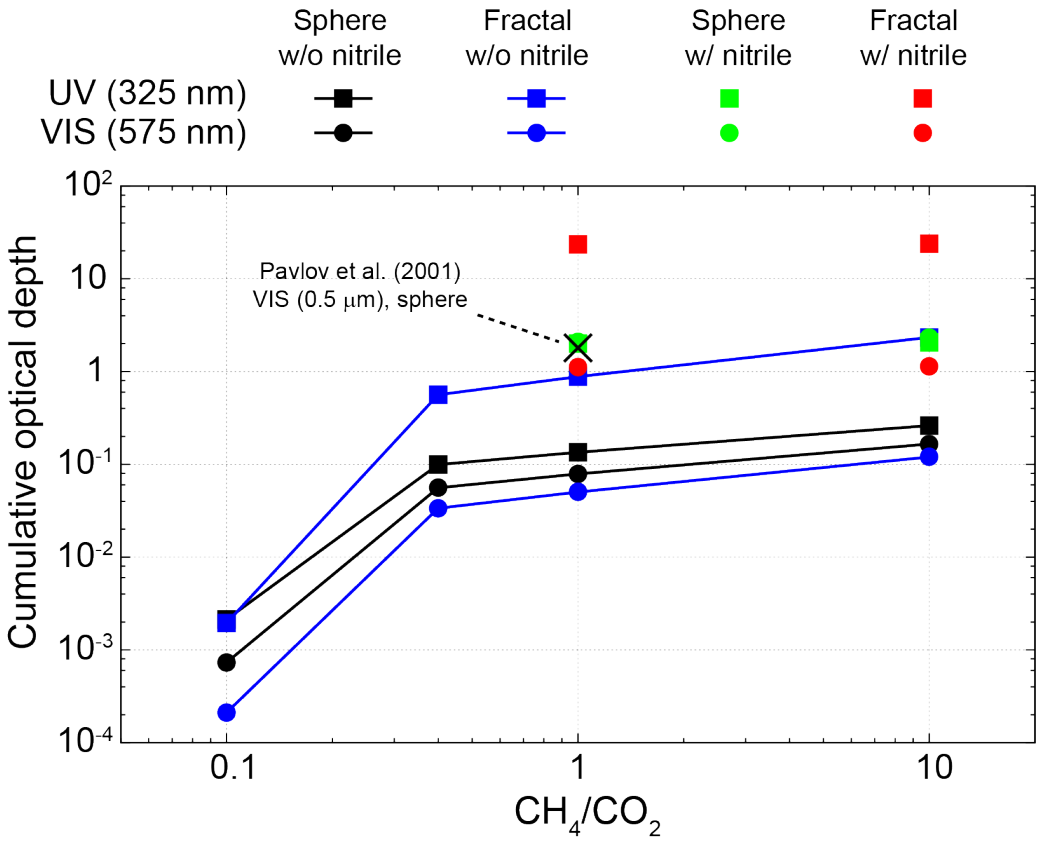

Figure 2.24. Cumulative optical depth of organic haze layers calculated for both sphere and fractal particles at a UV wavelength (325 nm) and a visible wavelength (575 nm). The total mixing ratios of CH_4 and CO_2 are from 2000 to 3500 ppm. Two aerosol production mechanisms are considered (production only by benzene pathways, or production by benzene and nitrile pathways). Also shown is the visible optical depth calculated by Pavlov et al. (2001). The optical depths of fractal particles are derived by interpolating the results of Wolf and Toon (2010) (See Figure 2.25). Only the cases using fractal particles and aerosol production with nitrile pathways show significant UV optical depths.

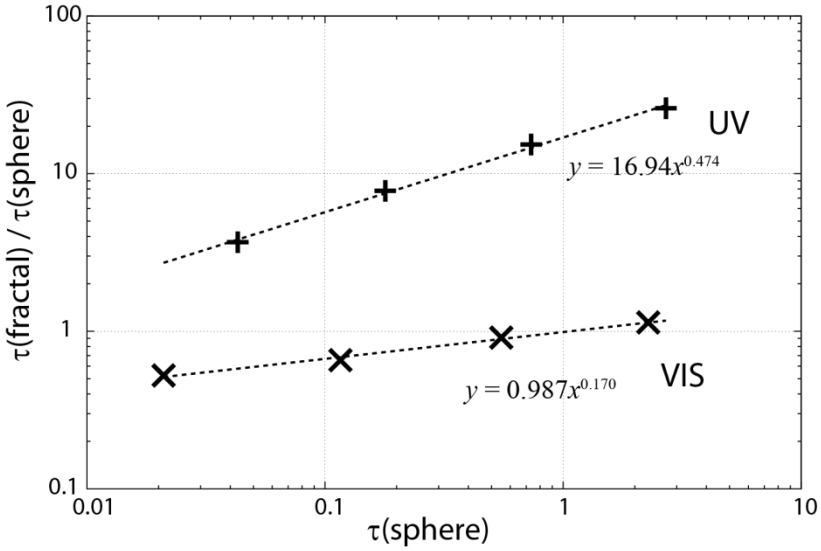

Figure 2.25. The ratio of cumulative optical depth of fractal particles to those of spherical particles as a function of the cumulative optical depth of spherical particles, calculated by Wolf and Toon (2010). The wavelengths are 197 nm and 564 nm for UV and visible, respectively. Also shown are the least square regression lines and their equations.

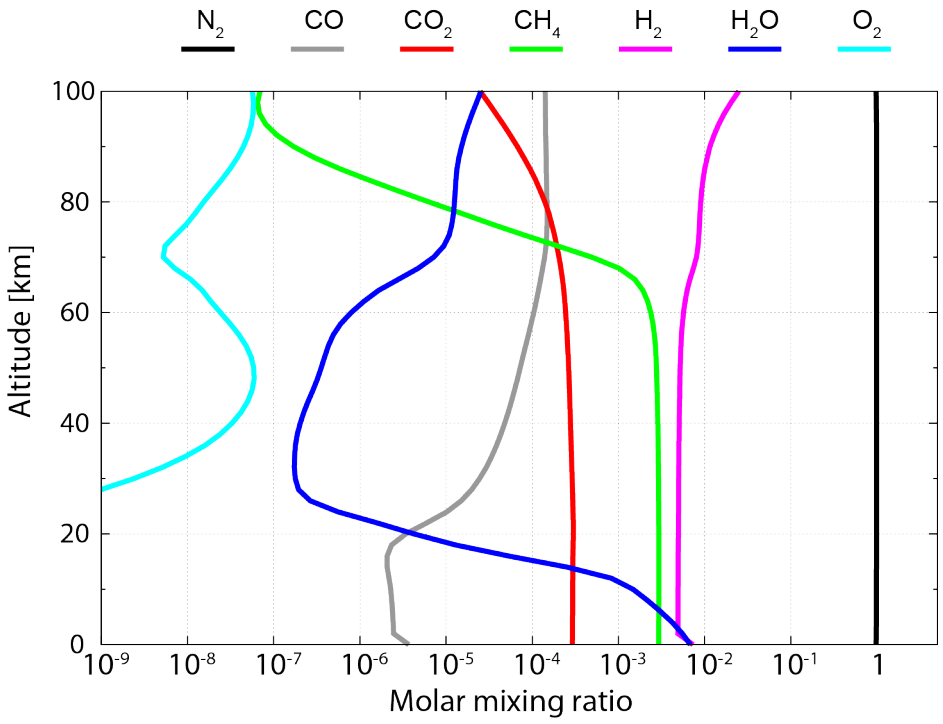

Figure 2.26 – *Continuted.*

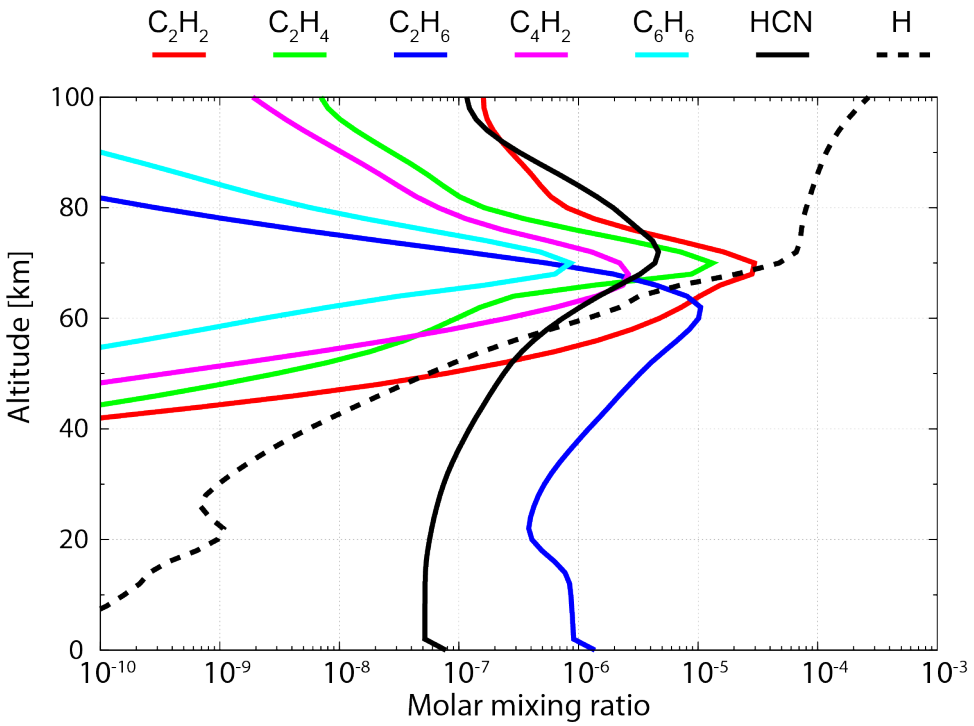

Figure 2.26. Altitude profiles of some major gases for the $CH_4/CO_2 = 10$ case including aerosol production by nitrogen chemistry.

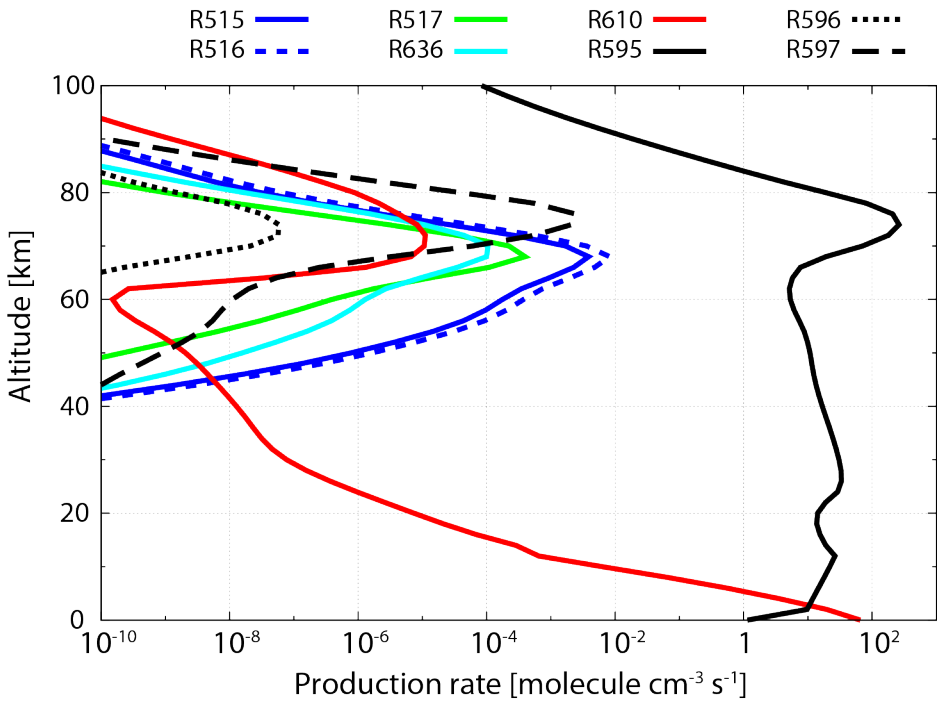

Figure 2.27. Production rate profiles for aerosol production mechanisms for the $CH_4/CO_2 = 10$ case including aerosol production by nitrogen chemistry. Nitrile reactions (R595 and R610) dominate the aerosol production at all altitudes.

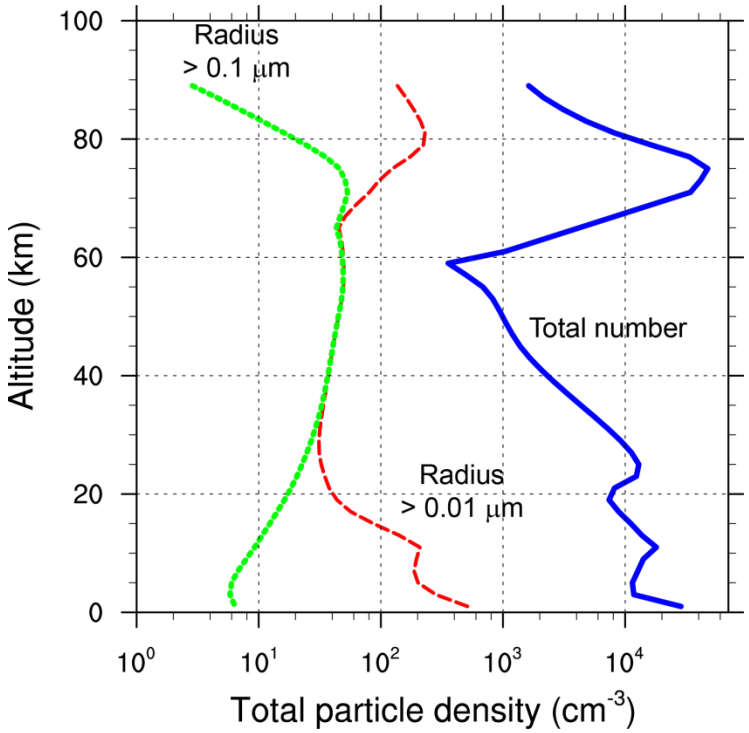

Figure 2.28. Number density profiles for various aerosol particle radii for the $CH_4/CO_2 = 10$ case including aerosol production by nitrogen chemistry.

2.5 Conclusions

We coupled a photochemical model to microphysical and radiative transfer models using the monomer production reactions experimentally constrained in the Chapter 1. Using the coupling model, we investigate the influence of organic aerosols on the radiative transfer process in reducing atmospheres. Polymerization reactions of benzene are incorporated as the monomer production reactions. We then investigate the influence of organic aerosols on the radiative transfer processes in the atmospheres of Titan and early Earth. Our results show that polymerization reactions of benzene contribute only ~10% of the total aerosol production and cannot explain the observed profile of organic aerosol layer in Titan's atmosphere. In contrast, we found the aerosol production would be dominated by nitrile polymerization in Titan's atmosphere, which requires high-energy particle irradiation to initiate the reactions. In early Earth's atmosphere, our results suggest that the organic aerosol layers produced by benzene

pathways are optically thin. Neither indirect greenhouse nor anti-greenhouse effects of organic haze layer would have been efficient if organic aerosols are formed only by polymerization of benzene, contrary to the previous predictions. This is because the previous studies included all of polymerization reactions and overestimated the amount of the organic aerosols actually formed in the atmosphere. The absence of strong anti-greenhouse effect by organic aerosols suggests that a combination of greenhouse effects of ethane would have worked efficiently even under CH_4-rich conditions to keep the Archean surface from freezing. We also suggest that if aerosol production occurs through nitrile polymerization, this would have resulted in thick aerosol layers. Assuming aggregate-shaped aerosol particles, such thick aerosols could have shielded NH_3 from UV photolysis. Nitrile polymerization in early Earth's atmosphere could have been important both for supporting the supply of NH_3 and for shielding it from UV irradiation, keeping the surface temperature above the freezing point of H_2O.

Summary

To couple chemical and physical processes occurred in CH_4-rich reducing atmospheres, we have conducted laboratory experiments of tholin formation and photochemical calculations to identify the parent molecules and chemical reactions that control the tholin production by irradiation of FUV light ($120 < \lambda < 200$ nm). Our results show that the tholin production rate is a linear function of actinic UV flux, which suggests that the aerosol production is limited by polymerization reactions between intermediate products produced from the photochemistry of methane. Our results also indicate that the tholin production rate remains almost constant as a function of CH_4/CO_2 ratio for higher CH_4/CO_2 (> 1), whereas the production rate drops remarkably with increasing CO_2 concentration when CH_4/CO_2 ratio is less than unity. Photochemical calculations show that the behavior of tholin production as a function of CH_4/CO_2 ratio is in a good agreement with polymerization reaction rates involving benzene. These results suggest that benzene play the intermediate products that control the tholin production. On the other hand, polymerization reactions involving polyynes would not contribute to the tholin production, contrary to the assumptions of the previous studies.

We then coupled a photochemical model to microphysical and radiative transfer models based on our experimental results that polymerization reactions of benzene control the production of aerosol monomers in CH_4-rich atmosphere. Our results show that polymerization reactions of benzene cannot explain the proposed aerosol production rates in Titan's atmosphere. In contrast, our results suggest that the organic aerosols in Titan's atmosphere are largely produced by nitrile polymerization, which require high-energy particles to initiate the reactions. There results imply that Titan's climate and surface environments would have been very sensitive to variations in the magnetic field of Saturn and solar wind flux in long-term evolution.

In early Earth's atmosphere, the organic aerosol layers produced by benzene polymerization would have been optically thin, insufficient to have both indirect greenhouse and anti-greenhouse effects. The absence of strong anti-greenhouse effect in turn suggests that the greenhouse effect of ethane would have worked efficiently to keep the Archean surface from freezing, especially under CH_4-rich atmospheric conditions. The supply and loss of both CO_2 and CH_4 through biogeochemical processes are a function of surface temperature. Given that ethane concentration also varies as a function of CH_4/CO_2 ratio of the atmosphere, there would have been a feedback between surface temperature and ethane concentration. On the other hand, if aerosol production also proceeds through nitrile polymerization, thick aerosol layers would have been formed, sufficient for UV shielding of NH_3 on early Earth. Further

investigation of nitrile polymerization by laboratory experiments will be important in future studies to evaluate the role of organic aerosols in early Earth's atmosphere.

Appendices

A. Photochemical scheme

Original No. denotes the reaction number for the appendix of Hebrard et al. (2006). Rate coefficients of first-order, second-order (two-body) and third-order (three-body) reactions are given in s^{-1}, cm^3 s^{-1} and cm^6 s^{-1}, respectively.

No.	Name	Note	No.	Name	Note	No.	Name	Note	No.	Name	Note	No.	Name	Note
1	H		28	C_4H_3		55	C_6H_9	P	82	CHCN		109	N_2H_4	$h\nu$
2	H_2	$h\nu$	29	C_4H_4	$h\nu$	56	C_6H_{10}	P	83	CH_2CN	P	110	$O(^1D)$	
3	C		30	C_4H_5		57	C_6H_{11}	P	84	CH_2NH	P	111	$O(^3P)$	
4	CH		31	C_4H_6	$h\nu$	58	C_6H_{12}	P	85	CH_2NH_2	P	112	O_2	$h\nu$
5	$^1CH_2$		32	C_4H_7	P	59	C_6H_{13}	P	86	CH_3CN	$h\nu$	113	O_3	$h\nu$
6	$^3CH_2$		33	C_4H_8		60	C_6H_{14}	P	87	CH_3NH	P	114	CO	
7	CH_3	$h\nu$	34	C_4H_9	P	61	C_7H_3	P	88	CH_3NH_2		115	CO_2	$h\nu$
8	CH_4	$h\nu$	35	C_4H_{10}		62	C_7H_4	P	89	C_2N		116	NO	$h\nu$
9	C_2		36	C_5H_2	P	63	C_7H_5	P	90	C_2N_2	$h\nu$	117	OH	$h\nu$
10	C_2H		37	C_5H_3		64	C_7H_6	P	91	C_2H_3CN		118	H_2O	$h\nu$
11	C_2H_2	$h\nu$	38	C_5H_4	P	65	C_7H_7	P	92	$C_2H_3NH_2$	P	119	HO_2	$h\nu$
12	C_2H_3	$h\nu$	39	C_5H_5	P	66	C_7H_8	P	93	C_2H_5CN	P	120	H_2O_2	$h\nu$
13	C_2H_4	$h\nu$	40	C_5H_6	P	67	C_7H_9	P	94	C_3N		121	HCO	
14	C_2H_5		41	C_5H_7	P	68	C_7H_{10}	P	95	C_3H_2CN	P	122	H_2CO	$h\nu$
15	C_2H_6	$h\nu$	42	C_5H_8	P	69	C_8H	P	96	C_3H_3CN	P	123	CH_2CO	$h\nu$
16	C_3H		43	C_5H_9	P	70	C_8H_2	$h\nu$	97	C_4H_2CN	P	124	CH_3O	
17	C_3H_2		44	C_5H_{10}	P	71	C_8H_3	P	98	C_4H_3CN	P	125	CH_3CO	
18	C_3H_3	$h\nu$	45	C_5H_{11}	P	72	C_8H_4	P	99	C_4N_2	$h\nu$	126	C_2H_4O	P
19	CH_3C_2H	$h\nu$	46	C_5H_{12}	P	73	C_8H_6	P	100	$N(^2D)$		127	CH_2OH	
20	CH_2CCH_2	$h\nu$	47	C_6H		74	CN		101	$N(^4S)$		128	CH_3OH	
21	C_3H_5		48	C_6H_2	$h\nu$	75	HCN	$h\nu$	102	NH		129	CH_3CHO	$h\nu$
22	C_3H_6	$h\nu$	49	C_6H_3	P	76	H_2CN		103	NH_2		130	C_2H_2OH	
23	C_3H_7		50	C_6H_4		77	HC_2N_2		104	NH_3	$h\nu$	131	C_2H_4OH	P
24	C_3H_8	$h\nu$	51	C_6H_5		78	HC_3N	$h\nu$	105	N_2	$h\nu$	132	C_2H_5CHO	$h\nu$
25	C_4H		52	C_6H_6	$h\nu$	79	H_2C_3N		106	N_2H	P	133	Ar	
26	C_4H_2	$h\nu$	53	C_6H_7	P	80	H_2C_3CN	L	107	N_2H_2		134	SOOT	
27	$C_4H_2^*$		54	C_6H_8		81	HC_5N	P	108	N_2H_3				

Pholollysis reactions

No.	original No.	Reactant 1	+ $h\nu$ →	Product 1	+	Product 2	+	Product 3	Cross sections	Quantum yields, q_x [wavelength in nm]	References for q_x
1	J1	H_2	+ $h\nu$ →	H	+	H			SwRI (no reference)	1.0	
2	J2	CH_3	+ $h\nu$ →	$^1CH_2$	+	H				1 [≠216 nm], 0 [216]	Parkes et al. (1973)
3	J3a	CH_4	+ $h\nu$ →	CH_3	+	H				1, 0.291 [Lyman α]	Wang et al. (2000)
4	J3b	CH_4	+ $h\nu$ →	$^1CH_2$	+	H	+	H		0.055 [Lyman α]	
5	J3c	CH_4	+ $h\nu$ →	$^1CH_2$	+	H_2				0.584 [Lyman α]	
6	J3d	CH_4	+ $h\nu$ →	CH	+	H_2	+	H		0.07 [Lyman α]	
7	J4a	C_2H_2	+ $h\nu$ →	C_2H	+	H				0.3	Okabe (1981); Okabe (1983); Seki & Okabe (1993)
8	J4b	C_2H_2	+ $h\nu$ →	C_2	+	H_2				0.1	
9	J5	C_2H_3	+ $h\nu$ →	C_2H_2	+	H			Fahr et al. (1998) vinyl radical	1.0	Fahr et al. (1998)
10	J6a	C_2H_4	+ $h\nu$ →	C_2H_2	+	H_2				0.58 [115–174]; 0.73 [> 175]	Holland et al. (1997); Chang et al. (1998)
11	J6b	C_2H_4	+ $h\nu$ →	C_2H_2	+	H	+	H		0.42 [115–174]; 0.27 [> 175]	
12	J7a	C_2H_6	+ $h\nu$ →	C_2H_4	+	H_2				0.56; 0.12 [Lyman α]	Akimoto et al. (1965); Hampson & McNesby (1965); Lias et al. (1970); Mount et al. (1977); Mount & Moos (1978)
13	J7b	C_2H_6	+ $h\nu$ →	C_2H_4	+	H	+	H		0.14; 0.30 [Lyman α]	
14	J7c	C_2H_6	+ $h\nu$ →	C_2H_2	+	H_2	+	H_2		0.27; 0.25 [Lyman α]	
15	J7d	C_2H_6	+ $h\nu$ →	CH_4	+	$^1CH_2$				0.02; 0.25 [Lyman α]	
16	J7e	C_2H_6	+ $h\nu$ →	CH_3	+	CH_3				0.01; 0.08 [Lyman α]	
17	J8a	C_3H_3	+ $h\nu$ →	C_3H_2	+	H				0.96	Jackson et al. (1991)
18	J8b	C_3H_3	+ $h\nu$ →	C_3H	+	H_2				0.04	
19	J9a	CH_3C_2H	+ $h\nu$ →	C_3H_3	+	H				0.56	Ho et al. (1998); Sun et al. (1999)
20	J9b	CH_3C_2H	+ $h\nu$ →	C_3H_2	+	H_2				0.44	
21	J10a	CH_2CCH_2	+ $h\nu$ →	C_3H_3	+	H				0.64	Seki & Okabe (1992); Ni et al. (1999); Sun et al. (1999)
22	J10b	CH_2CCH_2	+ $h\nu$ →	C_3H_2	+	H_2				0.36	
23	J11a	C_3H_6	+ $h\nu$ →	C_3H_5	+	H				0 [< 136]; 0 [136–155]; 0.565 [156–175]; 0.41 [> 175]	Collin (1988)
24	J11b	C_3H_6	+ $h\nu$ →	CH_3C_2H	+	H_2				0.11 [< 136]; 0.11 [136–155]; 0.01 [156–175]; 0.01 [> 175]	
25	J11c	C_3H_6	+ $h\nu$ →	CH_2CCH_2	+	H_2				0.17 [< 136]; 0.22 [136–155]; 0.01 [156–175]; 0.01 [> 175]	
26	J11d	C_3H_6	+ $h\nu$ →	C_2H_4	+	$^1CH_2$				0.06 [< 136]; 0.04 [136–155]; 0.02 [156–175]; 0.03 [> 175]	
27	J11e	C_3H_6	+ $h\nu$ →	C_2H_3	+	CH_3				0.21 [< 136]; 0.27 [136–155]; 0.335 [156–175]; 0.4 [> 175]	
28	J11f	C_3H_6	+ $h\nu$ →	C_2H_2	+	CH_4				0.05 [< 136]; 0.03 [136–155]; 0.05 [156–175]; 0.04 [> 175]	
29	J12a	C_3H_8	+ $h\nu$ →	C_3H_6	+	H_2				0.34 [< 136]; 0.66 [136–154]; 0.94 [> 154]	Johnston et al. (1978)
30	J12b	C_3H_8	+ $h\nu$ →	C_2H_6	+	$^1CH_2$				0.09 [< 136]; 0.04 [136–154]; 0 [> 154]	
31	J12c	C_3H_8	+ $h\nu$ →	C_2H_5	+	CH_3				0.35 [< 136]; 0.19 [136–154]; 0 [> 154]	
32	J12d	C_3H_8	+ $h\nu$ →	C_2H_4	+	CH_4				0.22 [< 136]; 0.11 [136–154]; 0.06 [> 154]	
33	J13a	C_4H_2	+ $h\nu$ →	C_4H	+	H				0.2 [< 181]; 0 [181–205]; 0 [> 205]	Glicker & Okabe (1987)
34	J13b	C_4H_2	+ $h\nu$ →	C_2H_2	+	C_2				0.1 [< 181]; 0.06 [181–205]; 0 [> 205]	
35	J13c	C_4H_2	+ $h\nu$ →	C_2H	+	C_2H				0.03 [< 181]; 0.01 [181–205]; 0 [> 205]	

36	J13d	C_4H_2	+ $h\nu$ →	$C_4H_2^*$								0.67 [< 181]; 0.93 [181–205]; 1 [> 205]	
37	J14a	C_4H_4	+ $h\nu$ →	C_4H_2	+	H_2					same as C_4H_2	0.8	Gladstone (1996)
38	J14b	C_4H_4	+ $h\nu$ →	C_2H_2	+	C_2H_2						0.2	
39	J15a	C_4H_6	+ $h\nu$ →	C_4H_4	+	H_2					Fahr & Nayak (1994) 1,3-Butadiene (218K)	0.05	Bergmann & Demtörder (1968)
40	J15b	C_4H_6	+ $h\nu$ →	C_2H_3	+	C_2H_3						0.1	
41	J15c	C_4H_6	+ $h\nu$ →	C_2H_4	+	C_2H_2						0.17	
42	J15d	C_4H_6	+ $h\nu$ →	C_3H_3	+	CH_3						0.4	
43	J15e	C_4H_6	+ $h\nu$ →	C_4H_5	+	H						0.28	
44	J16a	C_6H_2	+ $h\nu$ →	C_6H	+	H						0.2 [115–164]; 0 [165–300]	Wilson & Atreya (2003)
45	J16b	C_6H_2	+ $h\nu$ →	C_4H	+	C_2H						0.13 [115–164]; 0.07 [165–300]	
46	J17a	C_6H_6	+ $h\nu$ →	C_6H_5	+	H					Rennie et al. (1998) Bolovinos et al. (1981; 1982) Etzkorn et al. (1999) Feng et al. (2002)	0.8 [< 220]; 0 [221–270]	Wilson & Atreya (2003)
47	J17b	C_6H_6	+ $h\nu$ →	C_6H_4	+	H_2						0.16 [< 220]; 0.96 [221–270]	
48	J17c	C_6H_6	+ $h\nu$ →	C_5H_3	+	CH_3						0.04 [< 220]; 0.04 [221–270]	
49	J18a	C_8H_2	+ $h\nu$ →	C_4H	+	C_4H					same as C_6H_2	0.2 [115–164]; 0 [165–300]	Wilson & Atreya (2003)
50	J18b	C_8H_2	+ $h\nu$ →	C_6H	+	C_2H						0.13 [115–164]; 0.07 [165–300]	
51	J19	N_2	+ $h\nu$ →	$N(^4S)$	+	$N(^2D)$						1.0	
52	J20	NH_3	+ $h\nu$ →	NH_2	+	H						1.0	McNesby & Okabe (1962)
53	J21	HCN	+ $h\nu$ →	CN	+	H						1.0	Lee (1980)
54	J22a	HC_3N	+ $h\nu$ →	C_3N	+	H						0.09	Halpern et al. (1988, 1990); Clarke & Ferris (1995)
55	J22b	HC_3N	+ $h\nu$ →	CN	+	C_2H						0.3 [< 150]; 0.05 [> 150]	
56	J23	CH_3CN	+ $h\nu$ →	CN	+	CH_3						1.0	Halpern & Tang (1985)
57	J24	C_2N_2	+ $h\nu$ →	CN	+	CN						1.0	Cody et al. (1977); Jackson & Halpern (1979); Eng et al. (1996)
58	J25	C_4N_2	+ $h\nu$ →	C_3N	+	CN						0.3	Halpern et al. (1990)
59	J26a	H_2O	+ $h\nu$ →	OH	+	H						0.78 [< 145]; 1.0 [> 145]	Stief et al. (1975); Mordaunt et al. (1994)
60	J26b	H_2O	+ $h\nu$ →	$O(^1D)$	+	H_2						0.11 [< 145]; 0 [> 145]	
61	J26c	H_2O	+ $h\nu$ →	$O(^3P)$	+	H	+	H				0.11 [< 145]; 0 [> 145]	
62	J27	OH	+ $h\nu$ →	$O(^1D)$	+	H					from SwRI web van Dishoeck (1984)	1.0	
63	J28a	CO_2	+ $h\nu$ →	CO	+	$O(^3P)$						0 [< 167]; 1.0 [> 167]	Okabe (1978)
64	J28b	CO_2	+ $h\nu$ →	CO	+	$O(^1D)$						1.0 [< 167]; 0 [> 167]	
65	J29a	H_2CO	+ $h\nu$ →	CO	+	H_2						variable	Sander et al. (2011)
66	J29b	H_2CO	+ $h\nu$ →	HCO	+	H						variable	
67	J30	NO	+ $h\nu$ →	$O(^3P)$	+	$N(^4S)$						1.0	Huebner et al. (1992)
68		O_2	+ $h\nu$ →	$O(^3P)$	+	$O(^1D)$						based on SwRI web	
69		O_2	+ $h\nu$ →	$O(^3P)$	+	$O(^3P)$						based on SwRI web	
70		O_3	+ $h\nu$ →	O_2	+	$O(^1D)$						0.55 [< 193]; variable [193–220]; 0.90 [221–304]; variable [> 305]	Sander et al. (2011)
71		O_3	+ $h\nu$ →	O_2	+	$O(^3P)$						1.35 [< 193]; variable [193–220]; 0.10 [221–304]; variable [> 305]	
72		HO_2	+ $h\nu$ →	OH	+	$O(^3P)$						1.0	
73		H_2O_2	+ $h\nu$ →	OH	+	OH						1.0	
74		CH_2CO	+ $h\nu$ →	$^3CH_2$	+	CO						1.0	
75		CH_3CHO	+ $h\nu$ →	CH_3	+	HCO						0.5	Pavlov et al. (2001)
76		CH_3CHO	+ $h\nu$ →	CH_4	+	CO						0.5	
77		C_2H_5CHO	+ $h\nu$ →	C_2H_5	+	HCO					same as CH_3CHO	1.0	
78		N_2H_4	+ $h\nu$ →	N_2H_3	+	H						1.0	

Chemical Reactions used in P. Hong model 12.5.2013 Peng Hong
E:¥Hong¥Work¥Doctoral Thesis¥[haze_optical_depth.xlsx]Sheet1
Red: Corrected based on references
Blue rate coefficients: Termolecular reactions without k_0 or k_∞
Green rate coefficients: see the right equation

$$k(M,T) = \left(\frac{k_0(T)[M]}{1+\frac{k_0(T)[M]}{k_\infty(T)}}\right) 0.6^{\left\{1+\left[\log_{10}\frac{k_0(T)[M]}{k_\infty(T)}\right]^2\right\}^{-1}}$$

$$k(M,T) = \frac{k_0(T)[M]}{1+\frac{k_0(T)[M]}{k_\infty(T)}} F \quad \text{for (R860)}$$

No.	original No.	Reactant 1	+	Reactant 2	→	Product 1	+	Product 2	+	Product 3	Rate coefficients	References
R100	R321	$C_4H_2^*$			→	C_4H_2					$10\ s^{-1}$	Vuitton et al. (2003)
R101	R388	$N(^2D)$			→	$N(^4S)$					$2.3 \times 10^{-5}\ s^{-1}$	Okabe (1978)
R102	R535	$O(^1D)$			→	$O(^3P)$					$6.7 \times 10^{-3}\ s^{-1}$	Okabe (1978)
R150	R1	H	+	H	M →	H_2					$k_0 = 1.5 \times 10^{-29}\ T^{-1.3}$ $k_\infty = 1.0 \times 10^{-11}$	Tsang & Hampson (1986) (k_0) Estimated from Jacobs et al. (1965) by Lavvas et al. (2008) (k_∞)
R151	R2	H	+	CH	→	C	+	H_2			$1.31 \times 10^{-10}\ e^{-80/T}$	Harding et al. (1993)
R152	R3	H	+	$^1CH_2$	→	CH	+	H_2			2.71×10^{-10}	Tsang & Hampson (1986)
R153	R4	H	+	$^3CH_2$	→	CH	+	H_2			$3.54 \times 10^{-11}\ T^{0.32}$	Fulle & Hippler (1997)
R154	R5	H	+	$^3CH_2$	M →	CH_3					$k_0 = 3.1 \times 10^{-30}\ e^{457/T}$ $k_\infty = 1.5 \times 10^{-10}$	Gladstone et al. (1996)
R155	R6	H	+	CH_3	→	$^3CH_2$	+	H_2			$1.0 \times 10^{-10}\ e^{-7600/T}$	Baulch et al. (1992)
R156	R7	H	+	CH_3	M →	CH_4					$k_0 = 6.33 \times 10^{-21}\ T^{-2.98}\ e^{-635/T}$ $k_\infty = 3.5 \times 10^{-10}$	Forst (1991) Baulch et al. (1994)
R157	R8	H	+	CH_4	→	CH_3	+	H_2			$2.18 \times 10^{-20}\ T^3\ e^{-4045/T}$	Baulch et al. (1992)
R158	R9	H	+	C_2H	M →	C_2H_2					$k_0 = 1.26 \times 10^{-18}\ T^{-3.1}\ e^{-721/T}$ $k_\infty = 3.0 \times 10^{-10}$	Tsang & Hampson (1986)
R159	R10	H	+	C_2H_2	→	C_2H	+	H_2			$1.0 \times 10^{-10}\ e^{-11200/T}$	Tsang & Hampson (1986)
R160	R11	H	+	C_2H_2	M →	C_2H_3					$k_0 = 3.3 \times 10^{-30}\ e^{-740/T}$ $k_\infty = 1.4 \times 10^{-11}\ e^{-1300/T}$	Baulch et al. (1994)
R161	R12	H	+	C_2H_3	→	C_2H_2	+	H_2			7.6×10^{-11}	Monks et al. (1995)
R162	R13	H	+	C_2H_3	M →	C_2H_4					$k_0 = 5.76 \times 10^{-24}\ T^{-1.3}$ $k_\infty = 8.0 \times 10^{-11}$	Monks et al. (1995)
R163	R14	H	+	C_2H_4	M →	C_2H_5					$k_0 = 7.69 \times 10^{-30}\ e^{-383/T}$ $k_\infty = 6.6 \times 10^{-15}\ T^{1.28}\ e^{-650/T}$	Baulch et al. (1994)
R164	R15	H	+	C_2H_5	→	CH_3	+	CH_3			1.25×10^{-10}	Sillesen et al. (1993)
R165	R16	H	+	C_2H_5	→	C_2H_4	+	H_2			3.0×10^{-12}	Tsang & Hampson (1986)
R166	R17	H	+	C_2H_5	M →	C_2H_6					$k_0 = 5.5 \times 10^{-23}\ T^{-2}\ e^{-1040/T}$ $k_\infty = 1.66 \times 10^{-10}$	Teng & Jones (1972) Sillesen et al. (1993)
R167	R18	H	+	C_2H_6	→	C_2H_5	+	H_2			$2.35 \times 10^{-15}\ T^{1.5}\ e^{-3725/T}$	Baulch et al. (1992)
R168	R19	H	+	C_3H_2	M →	C_3H_3					$k_0 = 1.7 \times 10^{-26}$ $k_\infty = 1.0 \times 10^{-11}$	Laufer et al. (1983) Homann & Wellmann (1983)
R169	R20	H	+	C_3H_3	M →	CH_3C_2H					$k_0 = 1.7 \times 10^{-26}$ $k_\infty = 2.5 \times 10^{-10}$	Laufer et al. (1983) Atkinson & Hudgens (1999)
R170	R21	H	+	C_3H_3	M →	CH_2CCH_2					$k_0 = 1.7 \times 10^{-26}$ $k_\infty = 2.5 \times 10^{-10}$	Laufer et al. (1983) Atkinson & Hudgens (1999)
R171	R22	H	+	CH_3C_2H	M →	CH_3	+	C_2H_2			$k_0 = 8.0 \times 10^{-24}\ T^{-2}\ e^{-1225/T}$ $k_\infty = 9.7 \times 10^{-13}\ e^{-1550/T}$	Wagner & Zellner (1972a)
R172	R23	H	+	CH_3C_2H	M →	C_3H_5					$k_0 = 8.0 \times 10^{-24}\ T^{-2}\ e^{-1225/T}$ $k_\infty = 6.0 \times 10^{-11}\ e^{-1233/T}$	Whytock et al. (1976)
R173	R24	H	+	CH_2CCH_2	→	CH_3C_2H	+	H			$1.29 \times 10^{-11}\ e^{-1156/T}$	Alexandrov et al. (1980)
R174	R25	H	+	CH_2CCH_2	M →	CH_3	+	C_2H_2			$k_0 = 8.0 \times 10^{-24}\ T^{-2}\ e^{-1225/T}$ $k_\infty = 9.7 \times 10^{-13}\ e^{-1550/T}$	Wagner & Zellner (1972b)
R175	R26	H	+	CH_2CCH_2	M →	C_3H_5					$k_0 = 8.0 \times 10^{-24}\ T^{-2}\ e^{-1225/T}$ $k_\infty = 6.6 \times 10^{-12}\ e^{-1360/T}$	Whytock et al. (1976)
R176	R27	H	+	C_3H_5	→	C_2H_3	+	CH_3			6.0×10^{-11}	Estimated from R183
R177	R28	H	+	C_3H_5	→	CH_3C_2H	+	H_2			3.3×10^{-10}	Tsang (1991)
R178	R29	H	+	C_3H_5	→	CH_2CCH_2	+	H_2			3.0×10^{-11}	Tsang (1991)
R179	R30	H	+	C_3H_5	M →	C_3H_6					$k_0 = 1.0 \times 10^{-24}$ $k_\infty = 2.84 \times 10^{-10}$	Hanning-Lee & Pilling (1992)
R180	R31	H	+	C_3H_6	→	CH_3	+	C_2H_4			$1.2 \times 10^{-11}\ e^{-655/T}$	Tsang (1991)
R181	R32	H	+	C_3H_6	→	C_3H_5	+	H_2			$2.87 \times 10^{-19}\ T^{2.5}\ e^{-1245/T}$	Tsang (1991)
R182	R33	H	+	C_3H_6	M →	C_3H_7					$k_0 = 1.5 \times 10^{-29}$ $k_\infty = 3.7 \times 10^{-11}\ e^{-1040/T}$	Laufer et al. (1983)
R183	R34	H	+	C_3H_7	→	C_2H_5	+	CH_3			6.0×10^{-11}	Tsang (1988)
R184	R35	H	+	C_3H_7	→	C_3H_6	+	H_2			3.0×10^{-12}	Tsang (1988)
R185	R36	H	+	C_3H_7	M →	C_3H_8					$k_0 = 5.5 \times 10^{-23}\ T^{-2}\ e^{-1040/T}$ $k_\infty = 2.49 \times 10^{-10}$	Estimated from R166(k_0) Munk et al. (1986)
R186	R37	H	+	C_3H_8	→	C_3H_7	+	H_2			$2.2 \times 10^{-18}\ T^{2.54}\ e^{-3400/T}$	Tsang (1988)
R187	R38	H	+	C_4H	M →	C_4H_2					$k_0 = 1.26 \times 10^{-18}\ T^{-3.1}\ e^{-721/T}$ $k_\infty = 3.0 \times 10^{-10}$	Estimated from R158(k_0) Estimated from R158(k_∞)

R188	R39	H	+	C_4H_2	$\xrightarrow{M}$	C_4H_3				$k_0 = 3.3 \times 10^{-30} e^{-740/T}$ $k_\infty = 1.39 \times 10^{-10} e^{-1184/T}$	Estimated from R160(k_0) Nava et al. (1986)
R189	R40	H	+	C_4H_3	→	C_2H_2	+	C_2H_2		3.3×10^{-12}	Schwanebeck & Warnatz (1975)
R190	R41	H	+	C_4H_3	→	C_4H_2	+	H_2		1.2×10^{-11}	Schwanebeck & Warnatz (1975)
R191	R42	H	+	C_4H_3	$\xrightarrow{M}$	C_4H_4				$k_0 = 5.76 \times 10^{-24} T^{-1.3}$ $k_\infty = 8.56 \times 10^{-10} e^{-405/T}$	Estimated from R162(k_0) Duran et al. (1988)
R192	R43	H	+	C_4H_4	$\xrightarrow{M}$	C_4H_5				$k_0 = 8.76 \times 10^{-8} T^{-7.03} e^{-1390/T}$ $k_\infty = 3.3 \times 10^{-12}$	Schwanebeck & Warnatz (1975)
R193	R44	H	+	C_4H_6	→	C_4H_5	+	H_2		$1.05 \times 10^{-13} T^{0.7} e^{-3019/T}$	Weissman & Benson (1988)
R194	R45	H	+	C_6H	$\xrightarrow{M}$	C_6H_2				$k_0 = 1.26 \times 10^{-18} T^{-3.1} e^{-721/T}$ $k_\infty = 3.0 \times 10^{-10}$	Kiefer & von Drasek (1990)
R195	R46	H	+	C_6H_4	$\xrightarrow{M}$	C_6H_5				$k_0 = 1.96 \times 10^{+33} T^{-18.35} e^{-6694/T}$ $k_\infty = 1.06 \times 10^{-14} T^{1.11} e^{-705/T}$	Wang & Frenklach (1994)
R196	R47	H	+	C_6H_5	$\xrightarrow{M}$	C_6H_6				$k_0 = 1.82 \times 10^{+28} T^{-16.3} e^{-3526/T}$ $k_\infty = 1.66 \times 10^{-10}$	Wang & Frenklach (1997)
R197	R48	H	+	C_6H_6	→	C_6H_5	+	H_2		$4.15 \times 10^{-10} e^{-8052/T}$	Wang & Frenklach (1997)
R198	R49	H	+	C_6H_6	$\xrightarrow{M}$	C_6H_7				$k_0 = 3.3 \times 10^{-30} e^{-740/T}$ $k_\infty = 5.27 \times 10^{-11} e^{-1605/T}$	Estimated from R160(k_0) Mebel et al. (1997)
R199	R50	C	+	H_2	$\xrightarrow{M}$	$^3CH_2$				$k_0 = 7.0 \times 10^{-32}$ $k_\infty = 2.06 \times 10^{-11} e^{-55.4/T}$	Husain et al. (1975) Harding et al. (1993)
R200	R51	C	+	C	$\xrightarrow{M}$	C_2				$k_0 = 4.87 \times 10^{-27} T^{-1.6}$ $k_\infty = 2.16 \times 10^{-11}$	Slack et al. (1976) Martinotti et al. (1968)
R201	R53	C	+	CH_4	→	C_2H_4				2.0×10^{-15}	Husain et al. (1971) – Upper limit
R202	R54	C	+	C_2H_2	→	C_3H_2				$4.6 \times 10^{-10} T^{-0.08}$	Chastaing et al. (1999)
R203	R55	C	+	C_2H_4	→	CH_2CCH_2				$4.6 \times 10^{-10} T^{-0.07}$	Chastaing et al. (1999)
R204	R56	C	+	CH_3C_2H	→	C_4H_4				8.0×10^{-10}	Husain et al. (1997)
R205	R57	C	+	C_4H_6	→	C_3H_3	+	C_2H_3		1.1×10^{-9}	Husain et al. (1997)
R206	R58	CH	+	H_2	→	$^3CH_2$	+	H		$3.1 \times 10^{-10} e^{-1650/T}$	Brownsword et al. (1997)
R207	R52	CH	+	H_2	$\xrightarrow{M}$	CH_3				$k_0 = 4.7 \times 10^{-26} T^{-1.6}$ $k_\infty = 2.5 \times 10^{-10} T^{-0.08}$	Brownsword et al. (1997)
R208	R59	CH	+	CH	→	C_2H_2				1.99×10^{-10}	Braun et al. (1967)
R209	R60	CH	+	CH_4	→	C_2H_4	+	H		$3.96 \times 10^{-8} T^{-1.04} e^{-36.1/T}$	Canosa et al. (1997)
R210	R61	CH	+	C_2H_2	→	C_3H_2	+	H		$1.59 \times 10^{-9} T^{-0.23} e^{-16/T}$	Canosa et al. (1997)
R211	R62	CH	+	C_2H_4	→	CH_3C_2H	+	H		$3.87 \times 10^{-9} T^{-0.546} e^{-29.6/T}$	Canosa et al. (1997)
R212	R63	CH	+	C_2H_4	→	CH_2CCH_2	+	H		$3.87 \times 10^{-9} T^{-0.546} e^{-29.6/T}$	Canosa et al. (1997)
R213	R64	CH	+	C_2H_6	→	C_3H_6	+	H		$1.9 \times 10^{-8} T^{-0.859} e^{-53.2/T}$	Canosa et al. (1997)
R214	R65	CH	+	C_2H_6	→	C_2H_4	+	CH_3		$1.9 \times 10^{-8} T^{-0.859} e^{-53.2/T}$	Canosa et al. (1997)
R215	R66	CH	+	CH_3C_2H	→	C_4H_5				4.6×10^{-10}	Butler et al. (1991)
R216	R67	CH	+	C_3H_6	→	C_4H_6	+	H		$3.87 \times 10^{-9} T^{-0.546} e^{-29.6/T}$	Estimated from R211
R217	R68	CH	+	C_3H_8	→	C_4H_8	+	H		$1.9 \times 10^{-10} e^{240/T}$	Baulch et al. (1992)
R218	R69	CH	+	C_4H_2	→	C_5H_2	+	H		$1.59 \times 10^{-9} T^{-0.23} e^{-16/T}$	Estimated from R210
R219	R70	CH	+	C_4H_8	→	C_5H_8	+	H		$8.78 \times 10^{-9} T^{-0.529} e^{-33.5/T}$	Canosa et al. (1997)
R220	R71	$^1CH_2$	+	H_2	→	$^3CH_2$	+	H_2		1.26×10^{-11}	Braun et al. (1970)
R221	R72	$^1CH_2$	+	H_2	→	CH_3	+	H		1.2×10^{-10}	Tsang & Hampson (1986)
R222	R73	$^1CH_2$	+	$^1CH_2$	→	C_2H_2	+	H	+ H	5.0×10^{-11}	Tsang & Hampson (1986)
R223	R74	$^1CH_2$	+	$^3CH_2$	→	C_2H_2	+	H	+ H	3.0×10^{-11}	Tsang & Hampson (1986)
R224	R75	$^1CH_2$	+	CH_3	→	C_2H_4	+	H		3.0×10^{-11}	Tsang & Hampson (1986)
R225	R76	$^1CH_2$	+	CH_4	→	$^3CH_2$	+	CH_4		1.2×10^{-11}	Böhland et al. (1985b)
R226	R77	$^1CH_2$	+	CH_4	→	CH_3	+	CH_3		$7.14 \times 10^{-12} e^{-5052/T}$	Böhland et al. (1985b)
R227	R78	$^1CH_2$	+	C_2H	→	C_2H_2	+	CH		3.0×10^{-11}	Tsang & Hampson (1986)
R228	R79	$^1CH_2$	+	C_2H_2	→	$^3CH_2$	+	C_2H_2		8.14×10^{-11}	Baulch et al. (1992)
R229	R80	$^1CH_2$	+	C_2H_2	→	C_3H_3	+	H		9.62×10^{-11}	Baulch et al. (1992)
R230	R81	$^1CH_2$	+	C_2H_2	→	CH_3C_2H				9.62×10^{-11}	Baulch et al. (1992)
R231	R82	$^1CH_2$	+	C_2H_2	→	CH_2CCH_2				9.62×10^{-11}	Baulch et al. (1992)
R232	R83	$^1CH_2$	+	C_2H_3	→	C_2H_2	+	CH_3		3.0×10^{-11}	Tsang & Hampson (1986)
R233	R84	$^1CH_2$	+	C_2H_4	→	$^3CH_2$	+	C_2H_4		2.3×10^{-11}	Baulch et al. (1992)
R234	R85	$^1CH_2$	+	C_2H_4	→	C_3H_6				1.5×10^{-10}	Baulch et al. (1992)
R235	R86	$^1CH_2$	+	C_2H_5	→	C_2H_4	+	CH_3		1.5×10^{-11}	Tsang & Hampson (1986)
R236	R87	$^1CH_2$	+	C_2H_5	→	C_3H_6	+	H		1.5×10^{-11}	Tsang & Hampson (1986)
R237	R88	$^1CH_2$	+	C_2H_6	→	$^3CH_2$	+	C_2H_6		3.6×10^{-11}	Baulch et al. (1992)
R238	R89	$^1CH_2$	+	C_2H_6	→	C_2H_5	+	CH_3		1.9×10^{-10}	Tsang & Hampson (1986)
R239	R90	$^1CH_2$	+	CH_3C_2H	→	C_4H_5	+	H		9.62×10^{-11}	Estimated from R229
R240	R91	$^1CH_2$	+	CH_2CCH_2	→	C_4H_5	+	H		9.62×10^{-11}	Estimated from R229
R241	R92	$^1CH_2$	+	C_3H_5	→	C_4H_6	+	H		3.33×10^{-10}	Tsang (1991)
R242	R93	$^1CH_2$	+	C_3H_5	→	C_2H_4	+	C_2H_3		6.7×10^{-11}	Tsang (1991)
R243	R94	$^1CH_2$	+	C_3H_6	→	C_3H_5	+	CH_3		8.7×10^{-11}	Tsang (1991)
R244	R95	$^1CH_2$	+	C_3H_6	→	C_4H_8				8.1×10^{-11}	Tsang (1991)
R245	R96	$^1CH_2$	+	C_3H_7	→	C_2H_5	+	C_2H_4		3.0×10^{-11}	Tsang (1988)

R246	R97	$^1CH_2$	+	C_3H_7	→	C_3H_6	+	CH_3			3.0×10^{-12}	Tsang (1988)
R247	R98	$^1CH_2$	+	C_3H_8	→	C_2H_5	+	C_2H_5			1.6×10^{-10}	Tsang (1988)
R248	R99	$^1CH_2$	+	C_4H	→	C_4H_2	+	CH			3.0×10^{-11}	Estimated from R227
R249	R100	$^1CH_2$	+	C_4H_2	→	C_5H_3	+	H			9.62×10^{-11}	Estimated from R230
R250	R101	$^1CH_2$	+	N_2	→	$^3CH_2$	+	N_2			1.0×10^{-11}	Baulch et al. (1992)
R251	R102	$^3CH_2$	+	H_2	→	CH_3	+	H			5.0×10^{-15}	Tsang & Hampson (1986) – Upper limit
R252	R103	$^3CH_2$	+	$^3CH_2$	→	C_2H_2	+	H	+	H	$1.8 \times 10^{-10} e^{-400/T}$	Baulch et al. (1992)
R253	R104	$^3CH_2$	+	$^3CH_2$	→	C_2H_2	+	H_2			5.3×10^{-11}	Baulch et al. (1992)
R254	R105	$^3CH_2$	+	CH_3	→	C_2H_4	+	H			7.0×10^{-11}	Baulch et al. (1992)
R255	R106	$^3CH_2$	+	CH_4	→	CH_3	+	CH_3			$7.13 \times 10^{-12} e^{-5052/T}$	Böhland et al. (1985a) – Upper limit
R256	R107	$^3CH_2$	+	C_2H	→	C_2H_2	+	CH			3.0×10^{-11}	Tsang & Hampson (1986)
R257	R108	$^3CH_2$	+	C_2H_2	→	C_3H_2	+	H_2			$5.0 \times 10^{-12} e^{-3332/T}$	Böhland et al. (1988)
R258	R109	$^3CH_2$	+	C_2H_2	→	C_3H_3	+	H			$1.5 \times 10^{-12} e^{-3332/T}$	Böhland et al. (1988)
R259	R110	$^3CH_2$	+	C_2H_2	→	CH_3C_2H					$2.0 \times 10^{-11} e^{-3332/T}$	Baulch et al. (1992)
R260	R111	$^3CH_2$	+	C_2H_2	→	CH_2CCH_2					5.8×10^{-12}	Baulch et al. (1992)
R261	R112	$^3CH_2$	+	C_2H_3	→	C_2H_2	+	CH_3			3.0×10^{-11}	Tsang & Hampson (1986)
R262	R113	$^3CH_2$	+	C_2H_4	→	C_3H_6					$5.31 \times 10^{-12} e^{-2658/T}$	Kraus et al. (1993)
R263	R114	$^3CH_2$	+	C_2H_5	→	C_2H_4	+	CH_3			3.0×10^{-11}	Tsang & Hampson (1986)
R264	R115	$^3CH_2$	+	C_2H_6	→	C_2H_5	+	CH_3			$1.07 \times 10^{-11} e^{-3981/T}$	Böhland et al. (1985a)
R265	R116	$^3CH_2$	+	C_2H_6	→	C_3H_8					$8.13 \times 10^{-12} e^{-3332/T}$	Böhland et al. (1985a)
R266	R117	$^3CH_2$	+	C_3H_5	→	C_4H_6	+	H			5.0×10^{-11}	Tsang (1991)
R267	R118	$^3CH_2$	+	C_3H_5	→	C_2H_3	+	C_2H_4			1.6×10^{-11}	Tsang (1991)
R268	R119	$^3CH_2$	+	C_3H_6	→	C_3H_5	+	CH_3			$2.7 \times 10^{-12} e^{-2660/T}$	Tsang (1991)
R269	R120	$^3CH_2$	+	C_3H_6	→	C_4H_8					$2.71 \times 10^{-12} e^{-2664/T}$	Tsang (1991)
R270	R121	$^3CH_2$	+	C_3H_7	→	C_2H_4	+	C_2H_5			3.01×10^{-11}	Tsang (1988)
R271	R122	$^3CH_2$	+	C_3H_7	→	C_3H_6	+	CH_3			3.0×10^{-12}	Tsang (1988)
R272	R123	$^3CH_2$	+	C_3H_8	→	C_3H_7	+	CH_3			$1.5 \times 10^{-24} T^{3.65} e^{-3600/T}$	Tsang (1988)
R273	R124	$^3CH_2$	+	C_3H_8	→	C_4H_{10}					$8.14 \times 10^{-12} e^{-3332/T}$	Böhland et al. (1985a)
R274	R125	$^3CH_2$	+	C_4H	→	C_4H_2	+	CH			3.0×10^{-11}	Estimated from R256
R275	R126	$^3CH_2$	+	C_4H_2	→	C_4H	+	CH_3			$2.16 \times 10^{-11} e^{-2165/T}$	Böhland et al. (1988)
R276	R127	$^3CH_2$	+	C_4H_3	→	C_4H_2	+	CH_3			3.0×10^{-11}	Estimated from R261
R277	R128	CH_3	+	H_2	→	H	+	CH_4			$1.14 \times 10^{-20} T^{2.74} e^{-4740/T}$	Baulch et al. (1992)
R278	R129	CH_3	+	CH_3	→	C_2H_5	+	H			$8.28 \times 10^{-12} T^{0.1} e^{-5335/T}$	Stewart et al. (1989)
R279	R130	CH_3	+	CH_3	M →	C_2H_6					$k_0 = 2.2 \times 10^{-16} T^{-3.75} e^{-494/T}$ $k_\infty = 3.8 \times 10^{-9} T^{-0.69} e^{-88/T}$	Wang et al. (2003)
R280	R131	CH_3	+	C_2H	→	C_3H_3	+	H			4.0×10^{-11}	Tsang & Hampson (1986)
R281	R132	CH_3	+	C_2H_2	M →	C_3H_5					$k_0 = 3.3 \times 10^{-30} e^{-740/T}$ $k_\infty = 1.0 \times 10^{-12} e^{-3903/T}$	Estimated from R160(k_0) Baulch et al. (1992)
R282	R133	CH_3	+	C_2H_3	→	C_2H_2	+	CH_4			3.0×10^{-11}	Laufer et al. (2004)
R283	R134	CH_3	+	C_2H_3	→	C_3H_5	+	H			$3.42 \times 10^{-10} T^{-0.285}$	Stoliarov et al. (2000)
R284	R135	CH_3	+	C_2H_3	M →	C_3H_6					$k_0 = 2.2 \times 10^{-16} T^{-3.75} e^{-494/T}$ $k_\infty = 3.51 \times 10^{-12} T^{0.417} e^{161/T}$	Estimated from R279(k_0) Stoliarov et al. (2002)
R285	R136	CH_3	+	C_2H_4	→	C_2H_3	+	CH_4			$1.1 \times 10^{-23} T^{3.7} e^{-4780/T}$	Tsang & Hampson (1986)
R286	R137	CH_3	+	C_2H_4	M →	C_3H_7					$k_0 = 1.39 \times 10^{-29} e^{-562/T}$ $k_\infty = 3.5 \times 10^{-13} e^{-3700/T}$	Estimated from R163(k_0) Baulch et al. (1992)
R287	R138	CH_3	+	C_2H_5	→	C_2H_4	+	CH_4			1.9×10^{-12}	Baulch et al. (1992)
R288	R139	CH_3	+	C_2H_5	M →	C_3H_8					$k_0 = 8.0 \times 10^{+19} T^{-16.1} e^{-1904/T}$ $k_\infty = 5.6 \times 10^{-11}$	Laufer et al. (1983) Baulch et al. (1994)
R289	R140	CH_3	+	C_2H_6	→	C_2H_5	+	CH_4			$2.5 \times 10^{-31} T^{6} e^{-3043/T}$	Baulch et al. (1992)
R290	R141	CH_3	+	C_3H_3	M →	C_4H_6					$k_0 = 2.2 \times 10^{-16} T^{-3.75} e^{-494/T}$ $k_\infty = 1.5 \times 10^{-10}$	Estimated from R279(k_0) Fahr et al. (1999)
R291	R142	CH_3	+	CH_3C_2H	→	C_2H_6	+	C_2H			$8.32 \times 10^{-13} e^{-4428/T}$	Kerr & Parsonage et al. (1972)
R292	R143	CH_3	+	CH_2CCH_2	→	C_2H_5	+	C_2H_2			$3.32 \times 10^{-13} e^{-4076/T}$	Kerr & Parsonage et al. (1972)
R293	R144	CH_3	+	C_3H_5	→	CH_3C_2H	+	CH_4			$2.5 \times 10^{-12} T^{-0.32} e^{66/T}$	Tsang (1991)
R294	R145	CH_3	+	C_3H_5	→	CH_2CCH_2	+	CH_4			$2.5 \times 10^{-12} T^{-0.32} e^{66/T}$	Tsang (1991)
R295	R146	CH_3	+	C_3H_5	M →	C_4H_8					$k_0 = 2.2 \times 10^{-16} T^{-3.75} e^{-494/T}$ $k_\infty = 1.69 \times 10^{-10} T^{-0.32} e^{66/T}$	Estimated from R279(k_0) Tsang (1991)
R296	R147	CH_3	+	C_3H_6	→	C_3H_5	+	CH_4			$2.32 \times 10^{-13} e^{-4390/T}$	Kinsman et al. (1994)
R297	R148	CH_3	+	C_3H_6	M →	C_4H_9					$k_0 = 1.39 \times 10^{-29} e^{-562/T}$ $k_\infty = 1.34 \times 10^{-13} e^{-3330/T}$	Estimated from R163(k_0) Kinsman et al. (1994)
R298	R149	CH_3	+	C_3H_7	→	C_3H_6	+	CH_4			$1.9 \times 10^{-11} T^{-0.32}$	Tsang (1988)
R299	R150	CH_3	+	C_3H_7	M →	C_4H_{10}					$k_0 = 9.67 \times 10^{+28} T^{-18.5} e^{-2311/T}$ $k_\infty = 3.2 \times 10^{-10} T^{-0.32}$	Laufer et al. (1983) Tsang (1988)
R300	R151	CH_3	+	C_3H_8	→	C_3H_7	+	CH_4			$1.5 \times 10^{-24} T^{3.65} e^{-3600/T}$	Tsang (1988)
R301	R152	CH_3	+	C_4H	→	C_5H_3	+	H			4.0×10^{-11}	Estimated from R208
R302	R153	CH_3	+	C_4H_2	M →	C_5H_5					$k_0 = 3.3 \times 10^{-30} e^{-740/T}$ $k_\infty = 1.0 \times 10^{-12} e^{-3903/T}$	Estimated from R160(k_0) Estimated from R281(k_∞)
R303	R154	CH_3	+	C_4H_3	→	C_4H_2	+	CH_4			3.0×10^{-11}	Estimated from R282

R304	R155	CH_3	+	C_4H_3	→	C_3H_5	+	C_2H		$3.42 \times 10^{-10} T^{-0.285}$	Estimated from R283
R305	R156	CH_3	+	C_4H_3	M →	C_5H_6				$k_0 = 2.2 \times 10^{-16} T^{-3.75} e^{-494/T}$ $k_\infty = 3.51 \times 10^{-12} T^{0.417} e^{161/T}$	Estimated from R279(k_0) Estimated from R284(k_∞)
R306	R157	CH_3	+	C_4H_4	→	C_4H_3	+	CH_4		$6.61 \times 10^{-13} e^{-2502/T}$	Scherzer et al. (1985)
R307	R158	CH_3	+	C_4H_5	→	C_4H_4	+	CH_4		3.0×10^{-11}	Estimated from R282
R308	R159	C_2	+	H_2	→	C_2H	+	H		$1.77 \times 10^{-10} e^{-1469/T}$	Pitts et al. (1982)
R309	R160	C_2	+	CH_4	→	C_2H	+	CH_3		$5.05 \times 10^{-11} e^{-297/T}$	Pitts et al. (1982)
R310	R161	C_2	+	C_6H_6	→	SOOT				5.2×10^{-10}	Reisler et al. (1980)
R311	R162	C_2H	+	H_2	→	C_2H_2	+	H		$1.2 \times 10^{-11} e^{-998/T}$	Opansky & Leone (1996b)
R312	R163	C_2H	+	CH_4	→	C_2H_2	+	CH_3		$1.2 \times 10^{-11} e^{-491/T}$	Opansky & Leone (1996a)
R313	R164	C_2H	+	C_2H	→	C_2H_2	+	C_2		3.0×10^{-12}	Tsang & Hampson (1986)
R314	R165	C_2H	+	C_2H_2	→	C_4H_2	+	H		$9.53 \times 10^{-11} e^{30.8/T}$	Chastaing et al. (1998)
R315	R166	C_2H	+	C_2H_3	→	C_2H_2	+	C_2H_2		1.6×10^{-12}	Tsang & Hampson (1986)
R316	R167	C_2H	+	C_2H_3	→	C_4H_3	+	H		3.0×10^{-11}	Tsang & Hampson (1986)
R317	R168	C_2H	+	C_2H_4	→	C_4H_4	+	H		$7.8 \times 10^{-11} e^{134/T}$	Opansky & Leone (1996b)
R318	R169	C_2H	+	C_2H_5	→	C_2H_4	+	C_2H_2		3.0×10^{-12}	Tsang & Hampson (1986)
R319	R170	C_2H	+	C_2H_5	→	C_3H_3	+	CH_3		3.0×10^{-11}	Tsang & Hampson (1986)
R320	R171	C_2H	+	C_2H_6	→	C_2H_5	+	C_2H_2		$5.1 \times 10^{-11} e^{-76/T}$	Murphy et al. (2003)
R321	R172	C_2H	+	CH_3C_2H	→	C_5H_4	+	H		$1.2 \times 10^{-9} T^{-0.3}$	Carty et al. (2001)
R322	R173	C_2H	+	CH_2CCH_2	→	C_5H_4	+	H		$1.95 \times 10^{-9} T^{-0.4}$	Carty et al. (2001)
R323	R174	C_2H	+	C_3H_5	→	CH_2CCH_2	+	C_2H_2		1.2×10^{-11}	Tsang (1991)
R324	R175	C_2H	+	C_3H_6	→	C_2H_3	+	CH_3C_2H		2.0×10^{-11}	Tsang (1991)
R325	R176	C_2H	+	C_3H_6	→	C_4H_6	+	CH		2.0×10^{-11}	Tsang (1991)
R326	R177	C_2H	+	C_3H_6	→	C_5H_6	+	H		2.4×10^{-10}	Vakhtin et al. (2001a)
R327	R178	C_2H	+	C_3H_7	→	C_2H_5	+	C_3H_3		2.0×10^{-11}	Tsang (1988)
R328	R179	C_2H	+	C_3H_7	→	C_2H_2	+	C_3H_6		1.0×10^{-11}	Tsang (1988)
R329	R180	C_2H	+	C_3H_8	→	C_3H_7	+	C_2H_2		$9.8 \times 10^{-11} e^{-71/T}$	Murphy et al. (2003)
R330	R181	C_2H	+	C_4H	→	C_6H	+	H		3.0×10^{-12}	Estimated from R313
R331	R182	C_2H	+	C_4H_2	→	C_6H_2	+	H		$9.53 \times 10^{-11} e^{30.8/T}$	Estimated from R314
R332	R183	C_2H	+	C_4H_3	→	C_4H_2	+	C_2H_2		1.6×10^{-12}	Estimated from R315
R333	R184	C_2H	+	C_4H_3	→	C_6H_3	+	H		3.0×10^{-11}	Estimated from R316
R334	R185	C_2H	+	C_4H_8	→	C_6H_8	+	H		2.6×10^{-10}	Vakhtin et al. (2001a)
R335	R186	C_2H	+	C_4H_{10}	→	C_4H_9	+	C_2H_2		1.23×10^{-10}	Murphy et al. (2003)
R336	R187	C_2H	+	C_6H_2	→	C_8H_2	+	H		$9.53 \times 10^{-11} e^{30.8/T}$	Estimated from R314
R337	R188	C_2H	+	C_6H_6	→	SOOT				8.3×10^{-11}	Wang & Frenklach (1994)
R338	R189	C_2H	+	C_8H_2	→	SOOT	+	H		$9.53 \times 10^{-11} e^{30.8/T}$	Estimated from R314
R339	R190	C_2H_3	+	H_2	→	C_2H_4	+	H		3.01×10^{-20}	Fahr et al. (1995)
R340	R191	C_2H_3	+	CH_4	→	C_2H_4	+	CH_3		$2.4 \times 10^{-24} T^{4.02} e^{-2754/T}$	Tsang & Hampson (1986)
R341	R192	C_2H_3	+	C_2H_2	→	C_4H_4	+	H		$3.31 \times 10^{-12} e^{-2516/T}$	Fahr & Stein (1988)
R342	R193	C_2H_3	+	C_2H_2	M →	C_4H_5				$k_0 = 3.3 \times 10^{-30} e^{-740/T}$ $k_\infty = 4.17 \times 10^{-19} T^{1.9} e^{-1058/T}$	Estimated from R160(k_0) Weissman & Benson (1988)
R343	R194	C_2H_3	+	C_2H_3	→	C_2H_4	+	C_2H_2		2.4×10^{-11}	Fahr et al. (1991)
R344	R195	C_2H_3	+	C_2H_3	M →	C_4H_6				$k_0 = 2.2 \times 10^{-16} T^{-3.75} e^{-494/T}$ $k_\infty = 1.2 \times 10^{-10}$	Estimated from R279(k0) Fahr et al. (1991)
R345	R196	C_2H_3	+	C_2H_4	→	C_4H_6	+	H		$8.3 \times 10^{-13} e^{-3676/T}$	Tsang & Hampson (1986)
R346	R197	C_2H_3	+	C_2H_5	→	C_2H_4	+	C_2H_4		1.8×10^{-11}	Tsang & Hampson (1986)
R347	R198	C_2H_3	+	C_2H_5	→	C_2H_6	+	C_2H_2		9.8×10^{-12}	Tsang & Hampson (1986)
R348	R199	C_2H_3	+	C_2H_5	M →	C_4H_8				$k_0 = 2.2 \times 10^{-16} T^{-3.75} e^{-494/T}$ $k_\infty = 2.5 \times 10^{-11}$	Estimated from R279(k0) Tsang & Hampson (1986)
R349	R200	C_2H_3	+	C_2H_6	→	C_2H_4	+	C_2H_5		$9.98 \times 10^{-22} T^{3.3} e^{-5285/T}$	Tsang & Hampson (1986)
R350	R201	C_2H_3	+	CH_3C_2H	→	C_5H_6	+	H		$3.31 \times 10^{-12} e^{-2516/T}$	Estimated from R341
R351	R202	C_2H_3	+	CH_2CCH_2	→	C_5H_6	+	H		$3.31 \times 10^{-12} e^{-2516/T}$	Estimated from R341
R352	R203	C_2H_3	+	C_3H_5	→	C_2H_4	+	CH_2CCH_2		2.0×10^{-12}	Tsang (1991)
R353	R204	C_2H_3	+	C_3H_5	→	C_3H_6	+	C_2H_2		8.0×10^{-12}	Tsang (1991)
R354	R205	C_2H_3	+	C_3H_5	→	C_2H_4	+	CH_3C_2H		4.0×10^{-12}	Tsang (1991)
R355	R206	C_2H_3	+	C_3H_5	→	C_5H_6	+	H	+ H	8.0×10^{-11}	Tsang (1991)
R356	R207	C_2H_3	+	C_3H_6	→	C_3H_5	+	C_2H_4		$3.68 \times 10^{-24} T^{3.5} e^{-2356/T}$	Tsang (1991)
R357	R208	C_2H_3	+	C_3H_6	→	C_4H_6	+	CH_3		$1.2 \times 10^{-12} e^{-2520/T}$	Tsang (1991)
R358	R209	C_2H_3	+	C_3H_6	→	C_5H_8	+	H		$1.2 \times 10^{-12} e^{-3240/T}$	Tsang (1991)
R359	R210	C_2H_3	+	C_3H_7	→	C_3H_6	+	C_2H_4		2.0×10^{-12}	Tsang (1988)
R360	R211	C_2H_3	+	C_3H_7	→	C_3H_8	+	C_2H_2		2.0×10^{-12}	Tsang (1988)
R361	R212	C_2H_3	+	C_3H_7	M →	C_5H_{10}				$k_0 = 2.2 \times 10^{-16} T^{-3.75} e^{-494/T}$ $k_\infty = 1.6 \times 10^{-11}$	Estimated from R279(k0) Tsang (1988)
R362	R213	C_2H_3	+	C_3H_8	→	C_3H_7	+	C_2H_4		$1.0 \times 10^{-21} T^{2.3} e^{-5285/T}$	Tsang (1988)
R363	R214	C_2H_3	+	C_4H	→	C_4H_2	+	C_2H_2		1.6×10^{-12}	Estimated from R315
R364	R215	C_2H_3	+	C_4H	→	C_6H_3	+	H		3.0×10^{-11}	Estimated from R316
R365	R216	C_2H_3	+	C_4H_2	→	C_6H_4	+	H		2.4×10^{-11}	Estimated from R341
R366	R217	C_2H_3	+	C_4H_3	→	C_4H_4	+	C_2H_2		2.4×10^{-11}	Estimated from R343

R367	R218	C_2H_3	+	C_4H_3	→	C_6H_6			$4.77 \times 10^{-10} e^{-411/T}$	Duran et al. (1988)
R368	R219	C_2H_3	+	C_4H_5	→	C_6H_6	+	H_2	$3.05 \times 10^{-37} T^{7.07} e^{1823/T}$	Westmorelet et al. (1989)
R369	R220	C_2H_5	+	H_2	→	C_2H_6	+	H	$5.11 \times 10^{-24} T^{3.6} e^{-4253/T}$	Tsang & Hampson (1986)
R370	R221	C_2H_5	+	CH_4	→	C_2H_6	+	CH_3	$1.43 \times 10^{-25} T^{4.14} e^{-6322/T}$	Tsang & Hampson (1986)
R371	R222	C_2H_5	+	C_2H_2	→	C_2H_6	+	C_2H	$4.5 \times 10^{-13} e^{-11800/T}$	Tsang & Hampson (1986)
R372	R223	C_2H_5	+	C_2H_2	M →	C_4H_7			$k_0 = 3.3 \times 10^{-30} e^{-740/T}$ $k_\infty = 5.6 \times 10^{-14} e^{-3520/T}$	Estimated from R160(k0) Baulch et al. (1992)
R373	R224	C_2H_5	+	C_2H_4	→	C_2H_6	+	C_2H_3	$1.0 \times 10^{-21} T^{3.13} e^{-9063/T}$	Tsang & Hampson (1986)
R374	R225	C_2H_5	+	C_2H_4	M →	C_4H_9			$k_0 = 1.39 \times 10^{-29} e^{-562/T}$ $k_\infty = 1.8 \times 10^{-13} e^{-3670/T}$	Estimated from R163(k0) Tsang & Hampson (1986)
R375	R226	C_2H_5	+	C_2H_5	→	C_2H_6	+	C_2H_4	2.4×10^{-12}	Baulch et al. (1992)
R376	R227	C_2H_5	+	C_2H_5	M →	C_4H_{10}			$k_0 = 6.59 \times 10^{-6} T^{-6.39} e^{-301/T}$ $k_\infty = 1.26 \times 10^{-11} e^{-96/T}$	Laufer et al. (1983) Teng & Jones (1972)
R377	R228	C_2H_5	+	CH_3C_2H	M →	C_5H_9			$k_0 = 3.3 \times 10^{-30} e^{-740/T}$ $k_\infty = 5.6 \times 10^{-14} e^{-3520/T}$	Estimated from R160(k_0) Estimated from R372(k_∞)
R378	R229	C_2H_5	+	CH_2CCH_2	M →	C_5H_9			$k_0 = 3.3 \times 10^{-30} e^{-740/T}$ $k_\infty = 5.6 \times 10^{-14} e^{-3520/T}$	Estimated from R160(k_0) Estimated from R372(k_∞)
R379	R230	C_2H_5	+	C_3H_5	→	CH_2CCH_2	+	C_2H_6	$1.6 \times 10^{-12} e^{66/T}$	Tsang (1991)
R380	R231	C_2H_5	+	C_3H_5	→	C_3H_6	+	C_2H_4	$4.3 \times 10^{-12} e^{66/T}$	Tsang (1991)
R381	R232	C_2H_5	+	C_3H_5	M →	C_5H_{10}			$k_0 = 2.2 \times 10^{-16} T^{-3.75} e^{-494/T}$ $k_\infty = 3.33 \times 10^{-13} e^{66/T}$	Estimated from R279(k_0) Baulch et al. (1992)
R382	R233	C_2H_5	+	C_3H_6	→	C_3H_5	+	C_2H_6	$3.7 \times 10^{-24} T^{3.5} e^{-3340/T}$	Tsang (1991)
R383	R234	C_2H_5	+	C_3H_6	M →	C_5H_{11}			$k_0 = 1.39 \times 10^{-29} e^{-562/T}$ $k_\infty = 1.7 \times 10^{-13} e^{-3625/T}$	Estimated from R163(k_0) Tsang (1991)
R384	R235	C_2H_5	+	C_3H_7	→	C_3H_8	+	C_2H_4	1.9×10^{-12}	Tsang (1988)
R385	R236	C_2H_5	+	C_3H_7	→	C_3H_6	+	C_2H_6	2.4×10^{-12}	Tsang (1988)
R386	R237	C_2H_5	+	C_3H_7	M →	C_5H_{12}			$k_0 = 9.67 \times 10^{+28} T^{-18.5} e^{-2311/T}$ $k_\infty = 3.3 \times 10^{-11}$	Estimated from R299(k_0) Tsang (1988)
R387	R238	C_2H_5	+	C_3H_8	→	C_3H_7	+	C_2H_6	$1.5 \times 10^{-24} T^{3.65} e^{-4600/T}$	Tsang (1988)
R388	R239	C_2H_5	+	C_4H	→	C_2H_4	+	C_4H_2	3.0×10^{-12}	Estimated from R318
R389	R240	C_2H_5	+	C_4H	→	C_5H_3	+	CH_3	3.0×10^{-11}	Estimated from R319
R390	R241	C_2H_5	+	C_4H_2	M →	C_6H_7			$k_0 = 3.3 \times 10^{-30} e^{-740/T}$ $k_\infty = 5.6 \times 10^{-14} e^{-3520/T}$	Estimated from R160(k_0) Estimated from R372(k_∞)
R391	R242	C_2H_5	+	C_4H_3	→	C_4H_4	+	C_2H_4	1.8×10^{-11}	Estimated from R346
R392	R243	C_2H_5	+	C_4H_3	→	C_4H_2	+	C_2H_6	9.8×10^{-12}	Estimated from R347
R393	R244	C_2H_5	+	C_4H_3	M →	C_6H_8			$k_0 = 2.2 \times 10^{-16} T^{-3.75} e^{-494/T}$ $k_\infty = 2.5 \times 10^{-11}$	Estimated from R279(k_0) Estimated from R348(k_∞)
R394	R245	C_3H	+	CH_4	→	C_3H_2	+	CH_3	$1.2 \times 10^{-11} e^{-491/T}$	Estimated from R312
R395	R246	C_3H_2	+	H_2	→	C_3H_3	+	H	1.2×10^{-10}	Estimated from R221
R396	R247	C_3H_2	+	CH_4	→	C_3H_3	+	CH_3	5.9×10^{-11}	Estimated from R226
R397	R248	C_3H_2	+	C_2H_2	→	C_5H_3	+	H	9.62×10^{-11}	Estimated from R229
R398	R249	C_3H_2	+	C_2H_3	→	C_3H_3	+	C_2H_2	3.0×10^{-11}	Estimated from R232
R399	R250	C_3H_2	+	C_2H_4	→	C_5H_5	+	H	1.5×10^{-10}	Estimated from R234
R400	R251	C_3H_2	+	C_2H_5	→	C_3H_3	+	C_2H_4	1.5×10^{-11}	Estimated from R235
R401	R252	C_3H_2	+	C_2H_6	→	C_3H_3	+	C_2H_5	1.9×10^{-10}	Estimated from R238
R402	R253	C_3H_2	+	C_3H_6	→	C_3H_5	+	C_3H_3	8.7×10^{-11}	Estimated from R243
R403	R254	C_3H_2	+	C_3H_8	→	C_4H_5	+	C_2H_5	1.6×10^{-10}	Estimated from R247
R404	R255	C_3H_2	+	C_4H_2	→	C_7H_3	+	H	9.62×10^{-11}	Estimated from R229
R405	R256	C_3H_3	+	H_2	→	CH_3C_2H	+	H	$1.8 \times 10^{-19} T^{2.38} e^{-9557/T}$	Estimated from R417
R406	R257	C_3H_3	+	H_2	→	CH_2CCH_2	+	H	$1.8 \times 10^{-19} T^{2.38} e^{-9557/T}$	Estimated from R417
R407	R258	C_3H_3	+	CH_4	→	CH_3C_2H	+	CH_3	$6.6 \times 10^{-23} T^{3.4} e^{-11670/T}$	Estimated from R418
R408	R259	C_3H_3	+	CH_4	→	CH_2CCH_2	+	CH_3	$6.6 \times 10^{-23} T^{3.4} e^{-11670/T}$	Estimated from R418
R409	R260	C_3H_3	+	C_2H_2	M →	C_5H_5			$k_0 = 3.3 \times 10^{-30} e^{-740/T}$ $k_\infty = 5.3 \times 10^{-14} e^{-3500/T}$	Estimated from R160(k_0) Estimated from R419(k_∞)
R410	R261	C_3H_3	+	C_2H_4	→	C_5H_6	+	H	$1.0 \times 10^{-14} e^{-5776/T}$	Estimated from R420
R411	R262	C_3H_3	+	C_2H_6	→	CH_3C_2H	+	C_2H_5	$3.9 \times 10^{-22} T^{3.3} e^{-9986/T}$	Estimated from R421
R412	R263	C_3H_3	+	C_2H_6	→	CH_2CCH_2	+	C_2H_5	$3.9 \times 10^{-22} T^{3.3} e^{-9986/T}$	Estimated from R421
R413	R264	C_3H_3	+	C_3H_3	M →	C_6H_6			$k_0 = 2.2 \times 10^{-16} T^{-3.75} e^{-494/T}$ $k_\infty = 3.8 \times 10^{-9} T^{-0.69} e^{-88/T}$	Estimated from R279(k_0) Estimated from R279(k_∞)
R414	R265	C_3H_3	+	C_3H_6	→	C_6H_8	+	H	$1.0 \times 10^{-14} e^{-5776/T}$	Estimated from R426
R415	R266	C_3H_3	+	C_3H_8	→	CH_3C_2H	+	C_3H_7	$3.9 \times 10^{-22} T^{3.3} e^{-9986/T}$	Estimated from R430
R416	R267	C_3H_3	+	C_3H_8	→	CH_2CCH_2	+	C_3H_7	$3.9 \times 10^{-22} T^{3.3} e^{-9986/T}$	Estimated from R430
R417	R268	C_3H_3	+	C_4H_2	M →	C_7H_5			$k_0 = 3.3 \times 10^{-30} e^{-740/T}$ $k_\infty = 5.3 \times 10^{-14} e^{-3500/T}$	Estimated from R160(k_0) Estimated from R419(k_∞)
R418	R269	C_3H_5	+	H_2	→	C_3H_6	+	H	$1.8 \times 10^{-19} T^{2.38} e^{-9557/T}$	Tsang (1991)
R419	R270	C_3H_5	+	CH_4	→	C_3H_6	+	CH_3	$6.6 \times 10^{-23} T^{3.4} e^{-11670/T}$	Tsang (1991)

R420	R271	C_3H_5	+	C_2H_2	$\xrightarrow{M}$	C_5H_7				$k_0 = 3.3 \times 10^{-30} e^{-740/T}$ $k_\infty = 5.3 \times 10^{-14} e^{-3500/T}$	Estimated from R160(k_0) Tsang (1991)
R421	R272	C_3H_5	+	C_2H_4	→	C_5H_8	+	H		$1.0 \times 10^{-14} e^{-5776/T}$	Tsang (1991)
R422	R273	C_3H_5	+	C_2H_6	→	C_3H_6	+	C_2H_5		$3.9 \times 10^{-22} T^{3.3} e^{-9986/T}$	Tsang (1991)
R423	R274	C_3H_5	+	CH_3C_2H	$\xrightarrow{M}$	C_6H_9				$k_0 = 3.3 \times 10^{-30} e^{-740/T}$ $k_\infty = 5.3 \times 10^{-14} e^{-3500/T}$	Estimated from R160(k_0) Estimated from R419(k_∞)
R424	R275	C_3H_5	+	CH_2CCH_2	$\xrightarrow{M}$	C_6H_9				$k_0 = 3.3 \times 10^{-30} e^{-740/T}$ $k_\infty = 5.3 \times 10^{-14} e^{-3500/T}$	Estimated from R160(k_0) Estimated from R419(k_∞)
R425	R276	C_3H_5	+	C_3H_5	→	C_3H_6	+	CH_2CCH_2		$1.4 \times 10^{-13} e^{132/T}$	Tsang (1991)
R426	R277	C_3H_5	+	C_3H_5	$\xrightarrow{M}$	C_6H_{10}				$k_0 = 2.2 \times 10^{-16} T^{-3.75} e^{-494/T}$ $k_\infty = 1.7 \times 10^{-11} e^{132/T}$	Estimated from R279(k_0) Baulch et al. (1994)
R427	R278	C_3H_5	+	C_3H_6	→	C_6H_{10}	+	H		$1.0 \times 10^{-14} e^{-5776/T}$	Tsang (1991)
R428	R279	C_3H_5	+	C_3H_7	→	C_3H_6	+	C_3H_6		$2.4 \times 10^{-12} e^{66/T}$	Tsang (1991)
R429	R280	C_3H_5	+	C_3H_7	→	CH_2CCH_2	+	C_3H_8		$1.2 \times 10^{-12} e^{66/T}$	Tsang (1991)
R430	R281	C_3H_5	+	C_3H_7	$\xrightarrow{M}$	C_6H_{12}				$k_0 = 2.2 \times 10^{-16} T^{-3.75} e^{-494/T}$ $k_\infty = 3.4 \times 10^{-11} e^{66/T}$	Estimated from R279(k_0) Tsang (1991)
R431	R282	C_3H_5	+	C_3H_8	→	C_3H_6	+	C_3H_7		$3.9 \times 10^{-22} T^{3.3} e^{-9986/T}$	Tsang (1991)
R432	R283	C_3H_5	+	C_4H	→	CH_2CCH_2	+	C_4H_2		1.2×10^{-11}	Estimated from R362?
R433	R284	C_3H_5	+	C_4H_2	$\xrightarrow{M}$	C_7H_7				$k_0 = 3.3 \times 10^{-30} e^{-740/T}$ $k_\infty = 5.3 \times 10^{-14} e^{-3500/T}$	Estimated from R160(k_0) Estimated from R419(k_∞)
R434	R285	C_3H_5	+	C_4H_3	→	C_4H_4	+	CH_2CCH_2		2.0×10^{-12}	Estimated from R352
R435	R286	C_3H_5	+	C_4H_3	→	C_4H_2	+	C_3H_6		8.0×10^{-12}	Estimated from R353
R436	R287	C_3H_7	+	H_2	→	C_3H_8	+	H		$3.0 \times 10^{-21} T^{2.84} e^{-4600/T}$	Tsang (1988)
R437	R288	C_3H_7	+	CH_4	→	C_3H_8	+	CH_3		$4.0 \times 10^{-26} T^{4.02} e^{-5473/T}$	Tsang (1988)
R438	R289	C_3H_7	+	C_2H_2	→	C_2H_4	+	C_3H_5		$1.2 \times 10^{-12} e^{-4531/T}$	Tsang (1988)
R439	R290	C_3H_7	+	C_2H_4	→	C_3H_8	+	C_2H_3		$1.0 \times 10^{-21} T^{3.13} e^{-9063/T}$	Estimated from R373
R440	R291	C_3H_7	+	C_2H_4	$\xrightarrow{M}$	C_5H_{11}				$k_0 = 1.39 \times 10^{-29} e^{-562/T}$ $k_\infty = 7.5 \times 10^{-14} e^{-3470/T}$	Estimated from R163(k_0) Baulch et al. (1994)
R441	R292	C_3H_7	+	C_2H_6	→	C_3H_8	+	C_2H_5		$4.2 \times 10^{-25} T^{3.82} e^{-4550/T}$	Tsang (1988)
R442	R293	C_3H_7	+	CH_3C_2H	$\xrightarrow{M}$	C_6H_{11}				$k_0 = 3.3 \times 10^{-30} e^{-740/T}$ $k_\infty = 1.2 \times 10^{-12} e^{-4531/T}$	Estimated from R160(k_0) Estimated from R437(k_∞)
R443	R294	C_3H_7	+	CH_2CCH_2	$\xrightarrow{M}$	C_6H_{11}				$k_0 = 3.3 \times 10^{-30} e^{-740/T}$ $k_\infty = 1.2 \times 10^{-12} e^{-4531/T}$	Estimated from R160(k_0) Estimated from R437(k_∞)
R444	R295	C_3H_7	+	C_3H_6	→	C_3H_8	+	C_3H_5		$3.7 \times 10^{-24} T^{3.5} e^{-3340/T}$	Tsang (1991)
R445	R296	C_3H_7	+	C_3H_6	$\xrightarrow{M}$	C_6H_{13}				$k_0 = 1.39 \times 10^{-29} e^{-562/T}$ $k_\infty = 7.5 \times 10^{-14} e^{-3470/T}$	Estimated from R163(k_0) Baulch et al. (1994)
R446	R297	C_3H_7	+	C_3H_7	→	C_3H_8	+	C_3H_6		2.8×10^{-12}	Tsang (1988)
R447	R298	C_3H_7	+	C_3H_7	$\xrightarrow{M}$	C_6H_{14}				$k_0 = 6.59 \times 10^{-6} T^{-6.39} e^{-301/T}$ $k_\infty = 1.7 \times 10^{-11}$	Estimated from R376(k_0) Tsang (1988)
R448	R299	C_3H_7	+	C_4H	→	C_2H_5	+	C_5H_3		2.0×10^{-11}	Estimated from R327
R449	R300	C_3H_7	+	C_4H	→	C_4H_2	+	C_3H_6		1.0×10^{-11}	Estimated from R328
R450	R301	C_3H_7	+	C_4H_2	$\xrightarrow{M}$	C_7H_9				$k_0 = 3.3 \times 10^{-30} e^{-740/T}$ $k_\infty = 5.3 \times 10^{-14} e^{-3500/T}$	Estimated from R160(k_0) Estimated from R419(k_∞)
R451	R302	C_3H_7	+	C_4H_3	→	C_4H_4	+	C_3H_6		2.0×10^{-12}	Estimated from R359
R452	R303	C_3H_7	+	C_4H_3	→	C_4H_2	+	C_3H_8		2.0×10^{-12}	Estimated from R360
R453	R304	C_3H_7	+	C_4H_3	$\xrightarrow{M}$	C_7H_{10}				$k_0 = 2.2 \times 10^{-16} T^{-3.75} e^{-494/T}$ $k_\infty = 1.6 \times 10^{-11}$	Estimated from R361(k_0) Estimated from R212(k_∞)
R454	R305	C_4H	+	H_2	→	C_4H_2	+	H		$1.2 \times 10^{-11} e^{-998/T}$	Estimated from R311
R455	R306	C_4H	+	CH_4	→	C_4H_2	+	CH_3		$1.2 \times 10^{-11} e^{-491/T}$	Estimated from R312
R456	R307	C_4H	+	C_2H_2	→	C_6H_2	+	H		$9.53 \times 10^{-11} e^{30.8/T}$	Estimated from R314
R457	R308	C_4H	+	C_2H_4	→	C_6H_4	+	H		$7.8 \times 10^{-11} e^{134/T}$	Estimated from R317
R458	R309	C_4H	+	C_2H_6	→	C_4H_2	+	C_2H_5		$5.1 \times 10^{-11} e^{-76/T}$	Estimated from R320
R459	R310	C_4H	+	CH_3C_2H	→	C_7H_4	+	H		$9.53 \times 10^{-11} e^{30.8/T}$	Estimated from R314
R460	R311	C_4H	+	CH_2CCH_2	→	C_7H_4	+	H		$9.53 \times 10^{-11} e^{30.8/T}$	Estimated from R314
R461	R312	C_4H	+	C_3H_6	→	C_4H_3	+	CH_3C_2H		2.0×10^{-11}	Estimated from R324
R462	R313	C_4H	+	C_3H_6	→	C_4H_2	+	C_3H_5		2.4×10^{-10}	Estimated from R326
R463	R314	C_4H	+	C_3H_8	→	C_4H_2	+	C_3H_7		$9.8 \times 10^{-11} e^{-71/T}$	Estimated from R329
R464	R315	C_4H	+	C_4H	→	C_8H	+	H		3.0×10^{-12}	Estimated from R313
R465	R316	C_4H	+	C_4H_2	→	C_8H_2	+	H		$9.53 \times 10^{-11} e^{30.8/T}$	Estimated from R314
R466	R317	C_4H	+	C_4H_3	→	C_4H_2	+	C_4H_2		1.6×10^{-12}	Estimated from R315
R467	R318	C_4H	+	C_4H_3	→	C_8H_3	+	H		3.0×10^{-11}	Estimated from R316
R468	R319	C_4H	+	C_6H_2	→	SOOT	+	H		$9.53 \times 10^{-11} e^{30.8/T}$	Estimated from R314
R469	R320	C_4H	+	C_8H_2	→	SOOT	+	H		$9.53 \times 10^{-11} e^{30.8/T}$	Estimated from R314
R470	R322	$C_4H_2^*$	+	H_2	→	C_4H_2	+	H_2		1.4×10^{-15}	Zwier & Allen (1996)
R471	R323	$C_4H_2^*$	+	CH_4	→	C_4H_2	+	CH_4		1.4×10^{-15}	Zwier & Allen (1996)
R472	R324	$C_4H_2^*$	+	C_2H_2	→	C_6H_2				1.75×10^{-13}	Zwier & Allen (1996)
R473	R325	$C_4H_2^*$	+	C_2H_2	→	C_6H_2	+	H	+ H	1.75×10^{-13}	Zwier & Allen (1996)
R474	R326	$C_4H_2^*$	+	C_2H_4	→	C_6H_5	+	H		9.8×10^{-14}	Zwier & Allen (1996)

R475	R327	$C_4H_2^*$	+	C_2H_4	→	C_6H_4	+	H_2			3.69×10^{-13}	Zwier & Allen (1996)
R476	R328	$C_4H_2^*$	+	CH_3C_2H	→	C_7H_4	+	H_2			1.59×10^{-13}	Zwier & Allen (1996)
R477	R329	$C_4H_2^*$	+	CH_3C_2H	→	C_6H_2	+	CH_3	+	H	2.31×10^{-13}	Zwier & Allen (1996)
R478	R330	$C_4H_2^*$	+	CH_3C_2H	→	C_5H_4	+	C_2H_2			2.46×10^{-13}	Zwier & Allen (1996)
R479	R331	$C_4H_2^*$	+	CH_3C_2H	→	C_5H_3	+	C_2H_3			8.68×10^{-13}	Zwier & Allen (1996)
R480	R332	$C_4H_2^*$	+	C_3H_6	→	C_7H_6	+	H_2			1.63×10^{-13}	Zwier & Allen (1996)
R481	R333	$C_4H_2^*$	+	C_3H_6	→	C_6H_4	+	CH_3	+	H	3.76×10^{-13}	Zwier & Allen (1996)
R482	R334	$C_4H_2^*$	+	C_3H_6	→	C_5H_6	+	C_2H_2			2.29×10^{-13}	Zwier & Allen (1996)
R483	R335	$C_4H_2^*$	+	C_3H_6	→	C_5H_5	+	C_2H_3			4.9×10^{-13}	Zwier & Allen (1996)
R484	R336	$C_4H_2^*$	+	C_4H_2	→	C_8H_2	+	H	+	H	2.57×10^{-13}	Zwier & Allen (1996)
R485	R337	$C_4H_2^*$	+	C_4H_2	→	C_8H_2	+	H_2			2.57×10^{-13}	Zwier & Allen (1996)
R486	R338	$C_4H_2^*$	+	C_4H_2	→	C_6H_2	+	C_2H_2			8.17×10^{-13}	Zwier & Allen (1996)
R487	R339	$C_4H_2^*$	+	C_4H_2	→	C_8H_3	+	H			1.0×10^{-12}	Zwier & Allen (1996)
R488	R340	$C_4H_2^*$	+	C_4H_6	→	C_6H_6	+	C_2H_2			8.8×10^{-13}	Zwier & Allen (1996)
R489	R341	$C_4H_2^*$	+	N_2	→	C_4H_2	+	N_2			1.4×10^{-15}	Zwier & Allen (1996)
R490	R342	C_4H_3	+	H_2	→	C_4H_4	+	H			1.2×10^{-10}	Estimated from R221
R491	R343	C_4H_3	+	CH_4	→	C_4H_4	+	CH_3			5.9×10^{-11}	Estimated from R226
R492	R344	C_4H_3	+	C_2H_2	$\xrightarrow{M}$	C_6H_5					$k_0 = 1.3 \times 10^{+10}\ T^{-12.77}\ e^{-5888/T}$ $k_\infty = 2.8 \times 10^{-17}\ T^{0.47}\ e^{-3020/T}$	Wang & Frenklach (1994)
R493	R345	C_4H_3	+	C_2H_4	→	C_6H_6	+	H			1.5×10^{-10}	Estimated from R234
R494	R346	C_4H_3	+	C_2H_6	→	C_4H_4	+	C_2H_5			1.9×10^{-10}	Estimated from R238
R495	R347	C_4H_3	+	CH_3C_2H	→	C_7H_6	+	H			$3.3 \times 10^{-30}\ e^{-740/T}$	Estimated from R160(k_0)
R496	R348	C_4H_3	+	CH_2CCH_2	→	C_7H_6	+	H			$3.3 \times 10^{-30}\ e^{-740/T}$	Estimated from R160(k_0)
R497	R349	C_4H_3	+	C_3H_6	→	C_4H_4	+	C_3H_5			8.7×10^{-11}	Estimated from R243
R498	R350	C_4H_3	+	C_3H_6	→	C_6H_6	+	CH_3			$1.2 \times 10^{-12}\ e^{-2520/T}$	Estimated from R357
R499	R351	C_4H_3	+	C_3H_6	→	C_7H_8	+	H			$1.2 \times 10^{-12}\ e^{-3240/T}$	Estimated from R358
R500	R352	C_4H_3	+	C_3H_8	→	C_4H_4	+	C_3H_7			$1.0 \times 10^{-21}\ T^{2.3}\ e^{-5285/T}$	Estimated from R362
R501	R353	C_4H_3	+	C_4H_2	→	C_8H_4	+	H			9.62×10^{-11}	Estimated from R229
R502	R354	C_4H_3	+	C_4H_3	→	C_4H_4	+	C_4H_2			2.4×10^{-11}	Estimated from R343
R503	R355	C_4H_3	+	C_4H_3	$\xrightarrow{M}$	C_8H_6					$k_0 = 2.2 \times 10^{-16}\ T^{-3.75}\ e^{-494/T}$ $k_\infty = 1.2 \times 10^{-10}$	Estimated from R279(k_0) Estimated from R344(k_∞)
R504	R356	C_4H_5	+	H_2	→	C_4H_6	+	H			$6.61 \times 10^{-15}\ T^{0.5}\ e^{-1864/T}$	Weissman & Benson (1988)
R505	R357	C_4H_5	+	C_2H_2	→	C_6H_6	+	H			$3.16 \times 10^{-16}\ T^{1.47}\ e^{-2471/T}$	Westmorelet et al. (1989)
R506	R358	C_4H_5	+	C_2H_2	→	C_6H_6	+	H			$4.2 \times 10^{-19}\ T^{1.8}\ e^{-602/T}$	Weissman & Benson (1988)
R507	R359	C_6H	+	H_2	→	C_6H_2	+	H			$9.2 \times 10^{-18}\ T^{2.17}\ e^{-478/T}$	Opansky & Leone (1996b)
R508	R360	C_6H	+	CH_4	→	C_6H_2	+	CH_3			$1.2 \times 10^{-11}\ e^{-491/T}$	Estimated from R312
R509	R361	C_6H	+	C_2H_2	→	C_8H_2	+	H			$9.53 \times 10^{-11}\ e^{30.8/T}$	Estimated from R314
R510	R362	C_6H	+	C_2H_6	→	C_6H_2	+	C_2H_5			$5.1 \times 10^{-11}\ e^{-76/T}$	Estimated from R320
R511	R363	C_6H	+	C_4H_2	→	SOOT	+	H			$9.53 \times 10^{-11}\ e^{30.8/T}$	Estimated from R314
R512	R364	C_6H	+	C_6H_2	→	SOOT	+	H			$9.53 \times 10^{-11}\ e^{30.8/T}$	Estimated from R315
R513	R365	C_6H	+	C_8H_2	→	SOOT	+	H			$9.53 \times 10^{-11}\ e^{30.8/T}$	Estimated from R316
R514	R366	C_6H_5	+	H_2	→	C_6H_6	+	H			$9.48 \times 10^{-20}\ T^{2.43}\ e^{-3159/T}$	Mebel et al. (1997)
R515	R367	C_6H_5	+	C_2H_2	→	SOOT	+	H			$9.8 \times 10^{-13}\ T^{0.21}\ e^{-2516/T}$	Wang & Frenklach (1994)
R516	R368	C_6H_5	+	C_2H_2	$\xrightarrow{M}$	SOOT					$k_0 = 4.97 \times 10^{-19}\ T^{-4.08}\ e^{403/T}$ $k_\infty = 6.64 \times 10^{-17}\ T^{1.56}\ e^{-1914/T}$	Wang & Frenklach (1994)
R517	R369	C_6H_5	+	C_6H_6	→	SOOT	+	H			$1.35 \times 10^{-12}\ e^{-2105/T}$	Park et al. (1999)
R518	R370	$N(^4S)$	+	CH	→	CN	+	H			$2.77 \times 10^{-10}\ T^{-0.09}$	Brownsword et al. (1996)
R519	R371	$N(^4S)$	+	$^3CH_2$	→	HCN	+	H			1.6×10^{-11}	Tsai & McFadden (1990)
R520	R372	$N(^4S)$	+	CH_3	→	HCN	+	H	+	H	3.32×10^{-13}	Marston et al. (1989)
R521	R373	$N(^4S)$	+	CH_3	→	HCN	+	H_2			$4.3 \times 10^{-10}\ e^{-420/T}$	Marston et al. (1989)
R522	R374	$N(^4S)$	+	CH_3	→	H_2CN	+	H			$3.9 \times 10^{-10}\ e^{-420/T}$	Marston et al. (1989)
R523	R375	$N(^4S)$	+	C_2H_3	→	CH_2CN	+	H			6.16×10^{-11}	Payne et al. (1996)
R524	R376	$N(^4S)$	+	C_2H_3	→	C_2H_2	+	NH			1.23×10^{-11}	Payne et al. (1996)
R525	R377	$N(^4S)$	+	C_2H_3	→	CH_3CN					3.9×10^{-12}	Payne et al. (1996)
R526	R378	$N(^4S)$	+	C_2H_4	→	HCN	+	CH_3			4.2×10^{-14}	Miyazaki and Takahashi (1968)
R527	R379	$N(^4S)$	+	C_2H_5	→	H_2CN	+	CH_3			3.9×10^{-11}	Stief et al. (1995)
R528	R380	$N(^4S)$	+	C_2H_5	→	NH	+	C_2H_4			7.2×10^{-11}	Stief et al. (1995)
R529	R381	$N(^4S)$	+	$N(^4S)$	→	N_2					4.1×10^{-34}	Pravilov et al. (1991)
R530	R382	$N(^4S)$	+	NH	→	N_2	+	H			$1.1 \times 10^{-11}\ T^{0.5}$	Rate of maximul collision
R531	R383	$N(^4S)$	+	CN	→	C	+	N_2			3.01×10^{-10}	Baulch et al. (1994)
R532	R384	$N(^4S)$	+	H_2CN	→	HCN	+	NH			$1.0 \times 10^{-10}\ e^{-201/T}$	Nesbitt et al. (1990)
R533	R385	$N(^4S)$	+	C_2N	→	CN	+	CN			1.0×10^{-10}	Whyte and Phillips (1983)
R534	R386	$N(^4S)$	+	CHCN	→	C_2N_2	+	H			1.0×10^{-12}	Yung (1987)
R535	R387	$N(^4S)$	+	CH_3CN	→	HCN	+	HCN	+	H	$2.28 \times 10^{-15}\ e^{-813/T}$	Forst et al. (1957)
R536	R389	$N(^2D)$	+	Ar	→	$N(^4S)$	+	Ar			2.52×10^{-10}	Umemoto et al. (2000)
R537	R390	$N(^2D)$	+	N_2	→	$N(^4S)$	+	N_2			$5.4 \times 10^{-12}\ e^{-1624/T}$	Suzuki et al. (1993)
R538	R391	$N(^2D)$	+	H_2	→	NH	+	H			$4.2 \times 10^{-11}\ e^{-880/T}$	Herron (1999)
R539	R392	$N(^2D)$	+	CH_4	→	NH	+	CH_3			$1.44 \times 10^{-12}\ e^{-755/T}$	Herron (1999)
R540	R393	$N(^2D)$	+	CH_4	→	CH_2NH	+	H			$3.36 \times 10^{-12}\ e^{-755/T}$	Herron (1999)

R541	R394	$N(^2D)$	+	C_2H_2	→	CHCN	+	H			$1.6 \times 10^{-10} e^{-267/T}$	Herron (1999)
R542	R395	$N(^2D)$	+	C_2H_4	→	NH	+	C_2H_3			1.2×10^{-12}	Black et al. (1969)
R543	R396	$N(^2D)$	+	C_2H_4	→	CH_3CN	+	H			2.6×10^{-11}	Sato et al. (1999); Balucani et al. (2000)
R544	R397	$N(^2D)$	+	C_2H_6	→	NH	+	C_2H_5			1.9×10^{-11}	Herron et al. (1999)
R545	R398	$N(^2D)$	+	CO	→	CN	+	$O(^3P)$			1.7×10^{-12}	Piper et al. (1987)
R546	R399	$N(^2D)$	+	CO_2	→	NO	+	CO			3.6×10^{-13}	Herron et al. (1999)
R547	R400	NH	+	H	→	$N(^4S)$	+	H_2			1.7×10^{-11}	Baulch et al. (1994)
R548	R401	NH	+	CH_3	→	CH_2NH	+	H			4.0×10^{-11}	Lellouch et al. (1994)
R549	R402	NH	+	CH_3	→	$N(^4S)$	+	CH_4			4.0×10^{-11}	Lellouch et al. (1994)
R550	R403	NH	+	C_2H_3	→	$N(^4S)$	+	C_2H_4			4.0×10^{-11}	Lellouch et al. (1994)
R551	R404	NH	+	C_2H_5	→	$N(^4S)$	+	C_2H_6			4.0×10^{-11}	Lellouch et al. (1994)
R552	R405	NH	+	NH	$\xrightarrow{M}$	N_2	+	H_2			$k_0 = 1.0 \times 10^{-33}$ $k_\infty = 3.5 \times 10^{-12}$	Yung et al. (1984) Nicholas et al. (1986)
R553	R406	NH	+	NH_2	→	N_2H_3					1.6×10^{-10}	Pagsberg et al. (1979)
R554	R407	NH_2	+	H	$\xrightarrow{M}$	NH_3					$k_0 = 3.01 \times 10^{-30}$ $k_\infty = 2.66 \times 10^{-11}$	Schofield (1973) Pagsberg et al. (1979)
R555	R408	NH_2	+	H_2	→	NH_3	+	H			$2.09 \times 10^{-12} e^{-4277/T}$	Demissy & Lesclaux (1980)
R556	R409	NH_2	+	CH_3	$\xrightarrow{M}$	CH_3NH_2					$k_0 = 6.04 \times 10^{-18} T^{-3.85}$ $k_\infty = 1.19 \times 10^{-11} T^{0.42}$	Jodkowski et al. (1995)
R557	R410	NH_2	+	CH_4	→	NH_3	+	CH_3			$5.1 \times 10^{-23} T^{3.59} e^{-4540/T}$	Mebel & Lin (1999)
R558	R411	NH_2	+	C_2H_2	→	NH_3	+	C_2H			$1.11 \times 10^{-13} e^{-1850/T}$	Bosco et al. (1984)
R559	R412	NH_2	+	C_2H_4	→	NH_3	+	C_2H_3			$3.42 \times 10^{-14} e^{-1318/T}$	Bosco et al. (1984)
R560	R413	NH_2	+	C_2H_5	→	NH_3	+	C_2H_4			4.15×10^{-11}	Demissy & Lesclaux (1982)
R561	R414	NH_2	+	C_2H_6	→	NH_3	+	C_2H_5			$6.14 \times 10^{-13} e^{-3598/T}$	Lesclaux & Demissy (1978)
R562	R415	NH_2	+	NH_2	→	N_2H_2	+	H_2			1.3×10^{-12}	Stothard et al. (1995)
R563	R416	NH_2	+	NH_2	$\xrightarrow{M}$	N_2H_4					$k_0 = 8.74 \times 10^{-20} T^{-3.9}$ $k_\infty = 2.54 \times 10^{-11} T^{0.27}$	Fagerström et al. (1995)
R564	R417	NH_2	+	N_2H_4	→	N_2H_3	+	NH_3			5.14×10^{-13}	Gehring et al. (1971)
R565	R418	NH_3	+	H	→	NH_2	+	H_2			$7.78 \times 10^{-24} T^{3.93} e^{-4064/T}$	Espinosa-Garcia & Corchado (1994)
R566	R419	NH_3	+	CH	→	NH	+	CH_3			$4.11 \times 10^{-9} T^{-0.56} e^{-30.2/T}$	Bocherel et al. (1996)
R567	R420	NH_3	+	CH_3	→	NH_2	+	CH_4			$4.2 \times 10^{-21} T^{2.86} e^{-7340/T}$	Yu et al. (1998)
R568	R421	N_2H_2	+	H	→	N_2H	+	H_2			$1.4 \times 10^{-19} T^{2.63} e^{-115/T}$	Linder et al. (1996)
R569	R422	N_2H_2	+	NH_2	→	NH_3	+	N_2H			$1.5 \times 10^{-25} T^{4.05} e^{-810/T}$	Linder et al. (1996)
R570	R423	N_2H_3	+	H	→	NH_2	+	NH_2			2.66×10^{-12}	Gehring et al. (1971)
R571	R424	N_2H_3	+	N_2H_3	→	N_2H_4	+	N_2	+	H_2	6.0×10^{-11}	Atreya (1986)
R572	R425	N_2H_4	+	H	→	N_2H_3	+	H_2			$9.86 \times 10^{-12} e^{-1198/T}$	Stief & Payne (1976)
R573	R426	N_2H_4	+	CH_3	→	N_2H_3	+	CH_4			$1.66 \times 10^{-13} e^{-2516/T}$	Gray & Thynne (1964)
R574	R427	CN	+	H	$\xrightarrow{M}$	HCN					$k_0 = 2.4 \times 10^{-24} T^{-2.2} e^{-567/T}$ $k_\infty = 3.0 \times 10^{-9} T^{-0.5}$	Tsang et al. (1992)
R575	R428	CN	+	H_2	→	HCN	+	H			$3.2 \times 10^{-20} T^{2.87} e^{-820/T}$	Baulch et al. (1994)
R576	R429	CN	+	CH_4	→	HCN	+	CH_3			$5.73 \times 10^{-12} e^{-675/T}$	Sims et al. (1993)
R577	R430	CN	+	CH_4	→	CH_3CN	+	H			$2.08 \times 10^{-21} T^{2.64} e^{-78/T}$	Balla & Casleton (1991)
R578	R431	CN	+	C_2H_2	→	HC_3N	+	H			$5.26 \times 10^{-9} T^{-0.52} e^{-20/T}$	Sims et al. (1993); Sayah et al. (1988)
R579	R432	CN	+	C_2H_4	→	C_2H_3CN	+	H			$2.72 \times 10^{-9} T^{-0.69} e^{-31/T}$	Sims et al. (1993); Monks et al. (1993)
R580	R433	CN	+	C_2H_4	→	HCN	+	C_2H_3			$1.09 \times 10^{-8} T^{-0.69} e^{-31/T}$	Sims et al. (1993); Monks et al. (1993)
R581	R434	CN	+	C_2H_6	→	HCN	+	C_2H_5			$5.94 \times 10^{-12} T^{0.22} e^{58/T}$	Sims et al. (1993)
R582	R435	CN	+	CH_3C_2H	→	C_3H_3CN	+	H			4.1×10^{-11}	Carty et al. (2001)
R583	R436	CN	+	CH_2CCH_2	→	C_3H_3CN	+	H			4.1×10^{-11}	Carty et al. (2001)
R584	R437	CN	+	C_3H_6	→	CH_3CN	+	C_2H_3			$1.73 \times 10^{-10} e^{102/T}$	Sims et al. (1993)
R585	R438	CN	+	C_3H_8	→	HCN	+	C_3H_7			$2.4 \times 10^{-14} T^{1.19} e^{378/T}$	Yang et al. (1992a)
R586	R439	CN	+	C_4H_2	→	HC_5N	+	H			4.2×10^{-10}	Seki et al. (1996)
R587	R440	CN	+	C_4H_4	→	SOOT	+	H			$1.07 \times 10^{-7} T^{-0.82} e^{-228/T}$	Yang et al. (1992a)
R588	R441	CN	+	C_4H_6	→	SOOT					$2.57 \times 10^{-10} e^{171/T}$	Butterfield et al. (1993)
R589	R442	CN	+	NH_3	→	HCN	+	NH_2			$1.83 \times 10^{-8} T^{-1.14}$	Sims & Smith (1988)
R590	R443	CN	+	CN	$\xrightarrow{M}$	C_2N_2					$k_0 = 9.4 \times 10^{-23} T^{-2.61}$ $k_\infty = 9.4 \times 10^{-12}$	Tsang et al. (1992)
R591	R444	CN	+	HCN	→	C_2N_2	+	H			$2.5 \times 10^{-17} T^{1.71} e^{-770/T}$	Tsang et al. (1992)
R592	R445	CN	+	CH_3CN	→	C_2N_2	+	CH_3			$6.46 \times 10^{-11} e^{-1190/T}$	Zabarnick et al. (1989)
R593	R446	CN	+	C_3N	$\xrightarrow{M}$	C_4N_2					$k_0 = 9.4 \times 10^{-23} T^{-2.61}$ $k_\infty = 9.4 \times 10^{-12}$	Estimated from R590(k_0) Estimated from R590(k_∞)
R594	R447	CN	+	HC_3N	→	C_4N_2	+	H			1.69×10^{-12}	Halpern et al. (1989)
R595	R448	CN	+	C_2H_3CN	→	SOOT					$3.02 \times 10^{-11} e^{101/T}$	Butterfield et al. (1993)
R596	R449	CN	+	C_2N_2	→	SOOT					$2.19 \times 10^{-21} T^{2.7} e^{-325/T}$	Yang et al. (1992b)
R597	R450	CN	+	C_4N_2	→	SOOT					5.4×10^{-13}	Seki et al. (1996)
R598	R451	HCN	+	H	$\xrightarrow{M}$	H_2CN					$k_0 = 4.5 \times 10^{-24} T^{-2.73} e^{-3855/T}$ $k_\infty = 5.5 \times 10^{-11} e^{-2438/T}$	Tsang (1991)
R599	R452	HCN	+	$^3CH_2$	→	CH_2CN	+	H			$1.5 \times 10^{-12} e^{-3332/T}$	Estimated from R258

R600	R453	HCN	+	CH_3	$\xrightarrow{M}$	SOOT					$k_0 = 4.5 \times 10^{-24} T^{-2.73} e^{-3855/T}$ $k_\infty = 5.5 \times 10^{-11} e^{-2438/T}$	Estimated from R598(k_0) Estimated from R598(k_∞)
R601	R454	HCN	+	C_2H	→	HC_3N	+	H			$5.3 \times 10^{-12} e^{-769/T}$	Hoobler & Leone (1997)
R602	R455	HCN	+	C_2H_3	→	C_2H_3CN	+	H			4.5×10^{-14}	Monks et al. (1993)
R603	R456	HCN	+	C_2H_5	$\xrightarrow{M}$	SOOT					$k_0 = 4.5 \times 10^{-24} T^{-2.73} e^{-3855/T}$ $k_\infty = 5.5 \times 10^{-11} e^{-2438/T}$	Estimated from R598(k_0) Estimated from R598(k_∞)
R604	R457	HCN	+	C_3H_5	→	C_2H_5CN	+	H			4.5×10^{-14}	Estimated from R602
R605	R458	HCN	+	C_3H_7	$\xrightarrow{M}$	SOOT					$k_0 = 4.5 \times 10^{-24} T^{-2.73} e^{-3855/T}$ $k_\infty = 5.5 \times 10^{-11} e^{-2438/T}$	Estimated from R598(k_0) Estimated from R598(k_∞)
R606	R459	HCN	+	C_4H	→	HC_5N	+	H			4.5×10^{-14}	Estimated from R602
R607	R460	HCN	+	C_4H_3	→	C_4H_3CN	+	H			4.5×10^{-14}	Estimated from R602
R608	R461	HCN	+	H_2C_3CN	→	SOOT	+	H			4.5×10^{-14}	Estimated from R602
R609	R462	H_2CN	+	H	→	HCN	+	H_2			7.0×10^{-11}	Marston et al. (1989)
R610	R463	H_2CN	+	HCN	→	SOOT					$1.1 \times 10^{-15} e^{-900/T}$	Wilson & Atreya (2003)
R611	R464	H_2CN	+	H_2CN	→	HCN	+	HCN	+	H_2	7.7×10^{-12}	Nizamov & Dagdigian (2003)
R612	R465	CH_3NH_2	+	CH	→	$C_2H_3NH_2$	+	H			$3.1 \times 10^{-10} e^{-170/T}$	Zabarnick & Lin (1989)
R613	R466	CH_3NH_2	+	CH_3	→	CH_2NH_2	+	CH_4			$1.62 \times 10^{-13} e^{-4381/T}$	Gray & Thynne (1964)
R614	R467	CH_3NH_2	+	CH_3	→	CH_3NH	+	CH_4			$5.89 \times 10^{-15} e^{-2870/T}$	Gray & Thynne (1964)
R615	R468	C_2N_2	+	H	$\xrightarrow{M}$	HC_2N_2					$k_0 = 3.3 \times 10^{-30} e^{-740/T}$ $k_\infty = 1.5 \times 10^{-15}$	Estimated from R160(k_0) Phillips (1978)
R616	R469	CHCN	+	CHCN	→	C_4N_2	+	H_2			5.3×10^{-11}	Estimated from R253; Yung (1987)
R617	R470	CH_3CN	+	H	→	HCN	+	CH_3			$3.39 \times 10^{-12} e^{-3954/T}$	Jamieson et al. (1970)
R618	R471	CH_3CN	+	H	→	CN	+	CH_4			$1.66 \times 10^{-13} e^{-1505/T}$	Jamieson et al. (1970)
R619	R472	CH_3CN	+	C_2H	→	C_3H_3CN	+	H			$1.8 \times 10^{-11} e^{-766/T}$	Nizamov & Leone (2004)
R620	R473	C_3N	+	H_2	→	HC_3N	+	H			$1.2 \times 10^{-11} e^{-998/T}$	Estimated from R311
R621	R474	C_3N	+	$^3CH_2$	→	HC_3N	+	CH			3.0×10^{-11}	Estimated from R256
R622	R475	C_3N	+	CH_3	→	C_3H_2CN	+	H			4.0×10^{-11}	Estimated from R280
R623	R476	C_3N	+	CH_4	→	HC_3N	+	CH_3			$5.73 \times 10^{-12} e^{-675/T}$	Estimated from R575; Yung (1987)
R624	R477	C_3N	+	C_2H	→	SOOT	+	H			3.0×10^{-12}	Estimated from R313
R625	R478	C_3N	+	C_2H_2	→	HC_5N	+	H			$9.53 \times 10^{-11} e^{30.8/T}$	Estimated from R314
R626	R479	C_3N	+	C_2H_3	→	HC_3N	+	C_2H_2			1.6×10^{-12}	Estimated from R315
R627	R480	C_3N	+	C_2H_3	→	C_4H_2CN	+	H			3.0×10^{-11}	Estimated from R316
R628	R481	C_3N	+	C_2H_4	→	C_4H_3CN	+	H			$7.8 \times 10^{-11} e^{134/T}$	Estimated from R317
R629	R482	C_3N	+	C_2H_5	→	HC_3N	+	C_2H_4			3.0×10^{-12}	Estimated from R318
R630	R483	C_3N	+	C_2H_5	→	C_3H_2CN	+	CH_3			3.0×10^{-11}	Estimated from R319
R631	R484	C_3N	+	C_2H_6	→	HC_3N	+	C_2H_5			$5.94 \times 10^{-12} T^{0.22} e^{58/T}$	Estimated from R580; Yung (1987)
R632	R485	HC_3N	+	H	$\xrightarrow{M}$	H_2C_3N					$k_0 = 3.3 \times 10^{-30} e^{-740/T}$ $k_\infty = 1.1 \times 10^{-12} e^{-500/T}$	Estimated from R160(k_0) Parker et al. (2004)
R633	R486	HC_3N	+	C_2H	→	HC_5N	+	H			$9.53 \times 10^{-11} e^{30.8/T}$	Estimated from R314
R634	R487	HC_3N	+	C_2H_3	→	SOOT	+	H			$3.31 \times 10^{-12} e^{-2516/T}$	Estimated from R341
R635	R488	HC_3N	+	C_2H_5	→	SOOT					$4.5 \times 10^{-13} e^{-11800/T}$	Estimated from R371
R636	R489	HC_3N	+	C_6H_5	→	SOOT					$9.8 \times 10^{-13} T^{0.21} e^{-2516/T}$	Estimated from R514
R637	R490	H_2C_3N	+	H	→	C_2H_2	+	HCN			1.5×10^{-11}	Yung et al. (1984)
R638	R491	C_2N_2	+	H	→	HCN	+	CN			8.59×10^{-16}	Dunn et al. (1971)
R639	R492	C_2N_2	+	C	→	CN	+	C_2N			3.01×10^{-11}	Whyte & Phillips (1983)
R640	R493	HC_2N_2	+	H	→	HCN	+	HCN			$1.7 \times 10^{-13} e^{-110/T}$	Yung (1987)
R641	R494	$O(^3P)$	+	H	$\xrightarrow{M}$	OH					$1.3 \times 10^{-29} T^{-1}$ [cm^6 $molecule^{-2}$ s^{-1}]	Tsang & Hampson (1986)
R642	R495	$O(^3P)$	+	H_2	→	OH	+	H			$8.52 \times 10^{-20} T^{2.67} e^{-3163/T}$	Baulch et al. (1992)
R643	R496	$O(^3P)$	+	CH	→	CO	+	H			6.59×10^{-11}	Baulch et al. (1992)
R644	R497	$O(^3P)$	+	$^3CH_2$	→	CO	+	H	+	H	2.01×10^{-10}	Baulch et al. (1992)
R645	R498	$O(^3P)$	+	CH_3	→	H_2CO	+	H			1.4×10^{-10}	Atkinson et al. (1992)
R646	R499	$O(^3P)$	+	CH_3	→	CO	+	H_2	+	H	$1.95 \times 10^{-11} e^{-201/T}$	Fockenberg & Preses (2002)
R647	R500	$O(^3P)$	+	CH_3	→	CH_3O					$1.32 \times 10^{-8} T^{-2.12} e^{-312/T}$	Dean & Westmoreland (1987)
R648	R501	$O(^3P)$	+	CH_4	→	OH	+	CH_3			$1.15 \times 10^{-15} T^{1.56} e^{-4275/T}$	Baulch et al. (1992)
R649	R502	$O(^3P)$	+	C_2H	→	CO	+	CH			$2.41 \times 10^{-11} e^{-232/T}$	Devriendt & Peeters (1997)
R650	R503	$O(^3P)$	+	C_2H_2	→	CO	+	$^3CH_2$			$3.01 \times 10^{-11} e^{-1601/T}$	DeMore et al. (1997)
R651	R504	$O(^3P)$	+	C_2H_2	→	CH_2CO					2.1×10^{-13}	Gaedtke et al. (1973) – Upper limit
R652	R505	$O(^3P)$	+	C_2H_3	→	CH_2CO	+	H			1.6×10^{-10}	Tsang & Hampson (1986)
R653	R506	$O(^3P)$	+	C_2H_4	→	CH_3CO	+	H			$1.13 \times 10^{-17} T^{1.88} e^{-92/T}$	Baulch et al. (1994)
R654	R507	$O(^3P)$	+	C_2H_4	→	HCO	+	CH_3			$9.0 \times 10^{-18} T^{1.88} e^{-92/T}$	Baulch et al. (1994)
R655	R508	$O(^3P)$	+	C_2H_4	→	H_2CO	+	$^3CH_2$			$2.25 \times 10^{-18} T^{1.88} e^{-92/T}$	Baulch et al. (1994)
R656	R509	$O(^3P)$	+	C_2H_4	→	C_2H_4O					1.16×10^{-12}	Gaedtke et al. (1973)
R657	R510	$O(^3P)$	+	C_2H_5	→	CH_3CHO	+	H			1.33×10^{-10}	Tsang & Hampson (1986)
R658	R511	$O(^3P)$	+	C_2H_5	→	H_2CO	+	CH_3			2.67×10^{-11}	Tsang & Hampson (1986)
R659	R512	$O(^3P)$	+	C_2H_6	→	OH	+	C_2H_5			$1.66 \times 10^{-15} T^{1.5} e^{-2921/T}$	Baulch et al. (1992)
R660	R513	$O(^3P)$	+	C_3H_2	→	CO	+	C_2H	+	H	1.13×10^{-10}	Homann & Wellmann (1983)
R661	R514	$O(^3P)$	+	C_3H_3	→	SOOT	+	H			2.31×10^{-10}	Slagle et al. (1990b)
R662	R515	$O(^3P)$	+	C_3H_5	→	SOOT	+	H			3.01×10^{-10}	Slagle et al. (1990a)

R663	R516	$O(^3P)$	+	NH	→	OH	+	$N(^4S)$	1.16×10^{-11}	Cohen & Westberg (1991)
R664	R517	$O(^3P)$	+	NH	→	NO	+	H	1.16×10^{-10}	Cohen & Westberg (1991)
R665	R518	$O(^3P)$	+	NH_2	→	OH	+	NH	1.16×10^{-11}	Cohen & Westberg (1991)
R666	R519	$O(^3P)$	+	NH_2	→	NO	+	H_2	8.3×10^{-12}	Cohen & Westberg (1991)
R667	R520	$O(^3P)$	+	NH_3	→	OH	+	NH_2	$1.83 \times 10^{-18} T^{2.1} e^{-2624/T}$	Cohen & Westberg (1991)
R668	R521	$O(^3P)$	+	CN	→	CO	+	$N(^4S)$	1.69×10^{-11}	Baulch et al. (1992)
R669	R522	$O(^3P)$	+	HCN	→	CO	+	NH	$9.0 \times 10^{-16} T^{1.21} e^{-3822/T}$	Perry & Melius (1984)
R670	R523	$O(^3P)$	+	HCN	→	CN	+	OH	$5.5 \times 10^{-15} T^{1.58} e^{-13410/T}$	Perry & Melius (1984)
R671	R524	$O(^3P)$	+	CO	$\xrightarrow{M}$	CO_2			$1.7 \times 10^{-33} e^{-1510/T}$ [cm^6 molecule^{-2} s^{-1}]	Tsang & Hampson (1986)
R672	R525	$O(^3P)$	+	HCO	→	CO	+	OH	5.0×10^{-11}	Baulch et al. (1992)
R673	R526	$O(^3P)$	+	HCO	→	CO_2	+	H	5.0×10^{-11}	Baulch et al. (1992)
R674	R527	$O(^3P)$	+	H_2CO	→	HCO	+	OH	$6.9 \times 10^{-13} T^{0.57} e^{-1390/T}$	Baulch et al. (1992)
R675	R528	$O(^3P)$	+	CH_3O	→	H_2CO	+	OH	1.0×10^{-11}	Tsang & Hampson (1986)
R676	R529	$O(^3P)$	+	CH_2OH	→	H_2CO	+	OH	1.5×10^{-10}	Grotheer et al. (1988)
R677	R530	$O(^3P)$	+	CH_3OH	→	CH_2OH	+	OH	$3.2 \times 10^{-19} T^{2.5} e^{-1550/T}$	Tsang (1987)
R678	R531	$O(^3P)$	+	CH_3OH	→	CH_3O	+	OH	$3.2 \times 10^{-19} T^{2.5} e^{-1550/T}$	Tsang (1987)
R679	R532	$O(^3P)$	+	CH_3CO	→	CO_2	+	CH_3	2.4×10^{-10}	Miyoshi et al. (1989)
R680	R533	$O(^3P)$	+	CH_3CO	→	CH_2CO	+	OH	8.0×10^{-11}	Miyoshi et al. (1989)
R681	R534	$O(^3P)$	+	CH_3CHO	→	CH_3CO	+	OH	$1.79 \times 10^{-11} e^{-1103/T}$	DeMore et al. (1997)
R682	R536	$O(^1D)$	+	Ar	→	$O(^3P)$	+	Ar	5.0×10^{-13}	Shi & Barker (1990)
R683	R537	$O(^1D)$	+	N_2	→	$O(^3P)$	+	N_2	$1.8 \times 10^{-11} e^{-107/T}$	Atkinson et al. (2004)
R684	R538	$O(^1D)$	+	H_2	→	OH	+	H	1.1×10^{-10}	Atkinson et al. (2004)
R685	R539	$O(^1D)$	+	CH_4	→	OH	+	CH_3	1.13×10^{-10}	DeMore et al. (1997)
R686	R540	$O(^1D)$	+	CH_4	→	CH_2OH	+	H	7.51×10^{-12}	DeMore et al. (1997)
R687	R541	$O(^1D)$	+	CH_4	→	CH_3O	+	H	3.01×10^{-11}	DeMore et al. (1997)
R688	R542	$O(^1D)$	+	NH_3	→	NH_2	+	OH	2.51×10^{-10}	DeMore et al. (1997)
R689	R543	$O(^1D)$	+	H_2O	→	OH	+	OH	2.19×10^{-10}	Atkinson et al. (2004)
R690	R544	$O(^1D)$	+	CO	→	CO_2			8.0×10^{-11}	Tully (1975)
R691	R545	$O(^1D)$	+	CO_2	→	$O(^3P)$	+	CO_2	$7.41 \times 10^{-11} e^{121/T}$	DeMore et al. (1997)
R692	R546	OH	+	H	→	$O(^3P)$	+	H_2	$8.1 \times 10^{-21} T^{2.8} e^{-1950/T}$	Tsang & Hampson (1986)
R693	R547	OH	+	H	$\xrightarrow{M}$	H_2O			$6.1 \times 10^{-26} T^{-2}$ [cm^6 molecule^{-2} s^{-1}]	Baulch et al. (1992)
R694	R548	OH	+	H_2	→	H_2O	+	H	$7.7 \times 10^{-12} e^{-2100/T}$	Atkinson et al. (2004)
R695	R549	OH	+	$^3CH_2$	→	H_2CO			3.01×10^{-11}	Tsang & Hampson (1986)
R696	R550	OH	+	CH_3	→	H_2CO	+	H_2	$5.3 \times 10^{-15} e^{-2530/T}$	de Avillez Pereira et al. (1997)
R697	R551	OH	+	CH_3	$\xrightarrow{M}$	CH_3OH			$k_0 = 6.26 \times 10^{-18} T^{-3.8}$ $k_\infty = 8.2 \times 10^{-11} T^{0.1}$	Fagerström et al. (1994)
R698	R552	OH	+	CH_4	→	H_2O	+	CH_3	$1.85 \times 10^{-20} T^{2.82} e^{-987/T}$	Gierczak et al. (1997)
R699	R553	OH	+	C_2H	→	$O(^3P)$	+	C_2H_2	3.0×10^{-11}	Tsang & Hampson (1986)
R700	R554	OH	+	C_2H	→	CO	+	$^3CH_2$	3.01×10^{-11}	Tsang & Hampson (1986)
R701	R555	OH	+	C_2H_2	→	H_2O	+	C_2H	$3.04 \times 10^{-20} T^{2.68} e^{-6063/T}$	Tsang & Hampson (1986)
R702	R556	OH	+	C_2H_2	→	CH_2CO	+	H	1.0×10^{-13}	Siese & Zetzsch (1995) – Upper limit
R703	R557	OH	+	C_2H_2	$\xrightarrow{M}$	CH_3CO			$k_0 = 2.58 \times 10^{-26} T^{-1.5}$ $k_\infty = 9.35 \times 10^{-18} T^{2}$	Atkinson et al. (1999) DeMore et al. (1997)
R704	R558	OH	+	C_2H_3	→	CH_3CHO			5.0×10^{-11}	Tsang & Hampson (1986)
R705	R559	OH	+	C_2H_3	→	H_2O	+	C_2H_2	5.0×10^{-11}	Tsang & Hampson (1986)
R706	R560	OH	+	C_2H_4	→	H_2O	+	C_2H_3	$2.61 \times 10^{-20} T^{2.74} e^{-2100/T}$	Tsang & Hampson (1986)
R707	R561	OH	+	C_2H_5	→	H_2O	+	C_2H_4	4.0×10^{-11}	Tsang & Hampson (1986)
R708	R562	OH	+	C_2H_6	→	H_2O	+	C_2H_5	$6.9 \times 10^{-12} e^{-1007/T}$	Atkinson et al. (2001)
R709	R563	OH	+	OH	→	H_2O	+	$O(^3P)$	$2.3 \times 10^{-20} T^{2.6} e^{947/T}$	Atkinson et al. (2004)
R710	R564	OH	+	CO	→	CO_2	+	H	$2.81 \times 10^{-13} e^{-176/T}$	Frost et al. (1993)
R711	R565	OH	+	H_2CO	→	HCO	+	H_2O	$8.2 \times 10^{-12} e^{40.3/T}$	Atkinson et al. (1999)
R712	R566	OH	+	CH_2OH	→	H_2CO	+	H_2O	4.0×10^{-11}	Tsang (1987)
R713	R567	OH	+	CH_3OH	→	CH_2OH	+	H_2O	$3.1 \times 10^{-12} e^{-363/T}$	Atkinson et al. (2001)
R714	R568	OH	+	CH_3OH	→	CH_3O	+	H_2O	1.4×10^{-13}	Atkinson et al. (2001)
R715	R569	OH	+	CH_3CO	→	CH_2CO	+	H_2O	2.01×10^{-11}	Tsang & Hampson (1986)
R716	R570	OH	+	CH_3CHO	→	CH_3CO	+	H_2O	$4.4 \times 10^{-12} e^{368/T}$	Atkinson et al. (2001)
R717	R571	H_2O	+	CH	→	CH_2OH			$9.48 \times 10^{-12} e^{383/T}$	Zabarnick et al. (1986)
R718	R572	H_2O	+	$^1CH_2$	→	CH_3OH			3.0×10^{-11}	Tsang & Hampson (1986)
R719	R573	H_2O	+	$^3CH_2$	→	CH_3	+	OH	1.6×10^{-16}	Tsang & Hampson (1986) – Upper limit
R720	R574	H_2O	+	CH_3	→	CH_4	+	OH	$8.0 \times 10^{-22} T^{2.9} e^{-7480/T}$	Tsang & Hampson (1986)
R721	R575	H_2O	+	CH_3O	→	CH_3OH	+	OH	$1.5 \times 10^{-15} T^{3.8} e^{-5786/T}$	Jodkowski et al. (1999)
R722	R576	H_2O	+	CH_2OH	→	CH_3OH	+	OH	$1.25 \times 10^{-11} T^{3} e^{-10420/T}$	Jodkowski et al. (1999)
R723	R577	CO	+	H	$\xrightarrow{M}$	HCO			$5.29 \times 10^{-34} e^{-373/T}$ [cm^6 molecule^{-2} s^{-1}]	Baulch et al. (1992)
R724	R578	CO	+	$^3CH_2$	$\xrightarrow{M}$	CH_2CO			$k_0 = 1.0 \times 10^{-28}$ $k_\infty = 1.0 \times 10^{-15}$	Yung et al. (1984)
R725	R579	CO	+	CH_3	$\xrightarrow{M}$	CH_3CO			$k_0 = 4.19 \times 10^{-36}$ $k_\infty = 8.4 \times 10^{-13} e^{-3465/T}$	Baulch et al. (1994)

R726	R580	CO	+	CH_3O	→	CO_2	+	CH_3			$2.61 \times 10^{-11} e^{-5940/T}$	Tsang & Hampson (1986)
R727	R581	HCO	+	H	→	CO	+	H_2			1.83×10^{-10}	Friedrichs et al. (2002)
R728	R582	HCO	+	H_2	→	H_2CO	+	H			$3.0 \times 10^{-18} T^2 e^{-8979/T}$	Tsang & Hampson (1986)
R729	R583	HCO	+	$^3CH_2$	→	CO	+	CH_3			3.01×10^{-11}	Tsang & Hampson (1986)
R730	R584	HCO	+	CH_3	→	CO	+	CH_4			2.01×10^{-10}	Tsang & Hampson (1986)
R731	R585	HCO	+	CH_3	→	CH_3CHO					3.01×10^{-11}	Tsang & Hampson (1986)
R732	R586	HCO	+	CH_4	→	H_2CO	+	CH_3			$1.21 \times 10^{-20} T^{2.85} e^{-11310/T}$	Tsang & Hampson (1986)
R733	R587	HCO	+	C_2H	→	CO	+	C_2H_2			1.0×10^{-10}	Tsang & Hampson (1986)
R734	R588	HCO	+	C_2H_3	→	CO	+	C_2H_4			1.5×10^{-10}	Tsang & Hampson (1986)
R735	R589	HCO	+	C_2H_5	→	CO	+	C_2H_6			2.01×10^{-10}	Tsang & Hampson (1986)
R736	R590	HCO	+	C_2H_6	→	H_2CO	+	C_2H_5			$7.79 \times 10^{-20} T^{2.72} e^{-9285/T}$	Tsang & Hampson (1986)
R737	R591	HCO	+	C_3H_5	→	CO	+	C_3H_6			1.0×10^{-10}	Tsang (1991)
R738	R592	HCO	+	C_3H_7	→	CO	+	C_3H_8			1.0×10^{-10}	Tsang (1991)
R739	R593	HCO	+	C_3H_8	→	H_2CO	+	C_3H_7			$3.4 \times 10^{-19} T^{2.5} e^{-9286/T}$	Tsang (1988)
R740	R594	HCO	+	H_2O	→	H_2CO	+	OH			$3.9 \times 10^{-16} T^{1.35} e^{-13.11/T}$	Tsang & Hampson (1986)
R741	R595	HCO	+	HCO	→	CO	+	CO	+	H_2	3.64×10^{-11}	Yee Quee & Thynne (1968)
R742	R596	HCO	+	HCO	→	H_2CO	+	CO			4.48×10^{-11}	Friedrichs et al. (2002)
R743	R597	HCO	+	CH_3O	→	CH_3OH	+	CO			1.5×10^{-10}	Tsang & Hampson (1986)
R744	R598	HCO	+	CH_2OH	→	CH_3OH	+	CO			2.01×10^{-10}	Tsang (1987)
R745	R599	HCO	+	CH_2OH	→	H_2CO	+	H_2CO			3.01×10^{-10}	Tsang (1987)
R746	R600	HCO	+	CH_3OH	→	CH_2OH	+	H_2CO			$1.61 \times 10^{-20} T^{2.9} e^{-6607/T}$	Tsang (1987)
R747	R601	HCO	+	CH_3CO	→	CH_3CHO	+	CO			1.5×10^{-11}	Tsang & Hampson (1986)
R748	R602	HCO	+	CN	→	HCN	+	CO			1.0×10^{-10}	Tsang (1992)
R749	R603	HCO	+	HCN	→	H_2CO	+	CN			$1.0 \times 10^{-11} e^{-17210/T}$	Tsang (1991)
R750	R604	H_2CO	+	H	→	HCO	+	H_2			$2.1 \times 10^{-16} T^{1.62} e^{-1093/T}$	Baulch et al. (1994)
R751	R605	H_2CO	+	$^3CH_2$	→	HCO	+	CH_3			1.0×10^{-14}	Tsang & Hampson (1986)
R752	R606	H_2CO	+	CH_3	→	HCO	+	CH_4			$6.79 \times 10^{-12} e^{-4450/T}$	Baulch et al. (1992)
R753	R607	H_2CO	+	C_2H_3	→	HCO	+	C_2H_4			$9.0 \times 10^{-21} T^{2.81} e^{-2951/T}$	Tsang & Hampson (1986)
R754	R608	H_2CO	+	C_2H_5	→	HCO	+	C_2H_6			$9.0 \times 10^{-21} T^{2.81} e^{-2951/T}$	Tsang & Hampson (1986)
R755	R609	H_2CO	+	CH_3O	→	CH_3OH	+	HCO			$1.69 \times 10^{-13} e^{-1500/T}$	Tsang & Hampson (1986)
R756	R610	H_2CO	+	CH_2OH	→	CH_3OH	+	HCO			$9.1 \times 10^{-21} T^{2.8} e^{-2950/T}$	Tsang (1987)
R757	R611	H_2CO	+	CH_3CO	→	CH_3CHO	+	HCO			$3.01 \times 10^{-13} e^{-6506/T}$	Tsang & Hampson (1986)
R758	R612	H_2CO	+	CN	→	HCN	+	HCO			$2.81 \times 10^{-19} T^{2.72} e^{-720/T}$	Yu et al. (1993)
R759	R613	CH_3O	+	H	→	H_2CO	+	H_2			3.01×10^{-11}	Baulch et al. (1992)
R760	R614	CH_3O	+	$^1CH_2$	→	H_2CO	+	CH_3			3.01×10^{-12}	Tsang & Hampson (1986)
R761	R615	CH_3O	+	$^3CH_2$	→	H_2CO	+	CH_3			3.01×10^{-13}	Tsang & Hampson (1986)
R762	R616	CH_3O	+	CH_3	→	H_2CO	+	CH_4			4.0×10^{-11}	Tsang & Hampson (1986)
R763	R617	CH_3O	+	CH_4	→	CH_3OH	+	CH_3			$2.61 \times 10^{-13} e^{-4450/T}$	Tsang & Hampson (1986)
R764	R618	CH_3O	+	C_2H	→	H_2CO	+	C_2H_2			4.0×10^{-11}	Tsang & Hampson (1986)
R765	R619	CH_3O	+	C_2H_3	→	H_2CO	+	C_2H_4			4.0×10^{-11}	Tsang & Hampson (1986)
R766	R620	CH_3O	+	C_2H_5	→	H_2CO	+	C_2H_6			4.0×10^{-12}	Tsang & Hampson (1986)
R767	R621	CH_3O	+	C_2H_6	→	CH_3OH	+	C_2H_5			$4.0 \times 10^{-13} e^{-3570/T}$	Tsang & Hampson (1986)
R768	R622	CH_3O	+	CH_3OH	→	CH_3OH	+	CH_2OH			$5.0 \times 10^{-13} e^{-2050/T}$	Tsang (1987)
R769	R623	CH_3O	+	CH_3CO	→	CH_2CO	+	CH_3OH			1.0×10^{-11}	Tsang & Hampson (1986)
R770	R624	CH_3O	+	CH_3CHO	→	CH_3CO	+	CH_3OH			8.3×10^{-15}	Kelly & Heicklen (1978)
R771	R625	CH_2OH	+	H	→	H_2CO	+	H_2			1.0×10^{-11}	Tsang (1987)
R772	R626	CH_2OH	+	H	→	OH	+	CH_3			1.6×10^{-10}	Tsang (1987)
R773	R627	CH_2OH	+	H_2	→	CH_3OH	+	H			$1.12 \times 10^{-18} T^2 e^{-6722/T}$	Tsang (1987)
R774	R628	CH_2OH	+	$^3CH_2$	→	OH	+	C_2H_4			4.0×10^{-11}	Tsang (1987)
R775	R629	CH_2OH	+	$^3CH_2$	→	H_2CO	+	CH_3			2.01×10^{-12}	Tsang (1987)
R776	R630	CH_2OH	+	CH_3	→	H_2CO	+	CH_4			4.0×10^{-12}	Tsang (1987)
R777	R631	CH_2OH	+	CH_4	→	CH_3OH	+	CH_3			$3.59 \times 10^{-23} T^{3.1} e^{-8166/T}$	Tsang (1987)
R778	R632	CH_2OH	+	C_2H	→	H_2CO	+	C_2H_2			5.99×10^{-11}	Tsang (1987)
R779	R633	CH_2OH	+	C_2H	→	OH	+	C_3H_3			2.01×10^{-11}	Tsang (1987)
R780	R634	CH_2OH	+	C_2H_2	→	H_2CO	+	C_2H_3			$1.2 \times 10^{-12} e^{-4532/T}$	Tsang (1987)
R781	R635	CH_2OH	+	C_2H_3	→	H_2CO	+	C_2H_4			5.01×10^{-11}	Tsang (1987)
R782	R636	CH_2OH	+	C_2H_3	→	OH	+	C_3H_5			2.01×10^{-11}	Tsang (1987)
R783	R637	CH_2OH	+	C_2H_4	→	SOOT					$8.0 \times 10^{-14} e^{-3505/T}$	Tsang (1987)
R784	R638	CH_2OH	+	C_2H_5	→	H_2CO	+	C_2H_6			4.0×10^{-12}	Tsang (1987)
R785	R639	CH_2OH	+	C_2H_5	→	CH_3OH	+	C_2H_4			4.0×10^{-12}	Tsang (1987)
R786	R640	CH_2OH	+	C_2H_6	→	CH_3OH	+	C_2H_5			$3.3 \times 10^{-22} T^3 e^{-7033/T}$	Tsang (1987)
R787	R641	CH_2OH	+	CH_2OH	→	CH_3OH	+	H_2CO			8.0×10^{-12}	Tsang (1987)
R788	R642	CH_2OH	+	CH_3O	→	CH_3OH	+	H_2CO			4.0×10^{-11}	Tsang (1987)
R789	R643	CH_2OH	+	CH_3OH	→	CH_3OH	+	CH_3O			$1.3 \times 10^{-14} e^{-6073/T}$	Tsang (1987)
R790	R644	CH_3OH	+	H	→	CH_2OH	+	H_2			$2.73 \times 10^{-17} T^2 e^{-2271/T}$	Li & Williams (1996)
R791	R645	CH_3OH	+	H	→	CH_3O	+	H_2			$6.64 \times 10^{-11} e^{-3067/T}$	Warnatz (1984)
R792	R646	CH_3OH	+	$^1CH_2$	→	CH_2OH	+	CH_3			2.5×10^{-12}	Tsang (1987)
R793	R647	CH_3OH	+	$^3CH_2$	→	CH_2OH	+	CH_3			$5.29 \times 10^{-23} T^{3.2} e^{-3609/T}$	Tsang (1987)
R794	R648	CH_3OH	+	$^3CH_2$	→	CH_3O	+	CH_3			$2.39 \times 10^{-23} T^{3.1} e^{-3490/T}$	Tsang (1987)

R795	R649	CH_3OH	+	CH_3	→	CH_2OH	+	CH_4			$5.29 \times 10^{-23}\ T^{3.2}\ e^{-3609/T}$	Tsang (1987)
R796	R650	CH_3OH	+	CH_3	→	CH_3O	+	CH_4			$2.39 \times 10^{-23}\ T^{3.1}\ e^{-3490/T}$	Tsang (1987)
R797	R651	CH_3OH	+	C_2H	→	CH_2OH	+	C_2H_2			1.0×10^{-11}	Tsang (1987)
R798	R652	CH_3OH	+	C_2H	→	CH_3O	+	C_2H_2			2.01×10^{-11}	Tsang (1987)
R799	R653	CH_3OH	+	C_2H_3	→	CH_2OH	+	C_2H_4			$5.29 \times 10^{-23}\ T^{3.2}\ e^{-3609/T}$	Tsang (1987)
R800	R654	CH_3OH	+	C_2H_3	→	CH_3O	+	C_2H_4			$2.39 \times 10^{-23}\ T^{3.1}\ e^{-3490/T}$	Tsang (1987)
R801	R655	CH_3OH	+	C_2H_5	→	CH_2OH	+	C_2H_6			$5.29 \times 10^{-23}\ T^{3.2}\ e^{-4613/T}$	Tsang (1987)
R802	R656	CH_3OH	+	C_2H_5	→	CH_3O	+	C_2H_6			$2.39 \times 10^{-23}\ T^{3.1}\ e^{-4502/T}$	Tsang (1987)
R803	R657	CH_3OH	+	CH_3CO	→	CH_3CHO	+	CH_2OH			$8.05 \times 10^{-21}\ T^{3}\ e^{-6214/T}$	Tsang (1987)
R804	R658	CH_2CO	+	H	→	CO	+	CH_3			$5.99 \times 10^{-12}\ e^{-1178/T}$	Slemr & Warneck (1975)
R805	R659	CH_2CO	+	$^3CH_2$	→	CO	+	C_2H_4			2.09×10^{-10}	Canosamas et al. (1984)
R806	R660	CH_3CO	+	H	→	CH_2CO	+	H_2			1.92×10^{-11}	Ohmori et al. (1990)
R807	R661	CH_3CO	+	H	→	HCO	+	CH_3			1.03×10^{-11}	Ohmori et al. (1990)
R808	R662	CH_3CO	+	H_2	→	CH_3CHO	+	H			$6.85 \times 10^{-18}\ T^{1.82}\ e^{-8868/T}$	Tsang & Hampson (1986)
R809	R663	CH_3CO	+	$^3CH_2$	→	CH_2CO	+	CH_3			3.01×10^{-11}	Tsang & Hampson (1986)
R810	R664	CH_3CO	+	CH_3	→	CH_2CO	+	CH_4			1.01×10^{-11}	Hassinen et al. (1990)
R811	R665	CH_3CO	+	CH_3	→	C_2H_6	+	CO			5.4×10^{-11}	Adachi et al. (1981)
R812	R666	CH_3CO	+	CH_4	→	CH_3CHO	+	CH_3			$3.6 \times 10^{-21}\ T^{2.88}\ e^{-10800/T}$	Tsang & Hampson (1986)
R813	R667	CH_3CO	+	C_2H	→	CH_2CO	+	C_2H_2			3.01×10^{-11}	Tsang & Hampson (1986)
R814	R668	CH_3CO	+	C_2H_3	→	SOOT	+	CH_3			3.01×10^{-11}	Tsang & Hampson (1986)
R815	R669	CH_3CO	+	C_2H_6	→	CH_3CHO	+	C_2H_5			$3.0 \times 10^{-20}\ T^{2.75}\ e^{-8828/T}$	Tsang & Hampson (1986)
R816	R670	CH_3CO	+	CH_3CO	→	CH_3CHO	+	CH_2CO			1.49×10^{-11}	Hassinen et al. (1990)
R817	R671	CH_3CHO	+	H	→	CH_3CO	+	H_2			$6.64 \times 10^{-11}\ e^{-2120/T}$	Warnatz (1984)
R818	R672	CH_3CHO	+	$^3CH_2$	→	CH_3CO	+	CH_3			$2.76 \times 10^{-12}\ e^{-1773/T}$	Böhland et al. (1985a)
R819	R673	CH_3CHO	+	CH_3	→	CH_3CO	+	CH_4			$3.3 \times 10^{-30}\ T^{5.64}\ e^{-1239/T}$	Baulch et al. (1992)
R820	R674	CH_3CHO	+	$N(^4S)$	→	HCO	+	HCN	+	H_2	1.99×10^{-14}	Lambert et al. (1968)
R821	R675	CO_2	+	C	→	CO	+	CO			1.0×10^{-15}	Husain & Young (1975) – Upper limit
R822	R676	CO_2	+	$^3CH_2$	→	H_2CO	+	CO			3.9×10^{-14}	Tsang & Hampson (1986)
R823		C	+	O_2	→	CO	+	$O(^3P)$			3.3×10^{-11}	Donovan & Hussain (1970)
R824		CH	+	O_2	→	CO	+	OH			5.9×10^{-11}	Butler et al. (1981)
R825		$^3CH_2$	+	O_2	→	HCO	+	OH			1.5×10^{-12}	Prasad & Huntress (1980)
R826		$^1CH_2$	+	O_2	→	HCO	+	OH			3.0×10^{-11}	Ashfold et al. (1981)
R827		CH_3	+	O_2	$\xrightarrow{M}$	H_2CO	+	OH			$k_0 = 4.5 \times 10^{-31}\ (300/T)^{-3.0}$ $k_\infty = 1.8 \times 10^{-12}\ (300/T)^{-1.7}$	DeMore et al. (1992)
R828		C_2	+	O_2	→	CO	+	$O(^3P)$			$1.5 \times 10^{-11}\ e^{-550/T}$	Baughcum & Oldenburg (1984)
R829		C_2H	+	O_2	→	CO	+	HCO			2×10^{-11}	Brown & Laufer (1981)
R830		C_2H_5	+	O_2	$\xrightarrow{M}$	CH_3	+	HCO	+	OH	$k_0 = 1.5 \times 10^{-28}\ (300/T)^{-3.0}$ $k_\infty = 8.0 \times 10^{-12}$	DeMore et al. (1992)
R831		H	+	O_3	→	OH	+	O_2			$1.4 \times 10^{-10}\ e^{-470/T}$	DeMore et al. (1992)
R832		H	+	O_2	$\xrightarrow{M}$	HO_2					$k_0 = 5.7 \times 10^{-32}\ (300/T)^{-1.6}$ $k_\infty = 7.5 \times 10^{-11}$	DeMore et al. (1992)
R833		H	+	HO_2	→	H_2	+	O_2			$8.1 \times 10^{-11} \times (0.08)$	DeMore et al. (1992)
R834		H	+	HO_2	→	H_2O	+	$O(^3P)$			$8.1 \times 10^{-11} \times (0.02)$	DeMore et al. (1992)
R835		H	+	HO_2	→	OH	+	OH			$8.1 \times 10^{-11} \times (0.90)$	DeMore et al. (1992)
R836		OH	+	$O(^3P)$	→	H	+	O_2			$2.2 \times 10^{-11}\ e^{120/T}$	DeMore et al. (1992)
R837		OH	+	HO_2	→	H_2O	+	O_2			$4.8 \times 10^{-11}\ e^{250/T}$	DeMore et al. (1992)
R838		OH	+	O_3	→	HO_2	+	O_2			$1.6 \times 10^{-12}\ e^{-940/T}$	DeMore et al. (1992)
R839		OH	+	OH	$\xrightarrow{M}$	H_2O_2					$k_0 = 6.9 \times 10^{-31}\ (300/T)^{-0.8}$ $k_\infty = 1.5 \times 10^{-11}$	DeMore et al. (1992)
R840		HO_2	+	$O(^3P)$	→	OH	+	O_2			$3.0 \times 10^{-11}\ e^{200/T}$	DeMore et al. (1992)
R841		HO_2	+	O_3	→	OH	+	O_2	+	O_2	$1.1 \times 10^{-14}\ e^{-500/T}$	DeMore et al. (1992)
R842		HO_2	+	HO_2	→	H_2O_2	+	O_2			$2.3 \times 10^{-13}\ e^{600/T}$ $+ 1.7 \times 10^{-33}\ e^{1000/T}$ [M]	DeMore et al. (1992)
R843		H_2O_2	+	$O(^3P)$	→	OH	+	HO_2			$1.4 \times 10^{-12}\ e^{-2000/T}$	DeMore et al. (1992)
R844		H_2O_2	+	OH	→	HO_2	+	H_2O			$2.9 \times 10^{-12}\ e^{-160/T}$	DeMore et al. (1992)
R845		$O(^1D)$	+	O_2	→	$O(^3P)$	+	O_2			$3.2 \times 10^{-11}\ e^{70/T}$	DeMore et al. (1992)
R846		$O(^3P)$	+	O_3	→	O_2	+	O_2			$8 \times 10^{-12}\ e^{-2060/T}$	DeMore et al. (1992)
R847		$O(^3P)$	+	$O(^3P)$	$\xrightarrow{M}$	O_2					$2.76 \times 10^{-34}\ e^{710/T}$ [M]	Campbell & Thrush (1967)
R848		$O(^3P)$	+	O_2	$\xrightarrow{M}$	O_3					$k_0 = 6.0 \times 10^{-34}\ (300/T)^{-2.3}$ $k_\infty = 1 \times 10^{-10}$	DeMore et al. (1992)
R849		C_2H_2	+	OH	$\xrightarrow{M}$	C_2H_2OH					$k_0 = 5.5 \times 10^{-30}$ $k_\infty = 8.3 \times 10^{-13}\ (300/T)^2$	DeMore et al. (1992)
R850		C_2H_4	+	OH	$\xrightarrow{M}$	C_2H_4OH					$k_0 = 1.0 \times 10^{-28}\ (300/T)^{-0.8}$ $k_\infty = 8.8 \times 10^{-12}$	DeMore et al. (1992)
R851		C_3H_7	+	$O(^3P)$	→	C_2H_5CHO	+	H			1.1×10^{-10}	Estimated from CH_3 + O in DeMore et al. (1992)
R852		C_2H_5OH	+	$O(^3P)$	→	OH	+	CH_2CO			$3.3 \times 10^{-11}\ e^{-2000/T}$	Miller et al. (1982)
R853		C_2H_5OH	+	H	→	H_2O	+	C_2H_2			5.0×10^{-11}	Miller et al. (1982)
R854		C_2H_5OH	+	H	→	H_2	+	CH_2CO			$3.3 \times 10^{-11}\ e^{-2000/T}$	Miller et al. (1982)

R855	C_2H_2OH	+	OH	→	H_2O	+	CH_2CO	$1.7 \times 10^{-11} e^{-1000/T}$	Miller et al. (1982)
R856	C_2H_4OH	+	$O(^3P)$	→	OH	+	CH_3CHO	$3.3 \times 10^{-11} e^{-2000/T}$	Zahnle (1986)
R857	C_2H_4OH	+	H	→	H_2O	+	C_2H_4	5×10^{-11}	Miller et al. (1982)
R858	C_2H_4OH	+	H	→	H_2	+	CH_3CHO	$3.3 \times 10^{-11} e^{-2000/T}$	Zahnle (1986)
R859	C_2H_4OH	+	OH	→	H_2O	+	CH_3CHO	$1.7 \times 10^{-11} e^{-1000/T}$	Zahnle (1986)
R860	CH_3	+	CO	$\xrightarrow{M}$	CH_3CO			$k_0 = 5.9 \times 10^{-36}$ $k_\infty = 3.1 \times 10^{-16} T^{1.05} e^{-2850/T}$ F = 0.6 (See the 1st page)	Baulch et al. (1994)
R861	NH	+	NH	→	NH_2	+	$N(^4S)$	$1.4 \times 10^{-14} (T/298)^{2.89} e^{1019/T}$	Xu et al. (1997)

References

Adachi, H., Basco, N., James, D., 1981. The acetyl radicals CH_3CO and CD_3CO studied by flash-photolysis and kinetic spectroscopy. Int. J. Chem. Kinet. 13 (12), 1251–1276.

Adamkovics, M., Boering, K.A., 2003. Photochemical formation rates of organic aerosols through time-resolved in situ laboratory measurements. J. Geophys. Res. 108 (E8), 5092. doi:10.1029/2002JE002028

Akimoto, H., Obi, K., Tanaka, I., 1965. Primary process in photolysis of ethane at 1236 Å. J. Chem. Phys. 42 (11), 3864–3868.

Aleksandrov, E., Arutyunov, V., Dubrovina, I., Kozlov, S., 1980. Study of the reaction of atomic hydrogen with allene. Kinet. Catal. 21, 1323–1326.

Allen, M., Pinto, J.P., Yung, Y.L., 1980. Titan: aerosol photochemistry and variations related to the sunspot cycle. Astrophys. J. 242, L125-L128.

Altermann, W., Kazmierczak, J., 2003. Archean microfossils: A reappraisal of early life on Earth, Res. Microbiol. 154, 611-617.

Ambrose, D., Sprake, C.H.S., 1970. Thermodynamic Properties of Oxygen Compounds. XXXVII. Vapour Pressures of Methanol, Ethanol, Pentan-1-ol, and Octan-1-ol from the Normal Boiling Temperature to the Critical Temperature. J. Chem. Thermodyn. 7, 185-190.

Ashfold, M.N.R., Fullstone, M.A., Hancock, G., Ketley, G.W., 1981. Singlet methylene kinetics. Chern. Phys. 55, 245-257.

Atkinson, R., Baulch, D., Cox, R., Crowley, J., Hampson, R., Hynes, R., Jenkin, M., Rossi, M., Troe, J., 2004. Evaluated kinetic and photochemical data for atmospheric chemistry: Volume I - Gas phase reactions of O_x, HO_x, NO_x and SO_x species. Atmos. Chem. Phys. 4, 1461–1738.

Atkinson, R., Baulch, D.L., Cox, R.A., Crowley, J.N., Hampson, R.F, Jr., Kerr, J.A., Rossi, M.J., Troe, J., 2001. Summary of Evaluated Kinetic and Photochemical Data for Atmospheric Chemistry. IUPAC Subcommittee on Gas Kinetic Data Evaluation for Atmospheric Chemistry Web Version December 2001, 1-56.

Atkinson, R., Baulch, D., Cox, R., Hampson, R., Kerr, J., Troe, J., 1992. Evaluated kinetic and photochemical data for atmospheric chemistry: Supplement IV - IUPAC subcommittee on gas kinetic data evaluation for atmospheric chemistry. J. Phys. Chem. Ref. Data 21 (6), 1125–1568.

Atkinson, R., Baulch, D., Cox, R., Hampson, R., Kerr, J., Rossi, M., Troe, J., 1999. Evaluated kinetic and photochemical data for atmospheric chemistry, organic species: Supplement VII. J. Phys. Chem. Ref. Data 28 (2), 191–393.

Atkinson, D., Hudgens, J., 1999. Rate coefficients for the propargyl radical self-reaction and oxygen addition reaction measured using ultraviolet cavity ring-down

spectroscopy. J. Phys. Chem. A 103 (21), 4242–4252.

Atreya, S., 1986. Atmospheres and ionospheres of the outer planets and their satellites. Springer-Verlag, New York, Berlin.

Atreya, S.K., Donahue, T.M., Kuhn, W.R., 1978. Evolution of a nitrogen atmosphere on Titan. Science 201, 611-613.

Au, J.W., Cooper, G., Burton, G.R., Olney, T.N., Brion, C.E., 1993. The valence shell photoabsorption of the linear alkanes, CnH2n+2 (n=1-8): Absolute oscillator strengths (7-220 eV). Chem. Phys. 173, 209-239.

Azzam, R.M., Bashara, N.M., 1977. Ellipsometry and polarized light. North-Holland Pub. Co., Amsterdam, 529p.

Balla, R., Casleton, K., 1991. Kinetic study of the reactions of CN with O_2 and CO_2 from 292 K to 1500 K using high-temperature photochemistry. J. Phys. Chem. 95 (6), 2344–2351.

Balucani, N., Cartechini, L., Alagia, M., Casavecchia, P., Volpi, G., 2000. Observation of nitrogen-bearing organic molecules from reactions of nitrogen atoms with hydrocarbons: A crossed beam study of N(^{2}D) + ethylene. J. Phys. Chem. A 104 (24), 5655–5659.

Banks, P.M., Kockarts, G., 1973. Aeronomy, Part B. Academic Press, NY.

Bar-Nun, A., Kleinfeld, I., Ganor, E., 1988. Shape and optical properties of aerosols formed by photolysis of acetylene, ethylene, and hydrogen cyanide. J. Geophys. Res. 93, 8383-8387.

Barron, E.J., 1984. Ancient climates: Investigation with climate models. Rep. Prog. Phys. 47, 1563–1599. doi:10.1088/0034-4885/47/12/001.

Barth, E.L., Toon, O.B., 2003. Microphysical modeling of ethane ice clouds in Titan's atmosphere. Icarus 162, 94-113.

Barth, E.L., Toon, O.B., 2004. Properties of methane clouds on Titan: Results from microphysical modeling. Geophys. Res. Lett. 31, L17S07.

Baughcum, S.L., Oldenburg, R.C., 1984. Measurement of the $C_2(a^3P_u)$ and $C_2(x^1Sg^+)$ disappearance rates with O_2 from 298 to 1300 K. in The Chemistry of Combustion Processes, edited by Sloane T.M., pp. 257-266, Am Chem. Soc., Washmgton, D. C.

Baulch, D., Cobos, C., Cox, R., Esser, C., Frank, P., Just, T., Kerr, J., Pilling, M., Troe, J., Walker, R., Warnatz, J., 1992. Evaluated kinetic data for combustion modeling. J. Phys. Chem. Ref. Data 21 (3), 411–734.

Baulch, D., Cobos, C., Cox, R., Frank, P., Hayman, G., Just, T., Kerr, J., Murrells, T., Pilling, M., Troe, J., Walker, R., Warnatz, J., 1994. Evaluated kinetic data for combustion modeling: Supplement I. J. Phys. Chem. Ref. Data 23 (6), 847–1033.

Bekker, A., Holland, H.D., Wang, P.-L., Rumble, III, D., Stein, H.J., Hannah, J.L., Coetzee, L.L., Beukes, N.J., 2004. Dating the rise of atmospheric oxygen. Nature 427, 117-120.

Benilan, Y.D., Andrieux, D., Khlifi, M., Bruston, P., Raulin, F., Guillemin, J.-C.,

Cossart-Magos, C., 1996. Temperature dependence of HC_3N, C_6H_2, and C_4N_2 mid-UV absorption coefficients: Application to the interpretation of Titan's atmospheric spectra. Astrophys. Space Sci., 236, 85–95.

Benilan, Y., Smith, N., Jolly, A., Raulin, F., 2000. The long wavelength range temperature variations of the mid-UV acetylene absorption coefficient. Planet. Space Sci. 48, 463-471.

Benn, K., Mareschal, J.-C., Condie, K.C. (Eds.), 2006. Archean Geodynamics and Environments. Geophys. Monogr. Ser. vol. 164, 320 pp., AGU, Washington, D. C.

Bergmann, K., Demtrode, W, 1968. Mass-spectrometric investigation of primary processes in photodissociation of 1,3-butadiene. J. Chem. Phys. 48 (1), 18–22.

Berner, R.A., Lasaga, A.C., Garrels, R.M., 1983. The carbonate-silicate geochemical cycle and its effect on atmospheric carbon dioxide over the past 100 million years. Am. J. Sci, 283 (7), 641–683.

Bertrand, C., Collin, G.J., Gagnon, H., 1975. Coefficients d'absorption et rendements quantiques ioniques de composés inorganiques et d'hydrocarbones insaturés, J. Chim. Phys. 72, 719-723.

Black, G., Slanger, T., Stjohn, G., Young, R., 1969. Vacuum-ultraviolet photolysis of N_2O. 4. Deactivation of $N(^2D)$. J. Chem. Phys. 51 (1), 116–121.

Bocherel, P., Herbert, L., Rowe, B., Sims, I., Smith, I., Travers, D., 1996. Ultralow-temperature kinetics of $CH(X^2\Pi)$ reactions: Rate coefficients for reactions with O_2 and NO (T = 13-708 K), and with NH_3 (T = 23-295 K). J. Phys. Chem. 100 (8), 3063–3069.

Boduch, P., Chantepie, M., Hennecart, D., Husson, X., Kucal, H., Lecler, D., Stolterfoht, N., Druetta, M., Fawcett, B., Wilson, M., 1992. Spectroscopic analysis of visible and near UV light emitted by Ar^{7+} and Ar^{6+} ions produced in Ar^{8+}-He and Ar^{8+}-H_2 collisions at 120 keV. Physica. Scripta. 45, 203-211.

Bohland, T., Temps, F., Wagner, H., 1985a. The contributions of intersystem crossing and reaction in the removal of $CH_2(\tilde{A}^1A_1)$ by hydrocarbons studied with the LMR. Ber. Bunsen-Ges. Phys. Chem. 89 (9), 1013–1018.

Bolovinos, A., Philis, J., Pantos, E., Tsekeris, P., Andritsopoulos, G., 1981. The methylbenzenes vis-a-vis benzene. Comparison of their spectra in the Rydberg series region. J. Chem. Phys. 75, 4343-4349.

Bolovinos, A., Philis, J., Pantos, E., Tsekeris, P., Andritsopoulos, G., 1982. The methylbenzenes vis-a-vis benzene. Comparison of their spectra in the valence shell transition region. J. Mol. Spectrosc. 94, 55-68.

Borucki, W.J., Levin, Z., Whitten, R.C., Keesee, R.G., Capone, L.A., Summers, A.L., Toon, O.B., Dubach, J., 1987. Predictions of the electrical conductivity and charging of the aerosols in Titan’s atmosphere. Icarus 72, 604-622.

Bosco, S., Nava, D., Brobst, W., Stief, L., 1984. Temperature and pressure-dependence of the absolute rate-constant for the reactions of NH_2 radicals with acetylene and

ethylene. J. Chem. Phys. 81 (8), 3505–3511.

Breuer, D., Spohn, T., 1995. Possible flush instability in mantle convection at the Archaean–Proterozoic transition. Nature 378, 608-610.

Brown, R.L., Laufer, A.H., 1981. Calculation of the activation energies for hydrogen-atom extinction reactions by radicals containing triple bonds. J. Phys. Chem. 85, 3826-3828.

Brownsword, R., Gatenby, S., Herbert, L., Smith, I., Stewart, D., Symonds, A., 1996. Kinetics of reactions between neutral free radicals - Rate constants for the reaction of CH radicals with N atoms between 216 and 584 K. J. Chem. Soc., Faraday Trans. 92 (5), 723–727.

Butler, J.E., Fleming, J.W., Goss, L.P., Lin, M.C., 1981. Kinetics of CH radical reactions with selected molecules at room temperature. Chem Phys. 56, 355-365.

Butterfield, M., Yu, T., Lin, M., 1993. Kinetics of CN reactions with allene, butadiene, propylene and acrylonitrile. Chem. Phys. 169 (1), 129–134.

Cable, M.L., Horst, S.M., Hodyss, R., Beauchamp, P.M., Smith, M.A., Wills, P.A., 2012. Titan tholins: Simulating Titan organic chemistry in the Cassini-Huygens Era. Chem. Rev. 112, 1882-1909.

Caldwell, J., Owen, T., Rivolo, A. R., Moore, V., Hunt, G. E., & Butterworth, P. S., 1981. Observations of Uranus, Neptune, and Titan by the International Ultraviolet Explorer. Astron. J.86, 298-305.

Campbell, J.M., Thrush, B.A., 1967. The association of oxygen atoms and their combination with nitrogen atoms. Proc. R. Soc. London, Ser. A, 296, 222-232.

Canosamas, C., Frey, H., Walsh, R., 1984. Studies of methylene chemistry by pulsed laser-induced decomposition of ketene. 1. Ketene in the presence of noble gases. J. Chem. Soc., Faraday Trans. II 80, 561–578.

Carty, D., Le Page, V., Sims, I., Smith, I., 2001. Low temperature rate coefficients for the reactions of CN and C_2H radicals with allene (CH_2=C=CH_2) and methyl acetylene (CH_3C_2H). Chem. Phys. Lett. 344 (3-4), 310–316.

Catling, D.C., Zahnle, K.J, McKay, C.P., 2001. Biogenic Methane, Hydrogen Escape, and the Irreversible Oxidation of Early Earth. Science 293, 839-843.

Chan, W.F., Cooper, G., Brion, C.E., 1993. Absolute optical oscillator strengths for discrete and continuum photoabsorption of carbon monoxide (7-200 eV) and transition moments for the $X^1\Sigma^+ \rightarrow A^1\Pi$ system. Chem. Phys. 170, 123-138.

Chan, W.F., Cooper, G., Brion, C.E., 1994. Discrete and continuum photoabsorption oscillator strengths for the electronic spectrum of nitrous oxide (5.5-203 eV). Chem. Phys. 180, 77-88.

Chang, A., Mebel, A., Yang, X., Lin, S., Lee, Y., 1998. Ab initio/RRKM approach toward the understanding of ethylene photodissociation. J. Chem. Phys. 109 (7), 2748–2761.

Chastaing, D., James, P., Sims, I., Smith, I., 1998. Neutral-neutral reactions at the

temperatures of interstellar clouds - Rate coefficients for reactions of C_2H radicals with O_2, C_2H_2, C_2H_4 and C_3H_6 down to 15 K. Faraday Discuss. 109, 165–181.

Cicerone, R.J., Zellner, R., 1983. The atmospheric chemistry of hydrogen cyanide (HCN). J. Geophys. Res. 88, 10,689-10,696.

Clarke, D., Ferris, J., 1995. Photodissociation of cyanoacetylene - Application to the atmospheric chemistry of Titan. Icarus 115 (1), 119–125.

Cody, R., Sabetydzvonik, M., Jackson, W., 1977. Laser-induced fluorescence of $CN(X^2\Sigma^+)$ produced by photolysis of C_2N_2 at 160 nm. J. Chem. Phys. 66 (5), 2145–2152.

Cohen, N., Westberg, K., 1991. Chemical kinetic data sheets for high-temperature reactions. Part II. J. Phys. Chem. Ref. Data 20, 1211–1311.

Coll, P., Coscia, D., Smith, N., Gazeau, M.-C., Ramirez, S.I., Cernogora, G., Israel, G., Raulin, F., 1999. Experimental laboratory simulation of Titan's atmosphere: aerosols and gas phase. Planet. Space Sci. 47, 1331-1340.

Collin, G., 1988. Photochemistry of simple olefins: Chemistry of electronic excited states or hot ground state? Adv. Photochem. 14, 135–176.

Connors, R. E., Roebber, J. L., Weiss, K., 1974. Vacuum ultraviolet spectroscopy of cyanogen and cyanoacetylenes. J. Chem. Phys., 60, 5011–5024.

Cooney, C.L., Wise, D.L., 1975. Thermophilic anaerobic digestion of solidwaste for fuel gas production. Biotechnol. Bioeng. 17, 1119–1135.

Cottin, H., Moore, M., Benilan, Y., 2003. Photodestruction of relevant interstellar molecules in ice mixtures. Astrophys. J. 590, 874-881.

Courtin, R., Gautier, D., McKay, C.P., 1995. Titan's thermal emission spectrum: Reanalysis of the Voyager infrared measurements. Icarus 114, 144–162.

Coustenis, A., Salama, A., Lellouch, E., Encrenaz, T., Bjoraker, G.L., Samuelson, R.E., de Graauw, T., Feuchtgruber, H., Kessler, M.F., 1998. Evidence for water vapor in Titan's atmosphere from ISO/SWS data. Astron. Astrophys. 336, L85–L89.

Coustenis, A., Salama, A., Schulz, B., Ott, S., Lellouch, E., Encrenaz, Th., Gautier, D., Feuchtgruber, H., 2003. Titan's atmosphere from ISO mid-infrared spectroscopy. Icarus 161, 383-403.

Coustenis, A., and 24 colleagues, 2007. The composition of Titan's stratosphere from Cassini/CIRS mi-infrared spectra. Icarus 189, 35-62.

Crowley, T.J., 1983. The geologic record of climatic change. Rev. Geophys. 21, 828–877. doi:10.1029/RG021i004p00828.

Cui, J., Yelle, R.V., Volk, K., 2008. Distribution and escape of molecular hydrogen in Titan's thermosphere and exosphere. J. Geophys. Res. 113, doi:10.1029/2007JE003032. E10004.

Davis, D., Braun, W., 1968. Intense vacuum ultraviolet atomic line sources. Appl. Opt.7 (10), 2071-2074.

Dean, A., Westmoreland, P., 1987. Bimolecular QRRK analysis of methyl radical

reactions. Int. J. Chem. Kinet. 19 (3), 207–228.

de Avillez Pereira, R., Baulch, D., Pilling, M., Robertson, S., Zeng, G., 1997. Temperature and pressure dependence of the multichannel rate coefficients for the CH_3 + OH system. J. Phys. Chem. A 101 (50), 9681–9693.

de Kok, R., and 12 colleagues, 2007. Oxygen compounds in Titan's stratosphere as observed by Cassini CIRS. Icarus 186, 354-363.

Demissy, M., Lesclaux, R., 1980. Kinetics of hydrogen abstraction by NH_2 radicals from alkanes in the gas-phase - A flash-photolysis laser resonance-absorption study. J. Am. Chem. Soc. 102 (9), 2897–2902.

Demissy, M., Lesclaux, R., 1982. Absolute rate constants for the reactions between amino and alkyl radicals at 298 K. Int. J. Chem. Kinet. 14 (1), 1–12.

DeMore, W.B., Golden, D.M., Hampson, R.F., Howard, C.J., Kurylo, M.J., Molina, M.J., Ravishankara, A.R., Sander, S.P., 1992. Chemical kinetics and photochemical data for use in stratospheric modeling. Evaluation 10. JPL Publ., 92-20.

DeMore, W.B., Sander, S.P., Golden, D.M., Hampson, R.F., Kurylo, M.J., Howard, C.J., Ravishankara, A.R., Kolb, C.E., Molina, M.J., 1997. Chemical Kinetics and Photochemical Data for Use in Stratospheric Modeling. Evaluation Number 12. JPL Publication 97-4.

Devriendt, K., Peeters, J., 1997. Direct identification of the $C_2H(X^2\Sigma^+)$ + $O(^3P)$ → $CH(A^2\Delta)$ + CO reaction as the source of the $CH(A^2\Delta \rightarrow X^2\Pi)$ chemiluminescence in C_2H_2/O/H atomic flames. J. Phys. Chem. A 101 (14), 2546–2551.

DeWitt, H.L., Trainer, M.G., Pavlov, A.A., Hasenkopf, C.A., Aiken, A.C., Jimenez, J.L., McKay, C.P., Toon, O.B., Tolbert, M.A., 2009. Reduction in haze formation rate on prebiotic Earth in the presence of hydrogen. Astrobiology 9, 447–453.

Ditchburn, R.W., 1955. Absorption cross-sections in the vacuum ultra-violet. III. Methane. Proc. Roy. Soc. London 229a, 44-62.

Donovan, R.J., Hussain, D., 1970. Recent advances in the chem1stry of electronically excited atoms. Chern Rev. 70, 489-516.

Driese, S.G., Jirsa, M.A., Ren, M., Brantley, S.L., Sheldon, N.D., Parker, D., Schmitz, M., 2011. Neoarchean paleoweathering of tonalite and metabasalt: Implications for reconstructions of 2.69 Ga early terrestrial ecosystems and paleoatmospheric chemistry. Precambrian Res. 189(1–2), 1–17.

Duncanson, A., Stevenson, R.W.H., 1958. Some Properties of Magnesium Fluoride crystallized from the Melt. Proc. Phys. Soc. London 72, 1001-1006.

Duran, R., Amorebieta, V., Colussi, A., 1988. Is the homogeneous thermal dimerization of acetylene a free-radical chain-reaction? Kinetic and thermochemical analysis. J. Phys. Chem. 92 (3), 636–640.

Dunn, M., Freeman, C., McEwan, M., Phillips, L., 1971. Photometric and mass spectrometric observations on reaction of hydrogen atoms with cyanogen. J. Phys. Chem. 75 (17), 2662–2665.

Eden, S., Limão-Vieira, P., Kendall, P., Mason, N.J., Hoffmann, S.V., Spyrou, S.M., 2003. High resolution photo-absorption studies of acrylonitrile, C_2H_3CN, and acetonitrile, CH_3CN. Eur. Phys. J. D 26, 201-210.

Ehrenfreund, P., Boon, J.J., Commandeur, J., Sagan, C., Thompson, W.R., Khare, B., 1995. Analytical pyrolysis experiments of titan aerosol analogues in preparation for the Cassini Huygens mission. Adv. Space Res. 15, 335-342.

Elkins-Tanton, L.T., Seager, S., 2008. Ranges of atmospheric mass and composition of super-earth exoplanets. Astrophys. J. 685, 1237-1246.

Eng, R., Lambert, H., Fei, R., Carrington, T., Filseth, S., 1996. Energy disposal in $CN(A^2\Pi)$ produced in the 157 nm photodissociation of C_2N_2. Chem. Phys. Lett. 261 (6), 651–658.

Eriksson, P.G., Altermann, W., Nelson, D.R., Mueller, W.U., Catuneanu, O. (Eds.) 2004. The Precambrian Earth: Tempos and Events. Dev. Precambrian Geol. vol. 12, Elsevier, Amsterdam.

Espinosa-Garcia, J., Corchado, J., 1994. Variational transition-state theory calculation using the direct dynamics method - $NH_3 + H \rightarrow NH_2 + H_2$ reaction. J. Chem. Phys. 101 (2), 1333–1342.

Etzkorn, T., Klotz, B., Sørensen, S., Patroescu, I.V., Barnes, I., Becker, K.H., Platt, U., 1999. Gas-phase absorption cross sections of 24 monocyclic aromatic hydrocarbons in the UV and IR spectral ranges. Atmos. Environ. 33, 525-540.

Fagerstrom, K., Jodkowski, J., Lund, A., Ratajczak, E., 1995. Kinetics of the self-reaction and the reaction with OH of the amidogen radical. Chem. Phys. Lett. 236 (1-2), 103–110.

Fagerstrom, K., Lund, A., Mahmoud, G., Jodkowski, J., Ratajczak, E., 1994. Pressure and temperature dependence of the gas phase reaction between methyl and hydroxyl radicals. Chem. Phys. Lett. 224 (1-2), 43–50.

Fahr, A., Hassanzadeh, P., Atkinson, D., 1998. Ultraviolet absorption spectrum and cross-sections of vinyl (C_2H_3) radical in the 225-238 nm region. Chem. Phys. 236 (1-3), 43–51.

Fahr, A., Laufer, A., Klein, R., Braun, W., 1991. Reaction-rate determinations of vinyl radical reactions with vinyl, methyl, and hydrogen-atoms. J. Phys. Chem. 95 (8), 3218–3224.

Fahr, A., Monks, P., Stief, L., Laufer, A., 1995. Experimental determination of the rate constant for the reaction of C_2H_3 with H_2 and implications for the partitioning of hydrocarbons in atmospheres of the outer planets. Icarus 116 (2), 415–422.

Fahr, A., Nayak, A., 1994. Temperature dependent ultraviolet absorption cross sections of 1,3-butadiene and butadiyne. Chem. Phys. 189, 725-731.

Fahr, A., Nayak, A., 1996. Temperature dependent ultraviolet absorption cross sections of propylene, methylacetylene, and vinylacetylene. Chem. Phys. 203, 351-358.

Fahr, A., Stein, S., 1988. Reactions of vinyl and phenyl radicals with ethyne, ethene and

benzene. Proc. Combust. Inst. 22, 1023–1029.

Feng, R., Cooper, G., Brion, C.E., 2002. Dipole (e,e) spectroscopic studies of benzene: quantitative photoabsorption in the UV, VUV and soft x-ray regions. J. Electron Spectrosc. Related Phenom. 123, 199-209.

Ferradaz, T., Benilan, Y., Fraya, N., Jollya, A., M.Schwell, M., Gazeau, M.-C. M.C., Jochims, H.W., 2009. Temperature-dependent photoabsorption cross-sections of cyanoacetylene and diacetylene in the mid-and vacuum-UV: Application to Titan's atmosphere. Planet. Space Sci. 57, 10-22.

Ferris, J., Tran, B., Joseph, J., Vuitton, V., Briggs, R., Force, M., 2005. The role of photochemistry in Titan's atmospheric chemistry. Adv. Space Res. 36, 251-257.

Feulner, G., 2012. The faint young sun problem. Rev. Geophys. 50, RG2006.

Flasar, F.M., and 44 colleagues, 2005. Titan's atmospheric temperatures, winds, and composition. Science 308, 975–978.

Fulle, D., Hippler, H., 1997. The temperature and pressure dependence of the reaction $CH + H_2 \rightleftarrows CH_3 \rightleftarrows CH_2 + H$. J. Chem. Phys. 106 (21), 8691–8698.

Fockenberg, C., Preses, J., 2002. Temperature dependence of the rate constant and product distribution of the reaction of CH_3 radicals with $O(^3P)$ atoms. J. Phys. Chem. A 106 (12), 2924–2930.

Forst, W., 1991. Microcanonical variational theory of radical recombination by inversion of interpolated partition function, with examples: CH_3 + H atom, CH_3 + CH_3. J. Phys. Chem. 95 (9), 3612–3620.

Forst, W., Evans, H., Winkler, C., 1957. The kinetics of nitrogen atom reactions accompanied by catalyzed recombination of atoms. J. Phys. Chem. 61 (3), 320–325.

Fowler, C.M.R., Ebinger, C.J., Hawkesworth, C.J. (Eds.), 2002. The Early Earth: Physical, Chemical and Biological Development. Geol. Soc. Spec. Publ., 199.

Friedrichs, G., Davidson, D., Hanson, R., 2002. Direct measurements of the reaction $H + CH_2O \rightarrow H_2 + HCO$ behind shock waves by means of Vis-UV detection of formaldehyde. Int. J. Chem. Kinet. 34 (6), 374–386.

Frost, M., Sharkey, P., Smith, I., 1993. Reaction between OH (OD) radicals and CO at temperatures down to 80 K - Experiment and theory. J. Phys. Chem. 97 (47), 12254–12259.

Fuchs, C., Goetzberger, O., Henck, R., Fogarassy, E., 1995. Polymer photoablation under windowless VUV hydrogen or helium discharge lamp. Appl. Phys. A 60, 505-507.

Fuchs, N.A., 1964. Mechanics of Aerosols, Pergamon, New York.

Gaedtke, H., Glaenzer, K., Hippler, H., Luther, K., Troe, J., 1973. Addition reactions of oxygen atoms at high pressures. Proc. Combust. Inst. 14, 295–303.

Gehring, M., Hoyermann, K., Wagner, H., Wolfrum, J., 1971. Die Reaktion von Atomarem Wasserstoff mit Hydrazin. Ber. Bunsen-Ges. Phys. Chem. 75 (12),

1287–1294.

Gierczak, T., Talukdar, R., Herndon, S., Vaghjiani, G., Ravishankara, A., 1997. Rate coefficients for the reactions of hydroxyl radicals with methane and deuterated methanes. J. Phys. Chem. A 101 (17), 3125–3134.

Gilpin, R., Welge, K.H., 1971. Time - of - Flight Spectroscopy of Metastable Photodissociation Fragments. N_2O Dissociation in the Vacuum UV. J. Chem. Phys. 55, 975-978.

Gladstone, G., Allen, M., Yung, Y., 1996. Hydrocarbon photochemistry in the upper atmosphere of Jupiter. Icarus 119 (1), 1–52.

Glicker, S., Okabe, H., 1987. Photochemistry of diacetylene. J. Phys. Chem. 91 (2), 437–440.

Gough, D.O., 1981. Solar interior structure and luminosity variations. Sol. Phys. 74, 21-34.

Gray, P., Thynne, J., 1964. Arrhenius parameters for elementary combustion reactions: H-atom abstraction from N-H bonds. Proc. Combust. Inst. 10, 435–443.

Groth, W.E., Schierholz, H., 1959. The photolysis of nitrous oxide in the far ultraviolet. Planet. Space Sci. 1, 333-336.

Grotheer, H., Riekert, G., Walter, D., Just, T., 1988. Reactions of hydroxymethyl and hydroxyethyl radicals with molecular and atomic oxygen. Proc. Combust. Inst. 22, 963–972.

Güdel, M., 2007. The Sun in time: Activity and environment. Living Rev. Solar Phys. 4, 3.

Hale, C.J., 1987. The intensity of the geomagnetic field at 3.5 Ga: paleointensity results from the Komati Formation, Barberton Mountain Land, South Africa. Earth Planet. Sci. Lett. 86, 354-364.

Halpern, J., Miller, G., Okabe, H., 1989. The reaction of CN radicals with cyanoacetylene. Chem. Phys. Lett. 155 (4-5), 347–350.

Halpern, J., Miller, G., Okabe, H., Nottingham, W., 1988. The UV photochemistry of cyanoacetylene. J. Photochem. Photobiol. A - Chem. 42 (1), 63–72.

Halpern, J., Petway, L., Lu, R., Jackson, W., McCrary, V., Nottingham, W., 1990. Photochemistry of cyanoacetylene and dicyanoacetylene at 193 nm. J. Phys. Chem. 94 (5), 1869–1873.

Halpern, J., Tang, X., 1985. Production of $CN(A^2\Pi_i)$ in the photolysis of acetonitrile at 158 nm. Chem. Phys. Lett. 122 (3), 294–299.

Hamill, P., Toon, O.B., Kiang, C.S., 1977. Microphysical processes affecting stratospheric aerosol particles. J. Atmos. Sci. 34, 1104-1119.

Hanning-Lee, M., Pilling, M., 1992. Kinetics of the reaction between H-atoms and allyl radicals. Int. J. Chem. Kinet. 24 (3), 271–278.

Hampson, R., McNesby, J., 1965. Vacuum-ultraviolet photolysis of ethane at high temperature. J. Chem. Phys. 42 (6), 2200–2208.

Hampson, R.F. Jr., Okabe, H., 1970. Collisional Stimulation of the $O(^1S)$–$O(^1D)$ Emission of Oxygen Atoms Formed in Vacuum‐Ultraviolet Photolysis of Nitrous Oxide. J. Chem. Phys. 52, 1930-1933.

Harding, L., Guadagnini, R., Schatz, G., 1993. Theoretical-studies of the reactions H + CH → C + H_2 and C + H_2 → CH_2 using an abinitio global ground-state potential surface for CH_2. J. Phys. Chem. 97 (21), 5472–5481.

Haqq-Misra, J.D., Domagal-Goldman, S.W., Kasting, P.J., Kasting, J.F., 2008. A revised, hazy methane greenhouse for the Archean Earth. Astrobiology 8, 1127-1137.

Hasenkopf, C.A., Beaver, M.R., Trainer, M.G., DeWitt, H.L., Freedman, M.A., Toon, O.B., McKay, C.P., Tolbert, M.A., 2010. Optical properties of Titan and early Earth haze laboratory analogs in the mid-visible. Icarus 207, 903-913.

Hassinen, E., Kalliorinne, K., Koskikallio, J., 1990. Kinetics of reactions between methyl and acetyl radicals in gas phase produced by flash-photolysis of acetic anhydride. Int. J. Chem. Kinet. 22 (7), 741–745.

Hebrard, E., Dobrijevic, M., Benilan, Y., Raulin, F., 2006. Photochemical kinetics uncertainties in modeling Titan's atmosphere: A review. J. Photoch. Photobio. C 7, 211-230.

Hebrard, E., Dobrijevic, M., Benilan, Y., Raulin, F., 2007. Photochemical kinetics uncertainties in modeling Titan's atmosphere: First consequences. Planet. Space Sci. 55, 1470-1499.

Herron, J., 1999. Evaluated chemical kinetics data for reactions of $N(^2D)$, $N(^2P)$, and $N_2(A^3\Sigma^+_u)$ in the gas phase. J. Phys. Chem. Ref. Data 28 (5), 1453–1483.

Hessler, A.M., Lowe, D.R., Jones, R.L., Bird, D.K., 2004. A lower limit for atmospheric carbon dioxide levels 3.2 billion years ago. Nature 428, 736–738.

Hidayat, T., A. Marten, B. Bezard, D. Gautier, T. Owen, H. E. Matthews, G. Paubert, 1998. Millimeter and submillimeter heterodyne observations of Titan: The vertical profile of carbon monoxide in its stratosphere. Icarus, 133, 109–133. doi:10.1006/icar.1998.5908.

Hitchcock, A.P., Brion, C.E., Van der Wiel, M.J., 1980. Absolute oscillator strengths for valence-shell ionic photofragmentation of N_2O and CO_2 (8-75 eV). Chem. Phys. 45, 461-478.

Ho, G.H., Lin, M.S., Wang, Y.L., Chang, T.W., 1998. Photoabsorption and photoionization of propyne. J. Chem. Phys. 109, 5868-5879.

Holland, D., Shaw, D., Hayes, M., Shpinkova, L., Rennie, E., Karlsson, L., Baltzer, P., Wannberg, B., 1997. A photoabsorption, photodissociation and photoelectron spectroscopy study of C_2H_4 and C_2D_4. Chem. Phys. 219 (1), 91–116.

Holland, H.D., 1978. The Chemistry of the Atmosphere and Oceans. Wiley, New York.

Holstein, T., 1947. Imprisonment of Resonance Radiation in Gases. Phys. Rev. 72, 1212-1233..

Homann, K., Wellmann, C., 1983. Kinetics and mechanism of hydrocarbon formation in

the system C_2H_2/O/H at temperatures up to 1300 K. Ber. Bunsen-Ges. Phys. Chem. 87 (7), 609–616.

Hoobler, R., Opansky, B., Leone, S., 1997. Low-temperature rate coefficients for reactions of ethynyl radical (C_2H) with propane, isobutane, n-butane, and neopentane. J. Phys. Chem. A 101 (7), 1338–1342.

Hubrich, C., Stuhl, F.J., 1980. The ultraviolet absorption of some halogenated methanes and ethanes of atmospheric interest. J. Photochem. 12, 93-107.

Huebner, W., Keady, J., Lyon, S., 1992. Solar photo rates for planetary atmospheres and atmospheric pollutants, Kluwer Academic, Dordrecht, Boston.

Hunten, D.M., 1973a. The escape of H_2 from Titan. J. Atmos. Sci. 30, 726–732.

Hunten, D.M., 1973b. The escape of light gases from planetary atmospheres. J. Atmos. Sci. 30, 1481–1494.

Husain, D., Young, A., 1975. Kinetic investigation of ground-state carbon-atoms, $C(2^3P_J)$. J. Chem. Soc., Faraday Trans. II 71, 525–531.

Iess, L., Rappaport, J., Jacobson, R.A., Racioppa, P., Stevenson, D.J., Tortora, P., Armstrong, J.W., Asmar, S.W., 2010. Gravity field, shape, and moment of inertia of Titan. Science 327, 1367-1369.

Imanaka, H., Khare, B.N., Elsila, J.E., Bakes, E.L.O., McKay, C.P., Cruikshank, D.P., Sugita, S., Matsui, T., Zare, R.N., 2004. Laboratory experiments of Titan tholin formed in cold plasma at various pressures: implications for nitrogen-containing polycyclic aromatic compounds in Titan haze. Icarus 168, 344-366.

Imanaka, H., Smith, M.A., 2007. Role of photoionization in the formation of complex organic molecules in Titan's upper atmosphere. Geophys. Res. Lett. 34, L02204.

Imanaka, H., Smith, M.A., 2010. Formation of nitrogenated organic aerosols in the Titan upper atmosphere. P. Natl. Acad. Sci. USA 107, 12423–12428.

Jackson, W., Anex, D., Continetti, R., Balko, B., Lee, Y., 1991. Molecular-beam studies of the photolysis of allene and the secondary photodissociation of the C_3H_x fragments. J. Chem. Phys. 95 (10), 7327–7336.

Jackson, W., Halpern, J., 1979. Multiphoton ultraviolet photodissociation of C_2N_2. J. Chem. Phys. 70 (5), 2373–2377.

Jacob, D.J., 1999. Introduction to Atmospheric Chemistry. Princeton University Press, NJ.

Jacobs, T.A., Giedt, R.R., Cohen, N., 1965. Kinetics of decomposition of HF in shock waves. J. Chem. Phys. 43, 3688-3693.

Jamieson, J., Brown, G., Tanner, J., 1970. Reaction of atomic hydrogen with methyl cyanide. Can. J. Chem. - Rev. Can. Chim. 48 (23), 3619–3622.

Jodkowski, J., Ratajczak, E., Fagerstrom, K., Lund, A., Stothard, N., Humpfer, R., Grotheer, H., 1995. Kinetics of the cross reaction between amidogen and methyl radicals. Chem. Phys. Lett. 240 (1-3), 63–71.

Jodkowski, J., Rayez, M., Rayez, J., Berces, T., Dobe, S., 1999. Theoretical study of the

kinetics of the hydrogen abstraction from methanol. 3. Reaction of methanol with hydrogen atom, methyl, and hydroxyl radicals. J. Phys. Chem. A 103 (19), 3750–3765.

Johnston, G., Cuff, D., Price, D., 1978. Mechanisms for the photochemical production of hydrocarbons in gaseous hydrocarbon systems. Prog. React. Kinet. 8, 231–291.

Joseph, J.H., Wiscombe, W.J., Weinman, J.A., 1976. The delta-Eddington approximation for radiative flux transfer. J. Atmos. Sci. 33, 2452-2459.

Kasting, J.F., 1982. Stability of Ammonia in the Primitive Terrestrial Atmosphere. J. Geophys. Res. 87, 3091-3098.

Kasting, J.F., 1983. Photochemistry of methane in the Earth's early atmosphere. Precambrian Res. 20, 121-148.

Kasting , J.F., 1990. Bolide impacts and the oxidation state of carbon in the Earth's early atmosphere. Orig. Life. Evol. Biosph. 20, 199-231.

Kasting, J.F., 1993. Earth's early atmosphere. Science, 259, 920–926.

Kasting, J.F., 2005. Methane and climate during the Precambrian era. Precambrian Res. 137, 119–129.

Kasting, J.F., Brown, L.L., 1998. Setting the stage: The early atmosphere as a source of biogenic compounds. in The Molecular Origins of Life: Assembling the Pieces of the Puzzle. Eds. A. Brack, pp. 35-56, Cambridge Univ. Press, New York.

Kasting, J.F., Catling, D., 2003. Evolution of a habitable planet. Ann. Rev. Astron. Astrophys. 41, 429–463. doi:10.1146/annurev.astro.41.071601.170049.

Kasting, J.F., Donahue, T.M., 1980. The Evolution of Atmospheric Ozone. J. Geophys. Res. 85, 3255-3263.

Kasting, J.F., Grinspoon, D.H., 1991. The faint young Sun problem. in The Sun in Time, edited by C. P. Sonett, M. S. Giampapa, and M. S. Matthews, pp. 447–462, Univ. of Ariz. Press, Tucson.

Kasting, J.F., Liu, S.C., Donahue, T.M., 1979. Oxygen Levels in the Prebiological Atmosphere. J. Geophys. Res. 84, 3097-3107.

Kasting, J.F., Pavlov, A.A., Siefert, J.L., 2001. A coupled ecosystem-climate model for predicting the methane concentration in the Archean Atmosphere. Origins Life Evol. Biosphere 31, 271–285.

Kasting, J.F., Pollack, J.B., Crisp, D., 1984. Effects of high CO_2 levels on surface temperature and atmospheric oxidation state of the early Earth. J. Atmos. Chem. 1, 403–428. doi:10.1007/BF00053803.

Kasting, J.F., Walker, J.C.G., 1981. Limits on Oxygen Concentration in the Prebiological Atmosphere and the Rate of Abiotic Fixation of Nitrogen. J. Geophys. Res. 86, 1147-1158.

Kelly, N., Heicklen, J., 1978. Rate coefficient for reaction of CH_3O with CH_3CHO at 25°C. J. Photochem. 8 (2), 83–90.

Khare, B.N., Bakes, E.L.O., Imanaka, H., McKay, C.P., Cruikshank, D.P., 2002.

Analysis of the time-dependent chemical evolution of Titan haze tholin. Icarus 160, 172-182.

Khare, B.N., Sagan, C., Arakawa, E.T., Suits, F., Callcott, T.A., Williams, M.W., 1984a. Optical constants of organic tholins produced in a simulated Titanian atmosphere: From soft X-ray to microwave frequencies. Icarus 60, 127-137.

Khare, B.N., Sagan, C., Thompson, W.R., Arakawa, E.T., Suits, F., Callcott, T.A., Williams, M.W., Shrader, S., Ogino, H., Willingham, T.O., Nagay, B., 1984b. The organic aerosols of Titan. Adv. Space Res. 4, 59-68.

Khare, B.N., Sagan, C., Thompson, W.R., Arakawa, E.T., Votaw, P., 1987. Solid hydrocarbon aerosols produced in simulated Uranian and Neptunian stratospheres. J. Geophys. Res. 92, 15,067-15,082.

Kharecha, P., Kasting, J., Siefert, J., 2005. A coupled atmosphere-ecosystem model of the early Archean Earth. Geobiology 3, 53-76.

Kiehl, J.T., Dickinson, R.E., 1987. A study of the radiative effects of enhanced atmospheric CO_2 and CH_4 on early Earth surface temperatures. J. Geophys. Res. 92, 2991–2998.

Kirschvink, J.L., Gaidos, E.J., Bertani, L.E., Beukes, N.J., Gutzmer, J., Maepa, L.N., Steinberger, R.E., 2000. Paleoproterozoic snowball Earth: Extreme climatic and geochemical global change and its biological consequences. P. Natl. Acad. Sci. USA 97, 1400-1405.

Kloster-Jensen, E., Hanik, H.J., Christen, H., 1974. The electronic spectra of unsubstituted mono- to pentaacetylene in the gas phase and in solution in the range 1100 to 4000 Å. Helv. Chim. Acta 57, 1731-1744.

Kral, T.A., Brink, K.M., Miller, S.L., McKay, C.P., 1998. Hydrogen consumption by methanogens on the early Earth. Origins Life Evol. Biosphere 28, 311–319.

Krasnopolsky, V.A., 2009. A photochemical model of Titan's atmosphere and ionosphere. Icarus 201, 226-256.

Krasnopolsky, V.A., 2010. The photochemical model of Titan's atmosphere and ionosphere: A version without hydrodynamic escape. Planet. Space Sci. 58, 1507-1515.

Kuhn, W.R., Atreya, S.K., 1979. Ammonia photolysis and the greenhouse effect in the primordial atmosphere of the Earth. Icarus 37, 207–213.

Kump, L.R., 1991. Interpreting carbon-isotope excursions: Strangelove oceans. Geology 19, 299-302.

Kuramoto, K., Matsui, T., 1994. Formation of a hot proto-atmosphere on the accreting giant icy satellite: Implications for the origin and evolution of Titan, Ganymede, and Callisto. J. Geophys. Res. 99, 21,183-21,200.

Kuroiwa, K., Yamazaki, H., Tsuchiya, S., Kamisako, K., Tarui, Y., 1992. High-Intensity Vacuum Ultraviolet Light Source in Windowless Photochemical Vapor Deposition Reactor and Its Application to a-Si:H Deposition. Jpn. J. Appl. Phys. 31,

L518-L520.

Lambert, R., Christie, M., Golesworthy, R., Linnett, J., 1968. Mass spectrometric study of reaction of nitrogen atoms with acetaldehyde. Proc. R. Soc. A 302 (1469), 167–183.

Lara, L.M., Lellouch, E., Lopes-Moreno, J., Rodrigo, R., 1996. Vertical distribution of Titan's atmospheric neutral constituents. J. Geophys. Res. 101, 23,261-23,283.

Lasaga, A.C., Berner, R.A., Garrels, R.M., 1985. An improved geochemical model of atmospheric CO_2 fluctuations over the past 100 million years. in The Carbon Cycle and Atmospheric CO_2: Natural Variations Archean to Present, eds. Sundquist, E., Broecker, W., Am Geophys Union, Washington, DC, pp 397–411.

Laufer, A., Gardner, E., Kwok, T., Yung, Y., 1983. Computations and estimates of rate coefficients for hydrocarbon reactions of interest to the atmospheres of the outer Solar System. Icarus 56 (3), 560–567.

Lavvas, P.P., Coustenis, A., Vardavas, I.M., 2008a. Coupling photochemistry with haze formation in Titan's atmosphere, Part I: Model description. Planet. Space Sci. 56, 27-66.

Lavvas, P.P., Coustenis, A., Vardavas, I.M., 2008b. Coupling photochemistry with haze formation in Titan's atmosphere, Part II: Results and validation with Cassini/Huygens data. Planet. Space Sci. 56, 67-99.

Lavvas, P., Sander, M., Kraft, M., Imanaka, H., 2011. Surface chemistry and particle shape: processes for the evolution of aerosols in Tinta's atmosphere. Astrophys. J. 728, 80, 11p.

Lee, L., 1980. CN($A^2\Sigma_i \rightarrow X^2\Sigma^+$) and CN($B^2\Sigma^+ \rightarrow X^2\Sigma^+$) yields from HCN photodissociation. J. Chem. Phys. 72 (12), 6414–6421.

Lee, Y.-N., Schwartz, S.W., 1981. Evaluation of the rate of uptake of nitrogen dioxide by atmospheric and surface liquid water. J. Geophys. Res. 86, 11,971-11983.

Lellouch, E., Hunten, D.M., 1987. Titan atmosphere engineering model. Space Science Department of ESA, ESLAB 87/199.

Lellouch, E., Romani, P., Rosenqvist, J., 1994. The vertical distribution and origin of HCN in Neptune atmosphere. Icarus 108 (1), 112–136.

Lesclaux, R., Demissy, M., 1978. Kinetics of gas-phase reactions of NH_2 radicals with alkane and alkyl radicals. J. Photochem. 9 (2-3), 110–112.

Li, S., Williams, F., 1996. Experimental and numerical studies of two-stage methanol flames. Proc. Combust. Inst. 26, 1017 – 1024.

Lias, S., Collin, G., Rebbert, R., Ausloos, P., 1970. Photolysis of ethane at 11.6-11.8 eV. J. Chem. Phys. 52 (4), 1841–1851.

Liou, K., 2002. An Introduction to Atmospheric Radiation. 2nd Ed., pp. 583, Academic Press, Massachusetts.

Linder, D., Duan, X., Page, M., 1996. Thermal rate constants for R + N_2H_2 → RH + N_2H (R = H, OH, NH_2) determined from multireference configuration interaction

and variational transition state theory calculations. J. Chem. Phys. 104 (16), 6298–6307.

Lombos, B.A., Sauvageau, P., Sandorfy, C., 1967. The electronic spectra of *n*-alkanes. J. Mol. Spectrosc. 24, 253-269.

Lorenz, R.D., 1993. The life, death and afterlife of a raindrop on Titan. Planet. Space Sci. 41, 647-655.

Lorenz, R.D., McKay, C.P., Lunine, J.I., 1997. Photochemically driven collapse of Titan's atmosphere. Science 275, 642-644.

Lowe, D.R., 1980. Archean sedimentation. Annu. Rev. Earth Planet. Sci. 8, 145–167.

Marston, G., Nesbitt, F., Stief, L., 1989. Branching ratios in the N + CH_3 reaction - Formation of the methylene amidogen (H_2CN) radical. J. Chem. Phys. 91 (6), 3483–3491.

Marten, A., Gautier, D., Tanguy, L., Lecacheux, A., Rosolen, C., Paubert, G., 1988. Abundance of Carbon Monoxide in the Stratosphere of Titan from Millimeter Heterodyne Observations. Icarus 76, 558-562.

Marten, A., Hidayat, T., Biraud, Y., Moreno, R., 2002. New millimeter heterodyne observations of Titan: Vertical distributions of nitriles HCN, HC_3N, CH_3CN, and the isotopic ratio $^{15}N/^{14}N$ in its atmosphere. Icarus 158, 532–544.

Mason, E.A., Marreno, T.R., 1970. The diffusion of atoms and molecules. In: Bates, D.R., Esterman, I. (Eds.), Advances in Atomic and Molecular Physics. Academic, San Diego, Calif., pp. 155-232.

McEwan, M.J., Lawrence, G.M., Poland, H.M., 1974. Vacuum UV photolysis of N_2O. J. Chem. Phys. 61, 2857-2859.

McKay, C.P., 1996. Elemental composition, solubility, and optical properties of Titan's organic haze. Planet. Space Sci. 44, 741-747.

McKay, C.P., Coustenis, A., Samuelson, R.E., Lemmon, M.T., Lorenz, R.D., Cabane, M., Rannou, P., Drossart, P., 2001. Physical properties of the organic aerosols and clouds on Titan. Planet. Space Sci. 49, 79–99.

McKay, C.P., Pollack, J.B., Courtin, R., 1989. The thermal structure of Titan's atmosphere. Icarus 80, 23-53.

McNesby, J., Okabe, H., Tanaka, I., 1962. Vacuum ultraviolet photochemistry. 3. Primary processes in vacuum ultraviolet photolysis of water and ammonia. J. Chem. Phys. 36 (3), 605–607.

Meador, W.E., Weaver, W.R., 1980. Two-stream approximations to radiative transfer in planetary atmospheres: A unified description of existing methods and a new improvement. J. Atmos. Sci. 37, 630-643.

Mebel, A., Lin, M., 1999. Prediction of absolute rate constants for the reactions of NH_2 with alkanes from ab initio G2M/TST calculations. J. Phys. Chem. A 103 (13), 2088–2096.

Mebel, A., Lin, S., Yang, X., Lee, Y., 1997. Theoretical study on the mechanism of the

dissociation of benzene. The C_5H_3 + CH_3 product channel. J. Phys. Chem. A 101 (36), 6781–6789.

Miller, J.A., Mitchell, R.E., Smooke, M.D., Kee, R.J., 1982. Toward a comprehensive chemical kinetic mechanism for the oxidation of acetylene. Symp. Int. Combust. Proc. 19th, 181.

Miller, S.L., 1953. A production of amino acids under possible primitive Earth conditions. Science 117. 528-529.

Miller, S.L., Urey, H.C., 1959. Organic compound synthesis on the primitive Earth. Science 130, 245-251.

Miller-Ricci Kempton, E., Zahnle, K., Fortney, J.J., 2012. The atmospheric chemistry of GJ 1214b: Photochemistry and clouds. Astrophys. J. 745, 3, 13pp. doi:10.1088/0004-637X/745/1/3

Miyazaki, S., Takahashi, S., 1968. Reactions of nitrogen atom with methane and with ethylene. Bull. Chem. Soc. Jpn. 41 (6), 1456–1466.

Miyoshi, A., Matsui, H., Washida, N., 1989. Reaction of acetaldehyde and acetyl radical with atomic and molecular oxygen. J. Phys. Chem. 93 (15), 5813–5818.

Monks, P., Nesbitt, F., Payne, W., Scanlon, M., Stief, L., Shallcross, D., 1995. Absolute rate-constant and product branching ratios for the reaction between H and C_2H_3 at T = 213 and 298 K. J. Phys. Chem. 99 (47), 17151–17159.

Monks, P., Romani, P., Nesbitt, F., Scanlon, M., Stief, L., 1993. The kinetics of the formation of nitrile compounds in the atmospheres of Titan and Neptune. J. Geophys. Res.-Planets 98 (E9), 17115–17122.

Mordaunt, D., Ashfold, M., Dixon, R., Dissociation dynamics of H_2O (D_2O) following photoexcitation at the Lyman wavelength (121.6 nm). J. Chem. Phys. 100 (10), 7360–7375.

Morimoto, C., Otofuji, Y., Miki, M., Tanaka, H., Itaya, T., 1997. Preliminary palaeomagnetic results of an Archaean dolerite dyke of west Greenland: geomagnetic field intensity at 2.8 Ga. Geophys. J. Int. 128, 585-593.

Mount, G.H., Moos, H.W., 1978. Photoabsorption cross sections of methane and ethane, 1380-1600 Å, at T = 295 K and T = 200 K. Astrophys. J. 224, L35-L38.

Mount, G.H., Rottman, G.J., 1983. The solar absolute spectral irradiance 1150-3173 Å: May 17, 1982. J. Geophys. Res. 88, 5403-5410.

Mount, G., Warden, E., Moos, H., 1977. Photoabsorption cross-sections of methane from 1400 to 1850 Å. Astrophys. J. 214 (1), L47–L49.

Munk, J., Pagsberg, P., Ratajczak, E., Sillesen, A., 1986. Spectrokinetic studies of l-C_3H_7 and l-$C_3H_7O_2$ radicals. Chem. Phys. Lett. 132 (4-5), 417–421.

Murphy, J., Vakhtin, A., Leone, S., 2003. Laboratory kinetics of C_2H radical reactions with ethane, propane, and n-butane at T = 96-296 K: Implications for Titan. Icarus 163 (1), 175–181.

Nakata, R.S., Watanabe, K., Matsunaga, F.M., Absorption and photoionization

coefficients of CO_2 in the region 580-1670 Å. Science of Light 14, 54-71.
Nesbitt, F., Marston, G., Stief, L., 1990. Kinetic-studies of the reactions of H_2CN and D_2CN radicals with N and H. J. Phys. Chem. 94 (12), 4946–4951.
Ni, C., Huang, J., Chen, Y., Kung, A., Jackson, W., 1999. Photodissociation of propyne and allene at 193 nm with vacuum ultraviolet detection of the products. J. Chem. Phys. 110 (7), 3320–3325.
Nicholas, J., Spiers, A., Martin, N., 1986. Kinetics and mechanism in the decomposition of NH_3 in a radiofrequency pulse discharge. Plasma Chem. Plasma Process. 6 (1), 39–51.
Nicolet, M., Peetermans, W., 1972. Production of nitric oxide in the stratosphere by oxidation of nitrous oxide. Ann. Geophys. 28, 751-762.
Nisbet, E., Fowler, C., 2011. The evolution of the atmosphere in the archaean and early Proterozoic. Chin. Sci. Bull. 56, 4–13. doi:10.1007/s11434-010-4199-8.
Nisbet, E.G., Sleep, N.H., 2001. The habitat and nature of early life. Nature 409, 1083–1091. doi:10.1038/35059210.
Nizamov, B., Dagdigian, P., 2003. Spectroscopic and kinetic investigation of methylene amidogen by cavity ring-down spectroscopy. J. Phys. Chem. A 107 (13), 2256–2263.
Nizamov, B., Leone, S., 2004. Kinetics of C_2H reactions with hydrocarbons and nitriles in the 104-296 K temperature range. J. Phys. Chem. A 108 (10), 1746–1752.
Nuth, J.A., Glicker, S., 1982. The vacuum ultraviolet spectra of HCN, C_2N_2, and CH_3CN. J. Quant. Spectrosc. Radiat. Transfer 28, 223-231.
Ohmori, K., Miyoshi, A., Matsui, H., Washida, N., 1990. Studies on the reaction of acetaldehyde and acetyl radicals with atomic hydrogen. J. Phys. Chem. 94 (8), 3253–3255.
Okabe, H., 1967. Excited Species and Their Contribution to NO(β, γ) Fluorescence in the Photodissociation of N_2O. J. Chem. Phys. 47, 101-109.
Okabe, H., 1978. Photochemistry of small molecules. John Wiley and Sons, New York.
Okabe, H., 1981. Photochemistry of acetylene at 1470 Å. J. Chem. Phys. 75, 2772-2778.
Okabe, H., 1983. Photochemistry of acetylene at 1849 Å. J. Chem. Phys. 78 (3), 1312–1317.
Okabe, H., Becker, D.A., 1963. Vacuum ultraviolet photochemistry. VII. Photolysis of *n*-Butane. Chem. Phys. 39, 2549-2555.
Okabe, H., Dibeler, V.H., 1973. Photon impact studies of C_2HCN and CH_3CN in the vacuum ultraviolet; heats of formation of C_2H and CH_3CN. J. Chem. Phys. 59, 2430-2435. doi: 10.1063/1.1680354
Opansky, B., Leone, S., 1996a. Low-temperature rate coefficients of C_2H with CH_4 and CD_4 from 154 to 359 K. J. Phys. Chem. 100 (12), 4888–4892.
Opansky, B., Leone, S., 1996b. Rate coefficients of C_2H with C_2H_4, C_2H_6, and H_2 from

150 to 359 K. J. Phys. Chem. 100 (51), 19904–19910.

Owen, T., Cess, R.D., Ramanathan, V., 1979. Enhanced CO_2 greenhouse to compensate for reduced solar luminosity on early Earth. Nature 277, 640–642.

Pagsberg, P., Eriksen, J., CHristensen, H., 1979. Pulse-radiolysis of gaseous ammonia oxygen mixtures. J. Phys. Chem. 83 (5), 582–590.

Park, J., Burova, S., Rodgers, A., Lin, M., 1999. Experimental and theoretical studies of the $C_6H_5 + C_6H_6$ reaction. J. Phys. Chem. A 103 (45), 9036–9041.

Parker, J., Payne, W., Cody, R., Stief, L., 2004. Kinetics of the reaction of atomic hydrogen with cyanoacetylene from T = 200 to 298 K. J. Phys. Chem. A 108 (11), 1938–1945.

Parkes, D.A., Paul, D.M., Quinn, C.P., Robson, R.C., 1973. The ultraviolet absorption by alkylperoxy radicals and their mutual reactions. Chem. Phys. Lett. 23, 425-429.

Pavlov, A.A., Brown, L.L., Kasting, J.F., 2001. UV shielding of NH_3 and O_2 by organic hazes in the Archean atmosphere. J. Geophys. Res. 106, 23267-23287.

Pavlov, A.A., Hurtgen, M.T., Kasting, J.F., Arthur, M.A., 2003. Methane-rich Proterozoic atmosphere? Geology 31, 87-90.

Payne, W., Monks, P., Nesbitt, F., Stief, L., 1996. The reaction between $N(^4S)$ and C_2H_3: Rate constant and primary reaction channels. J. Chem. Phys. 104 (24), 9808–9815.

Perry, R., Melius, C., 1984. The rate and mechanism of the reaction of HCN with oxygen atoms over the temperature range 540-900 K. Proc. Combust. Inst. 20, 639–646.

Phillips, L., 1978. Reaction of H with C_2N_2 at pressures near 1 Torr. Int. J. Chem. Kinet. 10 (8), 899–904.

Piper, L., Donahue, M., Rawlins, W., 1987. Rate coefficients for $N(^2D)$ reactions. J. Phys. Chem. 91 (14), 3883–3888.

Pitts, W., Pasternack, L., McDonald, J., 1982. Temperature dependence of the C_2 reaction with H_2 and CH_4 and C_2 with O_2. Chem. Phys. 68, 417–422.

Pollack, J.B., 1979. Climatic change on the terrestrial planets. Icarus 37, 479–553. doi:10.1016/0019-1035(79)90012-5.

Pollack, J.B., 1991. Kuiper Prize Lecture: Present and past climates of the terrestrial planets. Icarus 91, 173–198. doi:10.1016/0019-1035(91)90017-N.

Pollack, J.B., Rages, K., Toon, O.B., Yung, Y.L., 1980. On the relationship between secular brightness changes of Titan and solar variability. Geophys. Res. Lett. 7, 829–832. doi: 10.1029/GL007i010p00829

Prasad, S.S., Huntress, W.T., 1980. A model for gas phase chemistry in interstellar clouds. Astrophys J. Suppl. Ser. 43, 1-35.

Pravilov, A., Smirnova, L., Vilesov, A., 1991. Kinetics and yield of xenon excitation in active nitrogen, studied by CCl_4 and Cl_2 sensitization techniques. J. Photochem. Photobiol. A - Chem. 60 (2), 133–147.

Pruppacher, H.R., Klett, J.D., 2010. Microphysics of clouds and precipitation. Second

revised and enlarged edition with an introduction to cloud chemistry and cloud electricity. Kluwer Academic Publishers, Dordrecht, Netherlands.

Rahman, A., Yalin, A.P., Surla, V., Stan, O., Hoshimiya, K., Yu, Z., Littlefield, E., Collins, G.J., 2004. Absolute UV and VUV emission in the 110-400 nm region from 13.56 MHz driven hollow slot microplasmas operating in open air. Plasma Sources Sci. Technol. 13, 537-547.

Rajappan, M., Buttner, M., Cox, C., Yates, J.T.Jr., 2010. Photochemical decomposition of N_2O by Lyman-α radiation: Scientific basis for a chemical actinometer. J. Phys. Chem. A 114, 3443-3448.

Rampino, M.R., Caldeira, K., 1994. The Goldilocks Problem: Climatic evolution and long-term habitability of terrestrial planets. Annu. Rev. Astron. Astrophys. 32, 83–114. doi:10.1146/annurev.aa.32.090194.000503.

Rannou , P., Hourdin, F., McKay, C.P., 2002. A wind origin for Titan's haze structure. Nature 418, 853-856.

Rannou, P., Hourdin, F., McKay, C.P., Luz, D., 2004. A coupled dynamics-microphysics model of Titan's atmosphere. Icarus 170, 443-462.

Raulin, F., Mourey, D., Toupance, G., 1982. Organic synthesis from CH_4-N_2 atmospheres — implications for Titan. Orig. Life Evol. Biosph. 12, 267–279.

Reisler, H., Mangir, M., Wittig, C., 1980. Kinetics of free-radicals generated by IR Laser Photolysis. 4. Intersystem crossings and reactions of C_2 ($X^1\Sigma^+_g$) and $C_2(a^3\Pi_u)$ in the gaseous-phase. J. Chem. Phys. 73 (5), 2280–2286.

Rennie, E.E., Johnson, C.A.F., Parker, J.E., Holland, D.M.P., Shaw, D.A., Hayes, M.A., 1998. A photoabsorption, photodissociation and photoelectron spectroscopy study of C_6H_6 and C_6D_6. Chem. Phys. 229, 107-123.

Reuben, B.G., 1969. Vapor Pressure of Ketene. J. Chem. Eng. Data 14, 235-236.

Ribas, I., Guinan, E.F., Gudel, M., Audard, M., 2005. Evolution of the solar activity over time and effects on planetary atmospheres. I. High-energy irradiances (1-1700 Å). Astrophys. J. 622, 680-694.

Richter, H., Howard, J.B., 2000. Formation of polycyclic aromatic hydrocarbons and their growth to soot – a review of chemical reaction pathways. Prog. Energy Combus. Sci. 26, 565-608.

Rosing, M.T., Bird, D.K., Sleep, N.H., Bjerrum, C.J., 2010. No climate paradox under the faint early Sun. Nature 464, 744–747. doi:10.1038/nature08955.

Rye, R., Kuo, P.H., Holland, H.D., 1995. Atmospheric carbon dioxide concentrations before 2.2 billion years ago. Nature 378, 603–605. doi:10.1038/378603a0.

Sagan, C., Chyba, C., 1997. The early faint Sun paradox: Organic shielding of ultraviolet-labile greenhouse gases. Science 276, 1217-1221.

Sagan, C., Mullen, G., 1972. Earth and Mars: Evolution of atmospheres and surface temperatures. Science 177, 52-56.

Samson, J.A.R., Marmo, F.F., Watanabe, K., 1962. Absorption and photoionization

coefficients of propylene and bunene-1 in the vacuum ultraviolet. J. Chem. Phys. 36, 783-786.

Samuelson, R.E., Hanel, R.A., Kunde, V.G., Maguire, W.C., 1981. Mean molecular weight and hydrogen abundance of Titan's atmosphere. Nature 292, 688–693.

Samuelson, R.E., Maguire, W.C., Hanel, R.A., Kunde, V.G., Jennings, D.E., Yung, Y.L., Aikin, A.C., 1983. CO_2 on Titan. J. Geophys. Res. 88, 8709-8715.

Sander, S., Friedl, R., Barker, J., Golden, D., Kurylo, Wine, P., Abbatt, J., Burkholder, J., Kolb, C., Moortgat, G., Huie, R., Orkin, V., 2011. Chemical kinetics and photochemical data for use in atmospheric studies. Evaluation number 17, JPL Publ. 10-6, 1–684.

Sato, K., Misawa, K., Kobayashi, Y., Matsui, M., Tsunashima, S., Kurosaki, K., Takayanagi, T., 1999. Measurements of thermal rate constants for the reactions of $N(^2D,^2P)$ with C_2H_4 and C_2D_4 between 225 and 292 K. J. Phys. Chem. A 103 (43), 8650–8656.

Sayah, N., Li, X., Caballero, J., Jackson, W., 1988. Laser-induced fluorescence studies of CN reactions with alkanes, alkenes and substituted aliphatic species. J. Photochem. Photobiol. A - Chem. 45 (2), 177–194.

Scattergood, T.W., Lau, E.Y., Stone, B.M., 1992. Titan's Aerosols I. Laboratory investigations of shapes, size distributions, and aggregation of particles produced by UV photolysis of model Titan atmospheres. Icarus 99, 98-105.

Scherzer, K., Claus, P., Karwath, M., 1985. Untersuchungen zur Kinetik und zum Mechanismus der Addition von Methylradicalen an Vinylacetylen. Z. Phys. Chemie - Int. J. Res. Phys. Chem. Chem. Phys. 266 (2), 321–328.

Schoen, R.I., 1962. Absorption, ionization, and ion-fragmentation cross sections of hydrocarbon vapors under vacuum-ultraviolet radiation. J. Chem. Phys. 37, 2032-2041.

Schofield, K., 1973. Evaluated chemical kinetic rate constants for various gas phase reactions. J. Phys. Chem. Ref. Data 2, 25–84.

Schopf, J.W., 2006. Fossil evidence for Archean life. Philos. Trans. R. Soc. B 361, 869-885.

Sciamma-O'Brien, E., Carrasco, N., Szopa, C., Buch, A., Cernogora, G., 2010. Titan's atmosphere: An optimal gas mixture for aerosol production? Icarus 209, 704-714.

Seinfeld, J.H., Pandis, S.N., 2006. Atmospheric chemistry and physics: From air pollution to climate change. 2nd ed. John Wiley & Sons, Inc., New Jersy.

Seki, K., Okabe, H., 1992. Photodissociation of methylacetylene at 193 nm. J. Phys. Chem. 96 (8), 3345–3349.

Seki, K., Okabe, H. 1993. Photochemistry of acetylene at 193.3 nm. J. Phys. Chem. 97 (20), 5284–5290.

Seki, K., Yagi, M., He, M., Halpern, J., Okabe, H., 1996. Reaction rates of the CN radical with diacetylene and dicyanoacetylene. Chem. Phys. Lett. 258 (5-6), 657–

662.

Sekine, Y., Genda, H., Sugita, S., Kadono, T., Matsui, T., 2011. Replacement and late formation of atmospheric N_2 on undifferentiated Titan by impacts. Nat. Geo. 4, 359–362.

Sekine, Y., Imanaka, H., Matsui, T., Khare, B.N., Bakes, E.L.O., McKay, C.P., Sugita, S., 2008a. The role of organic haze in Titan's atmospheric chemistry I. Laboratory investigation on heterogeneous reaction of atomic hydrogen with Titan tholin. Icarus 194, 186-200.

Sekine, Y., Lebonnois, S., Imanaka, H., Matsui, T., Bakes, E.L.O., McKay, C.P., Khare, B.N., Sugita, S., 2008b. The role of organic haze in Titan's atmospheric chemistry II. Effect of heterogeneous reaction to the hydrogen budget and chemical composition of the atmosphere. Icarus 194, 201-211.

Selkin, P.A., Gee, J.S., Tauxe, L., Meurer, W.P., Newell, A.J., 2000. The effect of remanence anisotropy on paleointensity estimates: a case study from the Archean Stillwater Complex. Earth Planet. Sci. Lett. 183, 403-416.

Selwyn, G., Podolske, J., Johnston, H.S., 1977. Nitrous oxide ultraviolet absorption spectrum at stratospheric temperatures. Geophys. Res. Lett. 4, 427-430.

Shaw, G., 2008. Earth's atmosphere–Hadean to early Proterozoic. Chem. Erde 68, 235–264. doi:10.1016/j.chemer.2008.05.001.

Sheldon, N.D., 2006. Precambrian paleosols and atmospheric CO_2 levels. Precambrian Res. 147, 148–155. doi:10.1016/j.precamres.2006.02.004.

Shemansky, D.E., Stewart, A.I.F., West, R.A., Esposito, L.W., Hallett, J.T., Liu, X., 2005. The Cassini UVIS stellar probe of the Titan atmosphere. Science 308, 978–982.

Shi, J., Barker, J., 1990. Kinetic studies of the deactivation of $O_2(^1\Sigma^+_g)$ and $O(^1D)$. Int. J. Chem. Kinet. 22 (12), 1283–1301.

Siese, M., Zetzsch, C., 1995. Addition of OH to acetylene and consecutive reactions of the adduct with O_2. Z. Phys. Chemie - Int. J. Res. Phys. Chem. Chem. Phys. 188, 75–89.

Sillesen, A., Ratajczak, E., Pagsberg, P., 1993. Kinetics of the reactions $H + C_2H_4 \rightarrow C_2H_5$, $H + C_2H_5 \rightarrow 2\,CH_3$ and $CH_3 + C_2H_5$ products studied by pulse-radiolysis combined with infrared diode-laser spectroscopy. Chem. Phys. Lett. 201 (1-4), 171–177.

Sims, I., Queffelec, J., Travers, D., Rowe, B., Herbert, L., Karthauser, J., Smith, I., 1993. Rate constants for the reactions of CN with hydrocarbons at low and ultra-low temperatures. Chem. Phys. Lett. 211 (4-5), 461–468.

Sims, I., Smith, I., 1988. Pulsed laser photolysis laser-induced fluorescence measurements on the kinetics of $CN(\nu = 0)$ and $CN(\nu = 1)$ with O_2, NH_3 and NO between 294 and 761 K. J. Chem. Soc., Faraday Trans. II 84, 527–539.

Slagle, I., Bernhardt, J., Gutman, D., Hanninglee, M., Pilling, M., 1990a. Kinetics of the reaction between oxygen-atoms and allyl radicals. J. Phys. Chem. 94 (9), 3652–

3656.

Slagle, I., Gmurczyk, G., Batt, L., Gutman, D., 1990b. Kinetics of the reaction between oxygen atoms and propargyl radicals. Proc. Combust. Inst. 23, 115–121.

Slemr, F., Warneck, P., 1975. Reactions of atomic hydrogen with ketene and acetaldehyde. Ber. Bunsen-Ges. Phys. Chem. 79 (2), 152–156.

Slinn, W.G.N., Hasse, L., Hicks, B.B., Hogan, A.W., Lal, D., Liss, P.S., Munnich, K.O., Sehmel, G.A., Vittori, O., 1978. Some aspects of the transfer of atmospheric trace constituents past the air-sea interface, Atmos. Environ. 12, 2055-2087.

Smith, N.S., Raulin, F., 1999. A box model of the photolysis of methane at 123.6 and 147 nm – comparison between model and experiment. J. Photochem. Photobiol. A Chemistry 124, 101-112.

Spence, R., Wild, W., 1935. The Vapour-Pressure Curve of Formaldehyde and Some Related Data. J. Chem. Soc. 138, 506-509.

Stephan, K., Krauss, R., Laesecke, A., 1987. Viscosity and thermal conductivity of nitrogen for a wide range of fluid states. J. Phys. Chem. Ref. Data 16, 993-1023.

Stevenson, D.J., Spohn, T., Schubert, G., 1983. Magnetism and thermal evolution of the terrestrial planets. Icarus 54, 466-489.

Stief, L., Nesbitt, F., Payne, W., Kuo, S., Tao, W., Klemm, R., 1995. Rate-constant and reaction channels for the reaction of atomic nitrogen with the ethyl radical. J. Chem. Phys. 102 (13), 5309–5316.

Stief, L., Payne, W., 1976. Absolute rate parameters for reaction of atomic-hydrogen with hydrazine. J. Chem. Phys. 64 (12), 4892–4896.

Stief, L., Payne, W., Klemm, R., 1975. Flash photolysis-resonance fluorescence study of formation of $O(^1D)$ in photolysis of water and reaction of $O(^1D)$ with H_2, Ar and He. J. Chem. Phys. 62 (10), 4000–4008.

Stothard, N., Humpfer, R., Grotheer, H., 1995. The multichannel reaction $NH_2 + NH_2$ at ambient temperature and low pressures. Chem. Phys. Lett. 240 (5-6), 474–480.

Strobel, D.F., 1974. The photochemistry of hydrocarbons in the atmosphere of Titan. Icarus 21, 466-470.

Strobel, D.F., 2008. Titan's hydrodynamically escaping atmosphere. Icarus 193, 588-594.

Strobel, D.F., 2009. Titan's hydrodynamically escaping atmosphere: escape rates and the structure of the exobase region. Icarus 202, 632–641.

Stull, D.R., 1974. Vapor Pressure of Pure Substances Organic Compounds. Ind. Eng. Chem. 39, 517-540.

Sun, H., Weissler, G.L., 1955. Absorption cross sections of methane and ammonia in the vacuum ultraviolet. J. Chem. Phys. 23, 1160-1164.

Sun, W., Yokoyama, K., Robinson, J., Suits, A., Neumark, D., 1999. Discrimination of product isomers in the photodissociation of propyne and allene at 193 nm. J. Chem. Phys. 110 (9), 4363–4368.

Suto, M., Lee, L.C., 1985. Photoabsorption cross section of CH_3CN: Photodissociation rates by solar flux and interstellar radiation. J. Geophys. Res. 90, 13037-13040.

Suzuki, T., Shihira, Y., Sato, T., Umemoto, H., Tsunashima, S., 1993. Reactions of $N(^2D)$ and $N(^2P)$ with H_2 and D_2. J. Chem. Soc., Faraday Trans. 89 (7), 995–999.

Tanguy, L., Bezard, B., Marten, A., Gautier, D., Gerard, E., Paubert, G., Lecacheux, A., 1990. Stratospheric profiles of HCN on Titan from millimeter observations. Icarus 85, 43–57.

Teanby, N.A., and 11 colleagues, 2007. Vertical profiles of HCN, HC_3N, and C_2H_2 in Titan's atmosphere derived from Cassini/CIRS data. Icarus 186, 364–384.

Teng, L., Jones, W., 1972. Kinetics of reactions of hydrogen atoms with ethylene and vinyl fluoride. J. Chem. Soc., Faraday Trans. I 68 (7), 1267–1277.

Thauer, R.K., 1998. Biochemistry of methanogenesis: A tribute to Marjory Stephenson. Microbiology 144(9), 2377–2406.

Thompson, W.R., Henry, T.J., Schwartz, J.M., Khare, B.N., Sagan, C., 1991. Plasma discharge in N_2 + CH_4 at low pressures: Experimental results and applications to Titan. Icarus 90, 57-73.

Tian, F., Kasting, J.F., Liu, H.-L., Roble, R.G., 2008a. Hydrodynamic planetary thermosphere model: 1. Response of the Earth's thermosphere to extreme solar EUV conditions and the significance of adiabatic cooling. J. Geophys. Res. 113, E05008. doi:10.1029/2007JE002946

Tian, F., Kasting, J.F., Zahnle, K., 2011. Revisiting HCN formation in Earth's early atmosphere. Earth Planet. Sci. Lett. 308, 417-423.

Tian, F., Solomon, S.C., Qian, L., Lei, J., Roble, R.G., 2008b. Hydrodynamic planetary thermosphere model: 2. Coupling of an electron transport/energy deposition model. J. Geophys. Res. 113, E07005. doi:10.1029/2007JE003043

Tobie, G., Lunine, J.I., Sotin, C., 2006. Episodic outgassing as the origin of atmospheric methane on Titan. Nature 440, 61-64.

Tomasko, M.G., Bezard, B., Doose, L., Engel, S., Karkoschka, E., Vinatier, S., 2008a. Heat balance in Titan's atmosphere. Planet. Space Sci. 56, 648-659.

Tomasko, M.G., Doose, L., Engl, S., Dafoe, L.E., West, R., Lemmon, M., Krakoschka, E., See, C., 2008b. A model of Titan's aerosols based on measurements made inside the atmosphere. Planet. Space Sci. 56, 669-707.

Tomasko, M.G., West, R.A., 2009. Aerosols in Titan's Atmosphere. In Titan form Cassini-Huygens. eds. Brown, R.H., Lebreton, J.-P., Waite, J.H., Springer, New York.

Toon, O.B., McKay, C.P., Ackerman, T.P., 1989. Rapid calculation of radiative heating rates and photodissociation rates in inhomogeneous multiple scattering atmospheres. J. Geophys. Res. 94, 16,287-16,301.

Toon, O.B., McKay, C.P., Griffith, C.A., Turco, R.P., 1992. A physical model of Titan's aerosols. Icarus 95, 24-53.

Toon, O.B., Pollack, J.B., Sagan, C., 1977. Physical properties of the particles composing the Martian dust storm of 1971-1972. Icarus 30, 663-696.

Toon, OB., Turco, R.P., Hamill, P., Kiang, C.S., 1979. A one-dimensional model describing aerosol formation and evolution in the Stratosphere: II. Sensitivity studies and comparison with observations. J. Atmos. Sci. 36, 718-736.

Toon, OB., Turco, R.P., Pollack, J.B., 1980. A physical model of Titan's clouds. Icarus 43, 260-282.

Toon, OB., Turco, R.P., Westphal, D., Malone, R., Liu, M.S., 1988. A multidimensional model for aerosols: Description of computational analogs. J. Atmos. Sci. 45, 2123-2143.

Toublanc, D., Parisot, J.P., Brillet, J., Gautier, D., Raulin, F., McKay, C.P., 1995. Photochemical modeling of Titan's atmosphere. Icarus 113, 2-26.

Trainer, M.G., Jimenez, J.L., Yung, Y.L., Toon, O.B., Tolbert, M.A., 2012. Nitrogen incorporation in CH_4-N_2 photochemical aerosol produced by Far Ultraviolet irradiation. Astrobiology 12, 315-326.

Trainer, M.G., Pavlov, A.A., Curtis, D.B., McKay, C.P., Worsnop, D.R., Delia, A.E., Toohey, D.W., Toon, O.B., Tolbert, M.A., 2004. Haze aerosols in the atmosphere of early Earth: Manna from Heaven. Astrobiology 4, 409-419.

Trainer, M.G., Pavlov, A.A., DeWitt, H.L., Jimenez, J.L., McKay, C.P., Toon, O.B., Tolbert, M.A., 2006. Organic haze on Titan and the early Earth. P. Natl. Acad. Sci. USA 103 (48), 18035-18042.

Trainer, M.G., Sebree, J.A., Yoon, Y.H., Tolbert, M.A., 2013. The influence of benzene as a trace reactant in Titan aerosol analogs. Astrophys. J. Lett. 766, L4 (5pp).

Tran, B.N., Ferris, J.P., Chera, J.J., 2003. The photochemical formation of a Titan haze analog. Structural analysis by X-ray photoelectron and infrared spectroscopy. Icarus 162, 114-124.

Tsai, C., McFadden, D., 1990. Gas-phase atom-radical kinetics of N-atom and O-atom reactions with CF and CF_2 radicals. Chem. Phys. Lett. 173 (2-3), 241–245.

Tsang, W., 1987. Chemical kinetic database for combustion chemistry. 2. Methanol. J. Phys. Chem. Ref. Data 16 (3), 471–508.

Tsang, W., 1988. Chemical kinetic database for combustion chemistry. 3. Propane. J. Phys. Chem. Ref. Data 17 (2), 887–952.

Tsang, W., 1991. Chemical kinetic database for combustion chemistry. 5. Propene. J. Phys. Chem. Ref. Data 20 (2), 221–273.

Tsang, W., 1992. Chemical kinetic database for propellant combustion - Reactions involving CN, NCO, and HNCO. J. Phys. Chem. Ref. Data 21 (4), 753–791.

Tsang, W., Hampson, R., 1986. Chemical kinetic database for combustion chemistry. 1. Methane and related-compounds. J. Phys. Chem. Ref. Data 15 (3), 1087–1279.

Tully, J., 1975. Reactions of $O(^1D)$ with atmospheric molecules. J. Chem. Phys. 62 (5), 1893–1898.

Turco R.P., Hamill, P., Toon, O.B., Whitten, R.C., Kiang, C.S., 1979. A one-dimensional model describing aerosol formation and evolution in the stratosphere: I. Physical processes and mathematical analogs. J. Atmos. Sci. 36, 699-717.

Umemoto, H., Terada, N., Tanaka, K., Oguro, S., 2000. Deactivation processes of highly excited atomic nitrogen, N($2p^2 3p^2 S$). Phys. Chem. Chem. Phys. 2 (15), 3425–3428.

van Dishoeck, E.F., 1984. Photodissociation and excitation of interstellar molecules; calculations and astrophysical applications, Ph. D. thesis, University of Leiden.

Vakhtin, A., Heard, D., Smith, I., Leone, S., 2001a. Kinetics of C_2H radical reactions with ethene, propene and 1-butene measured in a pulsed Laval nozzle apparatus at T = 103 and 296 K. Chem. Phys. Lett. 348 (1-2), 21–26.

Vervack Jr., R.J., Sandel, B.R., Strobel, D.F., 2004. New perspectives on Titan's upper atmosphere from a reanalysis of the Voyager 1 UVS solar occultations. Icarus 170, 91–112.

Vinatier, S., and 10 colleagues, 2007. Vertical abundance profiles of hydrocarbons in Titan's atmosphere at 15° S and 80° N retrieved from Cassini/CIRS spectra. Icarus 188, 120–138.

von Paris, P., Rauer, H., Lee Grenfell, J., Patzer, B., Hedelt, P., Stracke, B., Trautmann, T., Schreier, F., 2008. Warming the early Earth–CO_2 reconsidered. Planet. Space Sci. 56, 1244–1259.

Vuitton, V., Doussin, J.-F., Benilan, Y., Raulin, F., Gazeau, M.-C., 2006. Experimental and theoretical study of hydrocarbon photochemistry applied to Titan stratosphere. Icarus 185, 287-300.

Vuitton, V., Gee, C., Raulin, F., Benilan, Y., Crepin, C., Gazeau, M., 2003. Intrinsic lifetime of metastable excited C_4H_2: Implications for the photochemistry of C_4H_2 in Titan's atmosphere. Planet. Space Sci. 51 (13), 847–852.

Vuitton, V., Yelle, R.V., McEwan, M.J., 2007. Ion chemistry and N-containing molecules in Titan's upper atmosphere. Icarus 191, 722–742.

Wagner, H., Zellner, R., 1972a. Reaktionen von Wasserstoffatomen mit ungesattigten C_3 Kohlenwasserstoffen. II. Die Reaktion von H Atomen mit Methylacetylen. Ber. Bunsen-Ges. Phys. Chem. 76 (6), 518–525.

Wagner, H., Zellner, R., 1972b. Reaktionen von Wasserstoffatomen mit ungesattigten C_3 Kohlenwasserstoffen. III. Die Reaktion von H Atomen mit Allen. Ber. Bunsen-Ges. Phys. Chem. 76 (7), 667–672.

Waite Jr., J.H., and 21 colleagues, 2005. Ion neutral mass spectrometer results from the first flyby of Titan. Science 308, 982–986.

Waite Jr., J.H., Young, D.T., Cravens, T.E., Coates, A.J., Crary, F.J., Magee, B., Westlake, J., 2007. The process of tholin formation in Titan's upper atmosphere. Science 316, 870–875.

Wakeham, W.A., Slater, D.H., 1973. Diffusion coefficients for *n*-alkanes in binary gaseous mixtures with nitrogen. J. Phys. B Atom. Molec. Phys. 6, 886-896.

Walker, J.C.G., 1977. Evolution of the Atmosphere. Macmillan, New York.

Walker, J.C.G., 1982. Climatic factors on the Archean Earth. Palaeogeogr. Palaeoclimatol. Palaeoecol. 40, 1–11.

Walker, J.C.G., Hays, P.B., Kasting, J.F., 1981. A negative feedback mechanism for the long-term stabilization of the Earth's surface temperature. J. Geophys. Res. 86, 9776–9782.

Walker, J.C.G., Klein, C., Schidlowski, M., Schopf, J.W., Stevenson, D.J., Walter, M.R., 1983. Environmental evolution of the Archean-early Proterozoic Earth. in Earth's Earliest Biosphere: Its Origin and Evolution, edited by J.W. Schopf, pp. 260–290, Princeton Univ. Press, Princeton, N. J.

Wang, H., Frenklach, M., 1994. Calculations of rate coefficients for the chemically activated reactions of acetylene with vinylic and aromatic radicals. J. Phys. Chem. 98 (44), 11465–11489.

Wang, J., Liu, K., Min, Z., Su, H., Bersohn, R., Preses, J., Larese, J., 2000. Vacuum ultraviolet photochemistry of CH_4 and isotopomers. II. Product channel fields and absorption spectra. J. Chem. Phys. 113 (10), 4146–4152.

Wang, W.C., Yung, Y.L., Lacis, A.A., Mo, T., Hansen, J.E., 1976. Greenhouse effects due to man-made perturbations of trace gases. Science 194, 685-690.

Warnatz, J., 1984. Rate coefficients in the C/H/O system, in: Combustion Chemistry. Springer-Verlag, pp. 197–360.

Watanabe, K., Zelikoff, M., Absorption coefficients of water vapor in the vacuum ultraviolet. J. Opt. Soc. Am. 43, 753-754.

West, G.A., Berry, M.J., 1974. CN photodissociation and predissociation chemical lasers: Molecular electronic and vibrational laser emissions. J. Chem. Phys. 61, 4700-4716.

Westmoreland, P., Dean, A., Howard, J., Longwell, J., 1989. Forming benzene in flames by chemically activated isomerization. J. Phys. Chem. 93 (25), 8171–8180.

Weissman, M., Benson, S., 1988. Rate parameters for the reactions of C_2H_3 and C_4H_5 with H_2 and C_2H_2. J. Phys. Chem. 92 (14), 4080–4084.

Westley, M.S., Baraglola, R.A., Johnson, R.E., Baratta, G.A., 1995. Photodesorption from low-temperature water ice in interstellar and circumsolar grains. Nature 373, 405-407.

Whyte, A., Phillips, L., 1983. Rate of reaction of N with CN ($\nu = 0.1$). Chem. Phys. Lett. 98 (6), 590–593.

Whytock, D., Payne, W., Stief, L., 1976. Rate of reaction of atomic hydrogen with propyne over an extended pressure and temperature-range. J. Chem. Phys. 65 (1), 191–195.

Wilson, E., Atreya, S., 2003. Chemical sources of haze formation in Titan's atmosphere. Planet. Space Sci. 51 (14-15), 1017–1033.

Wilson, E.H., Atreya, S.K., 2004. Current state of modeling the photochemistry of

Titan's mutually dependent atmosphere and ionosphere. J. Geophys. Res. 109, E06002.

Wolf, E.T., Toon, O.B., 2010. Fractal organic hazes provided an ultraviolet shield for early Earth. Science 328, 1266-1268.

Wu, C.Y.R., Chen, F.Z., Judge, D.L., 2001. Measurements of temperature-dependent absorption cross sections of C_2H_2 in the VUV-UV region. J. Geophys. Res. 106 E, 7629-7636.

Xu, Z.-F., Fang, D.-C., Fu, X.-Y., 1997. Ab initio study on the reaction $2NH(X^3\Sigma^-) \rightarrow NH2(X^2B_1) + N(^4S)$. Chem. Phys. Lett. 275, 386-391.

Yamashita, I., 1975. Highly monochromatic Lyman alpha light source of plasma-jet type. Jpn. J. Appl. Phys. 14 (6), 833-839.

Yang, D., Yu, T., Lin, M., Melius, C., 1992a. CN radical reactions with hydrogen-cyanide and cyanogen - Comparison of theory and experiment. J. Chem. Phys. 97 (1), 222–226.

Yang, D., Yu, T., Wang, N., Lin, M., 1992b. Temperature-dependence of cyanogen radical reactions with selected alkanes - CN reactivities towards primary, secondary and tertiary C-H bonds. Chem. Phys. 160 (2), 307–315.

Yee Quee, M., Thynne, J., 1968. Pressure dependence of the decomposition of the isopropoxyl radical. J. Phys. Chem. 72 (8), 2824–2831.

Yelle, R.V., Strobel, D.F., Lellouch, E., Gautier, D., 1997. Engineering models for Titan's atmosphere, ESA SP-1177. European Space Agency, Noordwijk, 243-256.

Yelle, R.V., Cui, J., Muller-Wodard, I.C.F., 2008. Methane escape from Titan's atmosphere. J. Geophys. Res. 113, E10003.

Young, G.M., Long, D.G.F., Fedo, C.M., Nesbitt, H.W., 2001. Paleoproterozoic Huronian basin: product of a Wilson cycle punctuated by glaciations and a meteorite impact. Sediment. Geology 141-142, 233-254.

Yu, Y., Li, S., Xu, Z., Li, Z., Sun, C., 1998. An ab initio study on the reaction $NH_2 + CH_4 \rightarrow NH_3 + CH_3$. Chem. Phys. Lett. 296 (1-2), 131–136.

Yu, T., Yang, D., Lin, M., 1993. Kinetics of CN radical reactions with formaldehyde and 1,3,5-trioxane. Int. J. Chem. Kinet. 25 (12), 1053–1064.

Yung, Y.L., 1987. An update of nitrile photochemistry. Icarus 72, 468-472.

Yung, Y.L., Allen, M., Pinto, J.P., 1984. Photochemistry of the atmosphere of Titan: Comparison between model and observations. Astrophys. J. Suppl. 55, 465-506.

Yung, Y.L., DeMore, W.B., 1999. Photochemistry of Planetary Atmospheres. Oxford University Press, New York, 470p.

Zabarnick, S., Fleming, J., Lin, M., 1986. Temperature dependence of CH radical reactions with H_2O and CH_2O. Proc. Combust. Inst. 21, 713–719.

Zabarnick, S., Fleming, J., Lin, M., 1989. Kinetics of methylidyne $CH(X^2\Pi)$ radical reactions with ammonia and methylamines. Chem. Phys. 132 (3), 407–411.

Zabarnick, S., Lin, M., 1989. Kinetics of $CN(X^2\Sigma^+)$ radical reactions with HCN, BrCN

and CH3CN. Chem. Phys. 134 (1), 185–191.

Zahnle, K.J., 1986. Photochemistry of methane and the formation of hydrocyanic acid (HCN) in the Earth's early atmosphere. J. Geophys. Res. 91, 2819-2834.

Zahnle, K., Arndt, N., Cockell, C., Halliday, A., Nisbet, E., Selsis, F., Sleep, N.H., 2007. Emergence of a habitable planet. Space Sci. Rev. 129, 35–78.

Zahnle, K., Pollack, J.B., Grinspoon, D., 1992. Impact-generated atmospheres over Titan, Ganymede, and Callisto. Icarus 95, 1-23.

Zahnle, K.J., Walker, J.C.G., 1982. The evolution of solar ultraviolet luminosity. Rev. Geophys. 20, 280-292.

Zelikoff, M., Watanabe, K., 1953. Absorption coefficients of ethylene in the vacuum ultraviolet. J. Opt. Soc. Am. 43, 756-759.

Zerkle, A.L., Claire, M.W., Domagal-Goldman, S.D., Farquhar, J., Poulton, S.W., 2012. A bistable organic-rich atmosphere on the Neoarchaean Earth. Nat. Geo. 5, 359-363.

Zwier, T., Allen, M., 1996. Metastable diacetylene reactions as routes to large hydrocarbons in Titan’s atmosphere. Icarus 123 (2), 578–583.

笹森仁務，2012．初期地球大気における有機物ヘイズの生成実験と表層環境の安定性への応用．修士論文，東京大学大学院.